Effects of Mechanical Degradation on the Molecular Weight Distribution of High Molecular Weight Polymers

Montan University of Leoben

Department of Petroleum Engineering

Roman Schuetter, Bsc

Master Thesis

First Supervisor:
Univ.-Prof. Dipl.-Ing. Dr.mont.
Gerhard Thonhauser

Second Supervisor:
Fogh-lis. PhD. Shahin
Kord

EIDESSTATTLICHE ERKLÄRUNG

Ich erkläre an Eides statt, dass ich die vorliegende Diplomarbeit selbständig und ohne fremde Hilfe verfasst, andere als die angegebenen Quellen und Hilfsmittel nicht benutzt und die den benutzten Quellen wörtlich und inhaltlich entnommenen Stellen als solche erkenntlich gemacht habe.

AFFIDAVIT

I hereby declare that the content of this work is my own composition and has not been submitted previously for any higher degree. All extracts have been distinguished using quoted references and all information sources have been acknowledged.

Ort, Datum Unterschrift

Danksagung

Ich möchte mich hiermit für die Unterstützung und Hilfe während meines Studiums und ganz speziell bei der Erstellung meiner Diplomarbeit bei einigen speziellen Menschen und Institutionen bedanken.

Zuallerst gilt mein Dank natürlich dem universitären Betreuer meiner Arbeit Herrn Univ.-Prof. Dipl.-Ing. Dr.mont. Gerhard Thonhauser, der, eine Kapazität auf seinem Gebiet, die Führung des Insituts für Erdölwissenschaften übernommen hat und dem ich viel Wissen um mein Studium und diese Diplomarbeit verdanke. Weiters gebührt Herrn Fogh-lis. PhD. Shahin Kord mein ungeteilter Danke, der die operative Betreuung meiner Arbeit auf universitärer Ebene übernommen hat und mich durch diesen schwierigen Prozess geführt hat. Weiters will ich meine Anerkennung und Wertschätzung den zahlreichen Angehörigen des Departments Petroleum Engineering, des Departments Angewandte Geowissenschaften und Geophysik und vor allem den Mitarbeitern des Lehrstuhls für Reservoir Engineering aussprechen, die mittlerweile zu einem kleinen verschworenen Kreis geschrumpft, mich die letzten Semester meines Studiums begleitet haben. Vorallem für die frühen Jahre meines Studiums möchte ich meinen Dank der suddt. akad. Landsmannschaft Zornstein zu Leoben aussprechen, die mir Familie und Freunde waren und mich mit offenen Armen in Leoben aufgenommen haben. In weiterem Sinne danke ich natürlich auch der Gesamtheit meiner Alma Mater Leobiensis und all meinen übrigen Kommilitonen, mit denen ich viel Zeit meines Lebens verbracht habe und die mich stark geprägt haben.

Auf Seiten der OMV AG, der Firma, die diese Arbeit erst ermöglicht hat, möchte ich mich ganz besonders bei Herrn Dr. Thomas Gumpenberger bedanken, der mir Tag für Tag mit Rat und Tat zur Seite gestanden ist und mir sein unschätzbares Wissen zur Verfügung gestellt hat. Ohne sein Zutun und seine intensive Betreuung wäre dieses Werk hier nicht möglich gewesen. Weiters möchte ich Herrn Dipl.- Ing. Paul Toplak danken für seinen Input und Herrn Dr. Torsten Clemens, der für die Organisation und die grobe Richtung dieses Projekts verantwortlich zeichnet. Herr Dr. Clemens genießt in dieser Hinsicht meinen besonderen Respekt, da er sich speziell um die anwesenden Diplomanten und deren angemessene Arbeitsbedingungen gekümmert hat. Als letzten möchte ich noch Herrn Ing. Leopold Huber herausheben, der mich in die operativen Arbeiten des Labors eingeführt und mir einige nützliche Kniffe beigebracht hat. Am Ende meines Aufenthalts in der OMV musste ich leider erfahren, dass er einen Herzinfarkt erlitten hat und nun stationär behandelt wird. In diesem Sinne sind meine Gedanken bei ihm und seiner Familie und diese Arbeit ist selbstverständlich auch ihm gewidmet. Desweiteren danke ich natürlich der OMV in ihrer Gesamtheit und der gesamten Belegschaft für die freundliche Aufnahme.

Der wichtigste Dank gebührt zu guter Letzt meiner Familie und meiner Freundin, ohne all deren Hilfe ich niemals so weit gekommen wäre. Mein Vater, der mir grundlegende Lebensweisheiten mit auf den Weg gegeben hat und mir in meiner Erinnerung weiterhin als Vorbild dient. Meine Mutter, die immer für mich da war und mich unterstützt hat, wo sie nur konnte und die immer stolz auf mich war. Meine beiden Schwestern, die mir mit das wichtigste auf der Welt sind und schließlich meine Freundin, ohne deren Unterstützung die heiße Phase des Schreibens kaum schaffbar gewesen wäre und die mich immer aufs Neue ermuntert und motiviert hat.

All diesen besonderen Menschen möchte ich nochmals meinen tiefempfunden Dank aussprechen.

Abstract

Partially hydrolyzed polyacrylamides are viscosity enhancing polymers commonly used in enhanced oil recovery treatments as in the specific case of an OMV polymer project in the Matzen field, Lower Austria. The thesis at hand characterizes an analogue reservoir system, comprising 356 to 443 mD Berea Sandstones and 10 MDa 250 ppm FLOPAAM 3330 polymer solution. The two experimental methods applied here, were core flooding setups for the evaluation of apparent viscosity and size exclusion chromatography for the examination of according molecular weight distributions. At low far field flow rates of 1 to 20 m/day shear thickening apparent viscosity effects were notable with peak values of 35 mPas. A critical offset rate was recognized below which no significant mechanical degradation occurred. The offset flow rate lies at 60 m/day and leads to a flattening trend in shear thickening which transitions to shear thinning behavior and a drop of apparent viscosity at elevated near wellbore rates. Mechanical degradation is proven to occur exclusively at this level in a significant extent. Reinjecting previously degraded polymer solution into another core, leads to a similar viscosity profile but shifted to lower viscosities and higher flow rates. The averaged absolute viscosity loss due to mechanical degradation is as high as 58.1% with peak values of 84%. The average modal molecular weight of a 10 MDa HPAM solution is diminished to 8.4 MDa in the first place and further to 7.7 MDa after the second flood. In terms of average percentages, this equals a reduction of 16.4% in the first core flood and another 6.5% during a subsequent core experiment, adding up to 22.7% total loss. A combination of more elaborate core flooding experiments was designed to investigate time and temperature effects on degraded HPAM probes. Larger amounts of sample liquids were taken after a first experiment and stored for 2 months at temperatures of 8, 22, 50 and 80 °C . The lowest temperature scenario yielded an identical result as a normal reinjection experiment would have. The 80 °C configuration ended in a dramatically deteriorated viscosity profile in the range of 2 mPas, implying massive thermic degradation. The two temperature scenarios at 22 and 50 °C exhibited small amounts of viscosity healing and molecular size restoration. Further analysis of these data sets allowed the conclusion that a share of 15.8% of lost apparent viscosity is due to temporary effects and can be restored at certain conditions. The overall permanent damage must be considered not as grave as first measurements would suggest and can be stated to equal 48.7 instead of 58.1%. In terms of molecular size, this effect is much smaller. Only 1-3% of lost molecular weight is re-established over the same time span. This means that 1% of size growth is responsible for 15.8% of viscosity restoration. Permanent damage is considered to be the consequence of frequent chain scission processes. Temporary viscosity loss occurs most likely due to chain unfolding at higher temperatures and proved to be possibly undone given enough time.

Zusammenfassung

Hydratisierte Polyacrylamide werden bevorzugt für den Einsatz in EOR Behandlungen herangezogen, so auch im Matzen Feld im Zuge eines Polymerprojekts der OMV. Die hier vorliegende Diplomarbeit charakterisiert ein Lagerstättenanalogon, das sich aus 356 - 443 mD Berea Sandsteinen und 10 MDa 250ppm FLOPAAM 3330 wässriger Polymerlösung zusammensetzt. Die zwei angewandten Analysemethoden fußen auf Kernflutversuchen von unterschiedlicher Typologie zur Untersuchung der zugehörigen Viskositätsprofile und Größenausschlusschromatographie um resultierende Molekularmassenverteilungen dahingehend prüfen zu können. Niedrige Flussraten von 1 bis 20 m/d, äquivalent zu jenen tief in der Lagerstätte, weisen signifikantes scherverdickendes Verhalten auf mit Spitzenwerten von 35 mPas. Eine kritische Flussrate wurde festgestellt, unter welcher keine mechanische Degradation festgestellt werden konnte. Dieser Inversionspunkt liegt in etwa bei 60 m/d und zieht eine flachere Viskositätskurve und einen Übergang zu scherverdünnendem Verhalten bei höheren bohrlochnahen Raten nach sich. Mechanische Degradation vollzieht sich nachgewiesener Weise nur in diesem Bereich. Abermaliges Injizieren von bereits degradiertem Polymer in einen anderen Kern resultiert in ein ähnliches Viskositätsprofil mit niedrigeren Werten und höheren Flussraten. Der gemittelte absolute Viskositätsverlust auf Grund von Degradation beträgt 58.1% mit Extremwerten von 84%. Der mittlere Modalwert der Molekulargewichtsverteilung einer 10 MDa HPAM Lösung reduziert sich auf 8.4 MDa während des ersten Versuchs und weiters auf ein Minimum von 7.7 MDa während des zweiten Durchgangs. Ausgedrückt in Prozentzahlen entspricht das einem 16.4%igen Massenverlust im ersten Durchlauf und einem weiteren Verlust von 6.5% während des zweiten Experiments. Die Lösung erfährt einen Gesamtverlust von insgesamt 22.7%. Eine Kombination aus elaborierteren Flutversuchen wurde erstellt um Zeit- und Temperatureffekte auf die degradierte Lösung besser untersuchen zu können. Eine größere Menge an Polymerlösung wurde dem ersten Experiment entnommen und unter vier unterschiedlichen Temperaturbedingungen von 8, 22, 50 und 80 °C für zwei Monate ausgelagert. Das niedrigste Temperaturszenario ergab eine Viskositätskurve, die nahezu identisch einem regulären Reinjektionsexperiment ausfiel. Das bei 80 °C ausgelagerte Polymer wies ganz massiv verschlechtertes Viskositätsverhalten auf, was auf umfangreiche thermische Degradation rückschließen lässt. Die beiden Versuche mit mittleren und erhöhten Temperaturen erbrachten einen merklichen Heilungseffekt was Viskosität betrifft. 15.8% der verlorenen Viskosität konnte wiedergewonnen werden, was den Totalverlust von 58.1% auf 48.7% abmildern konnte. Derselbe Trend, nur weniger stark ausgeprägt, konnte für Untersuchungen der Molekulargewichtsverteilungen festgestellt werden. 1-3% der gemessenen Molekulargrößen konnten wiedergewonnen werden. Die Conclusio, die man aus beiden Beobachtungen ziehen kann, ist, dass eine kleine Erholung an Molekulargewicht für eine verhältnismäßig große Zunahme an wiedergewonnener Viskosität verantwortlich ist. Permanente Schädigung wird größtenteils Polymerkettenbrüchen zugeschrieben, temporäre Effekte hingegen der Entfaltung von vorher deformierten Molekularkettenknäueln.

Contents

1 Tertiary Oil Recovery

Enhanced oil recovery is a term that describes all hydrocarbon recovery techniques that are not attributed to primary or secondary oil recovery. Crude oil production normally undergoes three distinct phases of field deployment. These are primary, secondary, and tertiary recovery which are all connected to different production methods and technological challenges. Whilst primary recovery, natural reservoir pressure suffices to force hydrocarbons into the previously drilled wellbore. This natural drive combined with artificial lift methods delivers crude oil to the surface and hence to processing facilities. On average, nothing more than 10 to 20% of the reservoir's original hydrocarbons can be produced in the primary production phase. Secondary recovery techniques aim to extend a reservoir's productive lifetime by water or gas injection. The injected fluid shall displace the in situ hydrocarbons and squeeze them to a producer wellbore. Recovery factors for secondary recovery range in between 20 to 40% of the oil originally in place. Everything that goes beyond the above-mentioned techniques is called tertiary recovery, improved or enhanced oil recovery. (Buchwalter et al., 2008)

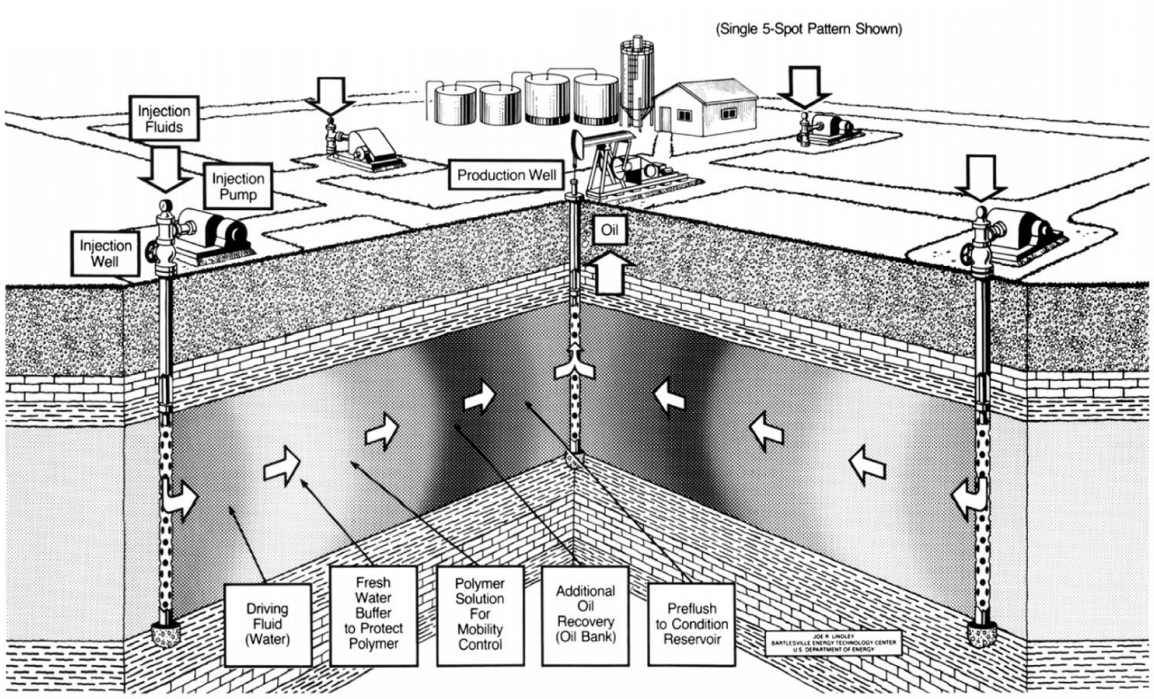

Figure 1: Polymer Flooding Schematic - A high viscous polymer bank mobilizes and displaces hydrocarbons. The polymer slug is followed by lower concentration polymer batches and pure injection water for costs reasons. (DOE, 2015)

1.1 Types of Enhanced Oil Recovery Techniques

Treatments that are most commonly referred to as enhanced oil recovery techniques can be grouped according to different characteristics. The Energy Department of the U.S. proposes a threefold division of tertiary recovery operations. (DOE, 2015)

- Thermal Recovery
- Gas Injection or Miscible Injection
- Chemical Injection

1.1.1 Thermal Recovery

Thermal injection or thermal recovery is an enhanced recovery method that intentionally introduces heat into a reservoir in order to lower viscosity and attenuate the heavy viscous oil or alter it's composition. These effects enable the oil to migrate through reservoir rock towards production facilities. Commercially applicable operations are cyclic steam injections, steam flooding and in situ combustion operations. These methods improve both the sweep efficiency and the displacement efficiency. (Satter and Iqbal, 2015)

1.1.2 Gas Injection

Miscible injection ushers gases such as natural gas, nitrogen or carbon dioxide downhole to replace hydrocarbons inside the reservoir and drive them towards a producer. These gases dissolve in crude oil and enhance the oil's ability to flow by lowering it's inherent viscosity. A miscible displacement process maintains the reservoir pressure and improves oil displacement due to the reduction of interfacial tension between hydrocarbons and water. The fluid most commonly used for miscible displacement is carbon dioxide. Oil displacement by carbon dioxide injection relies on the phase behavior of injection gas-oil mixtures which are strongly dependent on reservoir temperature, pressure and crude oil composition. (Buchwalter et al., 2008)

1.1.3 Chemical Injection

Chemical injection techniques split in two subgroups. On the one side polymer flooding, which involves the use of long-chained molecules to increase the effectiveness of water flooding operations by increasing the viscosity of the displacing fluid. These treatments are entirely based on mobility control. (Tarek, 2010) On the other side surfactant flooding. Such treatments utilize detergent-like surfactants to assist the diminution of surface tension which is very often the reason preventing oil droplets from migrating through the reservoir. In all of these methods, chemicals are injected into several wells. Production then is observed in adjacent wells. The downsides of chemical injection techniques are relatively high costs and in some cases unpredictability of effectiveness. (Buchwalter et al., 2008)

1.2 Targets of Improved Oil Recovery Operations

The major objective of tertiary oil production is to maximize recovery factors and by doing so increase ultimate oil recovery. Although the impact of an enhanced oil recovery process may not immediately or directly result into a surplus of production, the like treatments can very often improve the profitability of an entire operation and yield additional benefits. (Buchwalter et al., 2008) The primary objectives are

- Mobilization of Incremental Oil
- Improvement of Recovery Efficiency
- Reduction of Water Production
- Enlargement Productive Well Lifetime
- Reduction of Lifting Costs
- Reduction of Environmental Impact and Costs
- Minimization of Treatment and Disposal of Water
- Reduction of Well Maintenance Costs
- Satisfy Reservoir Management Objectives (Tarek, 2010)

1.3 Polymer Flooding

Polymer flooding is an enhanced oil recovery method that belongs to the chemical injection group. When conducting a polymer waterflood, high-molecular-mass polymers are combined with regular injection-water to improve oil water replacement. (Satter and Iqbal, 2015)

1.3.1 Mobility Control

The injected polymer features a viscosity enhancing effect, creating a stable polymer-water front that decreases the flood-water's mobility and, as a consequence of that, improves the sweep efficiency of the flooding operation. This resulting sweep efficiency benefit concerns both vertical and areal sweep and is a consequence of the improved balance between the mobility of the displacing and the displaced phase. That mobility balance is expressed by a number called the mobility ratio. The diminution of this key figure is the main objective of mobility control. (Dake, 2015) Controlled addition of polymer powder to injection water also triggers a secondary permeability-reduction response in many cases. Polymer flooding is typically performed whenever the waterflood's mobility ratio or the heterogeneity of the reservoir is high. (Dake, 2001) The mobility ratio is defined as

$$M = \frac{\lambda_D}{\lambda_d} = \frac{k_{rD}}{\mu_D}\Big|_{S_D} \frac{\mu_{rd}}{k_{rd}}\Big|_{S_d} \tag{1}$$

Equation 1: Definition of Mobility Ratio

where k_{rD} is the relative permeability of the displacing fluid, k_{rd} the relative permeability of the displaced fluid, μ_D the viscosity of the displacing fluid, μ_d the viscosity of the displaced fluid, S_D the average saturation of the displacing phase in the region behind the displacing phase front and S_d the average saturation of the displaced phase in the region ahead of the displacing phase front. (Dake, 2015)

$$\lambda_i = \frac{k_{ri}}{\mu_i} \tag{2}$$

Equation 2: Definition of a phase's Mobility

Mobility for each phase is defined by equation 2 as the ratio of the rock's relative permeability to the phase's viscosity.

1.3.2 Viscous Fingering

Viscous fingering is a phenomenon in a porous medium, triggering the formation of certain patterns in a morphologically unstable interface between two fluids. It occurs when a less viscous fluid is injected into a reservoir, displacing a more viscous one. It can also occur due to gravity effects if the interface is horizontal, separating two fluids of different densities, being the heavier one above the other. As shown in figure 2, viscous fingering is more likely to occur at higher mobility ratios. (Dake, 2001) It is an utterly unfavorable effect in water flooding operations because it entails early water breakthrough and thus less displacement, higher water cuts and fewer incremental oil. The macroscopic explanation for this unwanted behavior is that the injected water attempts to take the fastest flow path through the reservoir, sparing more distant regions of the horizon from contact and displacement. The means for coping with this problem is mobility control via polymer flooding. Polymers influence the displacing fluid's viscosity and decrease the according mobility ratio. This reduces viscous fingering effects and provides a more stable and broader displacement front. A mobility ratio smaller than unity ensures that more and more regions of the reservoir are touched by the

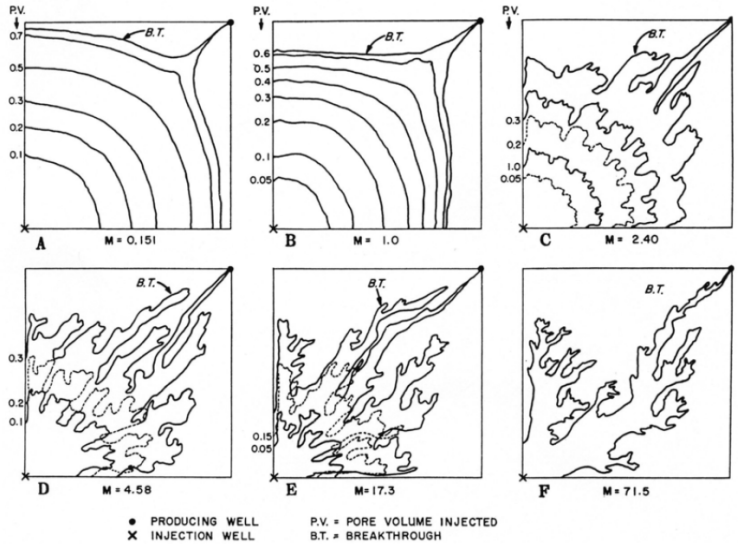

Figure 2: Effect of different mobility ratios on water breakthrough and the according displacement pattern. The higher the Mobility Ratio rises, the stronger viscous fingering effects will occur. Mobility ratios below unity will lead to a more even and stable displacement front with a much higher sweep efficiency. (Tarek, 2010)

displacing water and get properly swept. The result is an elevated hydrocarbon production. (Buchwalter et al., 2008)

2 Polymers

2.1 General Description

A polymer is by definition a large molecule or macromolecular complex assembled from many repeating chemical sub-entities called monomeres. Due to their broad range of properties both synthetic and natural polymers play an essential role in everyday life. The chemical process of joining together smaller monomers and forming polymer chains is referred to as the polymerization reaction process. Their consequently larger molecular mass relative to small molecule compounds results in unique physical properties, including such features as special toughness or viscoelasticity, features that are sought and come in very handy with respect to specific engineering applications. Polymers are manufactured in liquid form or in pure solid form further being dissolved into liquids.

2.2 Enhanced Oil Recovery Polymers

The two kinds of polymers that are most commonly used in polymer waterflooding operations are on the one side biopolymers with Xanthan as best known example and synthetic polymers like polyacrylamides on the other side.

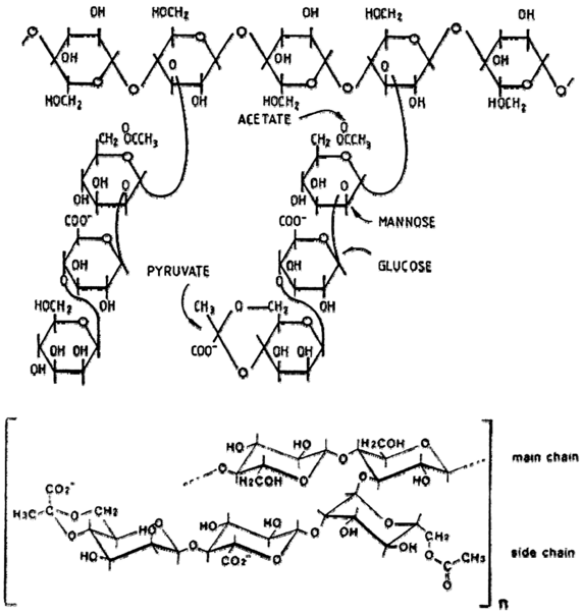

Figure 3: Chemical structure of a Xanthan molecule with the monosaccharidic main chain and according side branches (Lake, 1989)

2.2.1 Biopolymers

Biopolymers that are used for polymerflooding treatments are most commonly polysaccharides. The long polymer chains are constructed from monosaccharide units bound together by glycosidic linkages. The assembled carbohydrates have a multistranded conformation. They make up a very rigid and mechanically stable structure in an aqueous solution. This is a major advantage implying high resistance to mechanically induced degradation and relative insensitivity to high salinity. In addition to that, they are environmentally friendly and readily available. Their two primary downsides are due to their susceptibility to biological and chemical degradation. Furthermore injectability issues have to be considered resulting from

cell debris derived from the microorganism fermentation process whilst creation. Xanthan is the most common biopolymer used in polymer waterflooding. A Xanthan molecule with a molecular mass of 4 MDa comprises of repeating monosaccharide entities in the vicinity of 20 000 units. Xanthan is the fermentation product of the bacterium Xanthomonas campestris that usually leaves a substantial amount of cell debris in the final polymer solution. (Satter and Iqbal, 2015)

2.2.2 Synthetic Polymers

Synthetic polymers emerged to be the predominant type of polymers used in commercial flooding operations. Main advantages are their inherent chemical and biological stability alongside with injectivity- and cost-benefits. The downside of synthetic polymers is their high susceptibility to mechanical degradation. Main aspects of this degradation process haven't been entirely understood yet. Some facets of that problem are the focus of this research work. Synthetic polymers are usually composed from highly flexible molecules. The polymer backbone consists of a chemically stable carbon molecular chain with single and flexible carbon-carbon bonds. Pendant water-soluble chemical groups on the molecule like for example amide groups render the polymer soluble in water. (Lake, 1989)

2.2.3 Polyacrylamide

Acrylamide polymers have emerged to be the most widely used synthetic polymer family for application in synthetic polymer flooding treatments. Polyacrylamide or abbreviated PAM is the simplest and most basic form of an acrylamidic polymer. As for the entire group again their upsides are low costs and good availability, favorable chemical robustness and biological stability. A polyacrylamide molecular complex with a molecular mass of 7 MDa has a number of repeating monomer entities in the order of 100 000 units.

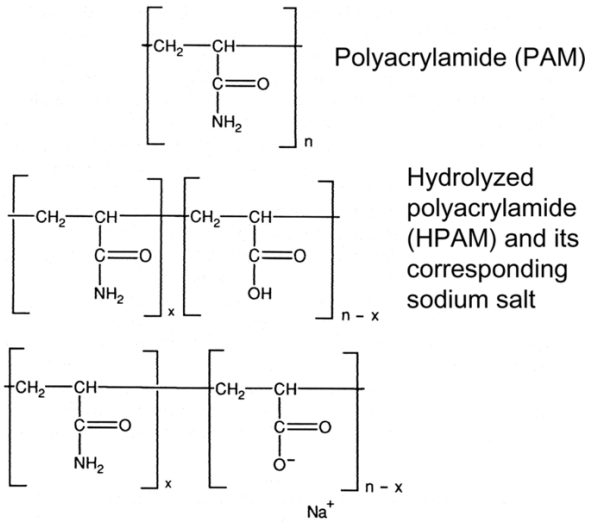

Figure 4: Chemical structure of Poylacrylamid (PAM) and Partially Hydrolysed Polyacrylamide (HPAM) molecules (Lake, 1989)

2.2.4 Partially Hydrolyzed Polyacrylamide

Pure polyacrylamide is slightly positively charged in an acidic or neutral pH environment. Thus polyacrylamide is prone to adsorb and stick onto reservoir rock surfaces especially sands and sandstone pore surfaces. In order to avoid this unfavorable effect the polymer is

subjected to a procedure that is called hydrolyzation or hydrolysis. When polyacrylamides are manufactured commercially they typically contain 1 to 2 mole percent of hydrolyzed content also referred to as carboxylate groups. This is an inadvertent byproduct of the manufacturing process. Although it is more or less an impurity in the production phase it is exactly the like that renders the product a better viscosity enhancing agent and enables the hydrolyzed polymer to propagate faster through a sandstone reservoir than mere polyacrylamide. Polyacrylamide is normally not referred to as partially hydrolyzed polyacrylamide or abbreviated HPAM until the carboxylate content exceeds approximately 2 mole percents. A 30% to 35% hydrolysis level within polyacrylamides is near the optimum in terms of simultaneously providing maximum viscosity enhancement and minimizing polymer adsorption onto reservoir rock surfaces during a flood operation. (Lake, 1989) It is not clear how sensitive partially hydrolyzed polyacrylamids are to elevated salinities. The most common opinion on this salinity issue is that HPAM performs best when flooded through a reservoir with low saline formation water. Yet, some researches like Maitin et al. state that HPAM also shows high performance in high salinity reservoir brine. (Maitin et al., 1990)

2.3 Polymer Specifications

The particular polymers used during the experimental phase were chosen to be partially hydrolyzed polyacrylamides of different nominal weights. All types of synthetic polymers were purchased from the same vendor SNF Floerger, SNF Group. Although more distinguishable polymer standards would have been better to calibrate the high performance liquid chromatograph and to quantify degradation more precisely, only five polymer standards were available, starting with the heavy 20 MDa FLOPAAM 3630 S to the light AB 305 VLM 1 MDa polymer.

Molecular Mass	Manufacturer	Product Name	Anionicity	Mother Solution
[MDa]	[x]	[x]	[%]	[ppm]
20	SNF	FLOPAAM 3630 S	35	5000
10	SNF	FLOPAAM 3330 S	35	5000
6	SNF	AN 934 BPM	35	5000
2.5	SNF	AB 305 MPM	35	5000
1	SNF	AB 305 VLM	35	5000

Table 1: Manufacturer's Polymer Specifications

All of the probes exhibit approximately the same anionicity of 35%, which lies perfectly within in the optimum range. The sales specification of the HPAM solutions is the viscosity modifying behavior. It is not based on the average or modal molecular weight. The stated nominal molecular weight of each polymer standard is estimated by the ratio of monomer units to the number of polymerisation starters. The manufacturer provided all polymers in powder form.

2.4 Polymer Preparation

The preparation of the polymer solution is based upon the detailed recommendation of the vendor. In order to generate batches with different concentrations, a 5000ppm mother

solution has to be created first and then be further diluted to target concentrations. The preparation work is based on the solution of polymer powder into an aqueous phase. The properties of the powder are provided by the manufacturer whereas the composition of the salt water has to be chosen separately. It should resemble the formation water as accurate as possible. A 3000ppm (w/w) aqueous potassium chloride solution was chosen as formation water equivalent. The actual reservoir water characterization and composition can be found in the following chapter about the geology and the depiction or translation of these values into an experimental analogue. For the moment it shall suffice to understand a 3% KCl solution as reservoir brine counterpart. The impact of divalent ions in the reservoir brine was presumed to be minor. To minimize the effect of different ion concentrations, the maximum concentration tolerance of solution concentration was limited to $\pm$ 0.5%.

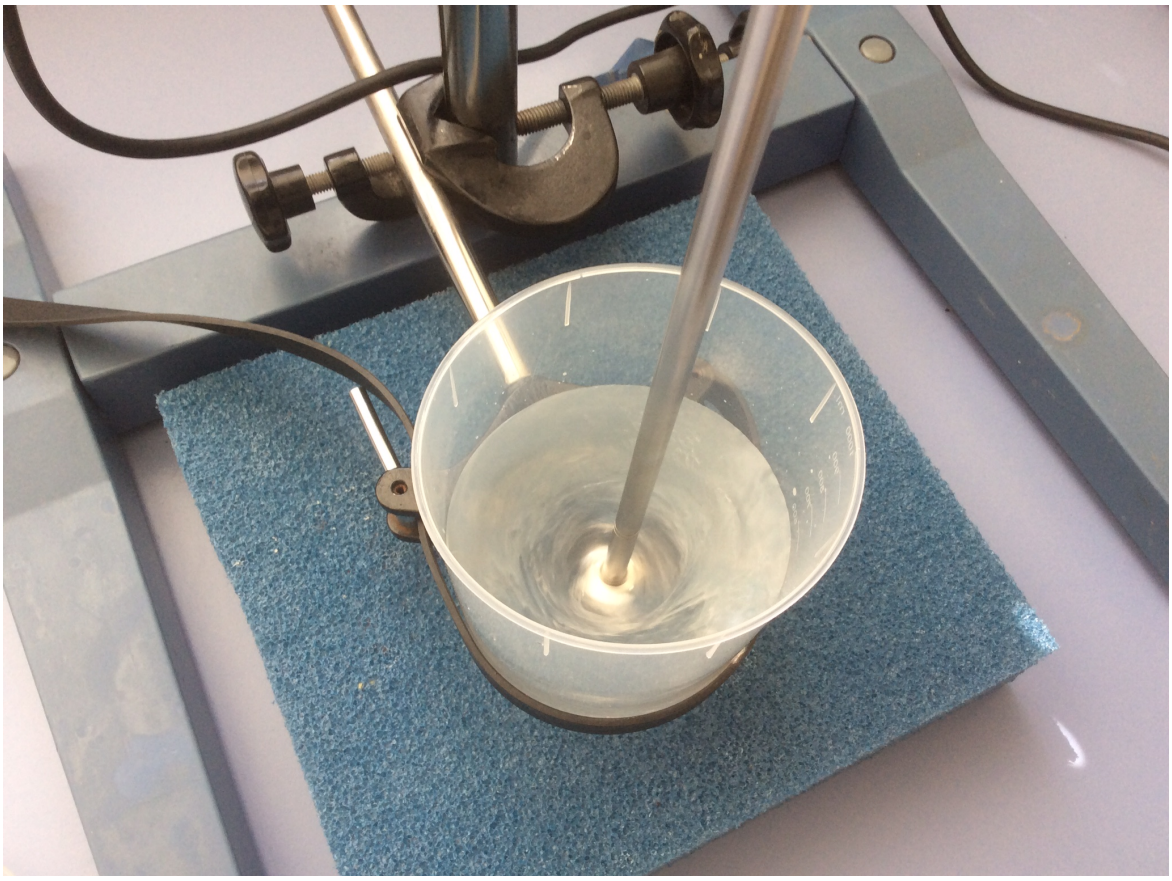

Figure 5: The 3000ppm potassium chloride vortex for the HPAM powder insertion created by a propeller stirrer at 500 RPM

For the purpose of preventing bacterial growth or other bacterial incidents a spoon tip of sodium azide NaN_3 was added to the solution because the time component and possible bacteria growth of certain extended experiments cannot be neglected. In order to purge the salt water solution from impurities it was vacuum filtered through $0.45\mu m$ Millipore filter paper and simultaneously roughly degassed. Contamination would distort the experimental findings and could eventually plug sensible parts of the instruments. Potassium chloride solutions were prepared on a regular basis and spent within few days. This measure shall reduce time dependent alteration effects that would otherwise influence measurements. The actual polymer solution is produced by cautiously blending polymer powder with the previously created brine solution. This is done by slowly and carefully sprinkling the polymer powder into the saltwater vortex generated by a propeller stirrer. After vigorously stirring

the blended solution at a speed of 500 RPM for 5 minutes, slower and gentle agitation is maintained for another 2 hours to entirely dissolve and mingle the powder in brine. The end product was degassed for 10min via a vacuum pump with the aim of keeping the polymer solution as pure and oxygen free as possible. The mother solution's strength is upped by an extra across the board allowance of 10% to account for residual moisture in the polymer powder. The strength required for a specific experiment is established by dilution with artificial brine to the target concentrations of 4000ppm, 1000ppm, 500ppm, 250ppm and 100ppm for each molecular weight of 20MDa, 10MDa, 6MDa, 2.5Ma and 1MDa in all combinations.

3 Definition of Physical Properties

The following sections shall convey the current scientific knowledge about polymer viscosity behavior. For that reason it is essential to denote certain rheological effects and precisely define key figures to handle these concepts properly. The definition section provides the basic toolkit to operate expressions and numbers necessary for the later experimental work.

3.1 Applicability of Rheological Definitions

All researches try to perform with common definitions and vastly acknowledged nomenclatures concerning physical traits. These standardized labels and concepts origin from different scientific disciplines most likely physics and try to catch major feats by simplifying and idealizing conditions. The problem that arises by doing so, is the fact that some technical problems are too complex to be distilled to simple on-the-sheet definitions. For example the term viscosity describes a fluid's resistance against flow. The physicists' idealized quantification of viscosity links it to flow between two ideal plates. This concept is not applicable for porous media flow, especially for the flow of large macro-molecular chains through porous media, because of vast differences in flow behavior. The standard viscosity approach is too simplistic for that purpose. Scientists who tried to get a grip on the matter soon realized that common approaches and definitions will lead to a dead end where blurry concepts and inappropriate definitions impede their scientific work. They soon came up with new definitions and key figures to describe the effects they were observing. Provided here, is a brief summary of common and new definitions of rheological properties and equations necessary to understand core flooding behavior.

3.2 Rheological Concepts

3.2.1 Newtonian Fluids

A Newtonian fluid is defined as a fluid whose flow related viscous stresses are linearly proportional to the local strain rate. This is equivalent to it's rate of deformation over time. In terms of definition, a fluid is Newtonian only, if the tensors that describe viscous stresses and the strain rate are related by a constant viscosity tensor that does not depend on the stress state and velocity of the flow. (Tipler et al., 2015)

3.2.2 Non-Newtonian Fluids

A Non-Newtonian fluid is by definition a fluid with properties that differ in any way from those of Newtonian fluids. The viscosity of a Non-Newtonian fluid is either dependent on shear rate, shear rate history or both. Time independent viscous behavior can be split up in shear thickening and shear thinning fluids. Shear thickening are those whose apparent viscosity increases with increased stresses. Shear thinning fluids are those whose viscosity decreases with increased stress. Time dependent viscosity behavior can be divided into rheopecty where viscosity increases with duration of stress and thixotropy, where viscosity decreases with duration of stress. (Tipler et al., 2015)

3.2.3 Dilatant Fluids

A dilatant or shear thickening fluid is a Non-Newtonian fluid whose shear viscosity increases with increasing shear stress. Shear thickening behavior is highly dependent on the volume fraction of solid particles suspended within the liquid and their size, shape and mass distribution. The higher the volume fraction, the less shear is required to initiate shear thickening

behavior. The actual mechanism of dilatancy depends on the ratio of Van der Waals forces to shear forces in the shear thickening suspension. As long as inter-particle forces like Van der Waals forces dominate, suspended particles will poise in ordered layers. Yet, whenever shear forces start to dominate, particles are transduced into a state of flocculation. They are no longer held in suspension and begin to behave like a solid. When shear forces are relieved from the fluid, the particles spread and form a stable suspension once again. (Tipler et al., 2015)

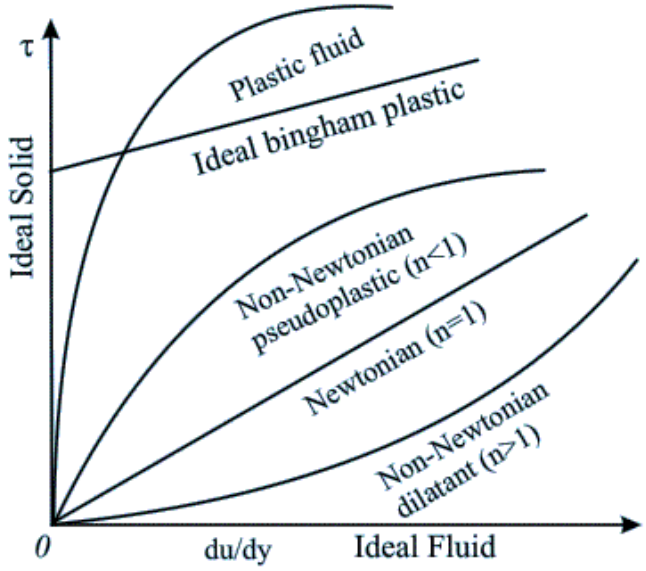

Figure 6: Relationships between shear stresses and deformation rate of different materials including ideal fluids, Newtonian fluids and several types of Non-Newtonian fluids with shear thickening and shear thinning behavior
(Tipler et al., 2015)

3.2.4 Pseudoplastic Fluids

A pseudoplastic or shear thinning fluid is a Non-Newtonian fluid which shows decreased apparent viscosity when subjected to shear stress. The mechanism that triggers shear thinning behavior is opposite to the above-mentioned shear thickening effect. The suspension is initially in a state of flocculation and gets more stable when stress is applied. The change of fluid structure leads to a state that facilitates particle flow and their planing on each other. This results in lower viscous macroscopic fluid properties. (Tipler et al., 2015)

3.2.5 Viscoelastic Fluids

Viscoelastic fluids are materials that behave like viscous liquids at low rates of deformation and partially like elastic solids at high rates of deformation. Elastic behavior is usually the result of bond stretching along crystallographic planes in an ordered solid, viscosity is the result of the diffusion of atoms or molecules inside an amorphous material. All materials exhibit in one way or the other viscoelastic traits and even these small amounts of viscoelasticity can result in significantly altered properties. Some anomalies in the polymer-porous-medium-interaction process that cannot be explained by simple viscous effects occur most probably due to elastic responses of the fluid. In this sense the term viscoelasticity is nothing more but an extended concepts of fluids or materials that include both viscous

and elastic interactions. Based upon each particular case there are constitutive models of linear viscoelasticity for the purpose of portraying these non conventional effects. The most famous models are the Maxwell model, the Kelvin-Voigt model and the generalized Maxwell model. (Tarek, 2010)

3.2.6 Rheopecty and Thixotropy

Rheopecty or rheopexy is the rare property of some Non-Newtonian fluids to show a time-dependent increase in viscosity. The longer the fluid is subjected to shearing forces, the higher will it's viscosity rise. The opposite type of behavior, in which fluids become less viscous the longer they undergo shear, is called thixotropy and is much more common. A thixotropic fluid is a fluid which takes a finite time to attain equilibrium viscosity when introduced to a change in shear rate. Some thixotropic fluids return to gel state almost instantly, others take much longer and can become nearly solid.

3.3 Rheological Key Figures

3.3.1 Viscosity

Viscosity is a measure of a fluid's ability to resist deformation by shear or tensile stresses. It corresponds to the fluid's flow resistance or to it's consistency as thick or thin while flowing. Viscosity is a property arising from collisions between neighboring particles in a fluid that are moving at different velocities. A fluid that has no resistance to shear stress is known as an ideal or inviscid fluid. Generally speaking a fluid's viscosity is its relation between strain rate and viscous stresses. In the Newtonian fluid model this relationship is described by the viscosity tensor. Multiplying this tensor by the strain rate tensor (expressed as the gradient of the flow's velocity) gives the viscous stress tensor. The viscosity tensor has typically nine independent degrees of freedom. For isotropic Newtonian fluids these can be reduced to two independent parameters. The most usual decomposition yields the stress viscosity.

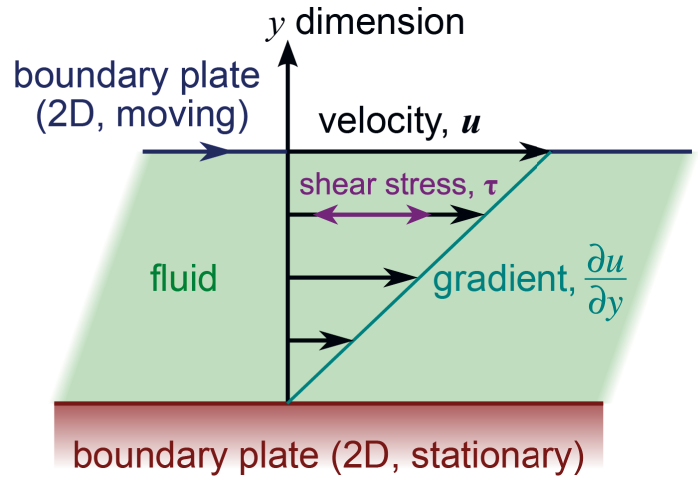

Figure 7: Velocity profile of parallel laminar shear flow. The shear stress is proportional to the gradient of the velocity. The proportionality constant is called dynamic viscosity (Tipler et al., 2015)

3.3.1.1 Dynamic Viscosity

As mentioned in the previous paragraph viscosity is an expression of a fluid's resistance to shearing flows. This property is also called dynamic or shear viscosity and bases on an idealized two plate model with adjacent layers moving parallel and with different speed to each other. This idealized concept is also known as Couette flow.

$$\mu = \frac{\tau}{\gamma} \tag{3}$$

Equation 3: Definition of Dynamic Viscosity

A fluid is trapped between two horizontal plates, one fixed and one moving horizontally at constant speed u. The plates are assumed to be sufficiently large so that no boundary conditions at the edges have to be considered. If the speed of the top plate is small enough, the fluid particles will move exactly parallel to it. The fluid particle speed will vary linearly from u at the top layer to zero at the fixed bottom plate. Each layer of fluid will move faster than the one right below it. The internal friction between layers and particles will result in a force resisting their relative motion. This force is defined via the fixed plate area, plate velocity and the gap height of the system via a proportionality constant μ, which is called dynamic viscosity. The definition of this shear viscosity is strongly related to the two plate model and is hardly and if so, with many constraints, translatable to the case of a core flooding experiment. (Tipler et al., 2015)

3.3.1.2 Kinematic Viscosity

The kinematic viscosity or "Momentum Diffusivity" is a convenient concept when analyzing the Reynolds number Re, expressing the ratio of inertial forces to viscous forces in a fluid's flow.

$$\eta = \frac{\mu}{\rho} \tag{4}$$

Equation 4: Definition of Kinematic Viscosity

Kinematic viscosity is usually denoted by the greek letter ν and is defined as the ratio of dynamic viscosity μ to the density ρ of a fluid.

3.3.1.3 Apparent Viscosity

The definition of dynamic viscosity μ is based upon the two-plate-model and defined for ideally viscous fluids. The liquid's viscosity is thought to be constant and independent of shear rate. Newtonian fluids match these requirements and feature such a constant viscosity. Non-Newtonian fluids however act in a more complex way and exhibit peculiar rheological behavior. Their viscosity values depend directly on the applied shear rate. A specific viscosity number related to the according shear rate is called "Apparent Viscosity", 'Apparent Shear Viscosity" or "Effective Viscosity" and is denoted η respectively η_{app} or η_{eff}.

$$\eta_{app} = \frac{\tau}{\gamma} \tag{5}$$

Equation 5: Common Definition of Apparent Viscosity

Every single value represents one point of the characteristic viscosity function and is only valid for the very shear rate it is related to. For the purpose of apparent viscosity comparison of different fluids and experimental setups it is necessary to specify shear conditions in advance. Regarding their quantification, the apparent viscosity of Newtonian fluids will remain constant and equals the Newtonian dynamic viscosity. The apparent viscosities of

Non-Newtonian fluids equal shear stress divided by the corresponding shear rate. For the purpose of core flooding experiments it is convenient to reshape Darcy's law in a way that the viscosity term is expressed by the other variables. Presuming identical metrics of the core, the fluid's viscosity will be governed mainly by the applied pressure drop, the nominal flow rate and the rock's water permeability.

$$\eta_{app} = \frac{k_w \ A \ \Delta p}{Q \ L} = \frac{A \ k_w}{Q} \ \frac{p_{out} - p_{in}}{L} \tag{6}$$

Equation 6: Core Flood Definition of Apparent Viscosity

Argillier et al. give a slightly different definition of apparent viscosity and call it "Apparent Relative Viscosity". Their definition is mainly the ratio of mobility reduction to permeability reduction. They claim that this relationship is better suited to catch the actual flow resistance of the fluid. Though, this formulation is almost equivalent to the one in equation 6, because the water permeability here is ruled by the pressure drop of the previous water flood. Inserting the reshaped Darcy relation and canceling out all metrics which are identical for both terms, leaves the pressure drop for the water flood and the polymer flood. This is identical to equation 7. Equation 6 will yield slightly different values than equation 7 due to the included metrics, but the general trend will be the same. (Argillier et al., 2013)

$$\eta_{app} = \frac{R_m}{R_k} = \frac{\Delta p_p}{\Delta p_f} \tag{7}$$

Equation 7: Pressure based Definition of Apparent Viscosity

The pressure based definitions of Argillier et al. will be discussed in more detail in the following sections about resistance factors and the residual resistance factor.

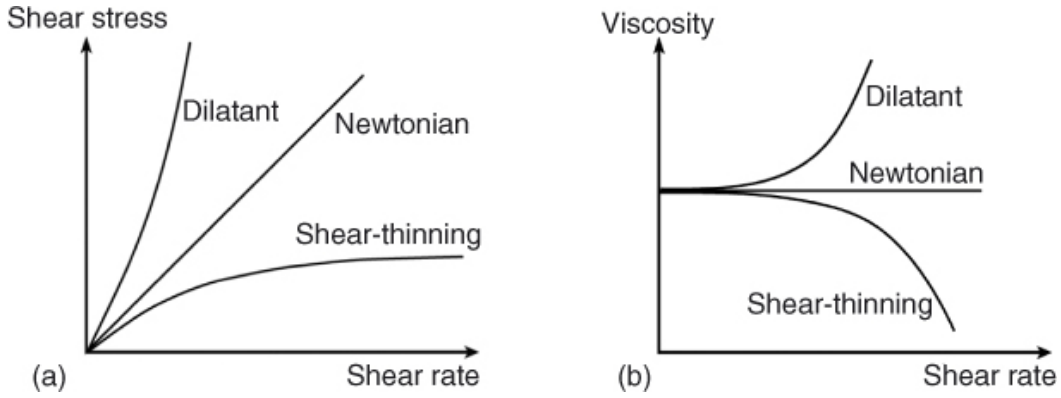

Figure 8: On the left side the typical behavior of Newtonian and Non-Newtonian fluids in a shear stress vs. shear rate plot. On the right side characteristic viscosity profiles for Newtonian, shear thickening and shear thinning fluids.

3.3.1.4 Pressure as measure for Viscosity

The interpretation of a coreflood calls for a different concept of viscosity. A porous medium, such as a sandstone plug, is hardly comparable to a two plate system. The intricate and winding flow path through a rock cannot be described exactly on a microscopic scale. The only means to get grip of the overall flow resistance of a polymer solution in a reservoir rock, is the relationship of fluid throughput vs. measured pressure drop. This relates again to the two plate simplification approach of dynamic viscosity. It is mainly the friction between fluid and boundaries and the internal friction that has to be overcome to enable

fluid movement. The pressure to activate fluid flow or more precisely the pressure drop that is caused by the fluid's reluctance to flow at a particular flow rate is an equivalent means for the quantification of viscosity in the sense of flow resistance. Looking back again to the Couette flow concept, this pressure can be defined as proportionality constant of the systems metrics and the force to keep the system flowing. This way of thinking is best suited for polymer core flooding experiments. It is similar to the concept of viscosity but bases on a different concept and a different point of view. Although this pressure based approach is not covered by the term viscosity entirely it shall be called this way to remain inside the limits of a historically established nomenclature to describe flow resistance. The concepts of resistance factors or apparent viscosity while core flooding are much better suited to quantify a fluid's flow reluctance in reservoir rock.

3.3.2 Resistance Factor

The Resistance Factor R_f, R, F_r, F, R_m, or $RTRF$ is defined as the ratio of pre-flooding brine mobility to the mobility of the actual polymer solution. It may be thought of as the relative apparent viscosity of a polymer solution in a porous medium. The mobility reduction at high rates is presumed to be connected to viscoelastic effects caused by increasing normal stresses exerted during primarily elongational flow. It seems that resistance factors respond much more sensitive to elongational forces than viscosities, which are typically associated with shear forces. This relation explains why screen-factor measurements correlate much more closely with resistance factors than with viscosities. (Seright, 1983)

$$R_f = \frac{\lambda_w}{\lambda_p} = \frac{k_w}{\mu_w} \frac{\mu_p}{k_p} \tag{8}$$

Equation 8: Common Definition of Resistance Factor

Resistance factors are not only a means for a fluid's inherent viscosity but also for the reduction of effective permeability. This is realised by the contribution of polymer and brine permeabilities. A more precise measure for permeability reduction is a derivative of the resistance factor called residual resistance factor. Again these permeabilities and effective viscosities are defined via pressure drops. This leads to a broad range of slightly different variations of the original resistance factor. They differ mostly based on the way permeability characteristics are included or neglected in the figure and how permeabilities and viscosities are expressed.

3.3.2.1 Mobility Reduction Factor

Argillier et al. suggest a resistance factor or mobility reduction factor R_M which equals a mere pressure drop ratio of brine flooding and polymer flooding measurements. This definition neglects all rock properties and reflects solely the fluid's viscosity loss expressed as pressure drops. (Argillier et al., 2013)

$$R_m = \frac{\Delta p_p}{\Delta p_w} \tag{9}$$

Equation 9: Definition of the Mobility Reduction Factor

3.3.2.2 Relative Total Resistance Factor

Sorbie and Roberts propose a Relative Total Resistance Factor which is again nothing more but a pressure drop ratio. These values are normalized by the according flow rates. Measurements at the same flow rate will cancel out the term Q, leaving again a pressure drop

ratio similar to the previously introduced Mobility Reduction Factor. (Sorbie and Roberts, 1984)

$$RTRF = \frac{\Delta p_p}{Q_p} \frac{Q_w}{\Delta p_w} \tag{10}$$

Equation 10: Definition of the Relative Total Resistance Factor

3.3.2.3 Flow Resistance Variable

Southwick and Manke suggest a definition of the Resistance factor or Flow Resistance Variable which is nothing more but a mere regrouping of Darcy's law. This key figure includes the effective viscosity, the according pressure drop and the rock's permeability in addition to the core metrics. Boiling it down to pressures, this figure contains the water-flood pressure drop via rock permeability and the pressure drop of the polymer flood in two different variations. Creating a ratio of brine and polymer flow resistance factor cancels out all identical values like core length, flooded area and nominal flow rate. The remaining variables are the two products of pressure drop and according mobilities. (Southwick and Manke, 1988)

$$R = \frac{A\ \Delta p\ k}{Q\ L\ \mu} \tag{11}$$

Equation 11: Definition of the Flow Resistance Variable

3.3.2.4 Similarities in Flow Resistance Variables

The above mentioned examples make clear that all types of slightly different resistance factors go down to a simple relationship between permeability, apparent viscosity or according pressure drops of brine and polymer floods. The gist of this flow resistance variable and the previously mentioned problems with regular viscosity, show that there is only one true measure of flow reluctance, which is the measured pressure drop during the flooding experiment. It is used directly or indirectly by some sort of apparent viscosity and / or Darcy's law regrouping (pressure drop in relation to nominal flow rate). Either way, all factors boil down to pressure drops.

3.3.3 Residual Resistance Factor

The residual resistance factor is a measure for the tendency of a polymer to adsorb to the surface of reservoir rock. In addition to that, the adsorption process partially blocks pores of the porous medium. The factor is defined as the core permeability prior and subsequent to the polymer flood. (Sorbie and Roberts, 1984)

$$R_{rf} = \frac{k_p}{k_w} \tag{12}$$

Equation 12: Common Definition of the Residual Resistance Factor

Rock permeability will decrease significantly during the flooding operation, leaving back post-polymer permeabilities of less than 30 % of the original brine permeability. Regarding the molecular weight distribution of the flooded solution, polymer chains with higher molecular weights tend to be preferentially adsorbed. The occurrence of residual polymers is wanted, because it prolongs the potency of the polymer flood. A post-polymer water-flood tends to dissolve previously adsorbed polymers again. This desorption process partially increases the

fluid's viscosity afterwards and leads to an improved sweep efficiency even though the actual polymer flood has already been executed. A slightly different definition is again given by Argillier et al. They express the permeability reduction as the ratio of brine pressure drop before the polymer flood and brine pressure drop after the polymer flood. Again this is a minimalistic way of expressing permeability reduction due to the omission of core metrics.

$$R_k = \frac{p_f}{p_p} \tag{13}$$

Equation 13: Pressure based Definition of the Residual Resistance Factor

This ratio equates the common definition of the permeability ratio, because they are also calculated by varying pressure drops and other constants that don't change. Comparing both formulations, they both origin from pressure ratios. (Argillier et al., 2013)

3.3.4 Screen Factor

The screen factor is a measure to quantify the viscoelastic character of a polymer solution. It is defined as the ratio of the time required for a fixed volume of polymer solution to flow through a stack of five 100-mesh screens to the flow time required for the same volume of brine to pass through the screens. A typical screen viscometer utilizes a measured fluid volume of about 40 ml and has a pack of five 0.25 in. diameter screens. Water flow time is 8 to 10 seconds. (Knight, 1973) During the experiment the fluid undergoes an abrupt elongational deformation as it accelerates through the screen openings. That is why it is thought to be related to the viscoelastic properties of the polymer. Like resistance factors screen factors are often more sensitive to mechanical degradation and larger than mere viscosities. (Seright, 1983) Screen factors are furthermore associated with the larger molecules in the polymers molecular weight distribution. The downside of this measurement is that a fresh polyacrylamide solution always experiences a measurable amount of mechanical degradation on just one pass through a screen viscometer, whereas many repetitions of viscometer measurements at high wall shear rates result in no detectable degradation. (Maerker, 1975)

3.3.5 Deborah Number

The Deborah number De or N_D is defined as ratio of the liquid relaxation time of a fluid to its characteristic time for fluid flow. The liquid relaxation time characterizes the duration of a fluid necessary to respond to a changing flow field or to adjust to applied stresses and deformations. The characteristic time scale of the experiment or fluid flow is characterized by the elongational rate epsilon.

$$De = \frac{t_c}{t_p} = \theta_{rel}\ \dot{\epsilon} \tag{14}$$

Equation 14: Definition of the Deborah Number

Polymer chains that hit a sand grain or a pore throat will be subjected to certain forces and deformations. When fluid flow is slow enough, the molecule has enough time to reshape. With increasing flow rates the time span for reacting to deformational stresses gets smaller and smaller. When a critical value of about 0.5 is reached, time is too short to respond to the acting forces. The molecules will start acting elastically and flow resistance will increases vastly due to the sharp increase in extensional viscosity. In other words, the Deborah number signifies the limit in the apparent viscosity plot, where shear thickening behavior will kick in. Polymer chains will not only act dilatant, they will eventually start rupturing beyond this point. (Sorbie and Roberts, 1984)

3.3.6 Trouton Number

The Trouton number or Trouton ratio T, T_r or N_{Tr} is defined as the relation of shear viscosity to elongational viscosity. It is a common means for comparing influences of diagonal and off diagonal parts of the stress tensor meaning shear and elongational forces and stresses.

$$T_r = \frac{\eta_{elongational}}{\eta_{shear}} \tag{15}$$

Equation 15: Definition of the Trouton Number

For a Newtonian fluid in planar extension the Trouton number is classically equal to 4. (Satter and Iqbal, 2015)

3.4 Conclusion

After a detailed discussion of all key figures, there is no overall better or worse. Every number has it's advantages and disadvantages. Figures that combine fluid properties and rock properties such as the apparent viscosity in equation 6 or the flow resistance variable in equation 5 are better suited to get a glimpse on the overall behavior of the system and the interaction of interlocked mechanisms. The more rock properties are included, that more expressive and individual will the figure become. This means on the other hand that poorer comparability is the result. For the purpose of examining specific details of the system other values are better suited. Rock properties like the reduction of permeability are best investigated via the residual resistance factor in equation 12. Pure fluid properties are best caught by the mobility reduction factor in equation 9.

3.5 Optical Concepts

3.5.1 Absorbance

Absorbance is defined as the logarithm of the ratio of incident to transmitted radiant power through a material. Absorbance is thought to be dimensionless. The term absorption refers to the physical process of absorbing light, while absorbance does not always measure absorption, which is a measure for attenuation of transmitted radiant power. Attenuation can be caused by absorption, but also reflection, scattering, and other physical processes.

$$A_\lambda = \frac{I_o}{I} = \varepsilon \; l \; c \tag{16}$$

Equation 16: Definition of Absorbance

4 Rheologial Behavior of Polymers

Having provided a proper toolset of definitions and concepts for investigation, it is now necessary to understand what physical process are up to be investigated and what is the current scientific knowledge about it. The aim, of course, is to understand how aqueous polymer solutions behave when pumped into a reservoir. The first and easiest methods to examine such a thing, are, for sure, simple laboratory measurements with shear viscometers. The problem at this point is, that the investigated solutions will exhibit completely different rheological traits in the laboratory than field data would suggest. This discrepancy calls for explanations and further investigation. Naturally, the means of choice are core flooding experiments. They simulate downhole fluid flow through porous rock material and should be able to catch the mismatch.

4.1 Shear Thinning Behavior in a Viscometer

At this point, it is crucial to understand that synthetic polymers exhibit completely different behaviors when examined via mere shear viscometers in comparison to core flooding experiments. Measurements with shear viscometers will result in a shear thinning characteristic viscosity profile, where apparent viscosity (after equation **??**) will continuously drop. Figure 9 visualizes this behavior for different salinities. The fluid is able to act as a whole and is only subjected to shear forces at the contact area of the viscometer.

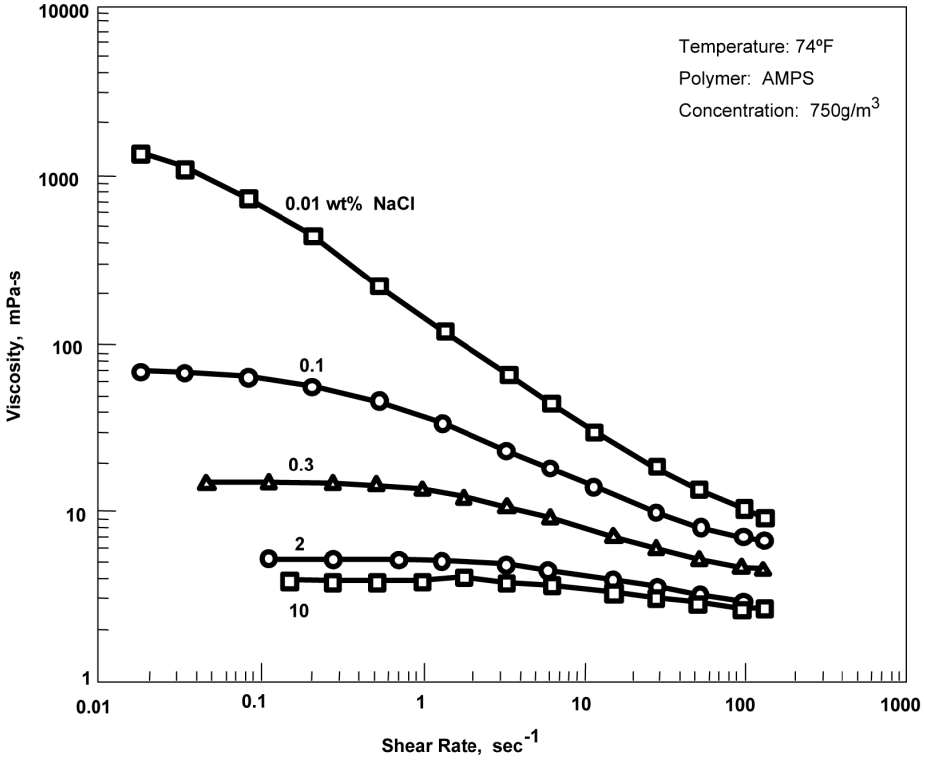

Figure 9: Viscosity Behavior of a synthetic polymer when subjected to shear stress in a shear viscometer. All experiments clearly show shear thinning behavior. (Lake, 1989)

4.2 Shear Thickening Behavior during Core Flooding

This is the huge difference to more elaborate core flooding experiments. Polymer solutions that are investigated by pumping them through rock material will be subjected to exceedingly

different shear conditions. A dense and winding pore net provides much more contact area entailing higher and different kinds of stresses and more possibilities for polymer chains to get adsorbed. A characteristic viscosity profile for such an experiment starts with very slight shear thinning behavior which is flipping over to shear thickening properties when a critical shear rate is overstepped going back to much stronger shear thinning effects at very high flow rates. An interpretation for this viscosity profile is that polymers in a core flood follow roughly the shear thinning trend of plain viscometer measurements but for different reasons, they are overlain by a vast shear thickening anomaly. The common explanation for this peculiar transition is, that at first, polymer chains are calmly floating in the polymer solution. At very low rates the solution finds similar conditions as in a shear viscometer with low shear rates and no major hindrances. This effect is vanishingly small and cannot be seen unless very small shear rates are examined.

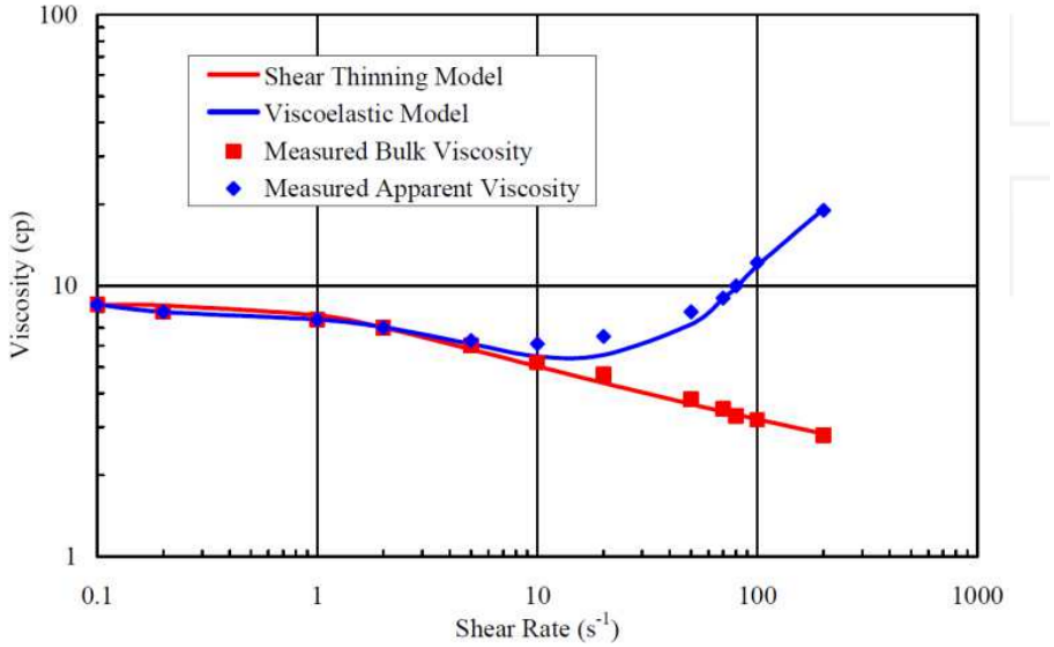

Figure 10: Viscosity vs. shear rate of HPAM measured in porous media and by viscometer. The shear thinning trend observed for both measurements at low rates is overruled by the shear thickening anomaly of the core flooding experiment. (Delshad et al.)

When flow at moderately low rates is established, molecular chains will start to migrate faster, touching each other, touching the rock's inner surface and bumping into each other. This shoving movement entails higher friction and impedes fluid flow through the pore net. At the same time, polymer chains will react to bounces and impacts by changing their shapes. In other words, the macro-molecules will be subjected to deformation. The polymer solution will act more and more as a viscoelastic fluid, with molecular chains elastically rebounding from reservoir rock and further contributing to the overall flow resistance. Both, deformation and drag will grow with increasing flow rates, giving the chains less time to react to grain or polymer impacts, increasing the relative amount of collisions and thus raising frictional forces. The result of this elevated flow resistance is called shear thickening behavior (calculated according to equation 6) This behavior has already been observed and described by numerous authors and is due to the fact that both shear and extensional flow coexist in porous media. At low velocities, the extensional viscosity of the polymer solutions can be neglected and the global pressure response will be dominated by shear viscosity. At high velocities, the apparent shear viscosity is slightly reduced due to shear-thinning

effects. Simultaneously, the extensional viscosity will increase far more steeply, dominating the overall viscosity and leading to an apparent shear thickening global viscosity response.

4.3 Shear Thinning due to Degradation

By further elevating flow rates respectively shear rates, particle interaction gets more and more complex. At a certain critical flow rate, shear thinning effects will kick in again and dominate fluid flow. Most researches didn't push their flow rates high enough to observe this effect, but at a certain point the apparent viscosity starts to fall off again very strongly.

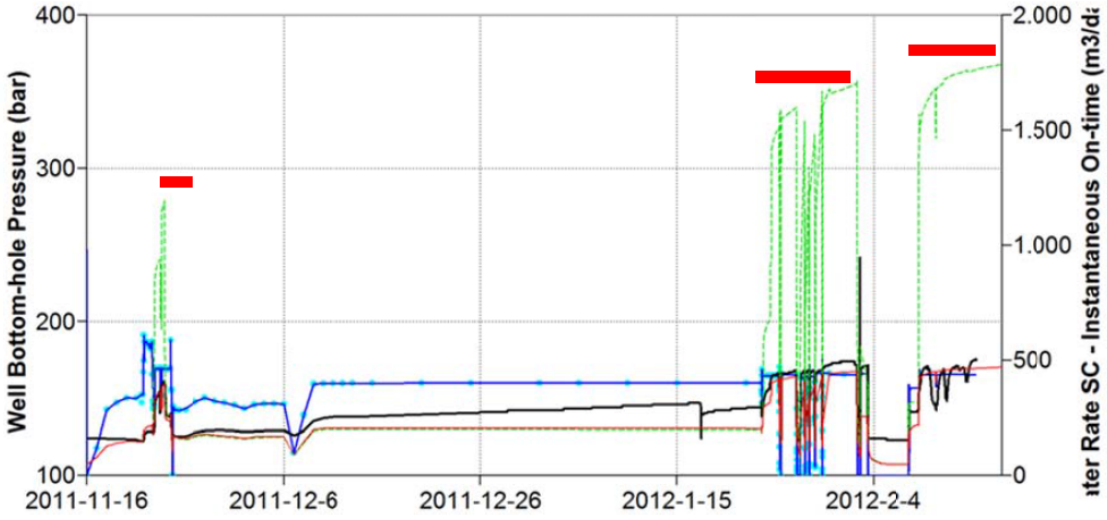

Figure 11: Response of the polymer injection pilot well in the Matzen field. The black shows the historical bottom hole pressure, the blue one the water injection rate. The green line stands for the simulated bottom hole pressure including shear thickening effects. The red line shows the simulated bottom hole pressure using the sheared polymer data. The thick red bars signify periods of polymer injection. (Clemens et al., 2013)

The most probable explanation for this behavior is mechanical degradation. Shear rates have grown high enough, that the polymer solutions starts to alter at molecular level. Polymer chains are breaking or being heavily deformed resulting in smaller particles with lower viscosity enhancing traits. The apparent viscosity starts to drop significantly. The damages done to the solution will most probably be permanent. Repeated core floods with the like degraded polymer solution will yield a much smaller viscosity profile than the original one. Viscosity profiles for such polymers, fresh and degraded, can be studied in figure 13. The observed mechanisms are also an explanation for another anomaly of real field behavior. For some flooding operations pressure responses are much lower than the shear thickening model of laboratory core floods would propose. Most probably has the injected polymer solution been degraded during the injection process and features now much lower viscosity enhancing traits for the actual immiscible flooding operation than expected from a fresh solution. The comparison of the shear thickening prediction to the degraded polymer model is illustrated in figure 10. It is clearly visible that the degraded version of the shear-thinning, shear-thickening, shear-thinning laboratory core flood model is applicable and matches actual field behavior. (Clemens et al., 2013) It is a model that demonstrably works for particular conditions. Generality has to be proven yet.

4.4 Chronological Milestones of Polymer Flooding Research

The previously discussed viscosity issues are assembled from different papers and are more or less the current scientific knowledge on the topic. Though, major uncertainties remain and theories exist, that are deviating or contradicting this perspective. It mustn't be forgotten that all of the above are just interpretations and theories prone to wrong assumptions or biased judgment. In order to understand the way this overall picture was assembled and in which tradition this master thesis is lining up, the research history on polymer flooding experiments shall briefly be portrayed. By discussing major progresses and localizing key findings the above assumptions shall be exposed to critical questioning and weak points shall be revealed.

The first attempts to make predictions about matrix-induced degradation were done by White et al. From this work, no general statements could be derived. The results were nothing but a recommended injection rate limit for minimizing polymer degradation for two specific wellbore completions. (White et al., 1973)

4.4.1 J. M. Maerker

The first systematic approach resulting to general theories about flow through porous media inducing degradation on polymer solutions go back to the findings of J. M. Maerker. His work is the starting point of many researchers, who devoted themselves to flooding issues. He described main aspects of mechanical degradation principles and defined figures and terminologies, that are still present and applied in nowadays degradation experiments. In his work,

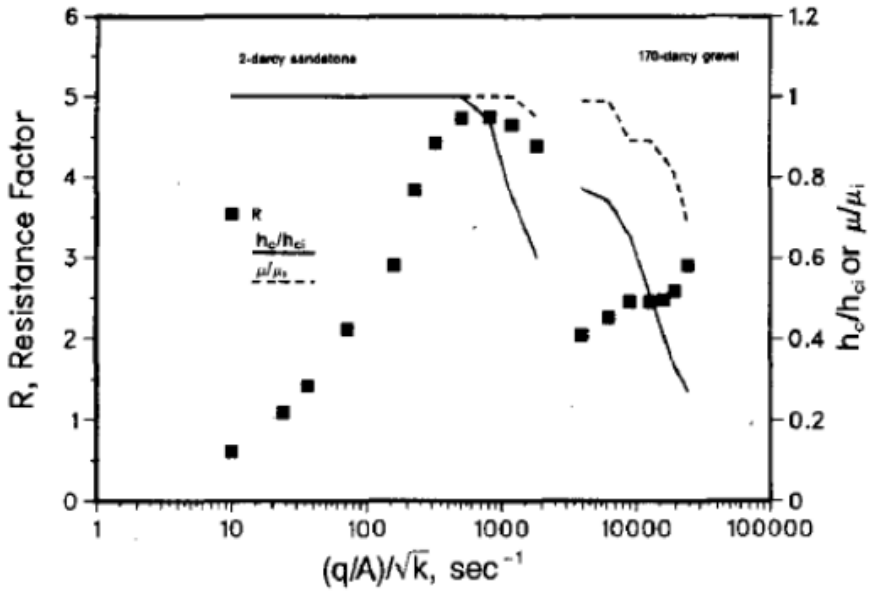

Figure 12: Resistance factors (squares) show the same trend as apparent viscosity with respect to shear thickening behavior and mechanical degradation (20% drop). The specific column height or elongational viscosity reacts much more sensitive to on-setting mechanical degradation. It losses more than 40% of it's original value. (Southwick and Manke, 1988)

he investigated polyacrylamide degradation by forcing polymer solutions and brines of varying salinity through sandstone cores. Maerker described the observed degradation process as being mechanically induced and suggested that the corresponding viscosity loss origins from large elongational stresses experienced by the viscoelastic polymer solution flowing through

constricted pore throats. He showed for the first time the characteristic shear thickening then shear thinning degradation pattern in a laboratory experiment for different scenarios and examined the influence of various parameters such as polymer concentration, molecular mass and core permeability on the degradation process. In order to be able to quantify elongational viscosity and the corresponding elongational degradation more precisely, he chose to use screen factors in combination with shear based apparent viscosity values. He proved that the screen factors respond much more sensitive to rock induced polymer degradation and suggested a correlation for screen factor loss based on the porous medium stretch rate and a dimensionless length. In a later paper, Maerker extended the screen factor correlation to include unconsolidated porous media by adding porosity to the term. (Maerker, 1975)

4.4.2 R. S. Seright

The most detailed studies on mechanical degradation in rock materials beyond the groundbreaking work of J.M. Maerker were done by R.S. Seright. Seright's experiments involved flowing polyacrylamide solutions through both linear and pie-shaped sandstone cores. Seright improved Maerker's screen factor correlation with the porous medium's average grain size rendering it applicable to various radial geometries independent of their specific length. During his linear core experiments he recognized an "entrance pressure drop" in cases where mechanical degradation was known to occur by screen factor and viscosity measurements on the core effluent. Seright interpreted this phenomenon in a way that degradation only occurs at the sand face of the porous medium and above some critical flux in a given core. Further analysis of the linear core experiments, in some cases using further data from previously sheared reinjected polymer, allowed Seright to formulate a simple correlation model for gross resistance factors. (Seright, 1983)

4.4.3 Sorbie and Roberts

Sorbie and Roberts tried to link viscosity losses and degradation processes to the molecular weight distribution of the polymer fluid. They introduced a sophisticated theoretical model for the prediction of a fluid's distribution alteration. Although it seems to work for the particular conditions, it is still based upon many idealizations, theoretical approximations and assumptions and is bulky to handle. Yet, the approach of examining the molecular weight distribution is a key step forward in polymer-rock investigations. (Sorbie and Roberts, 1984)

4.4.4 Southwik and Manke

Southwik and Manke introduced a new method of quantifying elongational viscosity via a ductless siphon apparatus. Their newly defined characteristic height or derived elongational viscosity indicates that the observed viscosity drop results mostly from huge losses of the fluid's elastic property at elevated rates. Southwik and Manke were able to work out Maerker's experiments in more detail, proofing that ductless siphon elastic viscosity is even more sensitive to viscosity losses during a coreflood experiment than screen factor measurements. (Southwick and Manke, 1988)

4.4.5 Polymer Researchers

In subsequent decades findings of material science and polymer rheological laboratories were introduced into core flooding research. Despite of the fact that these laboratories are not specialized on porous medium flow, they triggered new theories by giving new pulses and ideas on how mechanical degradation of polymer solutions works. Especially research from the 90ies and beyond found entrance in the research of polymer flooding. They are on the

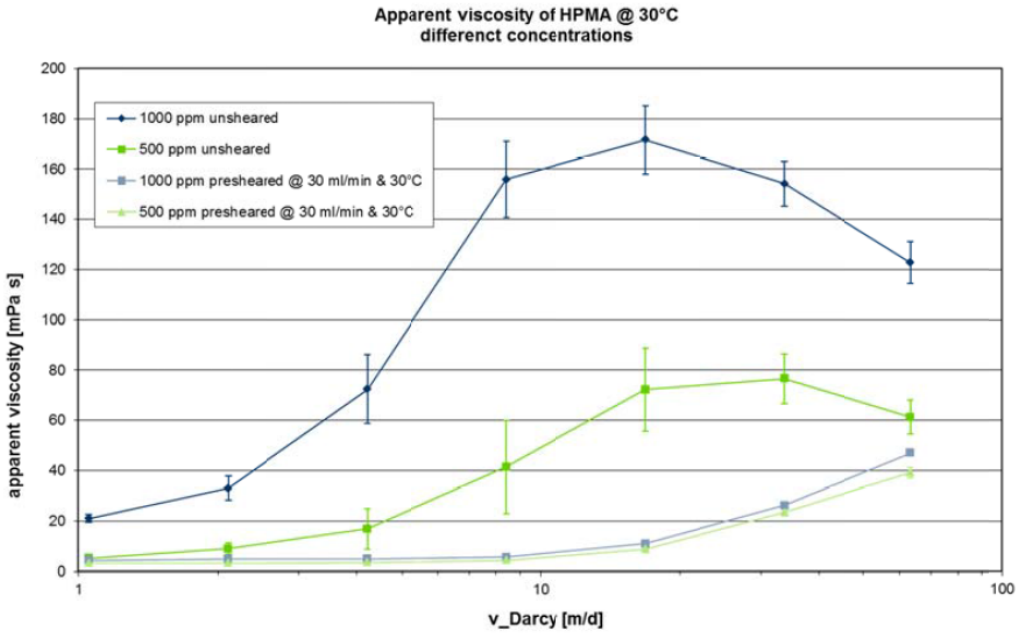

Figure 13: Typical behavior of apparent viscosity during core flooding. The typical viscosity profile features shear thinning (not visible here because of not sufficiently low flow rates), shear thickening and a shear thinning bump where mechanical degradation is thought to be triggered. The lower viscosity profiles belong to pre-sheared and degraded polymer solutions. The samples are 20MDa, 1000ppm and 500ppm HPAM solutions, sheared and presheared. (Zechner et al., 2013)

one hand scrutinizing the significance of elongational flow mechanisms (Muller et al., 1992) (Putz, 1992) and on the other hand investigating detailed mechanism of the chain rapture process and it's influence on the molecular weight distribution. (Buchholz et al., 2004).

4.4.6 Current Efforts

Recent research further investigates the basic theories that were based by Maerker and tries to push it further. Seright still publishes on the topic, expanding his experiments to broader areas, regarding different conditions, hydrocarbon flooding or the inclusion of rigid biopolymers. (Seright et al., 2010) Argillier et al. focus on elastic properties of the fluid and pressure based measurements. (Argillier et al., 2013) T. Clemens and T. Gumpenberger are the heads of an ongoing polymer project, trying to further describe mechanical degradation in a specific polymer flooding operation by combining laboratory core flooding experiments with examinations of the molecular weight distributions. (Clemens et al., 2013) (Zechner et al., 2013) This master thesis is part of the project and discusses the time and temperature related aspects of the degradation process.

4.5 Mechanical Degradation

Mechanical degradation is a term associated with the permanent or temporary viscosity loss of a polymer solution. It implies that changes on the molecular level of the solution cause a drop in flow resistance.

4.5.1 Sources of Viscosity Loss

Macroscopic viscosity losses of a polymer solution can emerge from different sources. Considering the above mentioned viscosity regimes, they mostly overlay each other and even tend to partially neutralize each other. The first source of viscosity alteration is the polymer's inherent tendency to shear-thinning behavior when subjected to increasing shear rates. This is some kind of partly visible background viscosity loss and shall be called primary viscosity loss. It is most of the time overruled by viscoelastic shear-thickening effects causing a steep rise in apparent viscosity. However, this dilatant behavior ceases at a high enough flow rate. Here the actual mechanical degradation kicks in, diminishing the fluid's viscosity again. This viscosity reduction shall be called secondary viscosity loss. It happens on the molecular level and entails molecular deformation or chain breakage.

4.5.2 Triggering of Mechanical Degradation

Mechanical degradation of polymer solutions is considered to occur when stresses developed during fluid flow become large enough to break the polymer molecular chains or to alter them in a way that the fluid looses part of it's original viscosity. Degradation is thought to be characteristic for extensional flow taking place in the pore throats. Shear forces play a minor role in the degradation process. (Seright, 1983) Mechanical degradation effects are considered secondary viscosity loss phenomena. They are linked to high shear rates and happen in the shear thickening regime of polymer fluid flow. Degradation is only possible to occur when the prerequisites of the Deborah number are met or beyond that. The eventuation of degration triggers a shear thinning effect in the typical viscosity profile and deteriorates the viscosity enhancing trait of the fluid.

4.5.3 Polymer Chain Alterations

The degradation process of a fluid entails an alteration of polymer chains. The macromolecules can change their state or their shape in multiple ways either decreasing or increasing it's viscosity.

- Viscosity Deterioration
  - Reversible Molecular Deformation
  - Permanent Molecular Deformation
  - Polymer Chain Breakage
- Viscosity Enhancement
  - Molecular Reshaping
  - Polymer Chain Entanglement

At low rates, losses will origin from the deformation of the solution's molecular chains in a way that they are no longer able to establish a certain flow resistance. These mechanically induced deformations can be undone when the polymer chains are reshaping. By regaining their original form, the fluid's viscosity will heal and attain the original value. If deformation endures, the viscosity losses will be permanent. These effects change the molecule's shape but not it's size. Whenever stresses during the deformation process grow sufficiently large, the polymer molecules are likely to break into fragments. Larger molecular chains will rupture into smaller entities, that aren't able any more to establish the same flow resistance as larger ones would do. The result is an irreversible loss of fluid viscosity. Chain scission viscosity

losses can partially be neutralized by an effect called chain entanglement. Smaller interacting chains begin to snag up and create a connection to each other. The newly built complex is called entangled and acts similar to a larger chain. This connection increases the solution's viscosity and hides former fragmentation.

4.5.4 Chain Scission and Entanglement

The chain breakage process is the most complex of all viscosity changing mechanisms. In order to understand how exactly the polymer solution's viscosity will change during the degradation process it is crucial to understand where a single macromolecular chain will break and when. Mechanical stress exerted on the polymer molecule is the primary cause of chain breakage. Most models use a statistical approach and describe the degradation process in terms of two probability functions. The first function depicts the probability that a polymer chain of a given length will break. The second function characterizes the probability that a molecule of a given length will result from the rupture process (Glynn et al., 1972). Despite this simple probabilistic framework, the underlying assumptions on frequency and location of the chain breakage are highly controversial.

Early theoretical works on polymer solutions in high shear fields indicate that chain scission at the center point of a molecular chain is most likely. (Bueche, 1960) Some experimental findings supported this theory. (Basedow et al., 1979). However, other researchers stated, that chain scission is most probably random. According to this theory, rupture of the macromolecule could happen at any point of the chain without any preference. (Sato and Nalepa, 1978) A third group claims that chain scissions are best modeled assuming a symmetric Gaussian breakage distribution at the chain center, which isn't necessarily identical to the midpoint of the polymer chain.(Glynn et al., 1972). Scission scenarios have also been studied by gel permeation chromatography and optical methods such as birefringence and dynamic light scattering. But again several different theories emerged from that, based on diverging findings. Some researchers state that mechanical degradation causes a mid-scission of the polymer chains. (Argillier et al., 2013) Others claim that chains will break randomly in the process. (Buchholz et al., 2004) (Muller et al., 1992) Even these sophisticated far-reaching investigation methods were not able to give a finite answer to the problem. A final decision cannot be made, yet.

A phenomenon closely related to microscopic chain scission is chain entanglement and polymer-polymer interaction. Southwick and Manke found that polymer coils in solution are most likely to overlap. They stated that polymer-polymer interaction forces turned out to be significant too, but most probably strong entanglements will not form out. Fluid properties are considered to depend mainly on single-chain polymer dynamics. (Southwick and Manke, 1988) Again the validity and applicability of such statements have to be received critically. Chain entanglement could play a much bigger role than expected.

Since there is no distinct determination possible on where and how chain scission or entanglement takes places, all according theories have to be assumed highly uncertain. All authors recommend further research and thus all correlation models and all attempts of detailed microscopic degradation description will feature significant uncertainties in their assumptions. This is a big weakness of polymer degradation research.

4.5.5 Degradation Influencing Parameters

Although huge difficulties in the microscopic descriptions of degradation processes aggravate core flooding investigations, macroscopic effects can readily be proven. Their influence on the overall viscosity response shall be discussed in this section. It is clear that mechanical degradation becomes more severe with larger fluxes due to higher shear rates. Beyond that, the fluid's molecular mass, it's concentration, it's salinity and the rock's permeability will alter the degree of polymer degradation in different ways.

4.5.6 Permeability

Considering rock permeability, a general trend was observed by several authors indicating that degradation increases as permeability decreases. This means that a loss of mobility control in certain formations caused by mechanical degradation is more severe with lower formation permeabilities. Isolated examples contradict this general conclusion, possibly because of different pore-size distributions, but the general trend is clear. Lower permeabilities entail higher degradation. The explanation for this phenomenon is easy to provide. A less permeable and thus denser rock leads to more polymer-rock interactions and thus to higher shear rates, more molecular deformation, a higher probability of chain scission and thus to a higher viscosity reduction. (Maerker, 1975)

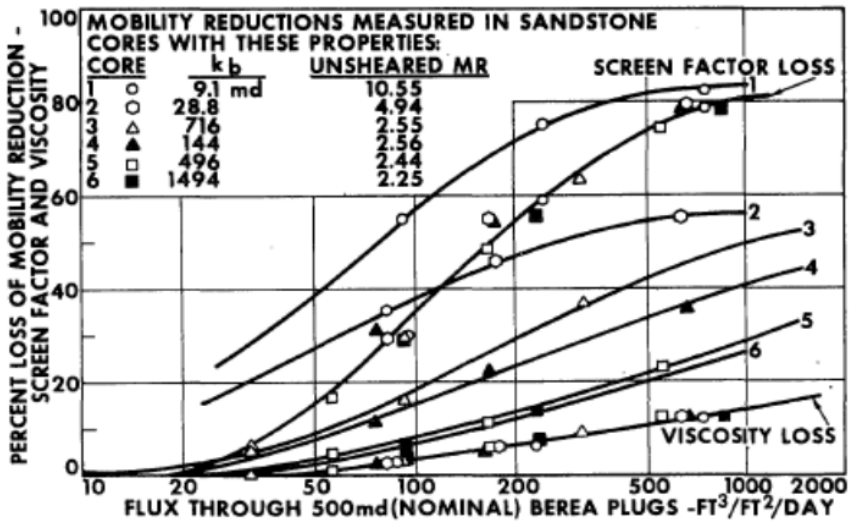

Figure 14: Influence of different rock permeabilities on the apparent viscosity during core floods. Degradation increases with decreasing permeability. Maerker (1975)

4.5.7 Molecular Weight

Longer and therefor heavier molecular chains offer more resistance to fluid flow due to their sheer size and larger contact area. They experience higher shear stresses and are consequently more likely to break. For a given shear stress there is a 'critical' molecular weight, below which no mechanical degradation will occur. (Argillier et al., 2013) With respect to the molecular weight distribution, it has been shown for several high molecular-weight polymer systems that mechanical degradation preferentially occurs within the high end of the weight distribution. Viscoelastic phenomena such as drag reduction and large normal-stress differences primarily depend on the largest molecular species in the distribution. Shear viscosity

on the other hand is related to the average molecular weight. Consequently, if the proportion of high molecular-weight material is small, the average molecular weight and therefore the shear viscosity would not be altered significantly after a certain amount of degradation. Screen factors and other key figures that respond more to elongational viscosity, indicate severe reduction in flow resistance. (Maerker, 1975)

4.5.8 Concentration

The original study by Maerker didn't focus so much on concentrations. He solely compared a 300ppm and a 600ppm PAM solution with each other, found no major difference and concluded that degradation is most likely independent of polymer concentration. (Maerker, 1975) Further investigations by Morris and Jackson however showed that Maerker's sample span-width was too small. By comparing 250, 500 and 2000ppm polymer solutions, they proved that smaller concentrations are more subject to degradation than higher ones. (Morris and Jackson, 1978) However, the influence of polymer concentration seems to be minor, ranging in-between few percents.

4.5.9 Salinity

The last mentionable property that could influence degradation is the polymer solution's salinity. Solvent salinity exerts a strong influence on the rheological properties of polyelectrolytes. Maerker examined salinity effects quite exhaustively. He produced a bunch of 600ppm solutions with different salinity concentrations and compositions. The general tendency is, that higher saline solutions tend to a higher level of degradation. An interesting discovery was, that greater losses of viscosity occurred with calcium chloride present. The relative magnitudes of screen-factor losses demonstrate that increasing ionic strength leads to more severe degradation. However, the effect of adding $CaCl_2$ is stronger than expected from a simple increase in ionic strength. In general a larger ionic strength solution will reduce molecular size because of more efficient neutralization of negative charges along the polymer chain. Therefore entanglement networks are not as easily removed by thermal Brownian motion and mechanical rupture of the polymer chains during elongational deformation is more probable. (Maerker, 1975)

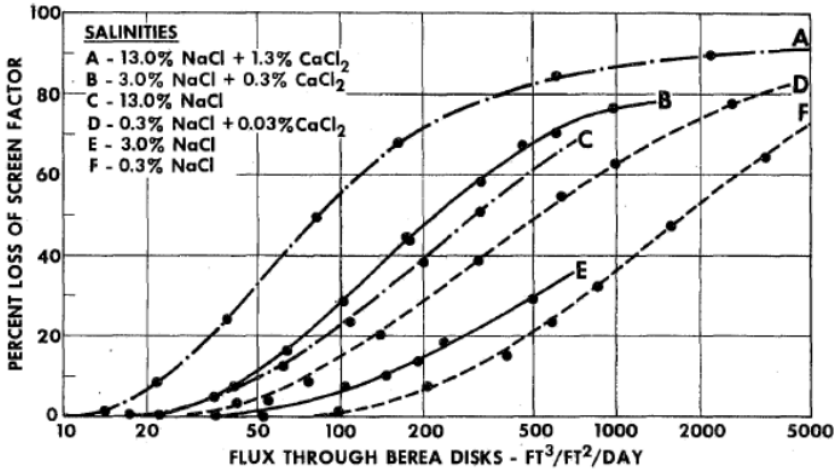

Figure 15: Influence of different solvent salinities on the apparent viscosity during core floods. Degradation increases with increasing salinity and ionic strenght. Maerker (1975)

5 Geological Analogue

This section introduces and describes the oil reservoir where OMV's polymer pilot project takes place. The first section deals with the field localization and description, the second chapter covers the related development and production history and the last ones explain on how field properties have been reproduced for the experimental work.

5.1 Field Description

The reservoir in question is part of the 8th Tortonian horizon of the Matzen field in Lower Austria. The field is situated approximately 30km north of the capital city of Vienna. It belongs to the Vienna Basin which is a well explored oil containing geological structure with a long and broad history of production and examination. The Tortonian age or stage belongs to the Late Miocene series or epoch which is part of the larger Neogene period or system. It spans chronologically the years between 11.608 ±0.005 Ma and 7.246 ±0.005 million years ago.

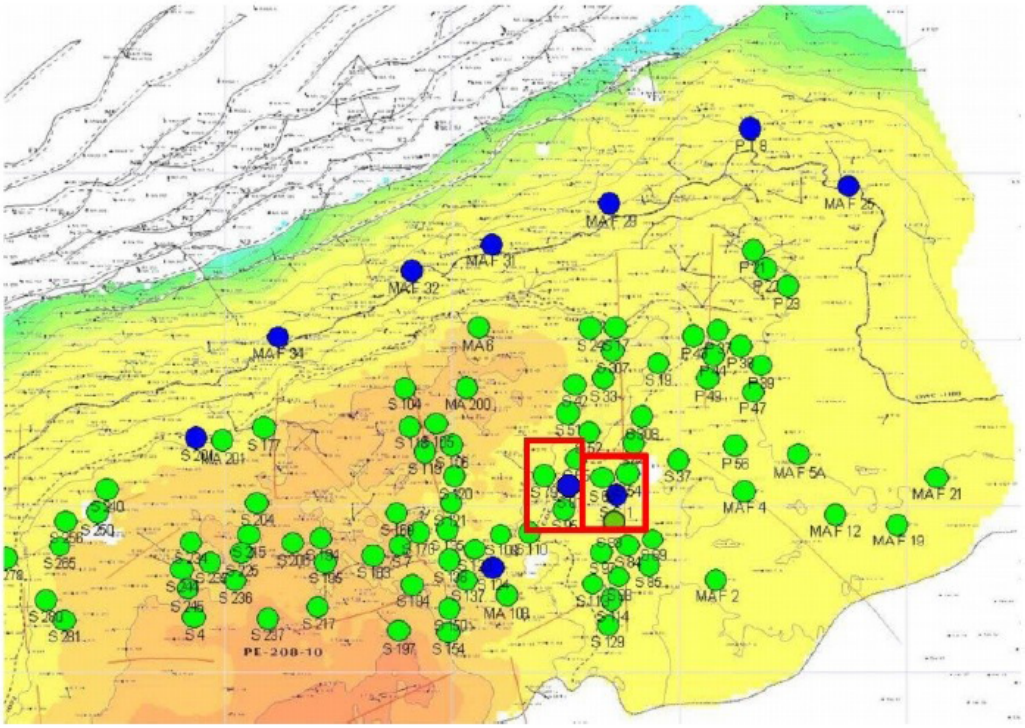

Figure 16: Top structure Map of the 8 Tortonian, Matzen Field, Austria. Green dots represent remaining producer and blue ones mark water injectors. The red rectangles point out polymer solution injection pilot areas. (Clemens et al., 2013)

The depositional environment of the 8th Tortonian reservoir was identified to be shallow marine which bestows the structure with considerably well reservoir conditions. It has an average gross thickness of approximately 40m. The sandstone reservoir is vertically and laterally heterogeneous with porosities between 20 and 30%. The permeability range of this structure lies in between 10 and 3000mD resulting in an average permeability of around 300 to 500mD. Nevertheless some high permeability streaks in excess of 1 Darcy are present entailing a high degree of heterogeneity. Even though the structure is laterally layered, the pilot was completed to just one individual stratum. The reservoir depth is about 1200m.

The initial reservoir pressure was reported to be 113 bar supported by a weak aquifer from the northern edge of the reservoir. There is no continuous pressure communication over the entire field. The initial oil viscosity is about 19 cP at 50 °C, the oil gravity is measured to be 20 ° API. The average in-situ water salinity is about 20 000 ppm whereas the produced water salinity shows values of about 15 000 ppm. (Clemens et al., 2013)

5.2 Production History

The field's oil production started in 1951 with a peak of 1980 $\frac{m^3}{d}$ in 1957 followed by an annual decline of 15%. Due to the weak aquifer, the reservoir pressure dropped from 130 to 80 bar in 1960. Performance analysis of drilled water injectors in the eastern and western part of the field showed low injectivity and low contribution to the overall reservoir pressure. Water injection into the aquifer was able to raise the average reservoir pressure and reduce pressure decline to 4% per year. The recovery factor of the field is about 26%. The field today is dominated by high water cuts of averagely 96%. (Zechner et al., 2013)

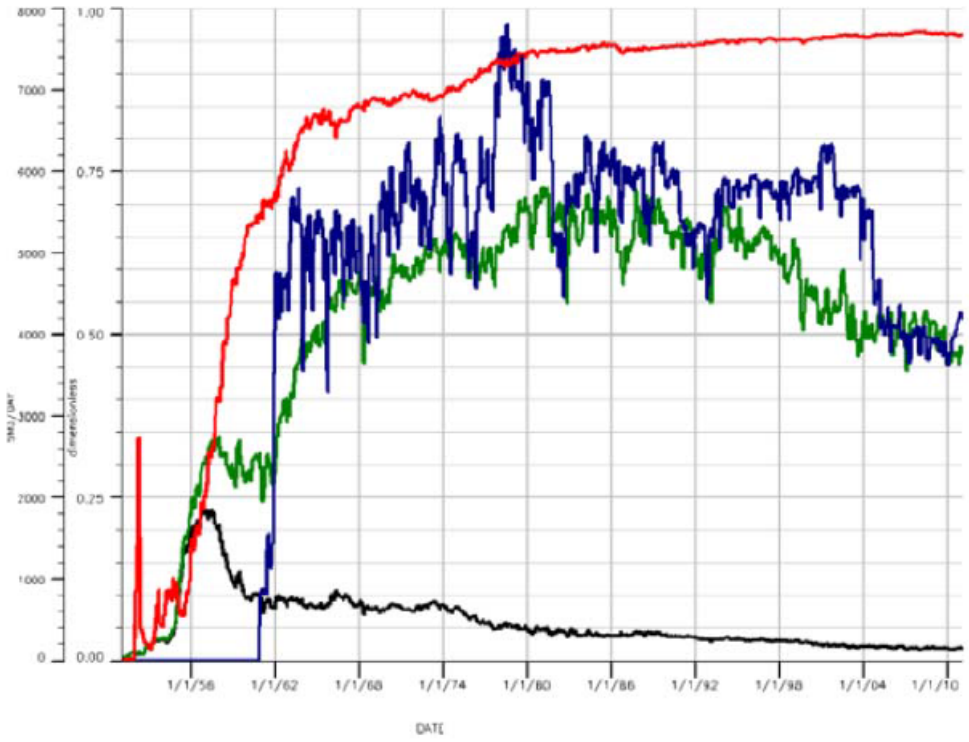

Figure 17: Oil production in black and liquid production in green from the 8th Tortonian. Water injection is shown in blue, water cut in red. (Clemens et al., 2013)

Enhanced oil recovery screening criteria indicated chemical flooding as potential improvement method to boost the field's recovery factor. Salinity, temperature, oil viscosity and permeability signaled favorable conditions for polymer flooding treatments. (Taber et al., 1997) The average well spacing of the field is 300m with 340 completed production wells. In 2012 80 producers and 11 injectors were engaged. A volume replacement rate of about 1 was achieved. Over the whole lifespan of the operation a total amount of 2.6 pore volumes of water was injected. In November 2001 a polymer injection pilot was realized to gain experience for a field wide implementation of the 8th Tortonian horizon. An experimental area was chosen in the middle of the reservoir. Since November 2014 the polymer injection is ongoing. (Clemens et al., 2013) For the overall establishment of polymer operations, tracer

tests were performed to evaluate flow patterns and producer-injector conductivity. Pressure fall-off tests were conducted to evaluate viscosities of injected polymer solutions. Polymers were injected right above the formation parting pressure to increase injectivity and to overcome high back-pressures. Several rheological laboratory investigations were conducted on the applied polymer in order to simulate near wellbore dynamics. (Clemens et al., 2013) (Clemens et al., 2003) This master thesis is a part of the afore-mentioned investigations.

5.3 Reservoir Fluid Analogue

The 8th Tortonian reservoir fluid is dominated by NaCl, CaCl and MgCl. The detailed composition is listed in the below table. Early experiments by Zechner et al. used brines that were assembled from the very same components. A 3000ppm potassium chloride solution turned out to yield equivalent results to the multicomponent fluid. In order to save time, this equivalent formation fluid was used in follow-up experiments. For the experimental setup of this master thesis, the 3% potassium chloride shall suffice as reservoir fluid analogue. Further information on the exact preparation of KCl solutions is provided in the polymer section. (Clemens et al., 2013)

Major Constituent	Concentration	Minor Constituent	Concentration
[x]	[mg/l]	[x]	[mg/l]
NaCl	20317.0	Na_2SO_4	28.7
$CaCl_2.2\ H_2O$	672.5	NaBr	69.3
$MgCl_2.6\ H_2O$	619.9	$BaCl_2.2\ H_2O$	22.2
KCl	166.8	$SrCl_2.6\ H_2O$	49.5

Table 2: Composition of Reservoir Fluid

5.4 Reservoir Rock Analogue

5.4.1 Sample Core Selection

The porous medium used in the following experiments has to suffice several contradictory requirements. On the one hand it should mirror as accurate as possible the real reservoir, on the other hand it must suffice laboratory requirements. In order to fulfill the prerequisite of depicting the real reservoir, it would be advisable to use actual cored reservoir rock. This has been done for several previous experiments. The disadvantage of this method is that the exact rock isn't readily and continuously available. It is costly to acquire downhole reservoir cores and the properties could be vastly distorted by heterogeneities dependent on where in the field the samples were cored.

Core Label	Permeability	Porosity	Diameter	Length	Saturation	Analogue
[x]	[mD]	[%]	[cm]	[cm]	[x]	[x]
Berea 6 / 108	365.559	20.766	2.98	6.69	3% KCl	ARP
Berea 6 / 109	386.615	20.404	2.97	6.73	3% KCl	ARP
Berea 6 / 110	356.683	20.769	2.98	6.72	3% KCl	ARP
Berea 6 / 111	379.669	20.782	2.99	6.69	3% KCl	ARP
Berea 6 / 112	359.956	21.130	2.99	6.77	3% KCl	ARP
Berea 6 / 113	356.015	21.725	2.98	6.78	3% KCl	ARP
Berea 6 / 100	420.400	20.256	3.00	6.75	3% KCl	ARP
Berea 6 / 101	417.500	20.270	3.00	6.74	3% KCl	ARP
Berea 6 / 117	380.000	20.489	3.00	6.86	3% KCl	ARP
Berea 6 / 119	371.600	20.549	3.00	6.8	3% KCl	ARP
Berea 6 / 121	443.400	20.757	3.00	6.78	3% KCl	ARP
Berea 6 / 123	427.800	21.876	3.00	6.86	3% KCl	ARP
Berea 25 / 08	230.000	22.791	3.00	6.92	3% KCl	ARP
NH 14 / 272	2141.020	22.820	3.00	6.88	3% KCl	HPS
NH 14 / 282	2100.530	22.790	3.00	6.93	3% KCl	HPS

Table 3: Reservoir Rock Analogues

To evade these considerable disadvantages it was decided to choose commercially available analogue rocks from well known quarries. These rocks were chosen to resemble the actual reservoir rock as closely as possible. For this very reservoir, the 8th Tortonian, Berea sandstones were found to be most suitable. The average reservoir permeability lies in between 300 and 500 mD. For the experiments Berea rocks in between a permeability range of 356 to 443 mD and an approximate porosity of more or less 20 % were picked. These rocks shall reproduce the average reservoir quality. An additional project for MALS measurements required a 2 Darcy analogue. Nordhorn sandstones with a permeability of approximately 2100mD were chosen for this case. These properties again shall resemble the high permeability streaks mentioned in the field description chapter. The metrics of all sandstone plugs are roughly 7cm in length and 3cm in diameter. Berea and Nordhorn rocks are very well known in the petroleum industry as analogue rocks. They are available in abundance, which was the main selection criterion with respect to repeatability and stable reservoir features necessary for laboratory use. The provided table lists all used cores with essential specifications, marking them as ARP = average reservoir permeability or HPS = high permeability streak analogues.

5.4.2 Core Preparation

For the reason of reproducing reservoir conditions regarding the simulation of formation water saturation, a particular well established preparation procedure was applied. First of all a fiber glass and epoxy resin isolation was coated around the core to seal it from radial flow. Prior to the actual experiment the pretreated core was vacuum saturated with brine (3% KCl) for at least 24 hours but mostly up to two to four days to improve the water saturation process. The core was fixed and sealed at the flowing surfaces by O-rings in order to force flow entirely through the core. Pressure transducers from HBM model P11 with a linearity deviation of smaller than ±0.5% and a standard deviation of reproducibility of less than ±0.1% were linked to the inlet and outlet face of the core to acquire data. The whole core plus pressure transducers and holding unit were submersed into a 30 degree tempered water bath in order to keep the system at a steady temperature. The chosen temperature of 30 °C represents the average near wellbore temperature expected downhole. The finished and readily prepared core samples approximate now the observed downhole conditions as can be seen in the below table.

Comparable Property	Reservoir	Unit	Experiment	Unit
Average Permeability upper	500	[mD]	443	[mD]
Average Permeability lower	300	[mD]	356	[mD]
High Permeability Streak	1000 - 3000	[mD]	2100	[mD]
Average Porosity	20 - 30%	[x]	20%	[x]
Formation Fluid	NaCl, $CaCl_2$, $MgCl_2$	[x]	KCl	[x]
Average Salinity	22 000	[ppm]	3000	[ppm]
Downhole Temperature	30	[°C]	30	[°C]

Table 4: Comparison of Reservoir Rock to Experimental Cores

6 Primary Research Objective

As mentioned in the literature section, the most common and broadest accepted theory of degradation implies that polymer chains, which are subjected to particular flow rates respectively velocities, will hit grains of the flooded rock and thus get deformed. If the flow rate is low enough, the polymer chain has enough time to restore it's original shape. The macro-molecule may continue on it's flow path without any sustaining damage or aftermath effect. If the flow velocity on the other hand exceeds a critical value, the acting forces will grow too grave, so that permanent deformation will result from that movement. Degradation, that origins from this process, is most commonly attributed to mechanical deterioration.

Degradation effects have been observed in abundance by several researches. The fact, that polymers somehow degrade while being flooded, is indisputable. But each researcher collected individually hints and indices during the process, crafting these to more or less applicable and diverging theories. Although there is, by now, a rough idea established, of what happens in the pores, it is still not clear how certain aspects of this degradation process work and if underlying assumptions really hold true. For example the theory that degradation is only taking place in the reservoir. Simplifications were made, sparing injection and production related facilities from experimental setups, assuming that this equipment is not responsible for polymer degradation. This hasn't been proven yet. Another issue is, that it is still not decided whether mere deformation is liable for the shear-thinning viscosity-loss or actual chain breakage. Furthermore and as a consequence of that, it hasn't been proven yet, if the induced viscosity damage is a permanent effect or if the polymer is somehow able to heal itself given sufficient time. These obscurities are the main focus of this work and shall be methodically worked out in the following chapters.

The first and primary target or "Objective I" is to discover the actual process behind degradation. There are two distinct options conceivable of what happens at the grains in a porous medium. This is either deformation or chain scission, eventually both of it.

6.1 Working Hypothesis I: Polymer Restoration

The first working hypothesis states that a polymer chain gets deformed at a pore or grain and changes it's shape when the flow velocity is high enough. If this happens to not just one single polymer chain but a statistically large enough amount of polymers, the macroscopic viscous behavior of the solution will be altered. The change of polymer viscosity origins in this scenario most likely from the deformation of molecular chains. This means that there is a possibility, that the deformed polymer chains can regain their original form over time and heal their viscosity loss. A second, less likely, explanation can be made by chain entanglement, when chain scission has occurred instead of mere deformation. But either way, in this approach, degradation is thought to be a temporary effect, that can be undone. The two possible explanations for viscosity healing are discussed in more detail now.

6.1.0.1 Hypothesis I-I: Coil Unfolding

Previously deformed polymer chains bestow the solution with lower viscosity, because the chain coils have been compressed during the flooding process. Whenever molecular chains hit each other or the core wall, they are squeezed together. Loose ends are folded into the core coil, reducing the hydrodynamic volume of the molecular coil. Void space inside the molecule sphere is displaced by previously free floating chain windings leading to a much denser packing of the molecule. At the end of the core flooding experiment, a much smaller, more compressed and denser coil is the result. Hypothesis I-I proposes that keeping the

polymer solution calm after this kind of core flooding stress, some of the previously induced deformation can be undone. The original molecular structure has a certain degree of stiffness and strives to regain its original state. If core induces stresses are suddenly absent, the backbone of the strucutre gets active and starts to slowley bend the chain branches back. The previously forced compression and densification is reversed. The molecular chains relaxes and expands. This leads to a larger hydrodynamic volume and thus a higher macroscopic viscosity.

6.1.0.2 Hypothesis I-II: Chain Entanglement

The second explanation presumes that polymer flooding through a rock core has triggered chain breakage. The chain scission process and effects will be discusses in Hypothesis II in more detail, but at this point it is sufficient to know, that an original polymer chain will be split into smaller entities. This will reduce the apparent viscosity of the polymer solution at hand, because although a higher concentration of particles is present, the hydrodynamical radius of these is dramatically diminished. They will be able to flow more smooth and exert less resistance to motion. Typically this phenomenon is a permanent effect and is therefor assigned to Hypothesis II. Under certain circumstances, for example a high concentration or charged parts of the molecule, the smaller molecular chains will start to interact or even bond. Branches of the smaller chains snag and entangle to each each. The newly created complex now acts similar to a large sole molecule and bestows the soltion with higher viscosity traits. As aforementioned, most researches confirm this effect, but neglect this effect. In comparison to Hypothesis I-I it is less likely, but could also be the reason for viscosity healing.

6.2 Working Hypothesis II: Permanent Damage

The second scenario implies permanent viscosity loss. Whenever a polymer chain hits a grain or gets in contact with a pore, the forces exerted on the molecular complex are high enough to damage the macro-molecule permanently. The macroscopic viscosity trait of the polymer solution is altered and leads to a much smaller flow resistance. In this approach no healing effects are thought to be active. Degradation damage is considered to endure. The permanent viscosity loss in this scenario can be attributed to two distinct explanations.

6.2.1 Hypothesis II-I: Chain Scission

On the one hand, permanent viscosity loss can be explained as the result of chain rupture. Stresses acting on molecular chains are in this approach considered high enough to fragment the mother molecule into two or more smaller chains. According to a macroscopic point of view, these smaller entities aren't any longer able to bestow the polymer solution with the same flow reluctance, than the virgin mother solution would have. Smaller apparent viscosity values will be observed under the premise that the newly created smaller chains will not form new connections. They exist and operate as individual entities in the fluid and are the sole reason for the solution's macroscopic viscosity.

6.2.1.1 Hypothesis II-I-a: Even Chain Scission

Inside this scenario, there exist again two possibilities. Hypothesis II-I-a proposes, that chain scission occurrence is uniformly distributed over the entire molecular weight distribution. This means, that both larger chains and smaller chains are equally subjected to chain breakage. The characteristic shape of the molecular weight distribution does not change, but the curve as a whole wanders to the section of smaller entities.

6.2.1.2 Hypothesis II-I-b: Preferred Chain Scission

It is very likely that the chain rupture process is not evenly spread over the size distribution. Most probably, longer and heavier molecular chains will be more vulnerable to scission than smaller ones. Whenever the degradation process prefers larger molecules, the resulting weight distribution will display a distinguishable altered shape in comparison to the original curve. The concentration of larger chains will be unproportionally reduced in favor of more frequent smaller ones. Their concentration will rise accordingly, because newly split, larger chain-fragments will add up to the untouched smaller chains resulting in an accumulation of smaller entities.

6.2.2 Hypothesis II-II: Permanent Deformation

The second permanent viscosity loss scenario assumes that the polymer could loose its viscosity by mere deformation. The molecular transformation in this case is considered permanent and cannot be undone. The polymer chains are in this approach somehow not able to regain their original shape and remain in their new and significantly deformed state. The change in size, alignment or coiling has the effect that the reshaped polymer chains are now able to flow much easier, bestowing the polymer solution with overall lower viscosity. The polymer sizes and thus the according molecular weight distributions remain untouched.

6.3 Working Hypothesis III: Partially Restorable Degradation

The third hypothesis is thought to be a mixture of hypothesis I and hypothesis II. It is presumed here, that a polymer solution will be subjected to both deformation and chain breakage whilst a flooding experiment. Some part of the viscosity loss can be restored over time, some part is lost forever and thus permanent. Both, chain scission and deformation are active. Again chain scission in Hypothesis II-I is likely to occur in even (II-I-a) or uneven variations (II-I-b) or chain entanglement effects like in Hypothesis I-II can be present. Deformation can either be restorable by unfolding due to Hypothesis I-I or permanent due to Hypothesis II-II. Complete polymer restoration is very unlikely. An entire viscosity loss is the assumption of all researches so far and must be rated very likely. This third hypothesis is alike thinkable and entails a determination of the ratio between permanent to restorable viscosity loss and the linkage to molecular size alteration.

7 Methodology I - Core Flooding Experiments

7.1 Definition and Purpose of Core Flooding Experiments

A core flooding experiment is designed to simulate fluid flow of possible hydrocarbons or formation water through reservoir rock towards a bore hole and production equipment. The setup is conceptualized to reproduce this downhole flow through porous media as accurate as necessary and as rough as possible. Nevertheless, a few simplifications had to be made to assure the experiment's feasibility under laboratory conditions and reproducibility within a similar framework of settings. A coreflooding framework always consists of a minimum of four basic elements:

- Pumping Unit
- Tubing System
- Core Holder plus Core
- Measurement System

7.1.1 Basic Coreflooding Elements

The pumping unit creates fluid flow and keeps the system in motion. It can be considered the power source of the experiment. The tubing system conveys fluid movement to the core-holder. It works as a kind of translation element, imparting pump forces on fluids

Figure 18: Core flooding equipment including HPLC pumps, hydraulic containers, a water bath, scales and the core.

and the actual core. The core-holder provides the framework for the actual experiment. It contains the rock core, assembles all other units and links them to the core. The core-holder isolates the rock plug from its environment and forces tubing flow into the entrance face of the core. In addition to that, the measurement system is in most coreflooding realizations integrated into the holding unit. The core, as main element of the system, represents the

reservoir. It is realized either as actual field material or as more homogenous outcrop rock and grants insights into sections of the real reservoir. The measurement system records physical data, such as pressure drops at various positions or fluid composition. The focus of the experiment is the rock-fluid interaction inside the core. Behind the core-holder, there is typically a catching container installed, collecting all possible fluid deposits.

7.1.2 Modifications for Polymer Flooding Experiments

The particular flooding experiment applied for the examination of polymer injection, follows roughly this basic concept of experimental setup. The conveying tubing system was extended by several hydraulic containers to puffer the polymer solution from direct contact with the pumping system. The measurement unit was realized in terms of pressure transducers at the entrance and exit face of the reservoir rock. The entire core complex and parts of the conduit system were submerged into a water bath in order to be able to control the temperature of the reservoir analogue. Behind the core holder a sampling installation was implemented to acquire altered polymer samples for further analysis. A detailed description of the flow path will be provided in the next section.

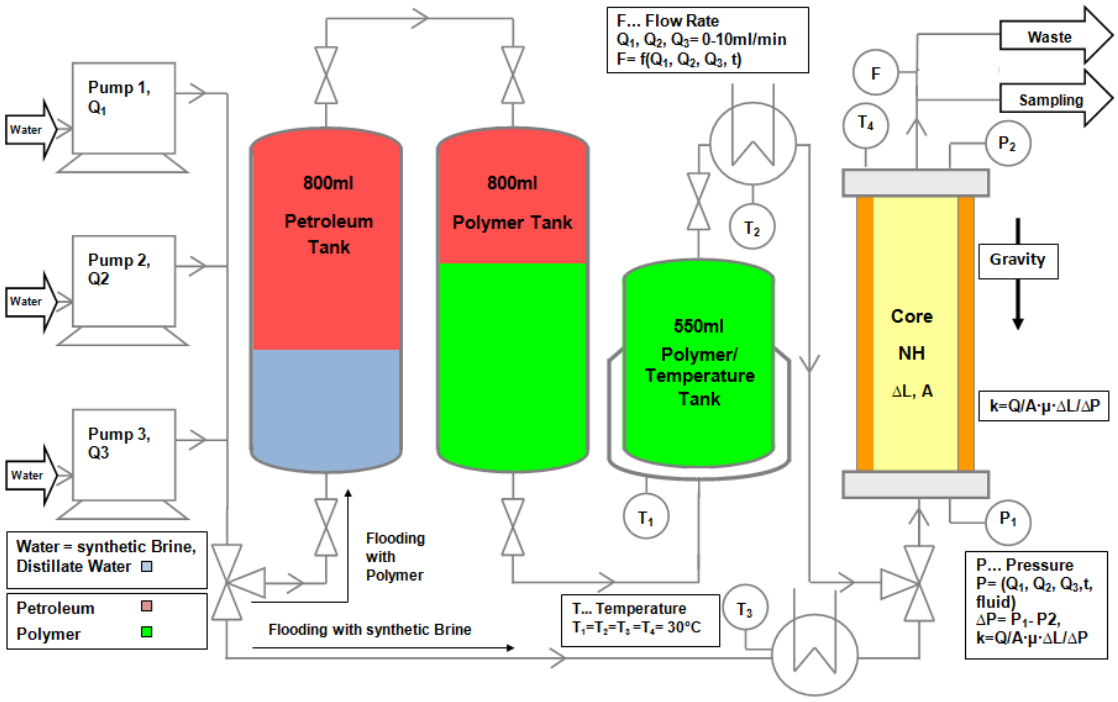

Figure 19: The fluid's flowpath through the coreflooding system (Sledz, 2015)

7.2 Fluid Flow Path

7.2.1 Pumping Unit

The power source of the system is realized via a combination of three parallel-type double plunger pumps. These three high performance liquid chromatograph pumps brand Shimadzu model LC-20AD are used to pump fluids through the assigned cores. They can adjust to pump rates from 0.1 μl /min to 10 ml/min and have a piston stroke volume of 10 μl. Their absolute flow rate accuracy is no more than 1% or 0.5 μl/min, whichever is greater. Maximum pressure pulsation lies below 0.1 MPa. Maximum discharge pressure is 40 MPa.

The three piston pumps can be worked in a parallel setup, achieving a maximum flow rate of 30 ml/min.
The minimum flow rate for the experiments is determined to be 0.2 ml/min, which can be easily adjusted within the absolute flow rate range.

7.2.2 Conveying System

The conveying system is in general realized by 1/4 inch and 1/12 inch plastic tubings, connecting each flooding unit with the other. There are two different flow paths available for the experiments, controlled by a two-way main valve and three pump valves. The direct flow path leads from a potassium chloride reservoir via the three piston pumps straight away to the core holder. This flowline is used whenever a water characterization or chase water re-characterization is performed. Potassium chloride brine is directly pumped through the core at previously assigned rate.

The second flow path is built to set the polymer solution in motion and force it through the core. In order to ensure that the polymer is by no means influenced by the HPLC plunger pumps, a flow path is constructed to keep the polymer solution in question far away from the mechanical parts of the pumping unit. Otherwise impurities of used liquids or some kind of pump degradation cannot be excluded. Three hydraulic containers are used to prevent the system from possible equipment degradation effects.

Figure 20: Hydraulic Containers

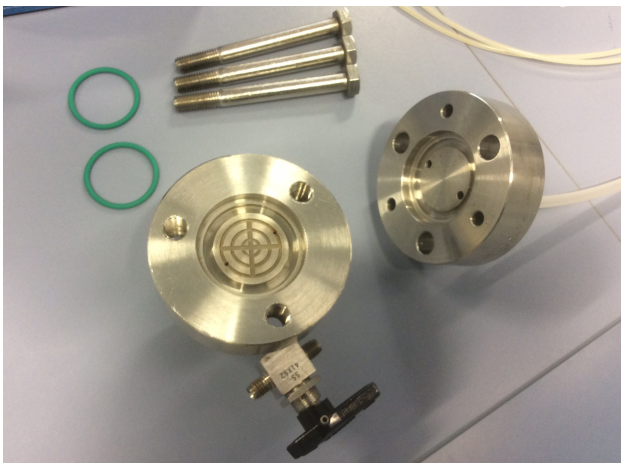

Figure 21: Core Holding Unit

The containers are filled with petroleum and polymer solution. The two large containers are made from plexiglas in order to be able to control the fluid consumption optically. The liquid boundaries between water, petroleum and polymer are clearly visible within the 800ml containers. Despite the advantages of transparency, the material selection bestows the system with an upper pressure limit of 30 - 40 bar. Whenever an experiment oversteps a pressure of 36 bar based upon a safety margin of 1%, the experiment is aborted and changed to operable conditions. The piston pumps are strictly prevented from contact with the polymer solution. They always impart their movement force on the driving medium, water. This water is set in motion and replaces the petroleum spirit inside the first column from below. A stable displacement front between the two liquids forms out, with water as denser fluid on the bottom. The lighter displaced petroleum is shoved upwards and conveyed to the second column via a hose. The polymer inside the second column is displaced downwards by the less dense petroleum replacement. Petroleum works in this case as a puffer medium in order to keep the driving water and the polymer apart and prevent them from mixing with each

other. This would otherwise spoil the flooding operation and thus further measurements. The polymer is pushed through a hose into a smaller polymer tank, from where the temperated polymer is pushed to the core holding complex. The actual core, the holding unit and the smaller 550ml polymer storage tank are submerged into a 30 °C tempered water bath to guarantee an even and accurate downhole temperature.

7.2.3 Core Complex

The core holding apparatus unites the core, the conduit system and the measurement setup in itself. The flooding liquid, be it brine or polymer through either of the both flow paths, enters the holding unit via a small hole on the bottom. A concentric flow pattern, milled in the steel bottom-face of the unit distributes the liquid evenly on the entrance face of the core for the purpose of an areal and uniform core flux. Rubber sealing rings prevent the fluids from escaping and direct the fluid towards and through the core.

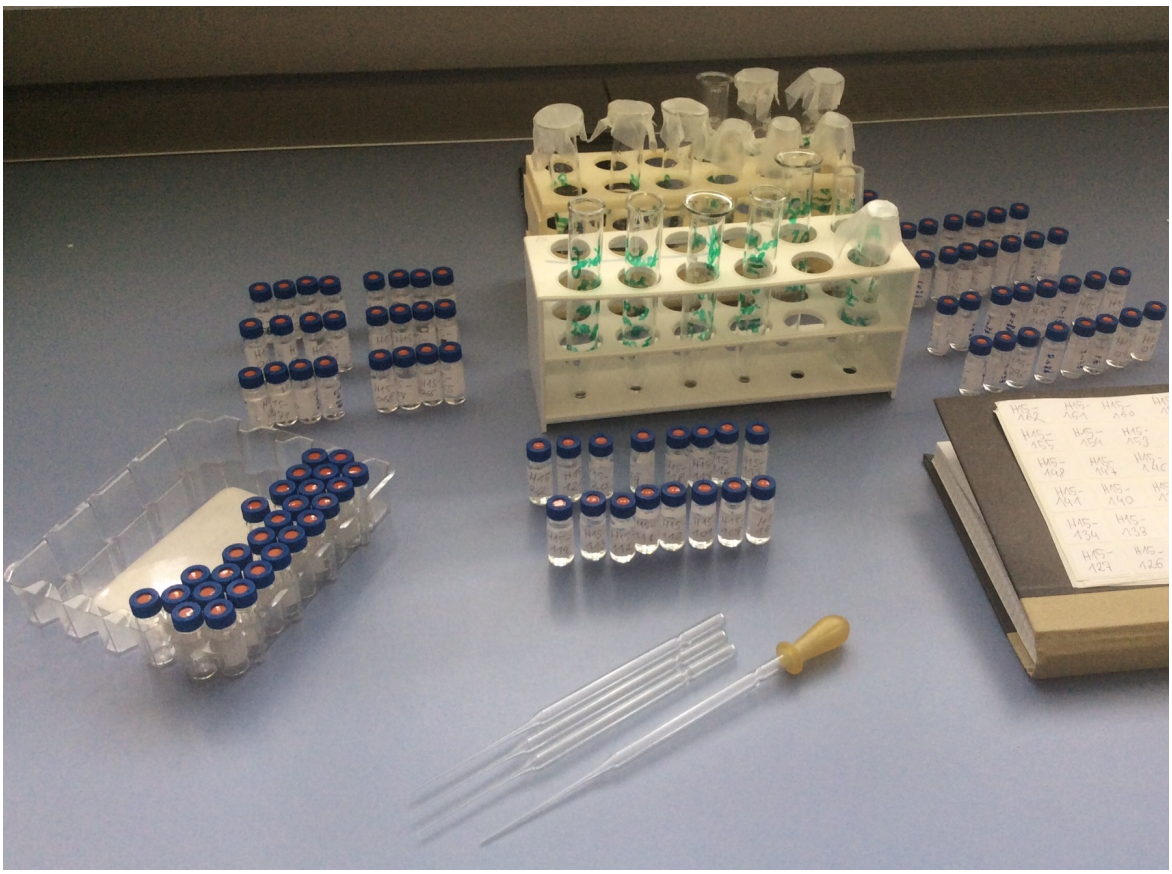

Figure 22: Fluid Samples and Vials

A second hole on the bottom is connected to a pressure transducer via plastic tubes. The upper unit is identical to the bottom one, consisting of an exit hole, a second measurement hole and the milled flow circles. The two parts are connected via large screws, clamping the core in-between and activating the sealing rings. This setup ensures that fluid flow is solely possible through the core. For further details on the selection and preparation of core rock, refer to the geological section with chapters discussing appropriate rock and fluid analogues and the transformation of reservoir conditions into an appropriate experimental setup.

7.2.4 Measurements

Quantification of polymer-rock interactions is the main issue of the entire flooding experiment. Acquired measurement data is the basis of all further analysis work and sample comparison. Most essential data sets for the experimental work are readings from the pressure transducer over time. These data in relation to the nominal flow rate of the HPLC pumps gives evidence on the rheological behavior of the polymer and rock-fluid flow properties resulting in apparent viscosities, resistance factors, permeabilities and residual resistance factors. The two pressure transducers connected to the core holder are chosen to be HBM P11 models with a linearity deviation of smaller than ± 0.5 and a standard deviation of reproducibility of less than ± 0.1.

The measured weight of the polymer, that has already passed the core, gives information on how much polymer is left in the columns and how many pore volumes have already passed the core. In combination with the necessary time to drop out, this data shows approximately which rate is currently applied. Especially knowledge about how many pore volumes passed the core, is crucial, due to sampling and pressure reading quality standards. For the reason of assuring that a certain sample or effect belongs to a certain flow rate and that it is not influenced by previous rates, every sample is taken subsequent to the throughput of three entire pore volumes. This secures clean and proper samples and stable fully developed pressure readings. For higher rates it was necessary to await the pass-through of more pore volumes in order to make sure that pressure readings equalizes at a stable end value. Entry pressure at the lower part of the core holder, exit pressure at the top unit, the resulting pressure difference, the approximated flow rate and the scale weight are continuously recorded via a LabView derivate and saved batchwise.

7.2.5 Fluid Sampling

When the rock affected fluid leaves the core, two different options are available. The fluid can either be conveyed to a sampling installment for the reason of sample extraction or it can be deposited to the waste container straight away. The deposit glas is connected to a scale with ± 0.1 g accuracy for determining the effluent mass and thus calculating flow and mass rate. The sampling installation consists of a holding unit with a clamp that directs the exit hose either to the waste container or the sampling vial. The vials are pre-labeled and systematically sealed and stored after the experiment for further analysis.

7.3 Types of Core Flooding Experiments

In order to get a grip on different traits of a fluid's viscous behavior and mechanical degradation, three kinds of core flooding setups were defined and performed in different variations and combinations. These are:

- Type I Simple Core Flood Experiment
- Type II Reinjection Core Flood Experiment
- Type III Temperated And Aged Core Flood Experiment

The different types of experiments are modifications of a basic core flooding set-up. They are assembled from smaller entities and shall be discussed in detail in the next chapters.

7.3.1 Type I Experiment - Simple Core Flooding

The simple core flooding experiment or type I experiment is the most basic experimental setup within the core flooding framework. It starts with the brine characterization of the chosen rock core. At this stage of the experiment, there is little known about the rock analogue, just plain metrics, porosity and gas permeability. In order to acquire brine permeability and, by doing so, capture the rock's response to Newtonian fluid flow, it is necessary to perform a water flood in the first place. The flooding liquid of choice is the simplified formation water analogue, a 3% potassium chloride solution. When setting up the system, the core is completely saturated with potassium chloride and all tubings are filled with formation brine. All gas bubbles have been removed from the flow path and measurement tubes in order to enable proper flooding behavior and undistorted pressure measurements. Since the whole system is filled and saturated with potassium chloride, the characterization phase can start directly by activating pumps and initiate fluid movement. Every flow rate is held constant for 5, in special cases 10 minutes, to obtain representative pressure readings. For the purpose of comparability, all flow rates, used for the polymer flood afterwards, shall be characterized. These are 0.2, 0.5, 1, 2, 4, 8, 16, 20 and 30 ml/min. The according pressure figures are used to calculate specific brine permeabilities for each rate.

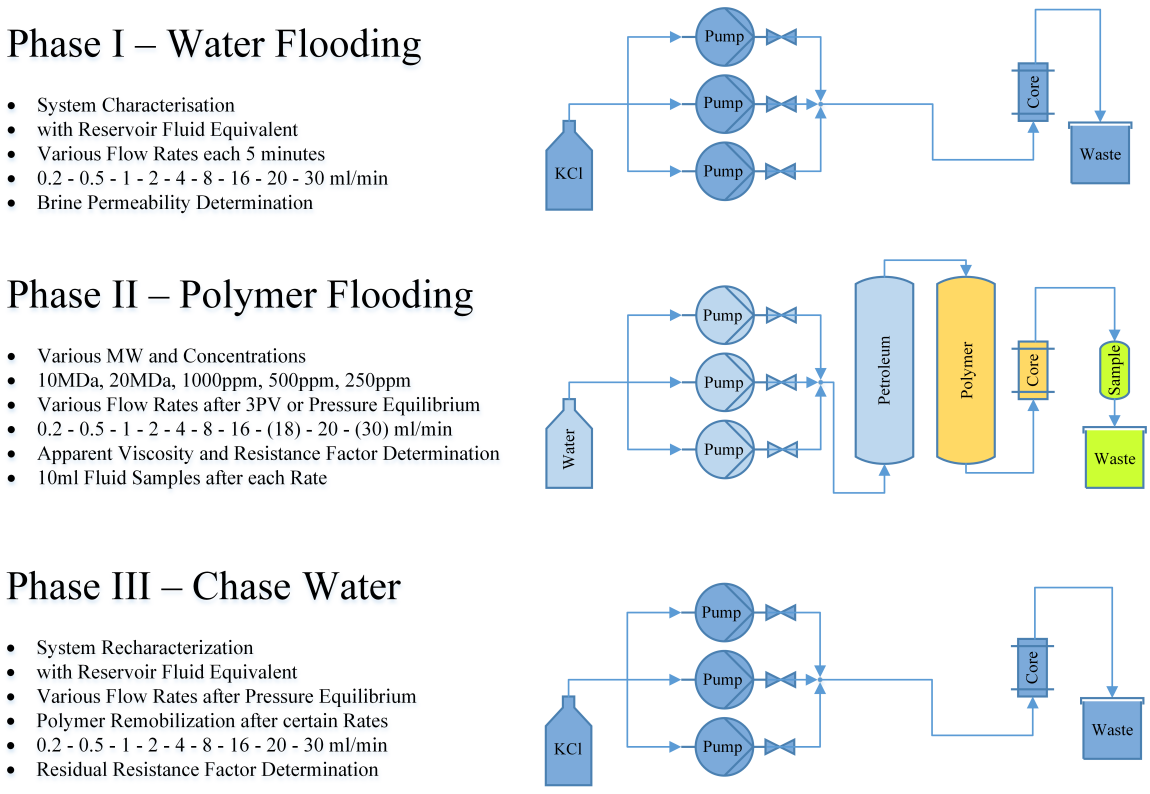

Figure 23: Schematic workflow of a type I core flooding experiment

Having characterized the system properly, the polymer flood is the next step at hand and simultaneously the core purpose of the experiment. The system is entirely filled with potassium chloride, like a section of the reservoir would be, solely saturated with formation water. The flow path is now switched to the hydraulic containers full of petroleum and polymer. Activating the pump units at the lowest rate of 0.2 ml/min, sets the fluid in motion, pushing petroleum into the next container and replacing polymer. The polymer solution is pushed further into the smaller container and conveyed via a long hose into the core holding unit.

Here it enters the KCl-saturated plug and continuously replaces the formation brine. The entire displacement process can take a significant amount of time. For the purpose of uncertainty reduction and enhanced measurement quality, it was decided to let three entire pore volumes pass, until samples are taken and the pressure is considered steady and equilibrated enough to be representative. After three pore volumes the exit tubular is deflected from the deposit container and directed towards the sampling installation. An additional 10 ml polymer is flooded through the core and sampled in designated vials. These vials are labeled, sealed and stored in the vicinity of the experimental setup. The pressure reading is supposed to have reached an equilibrium and is used for according resistance factor and apparent viscosity calculations. For the lowest rate of 0.2 ml/min this whole process takes up to 3.5 hours but grows successively faster with higher rates. Having acquired proper samples and pressure readings, the pump rate is raised and the whole process is repeated. In order to get a good overview on the viscous behavior of the polymer, flow rates of 0.2, 0.5, 1, 2, 4, 8, 16, 20 and 30 ml/min are examined. The pressure limits imposed by some parts of the equipment sometimes forced the setup to omit the highest rate of 30 ml/min using 20 ml/min in lieu of that. One experimental setup even overstepped the upper pressure boundary at a rate of 20 ml/min. For this exemption a rate of 18 ml/min was used instead. At elevated flow rates (8, 16, 20, 30) it is not sufficient to await the pass-through of just three pore volumes because the corresponding pressure cannot stabilize sufficiently, given just 30 to 60 seconds. For these rates it is necessary to wait till the pressure reading has equalized to a certain value, not until then the sampling and calculating can be executed. Having entirely carried out the second stage of the experiment, computed rock and fluid data plus according solution samples are available for the relevant flow rates.

After the actual polymer flood, the system must be characterized again with potassium chloride in order to understand how the inherent permeability of the core plug has changed during the experiment. For that reason, the flow path is switched again to the direct brine line, and the core is flooded with potassium chloride. In order to secure comparability, the same nominal flow rates of 0.2, 0.5, 1, 2, 4, 8, 16, 20 and 30 ml/min are taken, but this time the flooding behavior will be different. The first flow rate must be maintained until the complete possible polymer has been replaced by brine. The indicator for such a state is a stabilized pressure rate, which will be achieved after 1.5 hours. The second rate will stabilized after 30 minutes. All succeeding values will be done by 15 minutes. Although most of the polymer was displaced at the first rate, elevated flux will mobilize polymer fractions still adhering to the rock's inner surface at the beginning of each new rate. This will result in pressure bumps in the measurement record. The attained pressure values can be used to calculate post-polymer permeabilities. They tend to be significantly smaller than the original ones, with permeability losses of 60 to 80% compared to the untouched rock property. Relating original and post-flood permeability to each other, will yield the residual resistance factor for each individual rate.

7.3.2 Type II Experiment - Re-injection Core Flood

A "Re-injection Core Flood" or "Expanded Core Flood" is a combination of two type I flooding experiments performed with the same fluid. At first, a regular simple coreflooding experiment is performed, with water characterization, polymer flooding and chase water re-characterization, but with one striking difference in the polymer flooding phase. At a previously determined rate, most commonly the highest one, the polymer is not only sampled into a 10 ml vial but larger amounts of pumped-through polymer solution are collected. The quality standards are again applied, so that at least three pore volumes of polymer must have passed the core, in order to be declared representative for the according rate. After the first

set of type I experiments, the hydraulic container for the second experiment is refilled with collected post-core polymer and used as flooding medium for this second run. In order to be able to conduct an entire second type I experiment, at least 800 to 1000ml of core-influenced polymer must have been sampled from the first experiment. The two experiments shall be labeled "Type IIa Experiment" for the first fresh conduct and "Type IIb Experiment" for the second flood with previously used polymer.

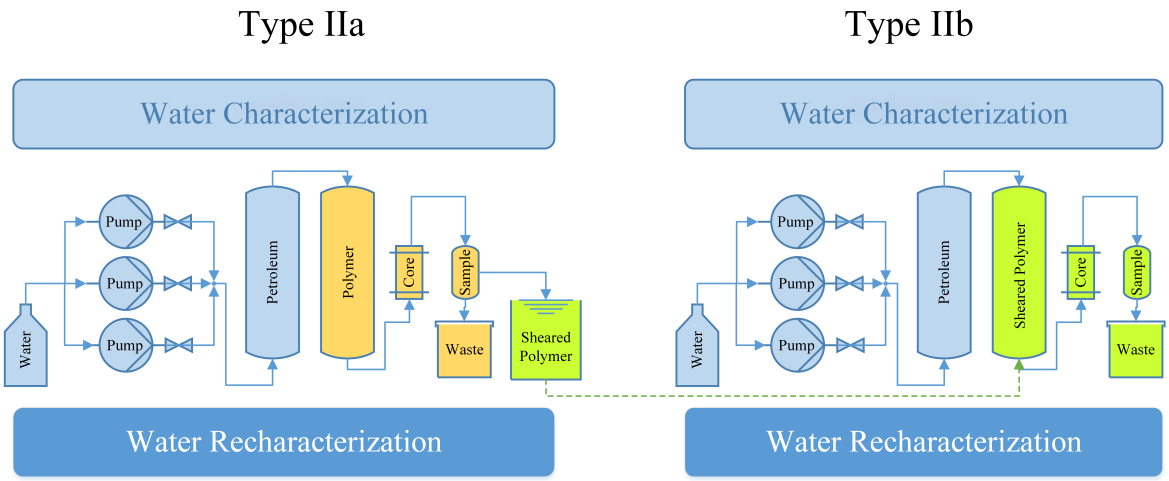

Figure 24: Schematic workflow of a type II core flooding experiment. On the left a Type IIa experiment. On the right a Type IIb experiment with reused polymer.

The concept behind this kind of experiment is, that the polymer solution is somehow subjected to mechanical deformation and degradation during the flood. The polymer, collected behind the core in IIa, will exhibit some kind of decreased viscosity. In order to quantify this reduction, the influenced polymer is reused for a second experiment IIb. Resistance factors and apparent viscosities will reach much smaller values in the second experimental setup due to former molecular alteration. Because of the expected smaller viscosities and smaller absolute pressures, high rates of 30 ml/min are possible within IIb experiments.

As already mentioned, the sample flow rate will most commonly be the highest possible rate during the first experiment, which is likely to be 20 or 18 ml/min dependent on the maximum pressure peak. One set of experiments is an exemption though, being sampled at a rate of 4 ml/min. This experimental run had the purpose of determining whether viscosity losses are already detectable by type IIb experiments at this rate or not. Previous experiments within the OMV polymer project did this in more detail by taking larger samples for each distinct flow rate of IIa experiments and performing according IIb experiments. The findings of this research can be looked up in figure 13.

7.3.3 Type III Experiment - Temperated And Aged Core Flood

Temperated and Aged Core Flooding Experiments or Type III floods are basically modifications of Type II experiments. The concept is basically the same. A simple type I or IIIa experiment is performed with larger amounts of polymer collected for the reuse in subsequent IIIb experiments. The difference in this variation is the time between experiment A and B. In plain re-injection Type II experiments, the sampled polymer is reinjected directly after the first flood IIa. The subsequent flood IIb is started within two hours. Not even a day

passes, between the degradation induction and the second flooding experiment. The modification Type III collects allegedly degraded polymer from the first flood IIIa and decants it to an appropriate container. The flask is properly labeled, evacuated and sealed for further storage. As mentioned in previous sections, the potassium chloride and the polymer solution have been mixed including small amounts of sodium azide in order to impede bacterial growth. The second measure to keep the sample clean over a longer time span is conducted right after the first part of the Type III experiment. The solution is degassed and rendered inert via nitrogen gas. This step shall keep the oxygen in any form from reacting with the polymer solution. By doing so, the degraded polymer samples are prevented from biological and chemical alteration over the entire storage time span.

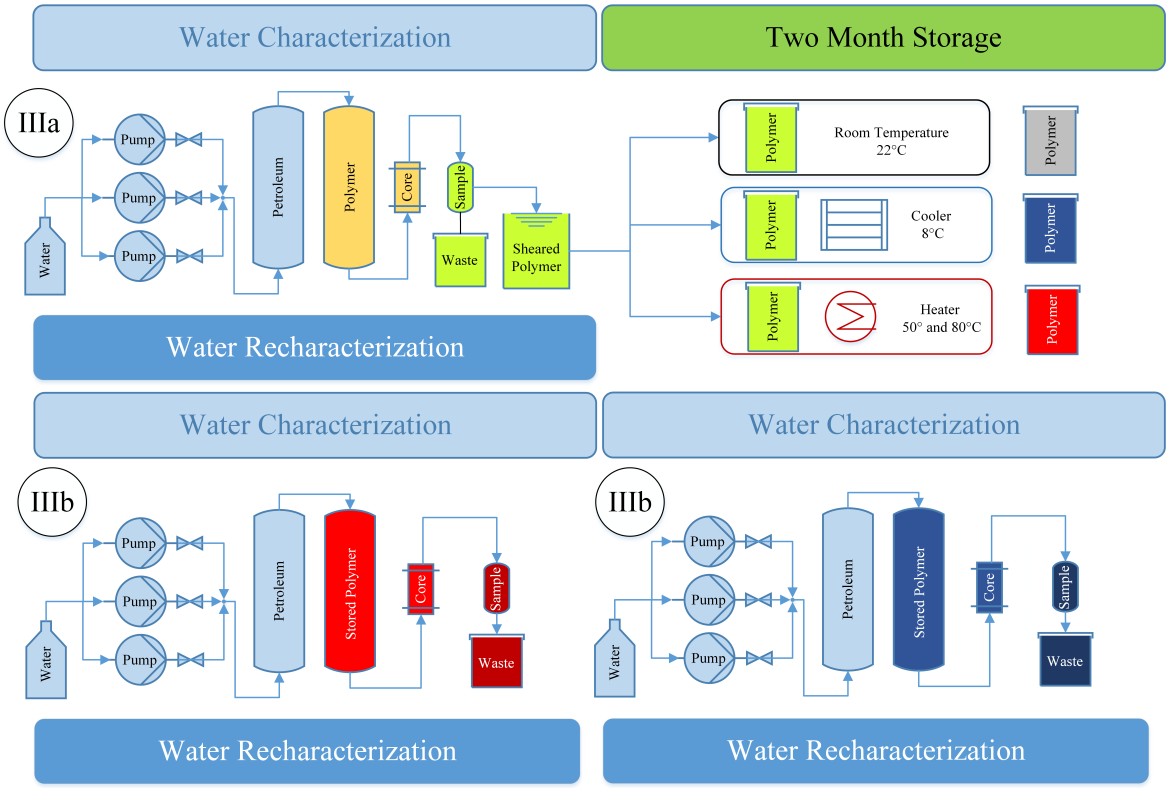

Figure 25: Schematic workflow of a type III core flooding experiment. On the left the original Type IIIa experiment. On the upper left storage condition. On the bottom two distinct IIIb experiments.

Properly prepared and sealed off, the core-influenced polymer sample is stored in opqaue containers at different temperature conditions for 2 months. The storage temperature ranges from cold 8 °C, over room temperature 22 °C, to elevated temperatures of 50 °C and 80 °C. After the designated storage time of 62 days, the polymer is used for another type I experiment.

Type III experiments are designed to examine the influence of time and temperature on the degraded polymer. The focus of this experimental setup lies upon the question if the stored and temperature influenced polymer will heal parts of it's viscosity or not. If degradation is permanent and no healing effects are present, the apparent viscosity will yield a similar curve as IIb experiments. If the polymer is somehow healing, the viscosity profile will more likely look like I, IIa or IIIb experiments. The objectives of this experiment and conditions

for interpretations are discussed in detail in the section about research objectives and the according validation methods.

8 Methodology II - Liquid Chromatography

8.1 Definition of Chromatography

The term "Chromatography" is a collective label for a series of laboratory techniques, that serve the purpose of mixture separation and quantification. The substance, that shall be examined, gets dissolved in a fluid called the mobile phase. This fluid carries the particles through a structure, that consists of another material, called the stationary phase. The various constituents of the mixture migrate at different velocities, causing them to separate accordingly. The separation is based upon a process of differential partitioning between mobile and stationary phases. Different materials for mobile and stationary phases lead to distinct separation principles and accordingly alternating classifications. Chromatography is nowadays accepted as probably the most powerful and versatile analytical technique available, because it can separate mixtures in a single step, and measure the amount of every component and their relative proportions.

8.2 Types of Chromatography

8.2.1 Gas Chromatography

Gas chromatography is a measurement technique, that relies on the usage of gas as mobile phase, usually an inert gas such as helium or a non-reactive gas like nitrogen. The stationary phase is realized as a microscopic layer of liquid or polymer on an inert solid support inside a piece of glass or metal tubing. As the carrier gas pushes the analyte molecules through the column, their particle motion is inhibited by adsorption processes onto the column wall. Since each type of molecule has a different rate of progression caused by varying adsorption impediment, the various components are separated as they progress through the column, reaching the end of the column at different times. A detector is utilized to monitor the outlet stream and identify single constituents by typically using a flame ionization detector or a mass spectrometer.

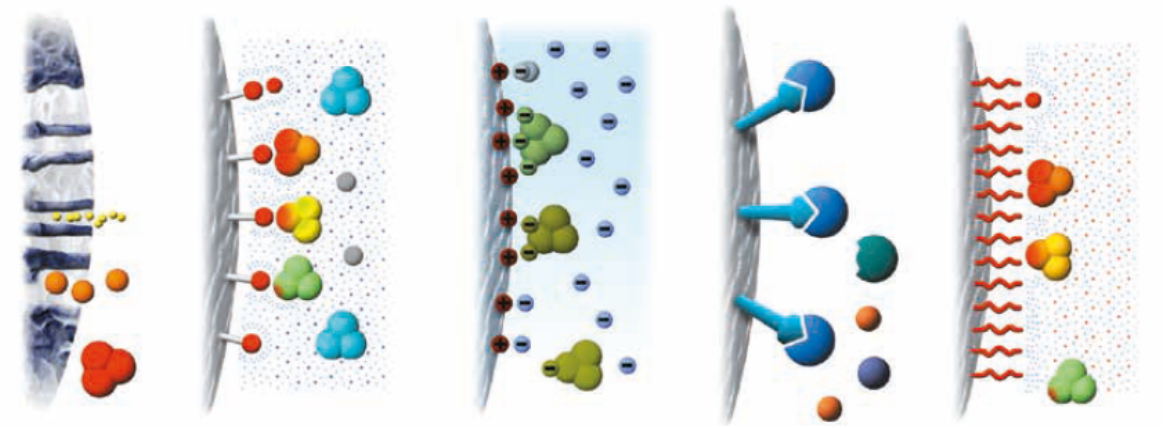

Figure 26: Schematic drawing of separation principles in chromatography purification. From left to right: Size exclusion chromatography SEC, Hydrophobic interaction chromatography HIC, Ion exchange chromatography IEX, Affinity chromatography AC, and Reversed phase chromatography RPC (GE-Liefscience, 2000)

8.2.2 Liquid Chromatography

Liquid chromatography is a separation technique, that relies on liquids as mobile phase. The procedure involves a sample being introduced into the stream of mobile phase percolating through a separation column. The constituents of the sample move through the column at different speed, being functions of specific physical interactions between the stationary phase and the analyte, be it bioaffinity, molecular size or polarization. The velocity of each component depends solely on its chemical nature, on the nature of the stationary phase and the composition of the mobile phase. The time at which a specific analyte elutes or emerges from the column, is called its specific retention time. The retention time measured under particular conditions is considered an identifying characteristic of a given analyte.

Present day liquid chromatography typically uses very small packing particles and relatively high pressures. Due to this operating conditions, it is most commonly referred to as "High Pressure Liquid Chromatography", "High Performance Liquid Chromatography" or simply "HPLC" which has become a synonym for plain liquid chromatography. Based upon particular properties of the liquid mobile phase and differing stationary phases there exist several distinct types of separation principles:

- Adsorption Chromatography
  - Normalphase Chromatography
  - Reversed-phase Chromatography
- Displacement Chromatography
- Ion-exchange Chromatography
- Bioaffinity Chromatography
- Size-exclusion Chromatography

8.2.2.1 Adsorption Chromatography

Adsorption chromatography separates analytes based on differences in their polarity. Normalphase chromatography involves a polar stationary phase such as silica and an unpolar mobile phase, such as Dioxan. The separation process is based on the analyte's ability to engage in polar interactions such as hydrogen-bonding or dipole-dipole interactions with the sorbent surface. Reverse-phase chromatography consists of a non-polar stationary phase and an aqueous, moderately polar mobile phase.

8.2.2.2 Displacement Chromatography

In displacement chromatography the analyte shows a different degree of dissolution in the mobile and the stationary phase. The better it solves in the stationary phase, the longer will the analyte linger there. As a result of that retention, the mobile phase won't be able to carry it very long. Conversely, an analyte that has a good solubility in the mobile phase, will be carried along much faster and longer. The separation principle is hence based on solubility differences.

8.2.2.3 Bioaffinity Chromatography

This chromatographic process relies on the property of biologically active substances to form stable and reversible compounds. The formation of such complexes involves the participation of common molecular forces such as the Van der Waals, electrostatic, dipole-dipole or hydrophobic interactions. The process itself can be thought of as an entrapment, with

the target molecule becoming trapped on the stationary phase. The other molecules in the mobile phase will not become trapped as they do not possess the triggering property.

8.2.2.4 Ion Exchange Chromatography

In ion-exchange chromatography, retention is based upon attraction forces between solute ions and charged parts of the stationary phase. Solute ions of the same charge belonging to the separation column are excluded from binding an pass along, while solute ions of the opposite charge retained on the column surface. This is the principle of ion exchange separation.

8.2.2.5 Size Exclusion Chromatography

Size-exclusion chromatography is a scientific method that achieves separation of molecules based on their differences in size or molecular weight. Size exclusion, hereinafter simply referred to as SEC, is a widely used polymer characterization method because of its ability to provide good molar mass distribution results for polymers. Based upon the choice of mobile phase there are two techniques distinguished. Gel Filtration Chromatography for aqueous solvents and Gel Permeation Chromatography for organic solvents. Due to limited acces-

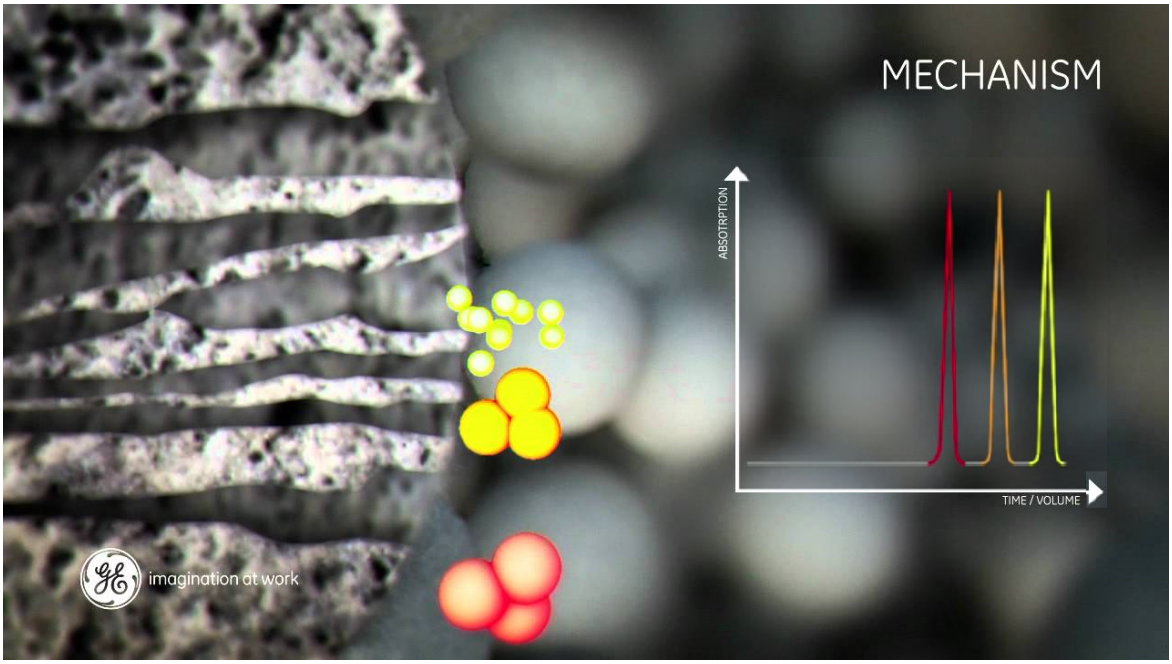

Figure 27: Schematic of a size exlusion bead and the ability of different molecular size to enter bead pores. (Siddiqui, 2015)

sibility of pore volume within the particles of the column packing, polymer molecules are separated according to their hydrodynamic volumes, with the larger size molecules exiting first, followed by the smaller ones. After a measurement, residence time then can be correlated with molecular weights. Since size-exclusion is the applied technique in this master thesis, it shall be explained in more detail in the next section.

8.3 Size Exclusion Principles

Size Exclusion Chromatography is a liquid chromatographic method that implies the separation of molecules or macro-molecular complexes by distinction of their size or molecular

weight. The principle of size exclusion is based upon different travel times assigned to varying molecule sizes. Whenever a chromatographic separation treatment is applied, polymer probes are injected into the mobile phase, also called eluation fluid or eluent. The combined fluid is then pumped through a so called separation column, containing a separatory stationary phase. This stationary phase is realized via chemically modified inorganic silicas or polymeric beads packed into the column. The mobile phase is able to travel between the beads and may also enter or exit all of their pores. In addition to that it carries the sample molecules, that shall be separated and examined. It is essential to understand, that these samples have been dissolved in the first place, because they must coil up on themselves in order to be properly measurable, forming spherical coil conformations, that resemble balls of strings. Despite their natural chain formation, they behave like tiny spheres during the exclusion process, with short and light-weight chains forming smaller balls and long heavy-weight chains coiling up to larger spheres. The dissolved polymer molecules move along the porous beads, as the mobile phase carries them down the column. At this point of the process, several things can happen.

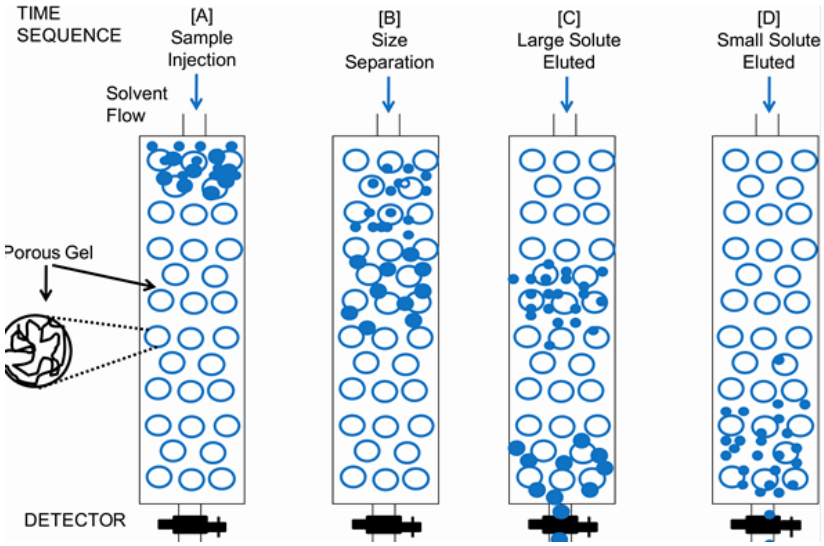

Figure 28: Schematic principle of size exclusion chromatography (Barron and Lin, 2009)

Whenever the coiled polymer chains are much larger than the biggest pores of the beads, they won't be able to enter them. The mobile phase carries the larger coils straight away and past the bead pores. If the polymer chains are a little bit smaller, they are able to enter the larger pores, but not the smaller ones, as they pass by. They are occupying some, but not all of the pores inside the stationary phase. Even smaller polymer coils will be able to intrude smaller and smaller pore space of the beads. If the coil size drops below the smallest available pore size of the stationary phase, they are free to migrate wherever they want and do not experience any restrictions in the choice of bead pores. As molecules of different sizes enter different pores with different frequency, a partitioning of molecules is achieved with diffusion urging the coils to enter or leave the pores. As a result of that, small polymer spheres may enter much more bead pores and accrue travel-time, leading to a much longer time span to migrate through the entire column. Therefore, they will leave the column at a much later time than others. Larger polymer spheres will diffuse in less bead pores, resulting in less travel-time and earlier column exit. Conversely to the smallest, highly diffusive molecules, larger coil chains will take the straightest path through the column, sparing all pores and exiting the column first and foremost. Thus, the way and the travel time of the molecules depends directly and very much on the size of molecules

and the size of the pores in the stationary phase. The separation process relies solely on the molecular size of each polymer component and its corresponding ability to diffuse in bead pores, rather than chemical interactions between particles and stationary phase.

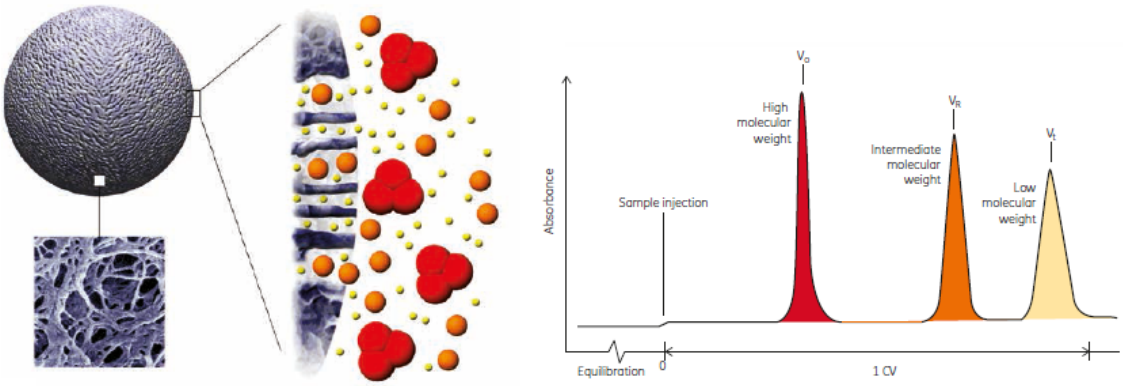

Figure 29: Schematic principle of size exclusion chromatography and its linkage to molecular weight distribution. (GE-Liefscience, 2000)

With regard to precise physical definitions, it must be stated that the separation principle is based upon the size or better the hydrodynamic volume and not the molecular weight of the polymer chains. The hydrodynamic volume is defined as the specific volume of a polymer coil when it is in solution. This volume may vary depending on how the polymer interacts with the solvent and the chain's uncoiled size. The term is very strongly related to the radius of gyration, meaning the characteristic length of a system that represents the distance in a rotating system between the point around which it is rotating and the point to or from which a transfer of energy has the maximum effect. Although the coil size is not straight away translatable to the polymer's molecular weight, the degree of correlation is high enough to link the two physical properties. The obtained correlation depends on the specific types of polymer and the overall size exclusion system.

8.4 Concentration Detection Methods

Once the polymer coils are sorted due their travel time and thus size or molecular weight, they are ready to be counted and quantified. The arrival time and time span between individual types of molecules must be recorded and their absolute frequency and concentration be determined. The quantification of these properties is realized via different detection methods. These can be:

- **Destructive Detectors**
  - Flame Ionization Detector (FID)
  - Flame Photometric Detector (FPD)
  - Nitrogen Phosphorus Detector (NPD)
  - Mass Spectrometer (MS)
  - Evaporative Light Scattering Detector (ELSD)
- **Non-destructive Detectors**
  - Ulta-Violet Detectors (UVD)
    - Diode Array Detector (DAD)

    - Photodiode Array Detector (PDA)
  - Thermal Conductivity Detector (TCD)
  - Fluorescence Detector
  - Electron Capture Detector
  - Photoionization Detector (PID)
  - Refractive Index Detector (RI or RID)

8.4.1 Ultra Violet Detection

8.4.1.1 Plain Ultra Violet Methods

Ultra violet detectors are most frequently used to measure components showing an absorption spectrum in the ultraviolet or visible light region. Most commonly, ultra violet detectors employ a deuterium discharge lamp as light source. For longer wavelengths, UV-VIS detectors are used, involving an additional tungsten lamp. The optical system of a plain UV detector features light from source lamps shining onto a diffraction grating. The light beam is dispersed into a broad range of wavelengths. When a measurement is performed with a certain wavelength, the angle of the diffraction grating is adjusted, so that only light of that very consistency may hit the flow cell. By monitoring the reference light divided from the light in front of the flow cell, the difference in intensity can be determined between the rear and the anterior of the flow cell.

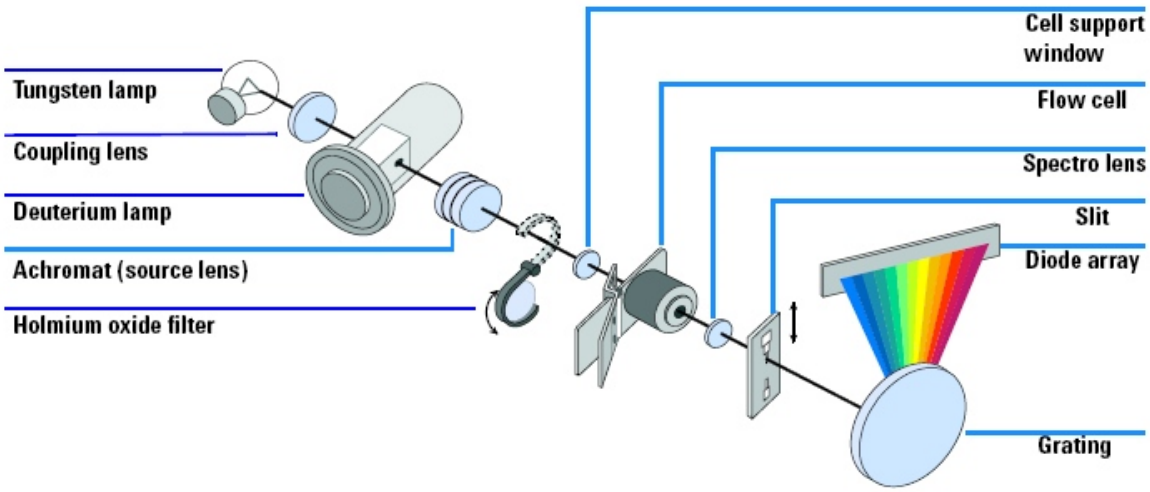

Figure 30: Schematic principle of diode array detection (Agilent, 2013)

8.4.1.2 Diode Array Detection

Diode array detectors are realized with photodiode arrays comprising a bundle of 512 to 1.024 semiconductor devices. A diode array detector is able to quantify absorption not only in the ultraviolet region but also in the visible light region. Whilst a plain UV-VIS detector has only one sample-side light-receiving section, a DAD has multiple photodiode arrays to obtain information over a wider range of wavelengths at one time. This is the preeminent merit of a diode array detector system.

In diode array measurement, the light is cast directly onto the flow cell. Light, that passes through the cell, is dispersed again by a diffraction grating. The amount of dispersed light is quantified for each wavelength in the photodiode arrays. The basic principle of DAD

utilization in HPL chromatography is based upon the measurement of light spectra during continuous eluate delivery. Detection time intervals are very small in order to capture all separated molecular sizes of the mobile phase stream. If the measurement is performed at a fixed wavelength, components are identified from their individual retention time. Thus, a minor deviation in retention time can render the identification of associated components an impossible task. In such a case, the detector provides the possibility to compare fill light spectra and improve distinguishability.

8.4.2 Refractive Index Detection

Refractive index detectors measure the refractive index of an analyte, relative to a particular solvent. The principle behind this measurement is the alteration of light beams when entering and leaving different materials. The light will either bend or refract. The refractive index of a material is a measure of how much the light beams bends when it enters. Refractometers consist of a flow cell with two distinct compartments. One chamber is destined for the sample

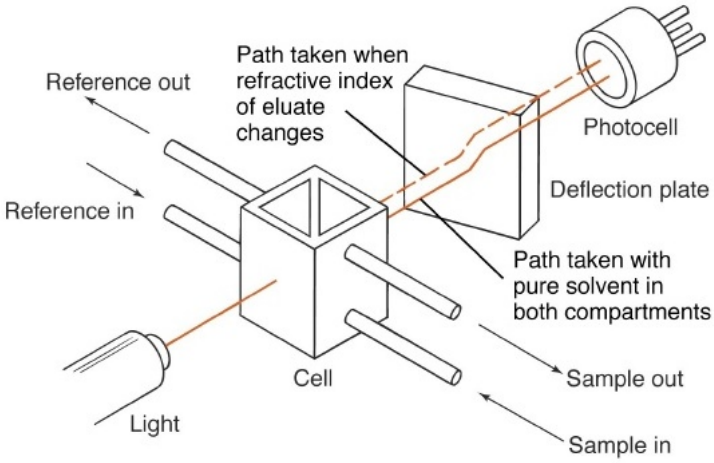

Figure 31: Schematic principle of refraction index detection (Kaumil, 2008)

under examination, the other one for the corresponding reference solvent. The detection unit measures both refractive indices and compares them. If the reference solvent is used as sample, the refractive index will yield unity, whereas diverging analytes will entail altered indexes. RIDs are considered universal detectors due to their ability to measure anything with a refractive index different from the solvent's. The major disadvantage of this method though, is its low sensitivity. For that reasons, they shall be used as diode array reference and consistency measure within this experimental setup.

8.4.3 Multi-Angle Light Scattering

Multiangle light scattering, abbreviated MALS, is a technique for the independent determination of absolute molar mass and the average size of particles in solution, by observing how individual constituents will scatter light. Collimated beams, generated by a laser, are the most frequently used source of light. A typical Rayleigh scattering process during such a detection operation involves a focused, single frequency polarized light beam, to illuminate the macromolecule solution. The electric field of the polarized light beam is generally produced perpendicular to the plane in which the intensity and angular dependence of the subsequently scattered light is to be measured. Intensity yields information about the molar

mass, while the angular dependence carries information about the size of the macromolecule.

The main advantage of this method is the direct measurability of molecular size and weight. Another benefit of this method is the acquisition of gyration radii or root mean squared radii. This data can be derived from the light scattering angle and grants deeper insights into sample composition.

8.5 Agilent Infinity 1290 LC System

8.5.1 Introduction to the Agilent System

Having discussed the principles of liquid chromatography, the applied separation techniques and the according detection principles, the specific chromatographic set-up and configurations shall be introduced in this section. The high performance liquid chromatograph, that was used for all measurements, was provided by OMV and manufactured by Agilent Technologies. The specific system belongs to the Infinity series and represents the latest chromatographic instrument of this brand. The installment is labeled "Agilent Infinity 1290 LC" and is assembled from different interchangeable modules, comprising basic and extended chromatographic functionality.

- **Pumping Unit**
  - Liquid Containers
  - Blending Valve
  - Degasing Unit
  - Quartenary Pumps
- **Autosampler**
  - Sample Container
  - Injection Needle
  - Bypass System
  - Flowpath Switch
- **Column Compartment**
  - Column Holding Units
  - Column Thermostat
  - Thermical Isolation
- **Diode Array Detector**
- **Refractive Index Detector**
  - RI Detector
  - Deposit Container

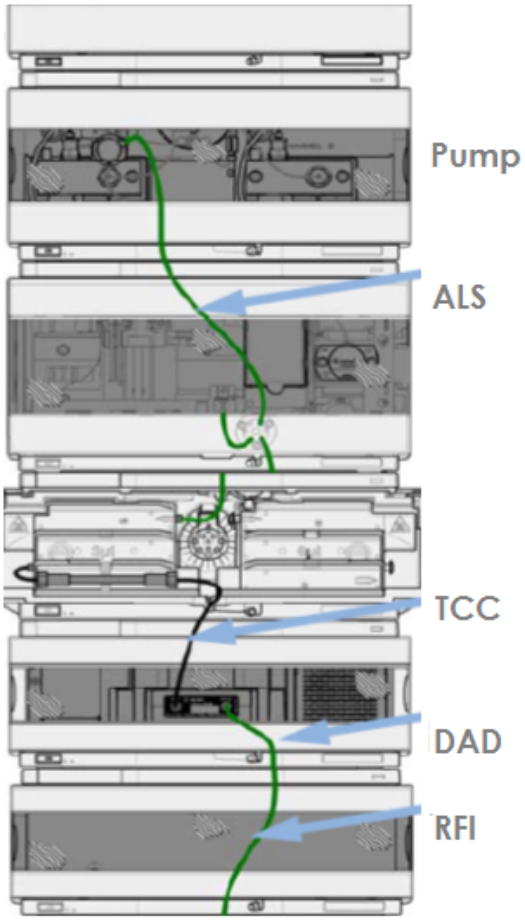

Figure 32: Agilent 1290 Series HPLC

8.5.2 Flowpath through the Agilent Infinity System

8.5.2.1 Liquid Containers

The storage system of the HPLC is installed on top of the system. It consists of four different bottles, that can be operated individually or blended in any possible combination. The four bottles and the corresponding channels are denoted A, B, C and D. The primary bottle has a capacity of 5 liter and is used as the mobile phase's reservoir. The according channel A is thus defined as the main flow path of the system. Bottle B, C, and D are realized as smaller flasks and serve the purpose of system cleanse and flowpath conditioning. Channel B is connected to a smaller bottle of isopropyl-alcohol, C_3H_8O, which was used for regular pump,

tubing and column purges. Bottles C and D are filled with distilled water for sweeping out the cleaning fluid and neutralizing the flow path. Distilled water was pumped through the system in order to condition and prepare the flowpath for the re-introduction of the mobile phase when starting a new measurement series.

8.5.2.2 Blending Valve

The blending unit enables the accurate regulation of circulation fluid. As previously mentioned, it is possible to switch between four individual channels or even blend liquids if necessary. For the purpose of system cleanse, it turned out to be practical and system-protecting to operate the cleaning fluids via gradients, meaning that the composition of liquids changes continuously from one to another (eg. isopropanol to distilled water). This portioning process is realized via an implemented multi-channel gradient valve.

8.5.2.3 Degassing Unit

The build-in degasser in the pumping module has the purpose of removing gas bubbles from the eluent liquids. This measure increases detector sensitivity and flow stability, especially at low flow rates. The manual, provided by Agilent, gives no further information on the degassing process, but it turned out to perform poorly for the specific experimental configuration.

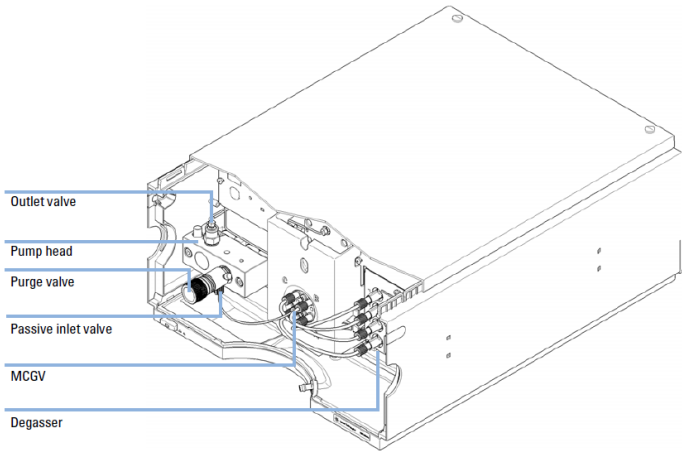

Figure 33: Schematic of the pumping module including the degasser unit, the blending valve and the quarternary Pump (Agilent, 2013)

Gas bubbles and resulting pressure pulses respectively signal fluctuations were a steady and vexing problem at the early stage of the project. These difficulties were finally brought under control by meticulous fluid preparation, like repeated vacuum degassing and a proper container selection. Although bubble issues were recurring sporadicaly, their occurance was seldom and short in time. Problems could be pushed back immediately and proper working conditions were soon re-established.

8.5.2.4 Quaternary Pump

The pumping unit of the system is realized via a quaternary plunger pump. The pump assembly consists of two identical piston-chamber units, both of them comprising a ball screw drive and a pump head with a sapphire piston for reciprocating movement. A servo-controlled variable reluctance motor drives the two ball screw drives in opposite directions. The drive gears have different circumferences, enabling the first piston to move at twice the

speed of the second one. The outer diameter of the piston is smaller than the inner, allowing the solvent to fill the gap in-between the two. The first piston has a stroke volume in the range of 20 to 100 μl depending on the flow rate. The microprocessor controls all flow rates in a range of 1 μl/min to 10 mL/min.

Installation Property	Manufacturer's Specification	Property Unit
Flow Rate Range	0.001 - 5	[ml/min]
Flow Rate Increments	1	[μl/min]
Flow Rate Accuracy	$\pm$1% or 10	[μl/min]
Ambient Operating Temperature	455	[°C]
Operating Pressure	120	[MPa]
Pressure Fluctuations	$< 1\%$	[Amplitude]
Gas Bubble Prevention	Degasser Unit	[x]

Table 5: Quarternary Pump Specifications

A purge valve is fitted to the pump outlet, enabling better cleaning conditions in case of pump errors. A damping unit is situated between the two piston chambers, smoothing pressure pulses and unwanted fluctuations. This active damping is combined with tuning algorithms embedded in the firmware to reduce ripples and associated UV noise in the detector signals. Fluctuation were held below 0.5 bar absolute pressure.

8.5.2.5 Autosampler

The autosampling module has two major purposes. It contains and stores different analytes systematically in a vial cluster and injects sampling fluid into the stream of mobile phase running through the system. Sample vials are heaved by a robot arm to the injection

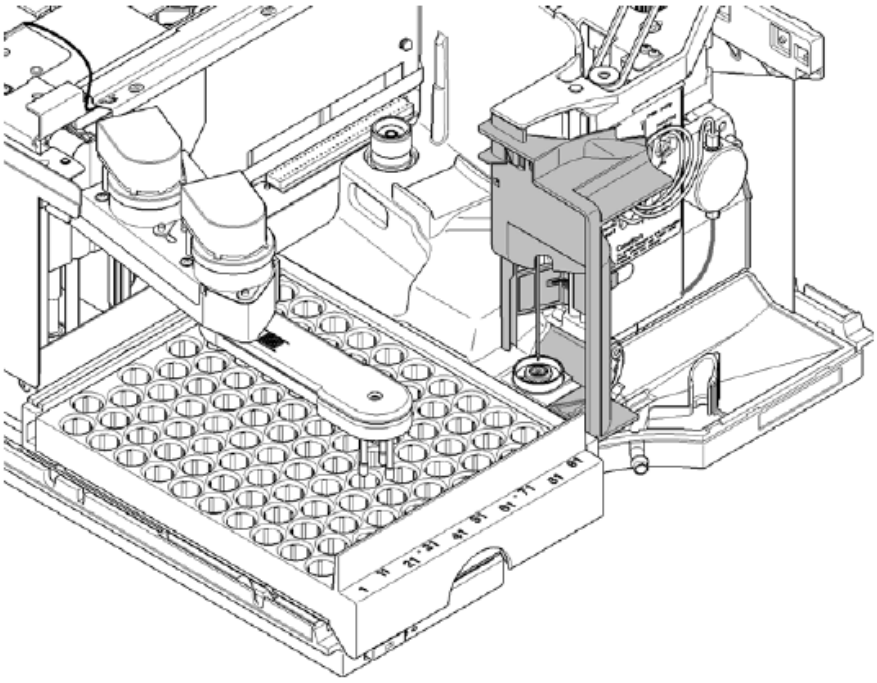

Figure 34: Schematic of the autosampling unit (Agilent, 2013)

needle. This transport mechanism utilizes an X-Z-Theta movement system to realize both vial positioning and return. A gripper arm picks up vials and positions them right below

the sampling unit. Both, the gripper transport mechanism and the sampling unit, are driven by stepper motors. Motion is monitored by optical sensors to ensure proper operation conditions. The sampling unit consists mainly of a needle, injecting small amounts of analyte into the flow stream of the system. The standard analytical head of the metering device provides injection volumes from 0.1 to 100 μl and can be operated at up to 600 bar. The metering device is flushed after each injection to ensure minimum carry-over effects.

Installation Property	Manufacturer's Specification	Property Unit
Sampling Range	0.1 - 100	$[\mu l]$
Sampling Increments	0.1	$[\mu l/\text{min}]$
Sampling Accuracy	$<$ 0.25% RSD, 5 – 100	$[\mu l]$
Sample Viscosity	0.2 - 50	[cp]
Replicate Injections	1 - 99 from one vial	[x]

Table 6: Autosampler Specifications

The six-port injection valve unit is driven by a high-speed hybrid stepper motor, bypassing the autosampler and directly connecting fluid flow from pumps to columns, when no measurement is going on. During injection and analysis phases, the valve unit directs flow straight away towards the autosampling unit, introducing small probes of analyte to the system. This ensures that the entire sample is completely and evenly fed into the separation column. Any sample residue is removed from the metering device and the needle before the next sampling sequence begins.

8.5.2.6 Flowpath Switch

In order to facilitate the handling of multiple columns or different column configurations in one set-up, an internal switching valve is installed. The switching option involves a hub, connecting different entrances and exits between the autosampler and the column compartment via capillary tubes. Based on the connection setup of the capillaries, two flow paths through different columns can be constructed and activated via a software command. The

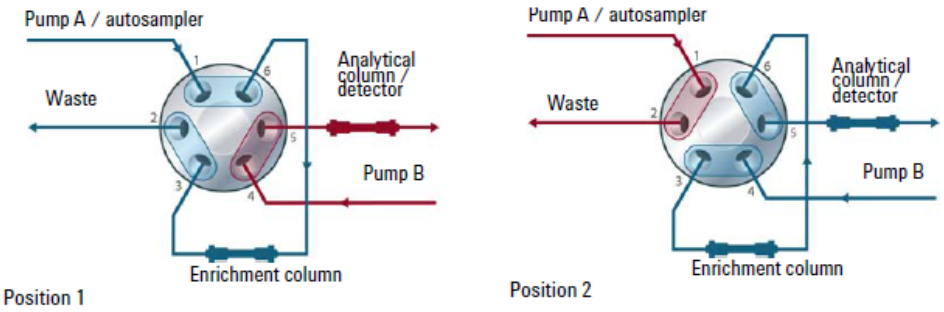

Figure 35: Schematic of the flow path switch (Agilent, 2013)

valve short-circuits either capillary 1 and 2 or 1 and 6 and forces the mobile phase to either path. This functionality can be applied to simple column switching, automatic column regeneration, sample preparation or column back-flushing operations.

8.5.2.7 Thermostatted Column Compartment

The Thermostatted Column Compartment, short TCC, serves the purpose of containing and securing separation columns and providing them appropriate working conditions. The

main purpose of this module is to host the separation columns. It is the crucial part of the chromatograph, where the actual size exclusion treatment is performed. The second purpose of this compartment is to control the temperature environment for both the mobile and the stationary phase during the separation process. The ambient temperature of the module is allowed to lie inbetween 10 °C and 100 °C at 2.5 ml/min and 80 °C at up to 5 ml/min. Temperature stability is limited to ±0.05 °C and accuracy to ±0.5 °C. These specification are

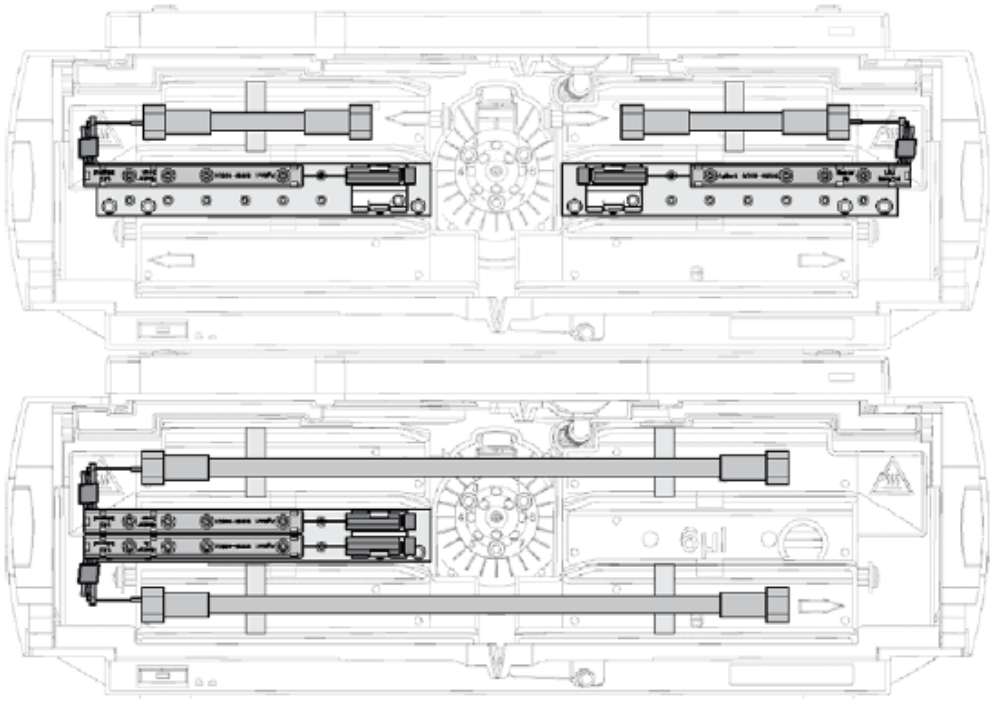

Figure 36: Schematic of the Thermostated Column Compartment. (Agilent, 2013)

achieved via a combination of conduction from contact with the thermostat vanes, still-air temperature in the column environment and as major factor by pre-heating or down-cooling the mobile phase via a heat exchanger. There are two independent temperature zones in each compartment, which can be combined for longer columns up to 300 mm length or be operated individually at different temperatures for short columns of 100 mm length or less.

Installation Property	Manufacturer's Specification	Property Unit
Temperature Range	10 below ambient to 100	[°C]
Temperature Stability	± 0.05	[°C]
Temperature Accuracy	± 0.8	[°C]

Table 7: Thermostated Column Compartment Specifications

The module comes with a 1.6 μl low dispersion heat exchanger. For the specification of used columns see the column selection chapter.

8.5.2.8 Diode Array Detector

The diode array detector module is the main measurement unit of the system. The illumination source is realized via a deuterium-arc-discharge lamp, individually tailored for the ultraviolet wavelength range. Its light is focused via a lamp mirror onto the entrance of an optofluidic-waveguides-containing cartridge flow-cell. Light beams exit the flow cell at the

other side of the cartridge and get focused through a slit assembly onto the holographic grating. They are getting dispersed then onto the core diode array. This optimized procedure allows the simultaneous access to all useable wavelength information of the system. The light source for this procedure is a long-life UV-lamp, which bases on plasma discharges in low-pressure deuterium gas. The discharge mechanism emits light over a range of 190 to approximately 800 nm wavelength. In order to improve optical measurements, a combina-

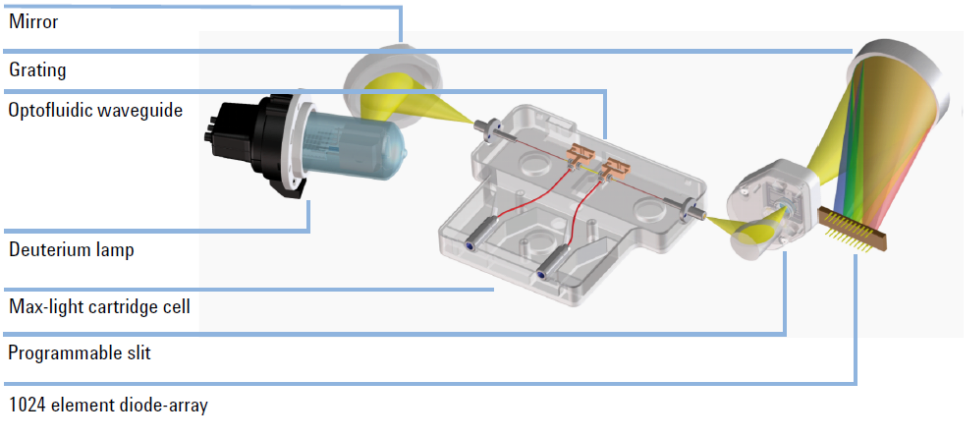

Figure 37: Schematic of Agilent Diode array detector. (Agilent, 2013)

tion of dispersion and spectral imaging is applied, accomplished via the usage of a concave holographic grating. The grating splits the light beam in question into all its constituent wavelengths and reflects the resulting components onto the photodiode array.

Installation Property	Manufacturer's Specification	Property Unit
Light source	Deuterium	[x]
Range of Wave Length	190 – 640	[nm]
Self Calibration	± 1	[nm]
Slit width	1,2,4,8	[nm]
Short-Term Noise	$< \pm 3x10^{-6}$	[AU]
Drift	$< 0.5x10^{-3}$	[AU/hr]

Table 8: Agilent Diode Array Detector Specifications

The diode array is a series of 1024 individual photodiodes and control circuits located on a ceramic carrier. It exhibits an effective wavelength range of 190 to 640 nm and a usable sampling interval of ±0.5 nm.

8.5.2.9 Refraction Index Detector

As a secondary quantification means and reference control measurement, a refraction index detector is installed.

Installation Property	Manufacturer's Specification	Property Unit
Type	Deflection method	[x]
Short-Term Noise	$\pm$ 2.510^{-9}	[RIU]
Drift	$< 200x10^{-9}$	[RIU/h]
Calibration	1.00- 1.75	[x]

Table 9: Refraction Index Detector Specifications

The RI detector inside the module is a differential refractometer, that measures the deflection of a light beam due to the difference in refraction between sample and reference cells. A beam of light passes through the flow cell, which is separated diagonally into a sample and a reference chamber. At the rear of the flow cell, a mirror reflects the light back via a

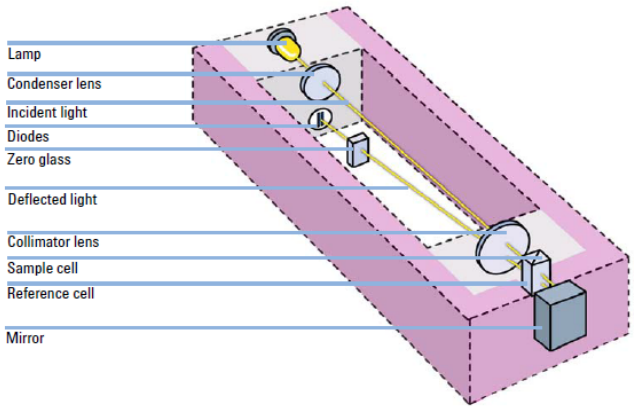

Figure 38: Schematic of Agilent refraction index detector. (Agilent, 2013)

zero glass affecting the optical path of the light beam receiver. The receptor consists of two diodes, each of which produces an electrical current, proportional to the amount of light that falls upon it. The relationship between the angle of incidence and the angle of refraction is described via Snell's refraction law and translated to according refraction indices. The refractometer provides the possibility of fluid recycling and has a purge valve implemented in order to optimize the measurement procedure.

8.5.2.10 Chemstation Software

The proprietary Agilent software bundle, called Chemstation, controls the whole chromatographic measurement process and provides multiple configuration and regulation options. All modules can be operated separately and be fine tuned to the very basic detail of the operation. Fluid composition, flow rate, temperature, flow path selection, injection volumes and measurement specifications are entirely controlled via the software interface. A specific set of configurations for a distinct measurement scenario can be saved as "method". These methods can be applied to a set of samples, aggregated as a so called "sample sequence". Methods and sequences can be written beforehand and assembled in any way that is convenient for later and automatized processing. The software comes in two instances, featuring one online mode and one offline mode. The online version controls the HPLC in real time. Whenever a change is applied, the relevant module is reacting immediately and operates due to the new conditions. The offline instance bestows the software bundle with the ability to simultaneously plan new methods and sequences and execute them a later point. At the same time, the software records all measured diode array signals and refraction indices. They are the actual measurement results of the entire process and so to say the end product. In addition to these core data-sets, all other pertinent operating conditions for the system, like mobile phase composition, overall pressure and diode voltage are recorded and saved to the according file. This secures data completeness and enables troubleshooting and the validation of surrounding conditions under which the optical signals have been taken. Chemstation provides an individual data analysis section, for further processing DAD and RF signals, but the built-in functions are bulky to handle and do not go far enough for the needs of this master thesis. It is obvious, that the system was designed for applications in different industries and for different purposes. Subsequent analysis and data usage will be handled outside the

Agilent system. For that reason it must be exported and converted to universally readable files. This issue will be discussed in further chapters, dealing with data conditioning and analysis. All modules can be operated separately and be fine tuned to the very basic detail

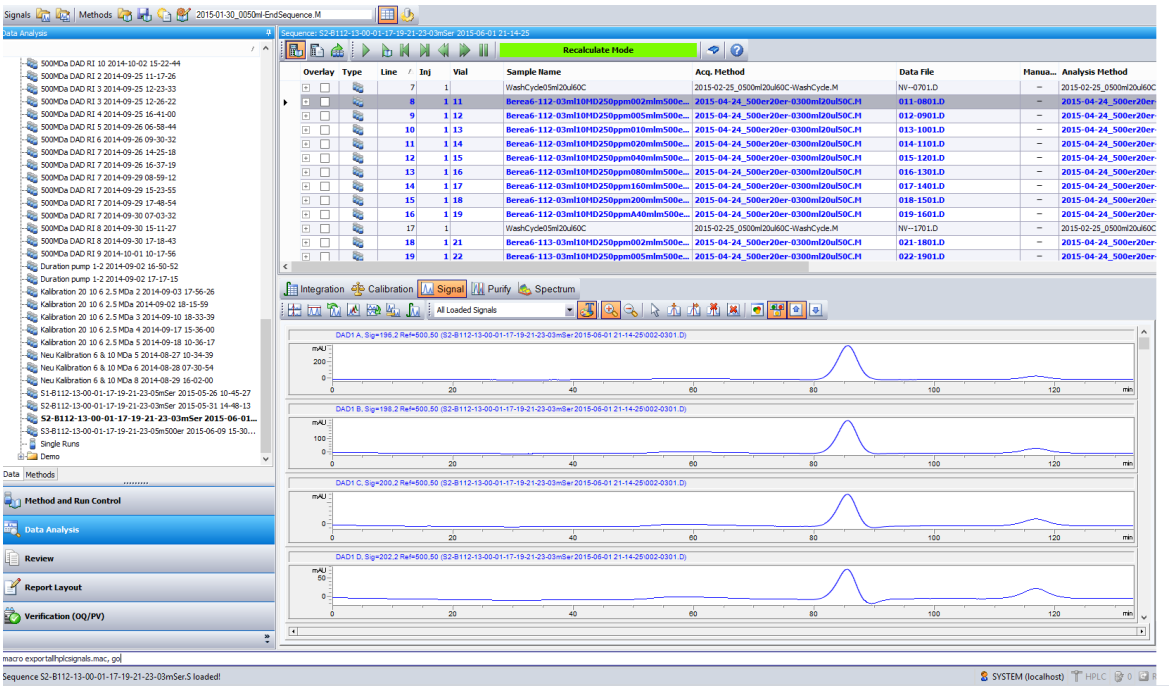

Figure 39: Chemstation Graphical Interface

of the operation. Fluid composition, flow rate, temperature, flow path selection, injection volumes and measurement specifications are entirely controlled via the software interface. A specific set of configurations for a distinct measurement scenario can be saved as "method". These methods can be applied to a set of samples, aggregated as a so called "sample sequence". Methods and sequences can be written beforehand and assembled in any way that is convenient for later and automatized processing. The software comes in two instances, featuring one online mode and one offline mode. The online version controls the HPLC in real time. Whenever a change is applied, the relevant module is reacting immediately and operates due to the new conditions. The offline instance bestows the software bundle with the ability to simultaneously plan new methods and sequences and execute them a later point. At the same time, the software records all measured diode array signals and refraction indices. They are the actual measurement results of the entire process and so to say the end product. In addition to these core data-sets, all other pertinent operating conditions for the system, like mobile phase composition, overall pressure and diode voltage are recorded and saved to the according file. This secures data completeness and enables troubleshooting and the validation of surrounding conditions under which the optical signals have been taken. Chemstation provides an individual data analysis section, for further processing DAD and RF signals, but the built-in functions are bulky to handle and do not go far enough for the needs of this master thesis. It is obvious, that the system was designed for applications in different industries and for different purposes. Subsequent analysis and data usage will be handled outside the Agilent system. For that reason it must be exported and converted to universally readable files. This issue will be discussed in further chapters, dealing with data conditioning and analysis.

8.6 Operating Conditions for the Agilent System

8.6.1 Mobile Phase Selection

The mobile phase of choice was selected due to the recommendations of the column manufacturer, being a diluted isocratic potassium dihydrogen phosphate solution. The used monopotassium phosphate, KH_2PO_4, is a soluble salt of potassium and dihydrogen phosphate ions and acts acidic when dissolved in water. The solution of choice was prepared on the usage of distilled water and vacuum filtration via $45\mu m$ paper. The tagert solution's molarity was chosen to be 0.5 mol of salt per liter solution and achieved with an accuracy of ± 0.1 g. Properties of the mobile phase play an important role on the overall system performance, including:

- Buffer capacity for the proper usage of field samples
- Establishment of disaggregated polymers
- Avoidance of shielding effects at the stationary phase
- Adsorption reduction
- Interaction with mass sensitive detectors
- Absorption of light

Due to the immaculate performance of monopotassium phosphate as buffer and mobile phase, no alternatives had to be considered.

8.6.2 Flow Rate Selection

The selected flow rates of the mobile phase range inbetween 0.1 and 1 ml/min. Previous HPLC measurements conducted by C. Sledz, operated with exceedingly low flow rates of 0.08 to 0.1 ml/min, leading to very long runtimes. The major difficulty here was to maintain separation sensibility. Long measurement durations increase the influences of drift and enlarge the probability of random effects on the result. Higher flow rates increase pressure fluctuations, signal unsteadiness and noise, leading to a global loss of signal quality. The main objective, with regard to flow rates, was to increase the speed of chromatographic measurements while simultaneously maintaining a sufficiently high data accuracy and expressiveness. The ideal compromise flow rate for conducting chromatography analyses is defined as a secondary target of this master thesis. A detailed discussion of results and causes is provided in the corresponding result chapter.

8.6.3 Injection Volume Selection

The chosen injection volumes were either 20 or 40 μl per sample depending on the target concentration of the examined solution. It was intended to keep the absolute sample concentration constant. The first core flooding experiments were started with 500 ppm HPAM solutions and examined by HPLC measurements featuring 20 μl injection volumes. In order to provide polymer standard comparability, it was sought to link it to both 500 ppm standards at an injection volume of 20 μl and 250 ppm standards with an injection volume of 40 μl. The same is true for 1000 ppm solutions of 20 μl and 500 ppm polymers with 40 μl. The greatest part of experiments was conducted with 250ppm HPAM solutions and an injection volume of 20 μl. This turned out to yield the best results. The injection error of the autosampler is strongly connected to the chosen injection volume but ranges below a value of 1%. Injection errors are assumed random errors, that do not influence the acrylamide calibration significantly.

8.6.4 Diode Array Wavelength Selection

A crucial property of the diode array detector is the chosen wavelength. C. Sledz, who set up the chromatographic frame-set at OMV, found a range inbetween 195 and 196 nm as most suitable for his experiments. However, these pre-set configurations were scrutinized and set under inspection for the current experiment. It turned out that a wavelength of 202.2 nm showed the highest contrast and thus, best resolutions for molecular weight distributions. The first measurement sequences were performed with pre-set 196,2 nm but successively replaced and compared with 202.2 nm. Despite of a better resolution for the acquisition of molecular weight with altered wavelengths, it was decided to continue simultaneously with lower wavelengths to keep the measurements within the same project consistent. The presented data is based upon 196,2 nm measurements. 202.2 nm data was used internally for higher expressiveness. An overall of 8 diode array channels were programmed within a range of 196 and 210 nm using 2 nm incremental steps. All of them were randomly crosschecked. The wavelengths of choice emerged to be the most viable compromise between highest absorption values and lowest signal-to-noise ratios. More detailed information can be obtained by full wavelength analysis.

8.7 Characteristic Molecular Weight Distribution

The result of a high performance liquid chromatographic measurement is the responding chromatogram or characteristic molecular weight distribution. As separated analyte components exit the column department and get detected via diode arrays, the elution behavior of the sample elicits a certain signal pattern called "chromatogram". The chromatographic pattern shows how much material left the separation column at any one time of the experiment. Higher molecular-weight coils will elute earlier, followed by successively lighter and therefore smaller molecular weight chains and smallest analyte constituents emerging last. A typical

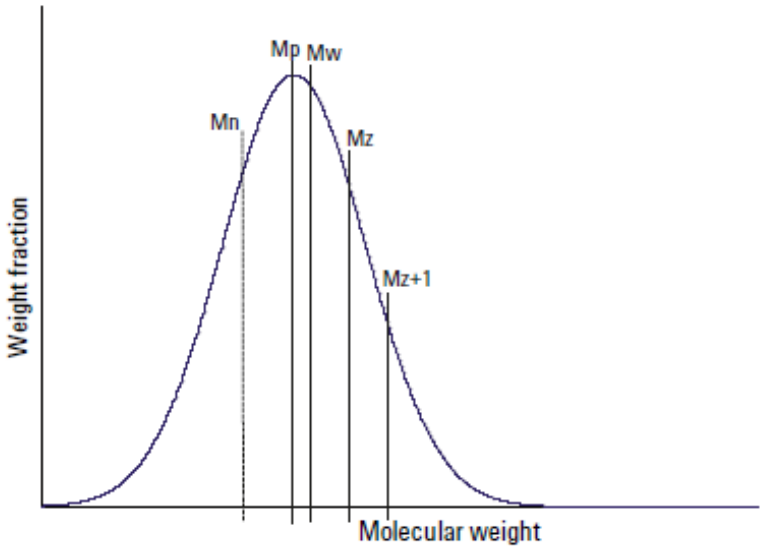

Figure 40: A typical molecular weight distribution in a weight vs fraction diagram. In order to describe molecular weight associated with the distribution curve, three key figures are common. The number average Mn, the weight average Mw and the z-average molecular weight Mz

chromatogram for the examined experiments consists of three characteristic bumps. The

first one is associated with the polymer samples, being the heaviest and largest molecular chains. The second peak is connoted with the salt components of the polymer solution. The third bump goes back to small amounts of sodium azide. The last two peaks will stay more of less untouched over a variety of different experiments. The major differences will hail from the first peak, the polymer peak. This curve section will be the focus of chromatographic examinations.

8.7.1 Molecular Size Linkage

The abscissa of the chromatogram reflects the time it takes, for a fraction of molecules of approximately the same size, to elute from the separation column. This time is referred to as retention time, being the duration these polymer coils have been retained inside the column. Assuming a more or less constant flow rate, this retention time can be translated to elution volume or EV by simply multiplying time with flow rate. The elution time has the the advantage of better comparability due to rate indecency, but shows the same tendency as plain retention time. Staying inside a certain flow rate for different measurements, renders this conversion gratuitous. The unit for retention time is minutes, the unit for elution volumes is milliliter for this set of experiments.

8.7.2 Molecular Concentration Linkage

The ordinate of an HPLC graph is a measure for the recorded light absorption, being a counter for the absolute occurrence frequency of polymer coils of a specific size. This means that diode array absorbance is directly connected to a particular polymer concentration. The unit most commonly assigned to the ordinate is the fictitious absorption unit [AU] or [mAU] for this case. Absorption is actually a dimensionless physical property being defined as the logarithm of the incoming beam's intensity I_o and the the transmitted beam's intensity I as in equation 16. The link between absorption and polymer concentration is given by Beer-Lambert's law, which states, that the absorbance of a specific wavelength λ is directly proportional to the length of a light beam l and the concentration of the light absorbing substance c via a proportionality constant ε, being called the molar attenuation coefficient of the material.

8.7.3 Diode Array Signal Interpretation

The diode array signal of a resulting chromatogram can therefore be interpreted as a size-concentration distribution. The height or y-value of the signal reflects a certain concentration with higher absorbance meaning higher concentrations. The position on the x-axis is connected to the measured molecular size with early signals indicating larger molecules and later values signifying subsequently smaller particles.

8.7.4 Accurate Size and Concentration Correlations

The accurate quantification of molecular size and concentrations is far from being trivial. Although concentration is directly linked to the measured absorbance via a physical law and would be straight-away computable with the Beer-Lambert's relation, the exact quantification of proportionality ε is complex. Hence, it is more common to use the area below the signal curve as correlation parameter. The linkage of molecular size to retention time respectively elution volume is even more treacherous and sophisticated than that. The basic principle is the usage of solutions with known molecular sizes and the comparison of analytes with these standards. This calibration technique works fine under normal working conditions

but evokes serious problems when applied to these experiments. The detailed procedure and a broad discussion on problems and conditions will be provided in the next chapter.

8.8 Calibration

8.8.1 Basic Principles of Molecular Size Calibration

The striven-for aim of chromatographic measurement in this thesis, is to get a glimpse on the molecular weight distribution of the investigated polymer samples. For this reason it is important to identify molecular sizes and weights and to assign them to according retention tims and concentrations. The problem is, that there is no directly computable link between retention time and elution volume on the one side and molecular size and mass on the other one. The only chance of pinning down individual molecule sizes to according time values, is to introduce size standards for the purpose of comparability.

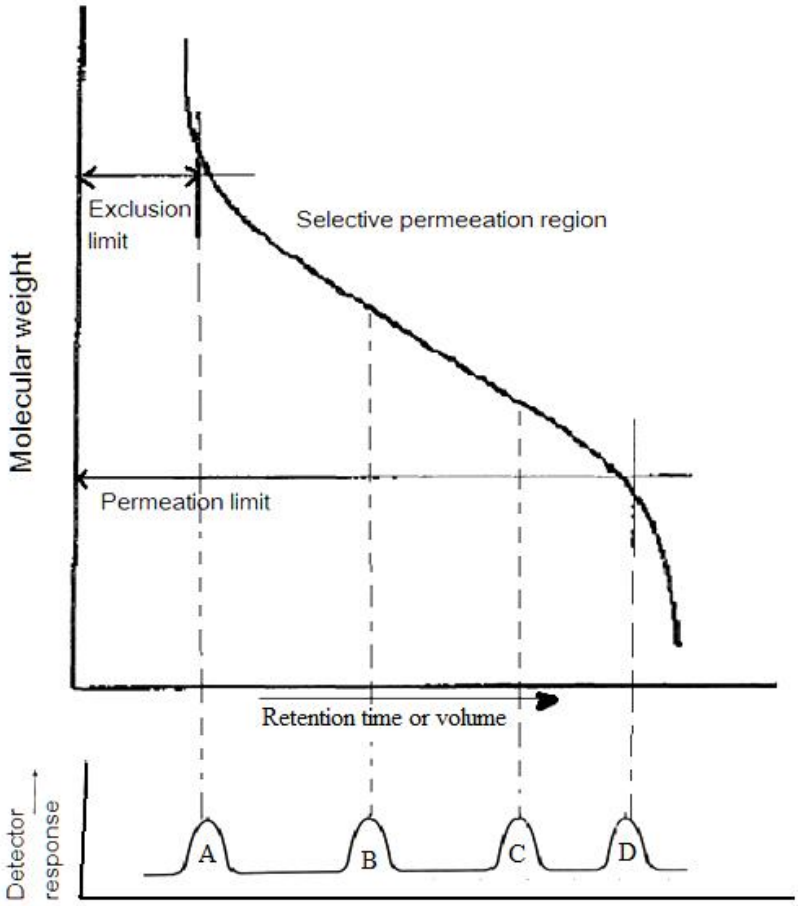

Figure 41: The Exclusion Limit or retention volume Vo is defined as void space of the column. Vi denotes the sum of void space Vo and total column porosity, also called the permeation limit. A separation column is solely able to performed within Vo and Vi. (Barron and Lin, 2009)

Having access to such fix points, enables proper interpolation between them, if it is proven, that there is some kind of proportionality existing between time and molecule size.

8.8.2 Available Calibration Range

The separation column manufacturer provides a calibration range between 200 and 1'000'000 g/mol meaning a range of 0.2 KDa and 1 MDa for Pullulan, a polysaccharide polymer often used for calibration purposes. The problem that arises with this official calibration range, is the fact, that the calibration curve for higher molecular weights up to the exclusion limit is not empirically given but simply interpolated. Since the experiments work in an average range of 20 to 5 MDa for the peak of the polymer curve, the manufacturer provided calibration is not sufficient.

With SNF polymer solutions it is possible to extend the calibration range by five additional calibration points, covering the range in-between 1 and 20 MDa. But this extension is deceitful and not directly applicable. The first issue is, that the two calibration ranges are defined via different substances, Pullulan and HPAM, and may not fit into one single model. In order to circumvent this obstacle, it is possible to define the calibration environment for every single sequence of measurements with SNF polymer in contrast to the low level Pullulan calibration range, separatley. The second problem is inherent to the used polyacrylamide solutions.

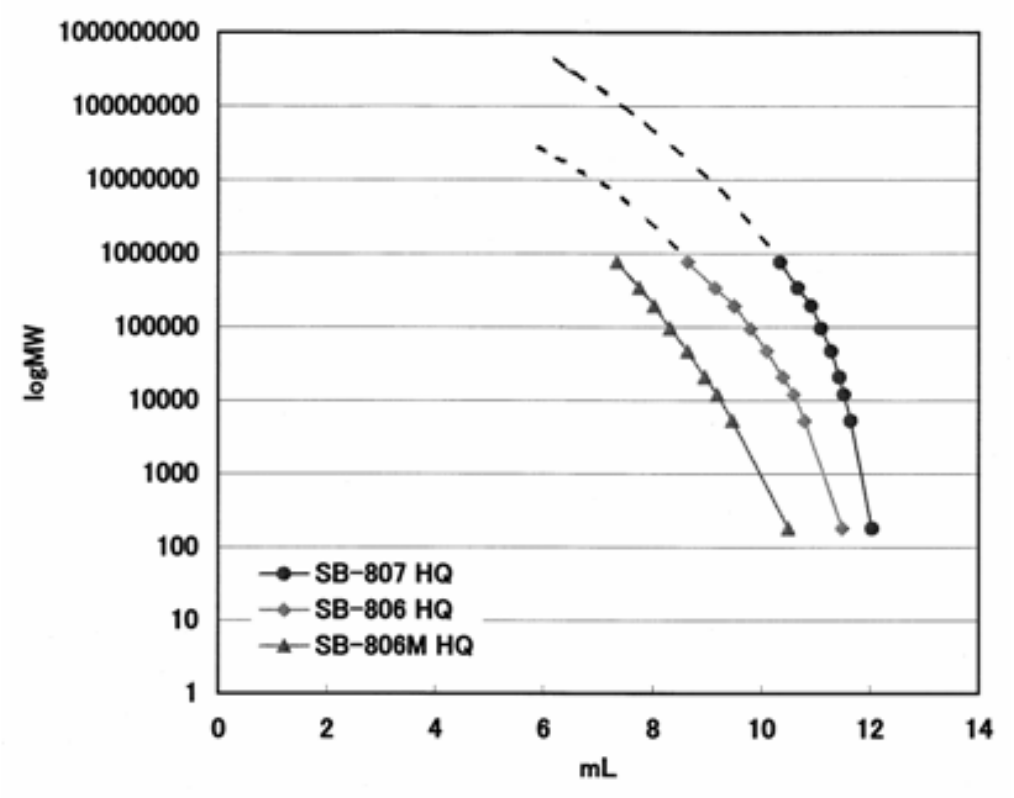

Figure 42: Calibration range of different columns based on Pullulan standards. Dark dots denote a 500 MDa exlusion limit. The other two profiles are associated with 20 MDa separation columns. (Shodex, 2015)

8.8.3 Characteristic Calibration Points

The polymer solution yields a certain molecular weight distribution during an HPLC measurement but these specific distribution provide no reference point to relate them to. The

powder may have an assigned nominal molecular weight, which is for this kind of experiment 20 MDa or 10 MDa, but it consists of a wide range of exceedingly diverging molecular chain lengths inbetween several hundred Dalton up to 500 MDa and even more. As stated in previous chapters, the polymer is defined by its viscosity enhancing effect and not by its molecular weight. Although it is most likely that the chain length with the highest concentration of the corresponding molecular weight curve, is simultaneously its nominal molecular weight, this is just an assumption and not confirmed by the manufacturer or experimental verifications. It would also be possible that the weighted average of all polymer coils equals the nominal molecular weight. Another issue is, that the molecular weight distribution for each SNF provided nominal weight could differ. This would render the calibration points inaccurate with the degree of imprecision unknown and highly uncertain. There is even a certain potential that reproducibility within a product standard is poor, although this can be minimized by normalization runs. Even HPLC properties like varying flow rates can influence the shape of the weight curve and alter its form, being broader, steeper or skewed. All these influences result in changing curves, making them somehow unsuitable for the usage as fixed anchor points for the calibration process. The only thing that is sure though, is the fact that the overall polymer composition is statistically distributed in a way that the resulting viscosity equates the viscosity of a pure polymer of this molecular weight. This issue is the result of industrial manufacturing techniques.

The assumptions to render this measurement technique applicable, even with constraints, is, to presume that the polymer solution's nominal molecular weight is equivalent to the molecular size with the highest concentration of the chromatographic measurement or the modal value of the polymer-associated part of the molecular weight distribution. The second assumption demands, that the structure and thus the weight distribution is similar for each kind of polymer standard provided by SNF. This means, that every single virgin polymer sample for each individual nominal molecular weight is afflicted by the same inaccuracies and blurring effects imparted by the statistical bell curve distribution of chain lengths and that this random errors do not accrue but are solely statistical. The modal value of a nominal 10 MDa polymer peak is assigned the molecular weight of 10 MDa based upon the size polymer coil with the highest frequency. The nomenclature of equating the manufacturer nominal molecular weight with the most frequent or modal coil size, is maintained over the rest of this thesis.

The problem that remains, is the simple fact, that there are no HPAM solutions available beyond 20 MDa and that calibration for this section must be interpolated and remain highly uncertain. This isn't too grave for the purpose of modal value comparison due to the fact, that most experiments are operated with 10MDa solutions and that the nominal value will most likely drop. For this purpose, the range of operability will suffice. A complete coverage would be necessary to increase the expressiveness of research results but it won't be achieved within this project.

8.8.4 Column Selection Criteria

8.8.4.1 Calibration Requirements

For the purpose of molecular separation two different types of columns with different exclusion limits were available. The first one, coming with a 20 MDa limit, the other one providing a 500 MDa. Obviously, they are both designed for different ranges of molecular weight and exhibit better separation quality for their designated gamut. When plotting modal values of different polymer standards against their elution volume or retention time, a clear shift can be observed, following a distinct retardation pattern. The separation process works the

better, the wider these modal values will spread or the better they are distinguishable. Since this method relies entirely on relativity, the absolute retention time values play just a minor role. For the purpose of interpolation, there are two options viable. The first one is a complex curve fit, that captures the exact calibration trend as precise as possible. The second one is a linear or log-linear interpolation between individual calibration points. The range of global validity lies inbetween 20 and 1 MDa. For the point-to-point correlation, this eased interpolation may only be applied within the according interval.

Figure 43: Two exemplary separation columns with different specifications by Agilent Technologies. (Agilent, 2013)

8.8.4.2 20 MDa Exclusion Limit

For the choice on which separation column to use, three distinct column set-ups where tested. The first one implied a single 20 MDa separation column, the second one a sole 500 MDa column and the third one a serial circuit of first the 20 MDa followed by the 500 MDa separation item. Scenario 1 showed poor separation quality, especially in the higher molecular weight regions. The slope of the interpolation is close to zero and significantly diverging from the linear curve fit at smaller molecular masses. This renders column 1 most suitable for the calibration of the lower molecular weight section, including the 1, 2.5 and 6 MDa sample.

8.8.4.3 500 MDa Exclusion Limit

Comparing it with column configuration 2 and 3, shows, that these scenarios show better resolution at higher molecular weights. The calibration anchors show a better spread and higher differences for discriminability. Both systems exhibit approximately the same separation performance. Following the rule of highest simplicity, involves choosing the 2nd configuration with just a plain 500 MDa column. The serial installment with the second column yields similar results but most likely involves higher degrees of interactions effects and blurring non-predictability due to the intricacy of assigning certain effects with an individual column. Thus, the 6, 10 and 20 MDa section, shall be calibrated and interpolated with a single 500 MDa column.

8.8.4.4 Non-Linearities

All three column set-ups, neither linearly correlated, nor logarithmic linearly calibrated, show a straight and proper fit. The separation mechnism does not work linearly. The are some kinds of non-linearities involved in the usage of SEC columns, especially at elevated molecular weights. This non-ideal effects renders calibration with industrial polymer solution even more problematic. The highlighted problems are tried to be captured and overcome in the trend fitting process.

8.9 Validity of Application

The entire chromatographic measurement technique hinges on the question of validity and repeatability. Sample sets of the same composition have to yield identical or at least similar

results. Sequences of different concentration, molecular weight or flow rates must move in the same framework of values and act similarly in order to be comparable. This is the prerequisite for the detection of molecular weight alterations. The relative standard deviation for each concentration sequence can be utilized as quality benchmark for the measurement. Previous experimental verifications showed a lower relative standard deviation for the brine peak (0.5 – 2 %) than for the polymer peak (3 – 9 %). Hence, it can be assumed that the brine peak is more robust in repeated experiments. This property can be used for correction treatments on possible preparation errors. It is also important to validate that different numbers of molecular mass end groups do not contribute to absorption behavior and consequently that the number of monomer units is proportional to the area below the diode array signal. Absorption strength at distinct concentration values shows no direct dependence on molecular weight, but a strong linear trend over the defined range. The consistency of this behavior proves that total absorption is a function of monomer units in solution and independent of molecular mass. Calibration development over time is sufficiently stable and exhibits only minor and neglectable variations.

Validity and repeatability is therefor proven for the given conditions and the defined field of operation. Each new set of analytes demands an individual correlation environment and a proper calibration fit with repeatability corrections. The quality of high performance liquid chromatographic measurements for this kind of experiment conditions is far from being ideal, because the whole system is operated at the very edge of its functionality involving far ultraviolet light, low pumping rates and very high viscosity of fluid samples. Nevertheless, the system is operable and yields sufficiently accurate data for the proof or rebuttal of previously defined hypotheses.

9 Secondary Methodological Objectives

Besides the main research objective and the focus on mechanical degradation, a few minor, secondary effects can be examined, related to the chromatographic measurement method.

9.1 Objective II: Automation of Chromatographic Analysis

Agilents proprietary software Chemstation is unwieldily and not designed for the kind of experiments intended for this stage of the project. The tradition of exporting data from Chemstation to an universal data format, a technique established in previous experiments, shall be carried on for this project. Preceding work on the high performance liquid chromatograph was utterly tedious due to the manual export of every individual sample and time consuming preparation and correction work. This data conditioning and preparation procedure was to that very moment entirely conducted by hand and devoured tremendous amounts of time and capacity, that could be used otherwise. The first objective was therefor to establish an easy, automatized way of exporting, conditioning and correcting multiple sample sequences simultaneously, systematically and accurately. The product of these efforts shall yield an easy workflow for handy data treatment in order to enable the fast and precise examination of polymer effects.

9.2 Objective III: Polymer Stability and Reproducibility

The first minor effect, that shall be investigated, is the stability of polymer samples and the repeatability of HPLC measurements. C. Sledz established a configuration and measurement method on the high performance liquid chromatograph, that enables the examination of heavy weight polymer solutions. The objective in this area is to proof the feasibility of his configuration and to ensure applicability on heavy weight polymer solutions. This shall be done by reproducing former findings within the toolset of proposed configurations. The second target is the comparison of original measurements with reproduced ones, in order to understand whether the 6 month storage did somehow alter the polymer samples or not. If the result is negative, they are considered chemically stable and time insensitive with regard to prevailing conditions. If alterations were measurable, they shall be described and discussed in detail.

9.3 Objective IV: Detectability of MWD Changes

The second theory, that has to be proven, is the assumption, that mechanical degradation is visible in the molecular weight distribution and measurable via a combination of size exclusion and diode array detection. This is a crucial issue, because without this means of distinguishability, degradation examination is solely limited to core flooding experiments. Preceding research within the OMV polymer project, prior to this master thesis, tried to capture changes in molecular weight concentrations, but the system turned out to be improper for that purpose. The application of 20 MDa FLOPAAM 3630 polymer solution diluted to a concentration of 1000 ppm in combination with 2000 mD Nordhorn cores, resulted in characteristic molecular weight distribution curves that couldn't be entirely resolved by the HPLC. The required resolution to distinguish an alteration in the distribution curve was too low. Although it was possible to observe the degradation process in an idealized capillary tube experiment, the Nordhorn flooding experiments did not yield usable results. In order to transfer the observability of degradation processes from capillary tube to core flooding experiments, a new configuration of the flooding system shall be established. For that reason, lower permeable Berea sandstone plugs shall be used in combination with low concentration

10 MDa FLOPAAM 3330 S solution. This denser and less viscous system is considered to lie within the observability range of the high performance liquid chromatograph. A positive result shall verify the assumption. A negative one entails the search for a different and more suitable system.

9.4 Objective V-a: Temperature Effects on HPLC Measurements

The following two subsections shall investigate the effects of changed parameters on the quality of HPLC measurements. The first one examines the response of diode array detection signals to changed temperature effects. If there is any difference in applied column temperature, it shall be described and discussed in order to obtain an ideal temperature recommendation.

9.5 Objective V-b: Rate Effects on HPLC Measurements

The second question deals with the effect of different flow rates on HPLC measurements. The objective of the experimental setup is to increase the speed of measurements and to decrease the overall duration needed for a set of samples. Previous measurements required several days up to one or two weeks of run-time to be completed, which is unpractical and inefficient. By speeding up the measurement process, the quality of the diode array signal will suffer, implying more fluctuations and heavily distorted baselines with much more unsteadiness and tilt. The sought-for aim is a well balanced compromise between signal quality and sequence duration.

9.6 Objective VI: Degradation due to Pumping Equipment

The last objective shall take a detailed look on a commonly assumed simplification in core flooding experiments. Major scientist, involved in polymer flooding research, presume that injection and production facilities do not harm the fresh polymer solution. They suggest, that mechanical degradation is entirely induced inside the reservoir by the porous rock system. Either they state this assumption directly, like Maerker and Seright (Maerker, 1975) (Seright, 1983) or they imply it indirectly like so many others by simply not mentioning this problem howsoever. Despite the fact that it is important to narrow down the research objectives and to simplify conditions to be able to perform proper examinations, facility degradation is an issue, that mustn't be neglected and shall not be neglected in this piece of research. Different injection and production facilities exhibit the capability of seriously damaging the polymer solution. Due to tight restrictions and relative movement, pumping units, throats and valves are most likely to induce degradation. In order to decide whether injection facilities impart degradation on solutions or not, a part of the injection path shall be removed and scrutinized exemplarily. The unit of choice is an eccentric screw pump or progressive cavity pump used for the mixing job within the polymer generation process. The comparison of fresh polymer solution and pumped solution will show, if degradation and if so, how much degradation can be attributed to this particular piece of pumping equipment.

10 Verification and Falsification Conditions

10.1 Available Analysis Instruments

10.1.1 General Overview on Analysis Methods

The toolset for coping with the imposed questions is split in two parts. The first technique implies different kinds of core flooding experiments and the examination of their apparent viscosity behavior. The second method takes a deeper look on the molecular weight distribution of taken fluid samples and how their characteristic molecular weight distribution changed.

- Method I - Viscosity Analysis
  - Type I-I Analysis: Viscosity Characterization
  - Type I-II Analysis: Apparent Viscosity Losses
  - Type I-III Analysis: Time and Temperature Effects
- Method II - Weight Distribution Analysis
  - Type II-IV Analysis: Time Shift of Maxima
    - Type II-IV-a: Modal Value Comparison
    - Type II-IV-b: Tangent Intersection Comparison
    - Type II-IV-c: Maximum of the Polynomial Fit to the Crest
  - Type II-V Analysis: Curve Flank Comparison
    - Type II-V-a: Flank Tangent Comparison
    - Type II-V-b: Differential Plot

10.1.2 Method I - Viscosity Analysis after Core Flood Experiments

Method I is strongly linked to core flooding experiments, so that a Type I-I analysis is defined as the examination of the apparent viscosity profile for brine and polymer floods of Type I core flooding experiments. Method I-II analysis is associated with the comparison of virgin and altered viscosity profiles of Type II flooding experiments. This analysis method shall detect and quantify viscosity losses after polymer reinjection. The last technique of type I examinations, method I-III, is connected to Type III experiments and compares the results of Type III-b experiments to ordinary II-b viscosity profiles, in order to detect and quantify changes in apparent viscosity losses over time and due to temperature effects.

10.1.3 Method II - Molecular Weight Distribution Comparisons

Method II analysis is done via the Agilent high performance liquid chromatograph. Having established an automatized, corrected, calibrated and proven measurement environment, it is possible to examine and compare molecular weight distributions of fluid samples, taken during Type I, II or III coreflooding experiments at various injection rates. Method II-IV compares the shift of polymer peak maxima and the influence of different core flooding injection rates compared to polymer standard maxima. A shift of these peaks indicates an alteration of molecular sizes respectively molecular weights as a whole. Method II-IV can be applied using the ordinary modal value of the distribution, defined as method IV-a, or the more sophisticated tangent intersection point called method II-IV-b. It is also possible to compare the changes of the peak maximum, derived from a polynomial curve fit of the signal crest, being called method II-IV-c. The last technique, method II-V, refines the practice

of molecular weight comparison by focusing on the flanks of the distribution. A change in either the left flank, indicating larger molecules, or the right flank, affecting the smaller chains, gives evidence about the composition or the alteration in composition of compared polymer samples. Here again exist subgroups, with method II-V-a using the tangents fitted to the inflection points of the flanks as a means of comparison and method II-V-b, focusing on the differential plot of diode array signals.

10.2 Primary Objective I - Thesis Core

The primary task of this master thesis is to investigate the title issue and to finally verify or falsify the previously defined working hypotheses. In order to decide whether of these theses are correct or wrong must be determined within the defined terminology and methodology.

10.2.1 Hypothesis I - Pure Temporary Viscosity Loss

The means for examining the temporary damage hypothesis, is a Type III analysis involving a couple of Type III core flooding experiments. Viscosity loss is considered temporary, when the follow-up III-b experiment shows a viscosity profile, that is anyhow diverging from reference II-b experiments, meaning, that the viscosity loss, observed at a simple reinjection experiment is by any means influenced via the two month storage time or the different temperature regimes. If the stored and tempered samples yield a viscosity curve nearer to Type II-a / III-a undegraded profiles, it must be assumed, that parts of the inflicted viscosity loss, or the entire loss, have been restored. Then, the regained viscosity loss, shall be considered a temporary effect.

10.2.2 Hypothesis I-I and I-II - Unfolding and Entanglement

The difference between Hypothesis I-I and I-II cannot be detected with the applied examination methods. When investigated with a Type IV-II peak comparison analysis, both effects will show the same effect. It does not matter if original polymer unravel or smaller ruptured chains form a larger one. Both processes will yield in an enlargement of hydrodynamic radius, which is es property measured by size exclusion chromatography. Either way, a larger molecule will be detected by the high performance liquid chromatograph. The same is true for Type II and Type III viscosity analysis. Larger molecules will endow the polymer solution with higher viscosity, hence, an elevated apparent viscosity curve is another indicator for larger molecule sizes. At this point, the two sub-theories cannot be distinguished, but it is possible to link them to their mother theory Hypothesis I by a Type II-IV analysis. With this means of peak comparison it can be investigated if viscosity restoration is really connected to chain size growth. When analysis method I-III shows a gain in apparent viscosity and analysis II-IV at the same time an increase in modal chain length, the link between molecular size and apparent viscosity is proven. The distinction between the two minor hyptheses are mentioned in order to give explanations on the effect rather than dividing them here.

10.2.3 Hypothesis II - Pure Permanent Viscosity Loss

The permanent damage theory is the exact opposite of Hypothesis I. If a III-b experiment ends up with a characteristic viscosity profile similar or identical to II-b reference measurements, it shall be presumed, that the core-flooding-induced damage is permanent and caused by either permanent deformation or chain scission. The two processes cannot be distinguished properly because both mechanism lead to smaller molecular chains and a permanent viscosity loss. The applied analysis method is again a Type I-III comparison that simply states if viscosity has been won back or not and a Type II-IV analysis explaining if

molecules did change their size or not. If no viscosity was restored, proved by an identical viscosity profile to II-b experiments and the molecular size is just the same for III-b diode array signals as for II-b signals, it must be presumed that the viscosity and chain size loss is permanent.

10.2.4 Hypothesis II-I and II-II - Chain Scission and Permanent Deformation

If permanent damage has been ascertained, a Type IV analysis shall be performed in order to trace down the source of observed viscosity loss. This analysis method involves the comparison of polymer peaks of different molecular weight distributions. If the according curves are shifted as a whole, indicated by some measure of characteristic behavior, it is proven, that the overall molecular weight or chain size has been reduced. The delay can either be indicated by a change of plain modal values as in IV-a, by a change in maxima, being defined as the intersection point of flank tangents according to IV-b or a change in the maximum of a polynomial fit to the crest as in IV-c methods. All three analysis methods shall be applied and compared in order to crosscheck consistency and pick the method with highest expressiveness in this matter. As previously mentioned it is again not possible to distinguish between permanent deformation and chain scission. What is possible to asses is the fact that molecular size and viscosity loss is connected to each other. A permanent viscosity loss is equal to loss in modal molecular size, if Hypothesis II-I and II-II can be declared verified. The preferred theory about permanent visocity loss in the literature is of course chain scission. Therefore, if size stagnation can be observed during IV-II analysis, theory II-I, chain scission shall be declared proven. Permanent deformation shall just be mentioned as alternative explanation model.

10.2.5 Hypothesis II-I-a - Even Chain Scission

If chain scission has been detected in the polymer solution, a deeper analysis method must be applied. In order to do that, method V was applied to grant deeper insights into the exact alteration of the molecular weight distribution. Within the Hypothesis II-I scenario, induced damage is considered permanent and hails from chain scission. It is possible, that the rupture process, turning larger polymer chains from the original distribution (Type I experiment) into smaller chains (Type II-b experiment), exhibits some kind of preference. This is not the case, if the characteristic shape of compared molecular weight distributions does not change. It means on the other hand, that all kinds of polymer chains are equally subjected to scission processes. This can be proven via a Type V-a or V-b analysis. Type V-a indicates uniform chain rupture, if the key values for the construction of inflection point tangents, fitted to both flanks, do not change significantly. Type V-b analysis is a proof for this Hypothesis, when the according differential plots show no major deviations been investigated samples.

10.2.6 Hypothesis II-I-b - Preferred Chain Scission

If there is some trend notable in Type V analysis methods, Hypothesis II-I-b must be declared correct. Both, the differential plot and the inflection point tangents, will yield a positive result, when a group of molecular sizes is preferentially degraded. As proposed by several researchers, these will most probably be the larger molecular chains of the solution. They provide more contact points and more vulnerable surface, where criticial forces and stresses can start the rupture process. In addition to that, larger molecules exhibit a larger momentum of intertia, which sets the whole molecule under higher tension when subjected

to bending or stretching. These aggravated stresses can lead to earlier and more likely chain breakages.

10.2.7 Hypothesis III - Mixed Viscosity Losses

In order to varify or falsify Hypothesis III, it is again necessary to conduct I-III viscosity analyses and II-IV peak comparisons. Opposite to theories I or II, the investigates apparent viscosities and molecular sizes will not match the results of either experiment I for full restoration or experiment II for permanent damage. The result of both analysis methods will lie inbetween the two extremes, meaning that a certain amount of viscosity / chain size has been healed and another part stays untouched and retains the inflicted damage. When Hypothesis III is correct, the major objective is to quantify the relation between restartable and permanent losses.

10.3 Secondary Objectives

Chronologically speaking, and not weighted by impact, the secondary or minor objectives of this master thesis, have to be examined and proven first, in order to verify or falsify the main working hypothesis of the above section.

10.3.1 Objective II - Conditioning and Correction Workflow

The first minor objective was to establish an automatized and easy workflow of data treatment. The proof, that these automatically generated corrections are accurate and true is easily provided. If the automatized process works properly, the results must be identical to hand-made data conditioning and similar to the built-in Chemstation results. If this is not the case, trouble-shooting and code revising must be the consequence. Identical results are taken as adequate proof for data conditioning objective II.

10.3.2 Objective III - Reproduction and Solution Stability

The proof for polymer stability and the proper HPLC configuration is given by simply reconducting earlier chromatographic measurements with earlier results by C. Sledz. The samples have been stored 6 months under atmospheric and room temperature conditions. Both, the HPLC configuration and sample stability, is assumed proven, if the resulting chromatograms are congruent with the early ones by C. Sledz. This is a necessary prerequisite for further usage of the established chromatographic framework and to improve the measurement process and finally apply them to the investigation of above mentioned working hypotheses.

10.3.3 Objective IV - Peak Retention Time Shift

Objective IV is considered fulfilled, when a time shift of polymer peaks is notable in a Method II-IV analysis. This has not been achieved yet by previous stages of the OMV polymer project, namely C. Sledz's work, due to the chosen core flooding system. The new, denser system should bring the expected time shift for chain ruptured solutions. This target shall be positively assessed, when the pattern already observed in capillary tube experiments, can be reproduced in core flooding experiments and thus in Method I molecular weight distribution examinations.

10.3.4 Objective V - Configuration Optimization

Temperature and Rate effects within this examination module shall simply be investigated, compared and then described. The favored outcome of this objective is an explanation for the observed configuration effects and a recommendation of optimum working conditions for further implementation in OMV projects.

10.3.5 Objective VI - Equipment Induced Mechanical Degradation

The last objective, which is part of this master thesis, is simultaneously the first and foremost, when it comes to the description and examination of polymer flooding operations. It is an exemplary check, if the assumption, made throughout the history of mechanical degradation research, holds true, namely the unaffectedness of polymer solutions, when in contact with pumping equipment. The experimental setup for that is easy. A progressive cavity pump, Type Nemo 4NE20 shall be filled with out-of-the-field polymer. This acrylamide solution shall be pumped from the storage tank to a deposit container then. The first experiment features just one pump-throughput of the polymer. The second experiment is realized by connecting the storage tank with the exit hose of the pump and circulating polymer solution for up to 2.5 hours. Liquid samples are taken after each rate for experiment 1 or after particular time intervals for experiment 2. They are examined with chromatographic measurements afterwards. A plain Type II-IV analysis is conducted comparing virgin polymer solution to pump-affected samples. If the sample molecular weight distribution is identical to the virgin solution, the assumption, that injection equipment does not induce damage on the polymer batches, is considered true. If degradation is detectable via a time shift of maxima values, mechanical degradation is proven to be inflicted by pumping facilities too and further examinations are advisable and shall be recommended with regard to this issue.

11 Coreflooding Analysis and Results

11.1 System Characterization - Pressure Performance

11.1.1 Schematic Water Flooding Behavior

A polymer flooding experiment of Type I typically starts with a rock characterization. The core plug's metrics have already been taken. Porosity and gas permeability is known at that point of the experimental workflow. In order to attain brine permeability, a water flooding experiment has to be performed. This water permeability gives evidence on how Newtonian fluids like salt water behave inside the core and give a rough glimpse on the core's capability to conduct liquids. Mostly these experiments will yield brine permeabilities of 90

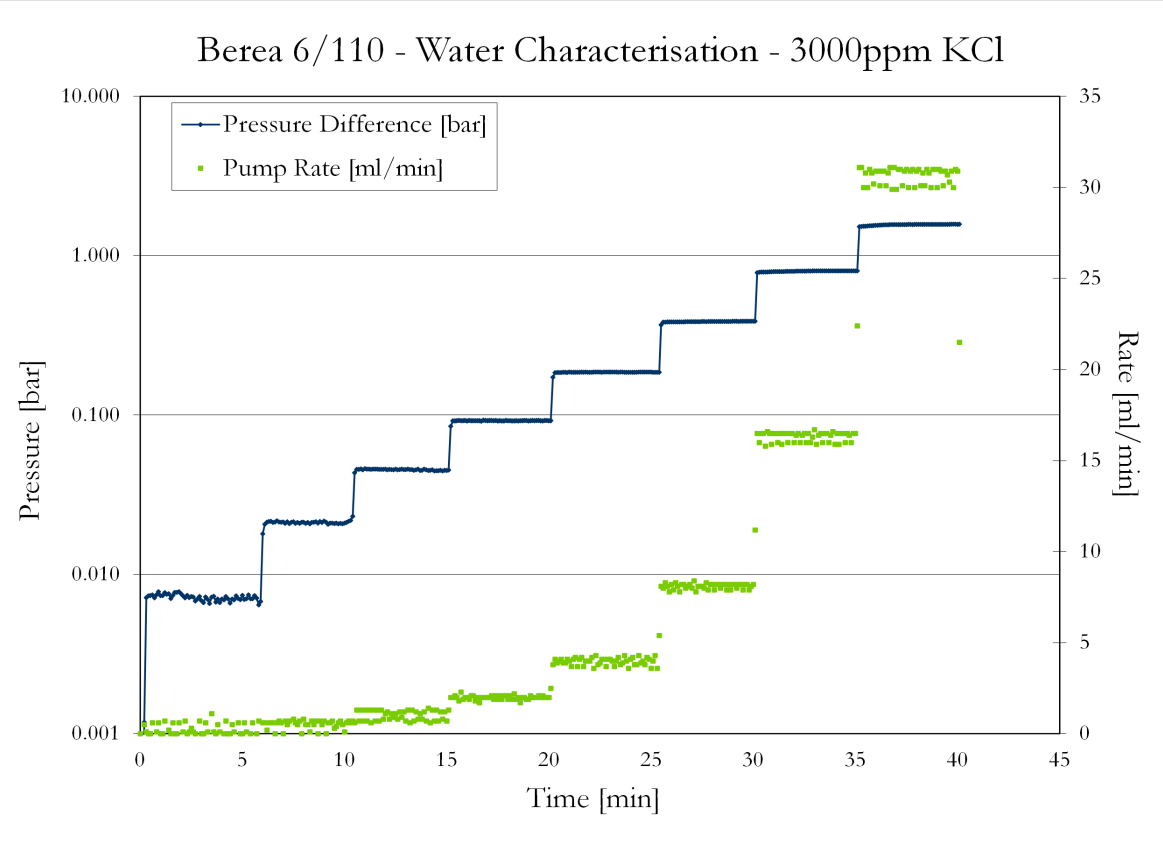

Figure 44: Water Flooding Experiment Berea 6-110. Pressure and Rate versus Time Plot.

to 60 percent of the measured gas permeability. The result of this kind of experiment is a stepwise increase of pressure difference due to elevated flow rates. Pressure drops and rates are linearly linked and can be used to compute brine permeability μ_b via a rearrangement of Darcys law. Figure 44 illustrates pressure and rate steps for an exemplary Berea 6-110 water characterization.

11.1.2 Schematic Polymer Flooding Behavior

By flooding the core with polymer solution and recording pressure data, it is possible to compute apparent viscosities according to equation 6. The fluid's viscosity behavior shows, as expected, a shear thickening and then shear thinning behavior, which has been stated typical for polymer floods known from the literature section. The first experiment, performed on core Berea 6-108, was destined to involve a FLOOPAM 3630 10MDa polymer solution

diluted to a target concentration of 500 ppm. This first test run had to be aborted due to high pressures encountered at rates of 16 ml/min peaking up to over 35 bar. The Plexiglas liquid columns wouldnt withstand higher pressures at further elevated flow rates and the striven for overcoming of the shear-thickening to shear-thinning translation hasn't been reached yet. 16 ml/min turned out to be not sufficiently high for that purpose. The experiment still operated under completely shear thickening conditions.

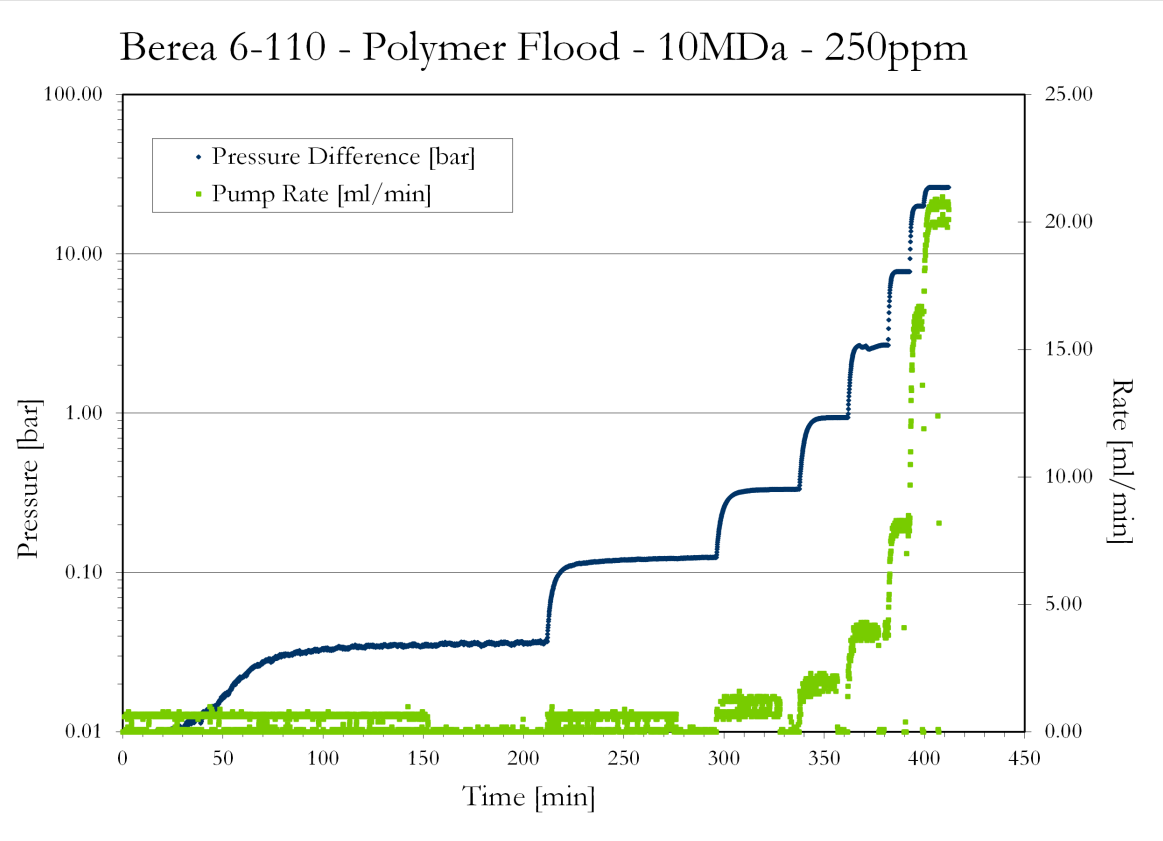

Figure 45: Pressure behavior of a polymer flood Type I through core Berea 6-110 with a 10 MDa partially hydrolyzed polyacrylamide solution with 250 ppm concentration. Pressure and Rate versus Time Plot

In order to extend the range of observability, it was decided to further dilute the 10 MDa hydrolyzed polyacrylamide solution to a target concentration of 250 ppm. This measure enabled the experimental setup to reach flow rates of 20 ml/min or even more and overstepped the shear thinning inversion point associated with mechanical degradation as required. The experimental setup of combining 356 - 443 mD cores with 10 MDa 250ppm HPAM solution proved to be suitable for the targeted issue and was maintained over the whole lifetime of the polymer sub-project.

Figure 45 and figure 46 show pressure plots of a typical core flooding experiment featuring core Berea 6-110 and standardized 10 MDa FLOPAAM 3630 polymer at a concentration of 250 ppm. One plot pictures pressure development over time, the other pressure development with regard to cumulative volume in order to get a better glimpse on pressures at higher flow rates. Both plots illustrate very neatly how pressure is building up, when a higher flow rate kicks in. The pressure buildup phase exhibits non-linear behavior and takes the longest for low core flooding rates. High flow rates entail successively shorter pressure readings due to the high throughput of polymer. This is a great challenge for the sampling procedure and

the previous experiment scheduling. It must be secured that the short duration of a certain rate results in proper and equilibrated pressure niveaus and usable polymer samples. Despite these difficulties, pressure readings turned out to be very stable over a distinct flow rate. Core flooding rates and the matching pressure differences aren't linearly coupled anymore as in previously discussed Newtonian brine flooding case. The relationship between these

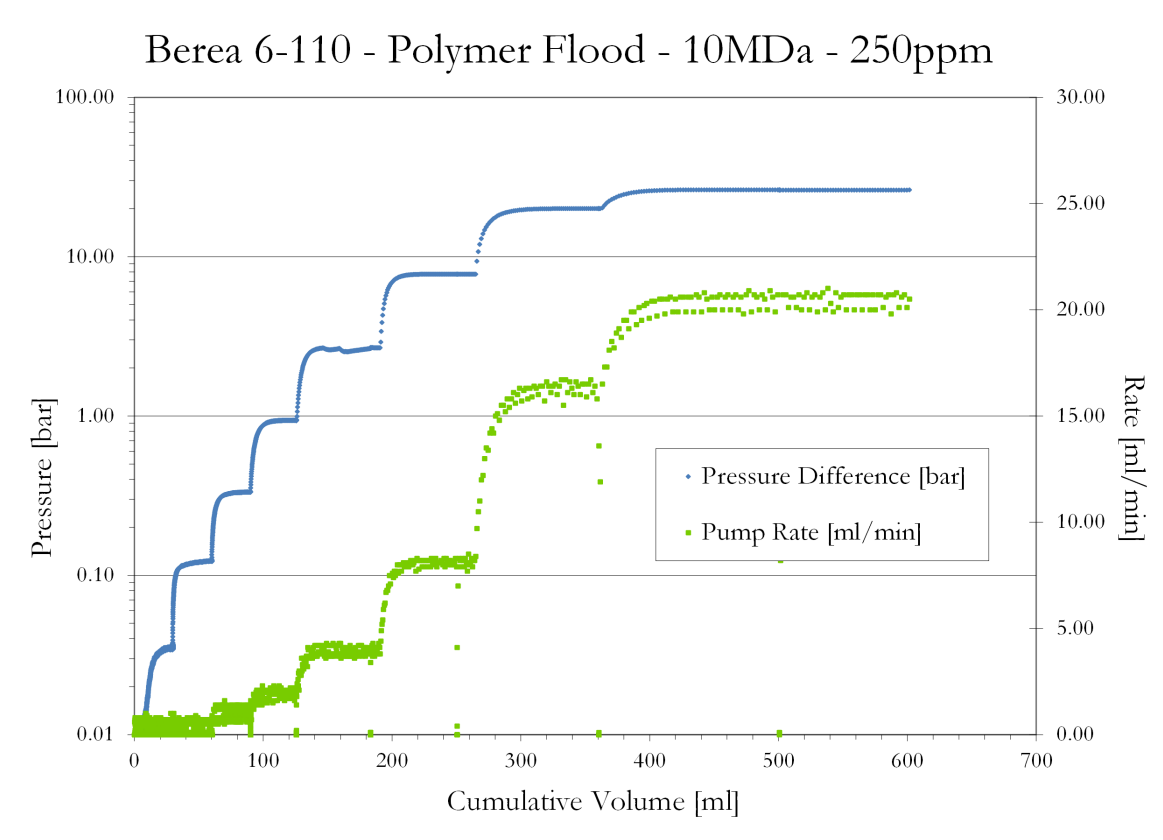

Figure 46: Pressure behavior of a polymer flood Type I through core Berea 6-110 with a 10 MDa partially hydrolyzed polyacrylamide solution with 250 ppm concentration. Pressure and Rate versus Cumulative Volume Plot

two parameters are somehow otherwise proportionally connected and shall be captured with the apparent viscosity approach. This will be discussed in more detail in the later viscosity analysis section.

11.1.3 Schematic Chase Water Behavior

The purpose of chase water flooding is a re-characterization of the system. Figure 47 shows the rate dependent pressure steps of the specific experimental setup. The flow line is re-switched to the potassium chloride reservoir and directed to a straight brine flush of the polymer affect core plug. This re-characterization flood has a slightly different time dependent configuration than a simple brine flood. Opposite to equal time intervals for the first brine characterization, an elevation of flow rate must await a complete pressure stabilization till the entire core is uniformly affected by induced changes. Especially for the first rate this can take a tremendous amount of time due to a combination of tediously low flooding rates and a complete replacement of polymer by brine. Most commonly this duration will span over 60 to 90 minutes of brine flooding. The second rate requires mostly 30 minutes. All other rates will be done in 10 to 15 minutes. A most prevalent phenomenon is a sharp

increase of pressure at a new rate. The introduced salt water is bestowed with a more energetic level and is able to mobilize another increment of adsorbed polymer. Nevertheless,

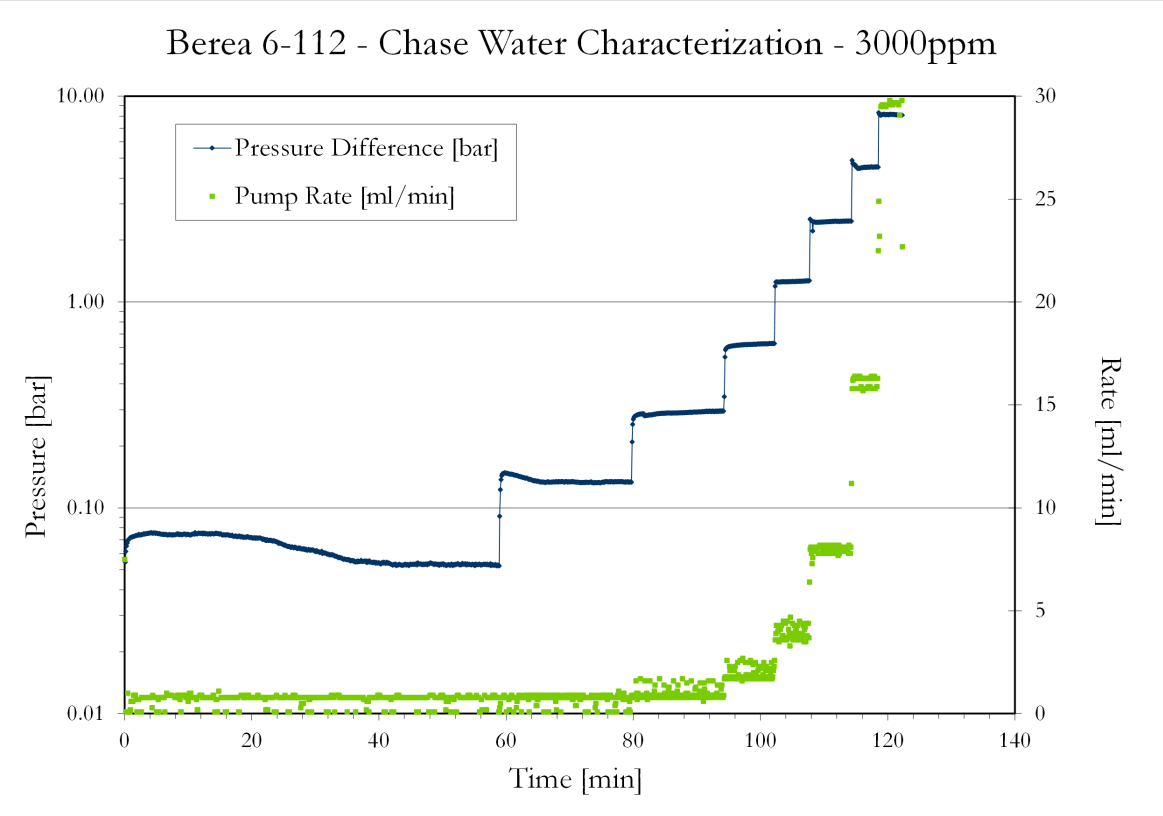

Figure 47: Chase Water Experiment Berea 6-112. Pressure and Rate versus Time Plot

the greater part of adsorbed molecules will remain inside the core, hindering recently introduced liquids to wander through the matrix. This effect is expressed as a drastically reduced brine permeability and can also be captured by the previously introduced residual resistance factor. The reduction of brine permeability can be as high as 70 % of the original property and beyond. The below table provised examplary residual resistance factors for different kinds of core flooding experiments. Virign Type I experiments show a greater reduction in brine permeability as reinjection II and storage III cores. The general trend is a growing permeability loss at higher flow rates.

Flow Rate	Type I Exp.	Type II Exp.	Type III Low	Type III High
[ml/min]	[x]	[x]	[x]	[x]
0.5	4.98	2.49	2.99	2.70
1	5.39	2.68	3.27	2.94
2	5.84	2.97	3.59	3.17
4	5.89	3.26	3.89	3.41
8	5.74	3.56	4.18	3.64
16	5.25	3.72	4.33	3.74
20	5.05	3.76	4.41	3.86

Table 10: Residual Resistance Factors for different kinds of Experiments.

11.2 Rheological System Characterization - Apparent Viscosity Profiles

11.2.1 Type I Analysis - Virgin Polymer Solution Experiments

As discussed in the previous section, there isn't anymore a linear linkage between flow rate and emerging pressures, when polymer is pumped through a porous system. The tool to illustrate this non-linearity is apparent viscosity or for higher expressiveness, characteristic apparent viscosity profiles for a given experimental setup. The first and simplest configuration is a Type I core flooding experiment. Figure 48 shows how 10 MDa polyacrylamide solutions with a concentration of 250 ppm behave in a porous medium with permeabilities in-between 356 and 443 mD. The chosen solution delivers, as expected, a shear thickening trend with a shear thinning trend reverse. The lowest rates of 0.2 ml/min or 2 m/day yield an apparent viscosity of roughly 10 mPas. Peak viscosity values are reached at the rate of

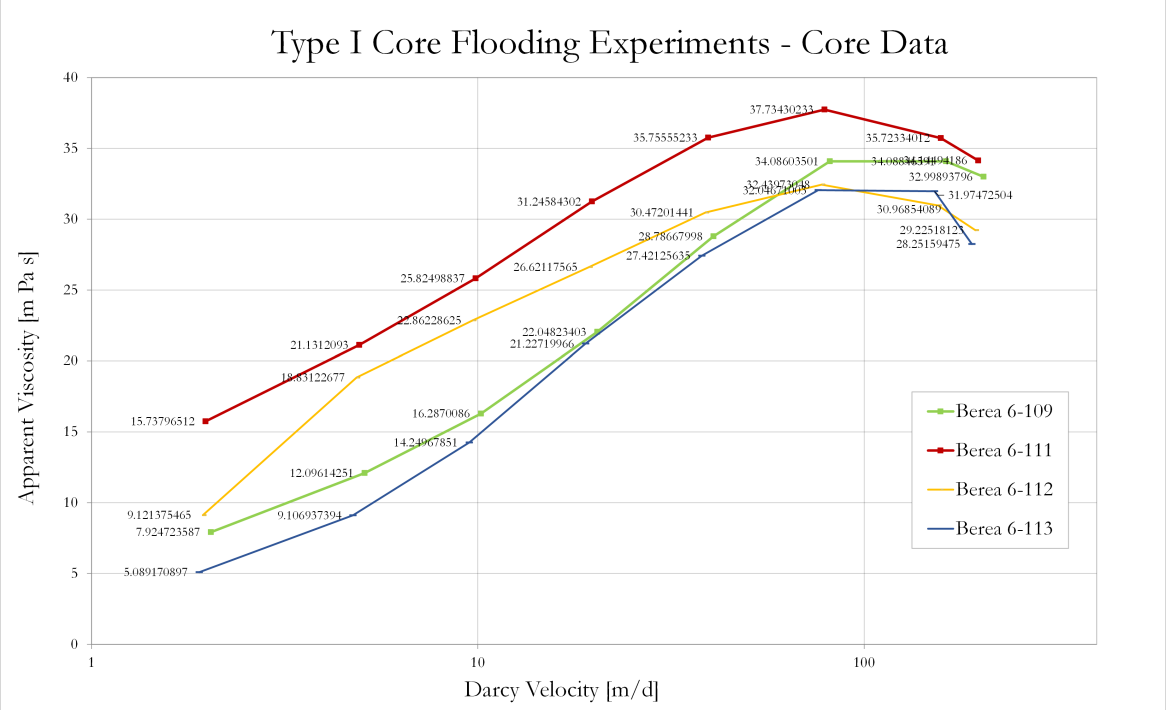

Figure 48: Apparent Viscosity Profile for Type I Experiments with individual Cores. Apparent Viscosity vs Darcy Velocity Plot. The characteristic curves for all four cores illustrates perfectly the expected traits, starting with a shear thickening behavior which is inverted to a shear shinning trend at higher rates.

8 ml/min or 76 m/d with a climax value of approximately 35 mPas. The inversion point between shear thickening and shear thinning behavior is marked by 4 ml/min or 38 m/d. Figure 49 is a summation of individual cores from figure 48, distilling the general trend out of specific samples by averaging corresponding viscosity levels and providing according standard deviations. In addition to that, a table is presented for numeric verification of the qualitative trend. What is striking when comparing individual cores in figure 48 or averaged values with standard deviations in figure 49 respectively the below table, is the fact, that individual core-fluid systems exhibit a fairly strong spread in viscosity profiles. Such a strong divergence seems to be entirely random because neither rock metrics nor other core properties indicate such a spread in viscous behavior. It can be taken for granted that this effect does not origin from the generation of polymer solution, because larger batches of identical solution were taken for multiple experiments and even if this wouldn't have been

the case, preparation recommendations were meticulously followed and executed with highest precision. This exclusion suggest that the wide spread of apparent viscosity is based on one particular or a combination of several rock property. More detailed scrutiny of available rock data did not result in a better explanation for the observed phenomenon.

Flow Rate	Av. Viscosity	Stan. Deviation	Lowest Value	Highest Value
[ml/min]	[mPas]	[x]	[mPas]	[mPas]
1.963	9.468	4.509	5.089	15.738
4.908	15.291	5.630	9.107	21.131
9.816	19.806	5.441	14.250	25.825
19.632	25.286	4.628	21.227	31.246
39.264	30.609	3.651	27.421	35.756
78.528	34.077	2.593	32.047	37.734
157.057	33.189	2.132	30.969	35.723
196.321	31.155	2.857	28.252	35.736

Table 11: Averaged Apparent Viscosity - Type I Experiment

Neither the first presumption, that air permeability or bulk porosity was responsible, nor the second theory that rock metrics, like length or diameter had an influence on the measured apparent viscosity, turned out to be true. Neither property showed a trend with regard to the spread of viscosity profiles. For that reason, no uni-causal or simple explanation

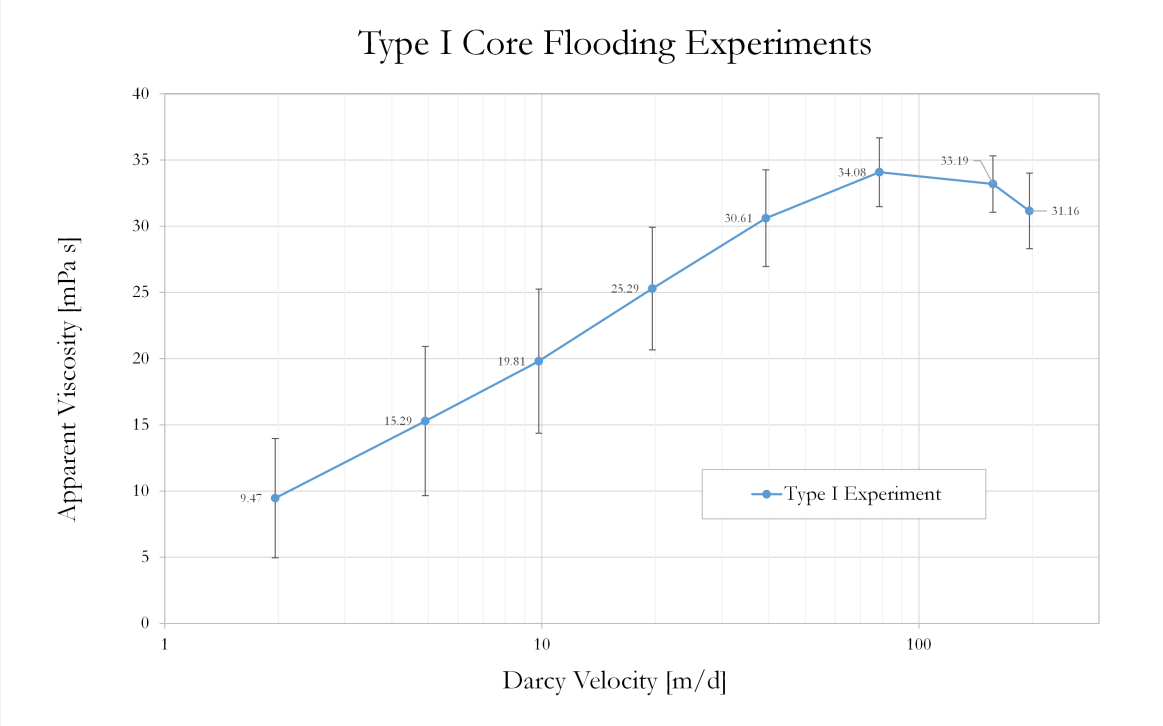

Figure 49: Averaged Type I Apparent Viscosity Profile with Error Bars

can be provided, illuminating the huge difference in viscosity profiles for similar rock-fluid systems. The most probable explanation is a broader divergence in the porous system of individual rock cores with largely deviating sorting and different pore size distributions. These microscopic changes were no part of the ongoing investigations and must remain in the dark for now. A second explanation would be the statistical unpredictability of rock-fluid

interaction. The probability of interactions between polymer chains and rock grains is not known to us, nor is the probability of deformation respectively degradation during such an interaction and the kind of alteration leading to viscosity losses. In addition to that, the real composition of the polymer solution is not exactly known. Irregularities in the polymer chain distribution or artifacts from the polymerization process could be the source of the viscosity spread too. Be that as it may, the framework for repeatability and consistency exhibits a medium degree of uncertainty due to this spread. Standard deviation ranges in-between 2 and 5 which must be declared as medium high for this system. The results are on the edge of expressiveness.

11.2.2 Type II Analysis - Reinjection Polymer Experiments

The second kind of viscosity profiles is caused by Type II experiments as presented in figure 50. The blue lines, belonging to cores Berea 6-109, 6-110, 6-112 and 6-113 indicate the first phase of this experiment Type II-a, which is identical to plain Type I core floods. The dis-

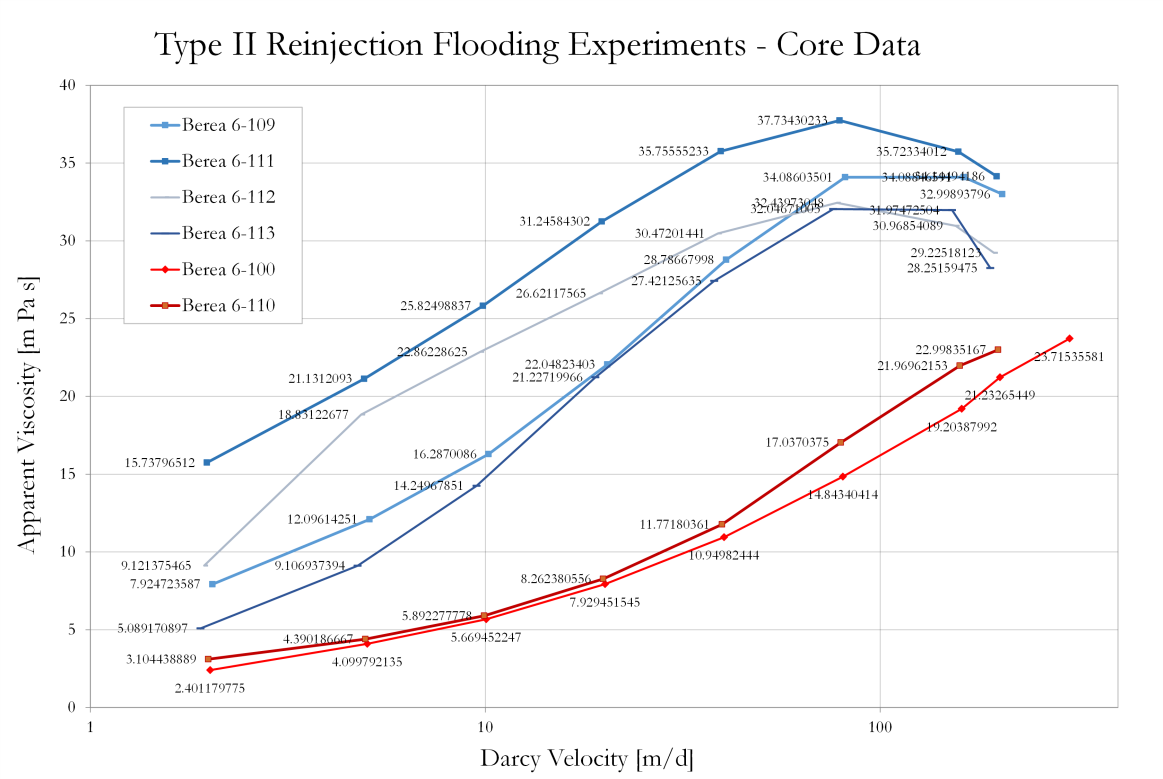

Figure 50: Apparent Viscosity Profiles for Type II Experiments - Core Data. Cores Berea 6-109, 6-111, 6-112 and 6-113 are Type I or Type II-a experiments. Cores Berea 6-100 and 6-110 were used for Type II-b reinjection experiments. Apparent viscosity curves are much lower for reinjection experiments but exhibit the same trend.

tinct cores on which Type II-b reinjection experiments have been performed are Berea 6-100 and Berea 6-110. Both polymer samples show significantly reduced apparent viscosity during the second core flood. Figure 51 shows again averaged viscosity properties for the Type II experimental setup including standard deviations as error bars. Due to these narrow error limits, it is obvious that degraded polymer solution behaves much more uniformly than in virgin Type I floods. Especially low rates result in almost identical apparent viscosities. This is most probably due to the loss of elongation viscosity during type II-a experiments. The solution seems to be subjected to alterations that result in a microscopically more uniform

polymer chain distribution. This theory will be discussed in more detail in the chromatographic analysis section. During Type II-a experiments at degrading rates above 8 ml/min, polymer chains will behave more chaotically entailing a lower degree of predictability. This could explain the large divergence of viscosity curves at elevated rates. The viscous regime

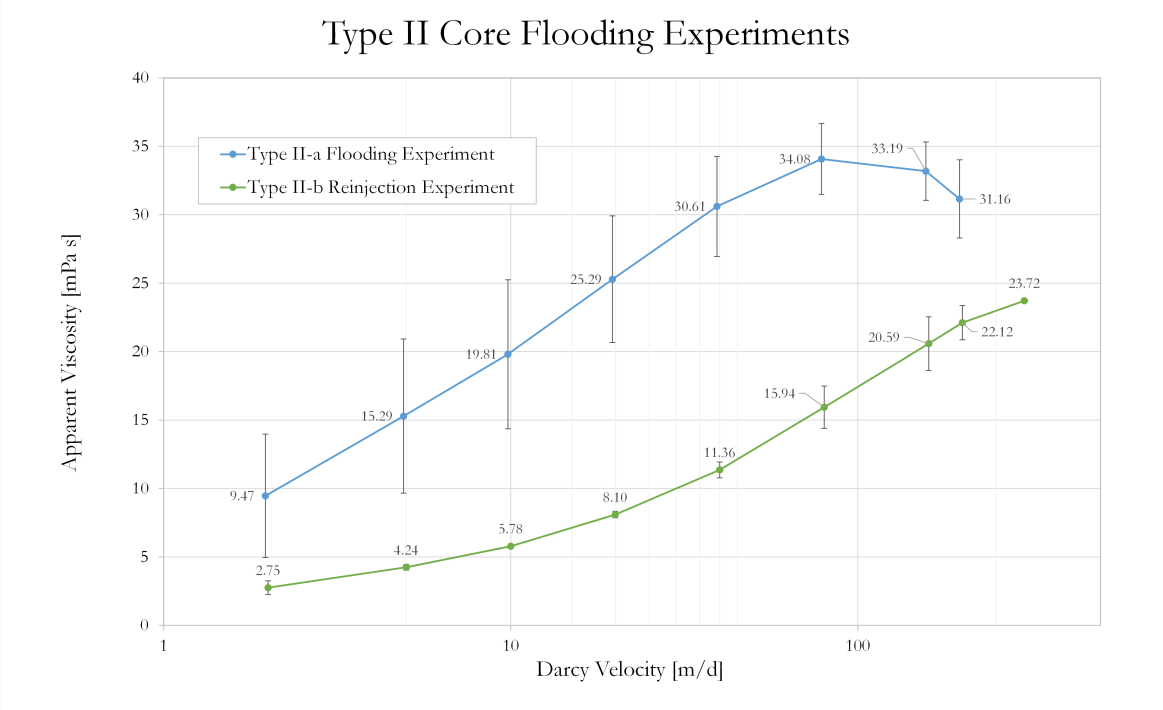

Figure 51: Averaged Type II Apparent Viscosity Profile with Error Bars. The blue lines represents a summation of previously introduced Type I experiments with standard deviations marked by error bars. The green line shows the averaged trend of Type II-b reinjection with error limits.

of Type II experiments is purely shear thickening. Different examination methods and a slight flattening trend at higher rates propose, that the shear thinning inversion point is right ahead, most probably at 35 to 40 ml/min. The comparison of Type II-a and Type II-b profiles shows that they feature roughly the same peculiarity. The difference is that reinjected samples are shifted downwards to lower viscosities and nudged to the right with higher rates necessary to reach the shear thinning are for further degradation.

Flow Rate	Av. Viscosity	Stan. Deviation	Lowest Value	Highest Value
[ml/min]	[mPas]	[x]	[mPas]	[mPas]
2.000	2.753	0.016	2.401	3.104
4.999	4.245	0.041	4.100	4.390
9.999	5.781	0.082	5.669	5.892
19.998	8.096	0.165	7.929	8.262
39.995	11.361	0.330	10.950	11.772
79.991	15.940	0.659	14.843	17.037
159.981	20.587	1.318	19.204	21.970
199.977	22.116	1.648	21.233	22.998

Table 12: Averaged Apparent Viscosity - Type II Experiment

11.2.3 Type III Analysis - Stored and Tempered Polymer Experiments

Averaged Type I and Type II apparent viscosity curves are the reference for Type III analyses. Different III-b viscosity curves with storage conditions at four different temperature levels shall be compared to these and evaluated. Figure 52 shows the entire set of the experimental schedule. The first four blue lines, comprising Berea 6-109, Berea 6-111, Berea 6-112 and Berea 6-113 are Type I respectively II/III-a virgin polymer experiments. The two black viscosity profiles of Berea 6-100 and 6-110 represent reference II-b reinjection experiments. The last four lines are III-b storage experiments with Berea 6-119 being the 22 °C sample, Berea 6-121 the 8 °C sample, Berea 6-123 the 50 °C sample and Berea 25-08 the 80 °C sample. The comparison of Type III experiments is difficult in this plot, but a trend of high temperature samples acting at the upper part of Type II references is still detectable as compared to the low temperature profile ranging in the limits of Type II experiments.

11.2.3.1 Storage Conditions with Lowered Temperature

The first stored sample that was chosen for a Type III experiment was sealed and stored for two months in a refrigerator at 8 °C. The expectation for that experiment was a blank result, yielding an apparent viscosity curve similar to Type II experiments. The two month

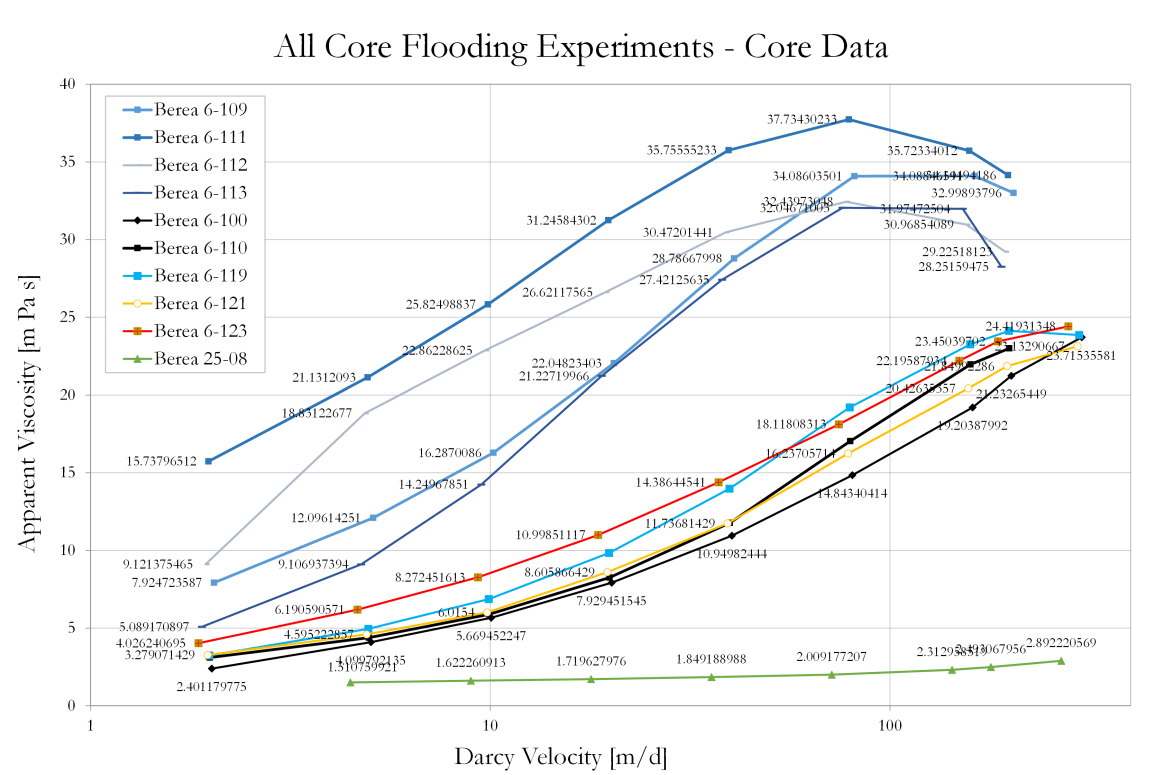

Figure 52: Apparent Viscosity Profiles for Type III Experiments - Core Data.

storage time at such a low temperature most probably won't change the original polymer solution at all. The expected outcome will be similar or identical to a viscosity profile, generated by Type II reinjection core flooding straight after an initial Type II-a core flood. Indeed, the Type III-b experiment at 8 °C storage condition resulted in an apparent viscosity profile that lay perfectly within the narrow margin of Type II-b error bars. Figure 53 shows the performance of core Berea 6-121 used for the target III-b storage experiment. Results matched expectations quite well. Deep temperatures provide a low energy environment in which polymer chains have no longer the inclination to move or change their shape. Neither

an unfolding movement is activated nor a chain entanglement process launched. Molecular strucutre and fluid composition remains the same for all two months. The polymer chains are

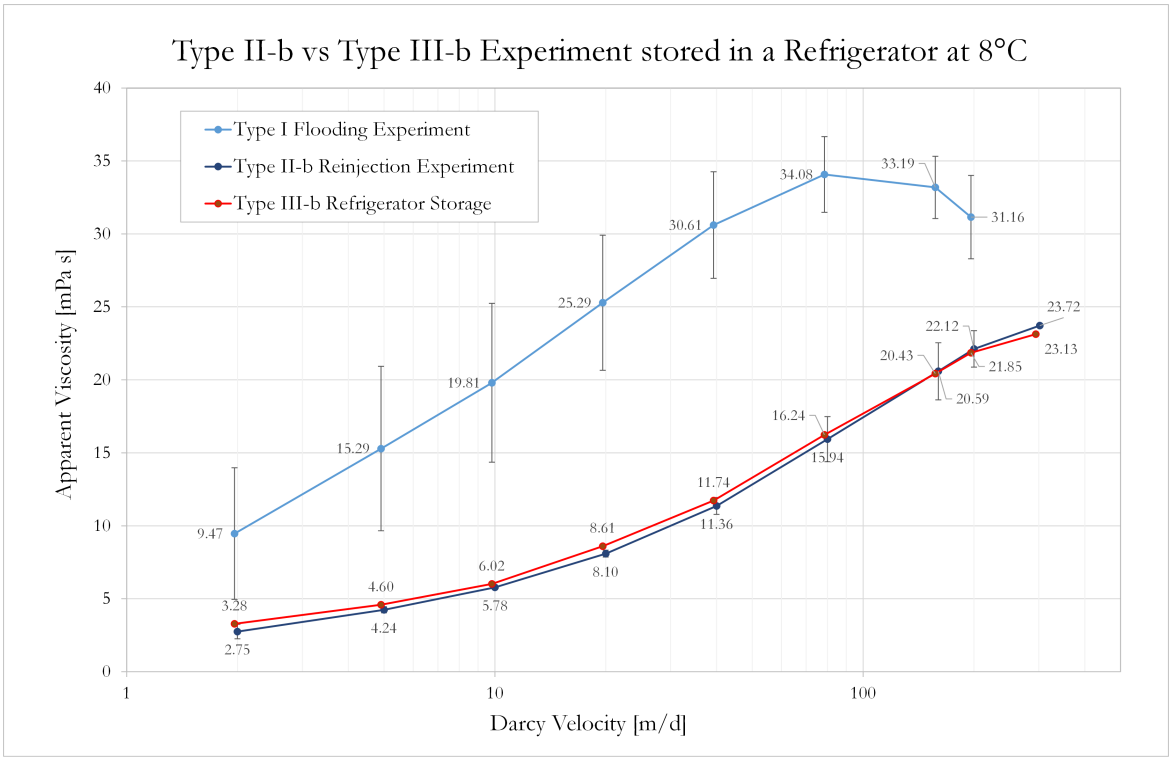

Figure 53: Comparison of Type III 8 °C Storage Apparent Viscosity Profile on Berea 6-121 with Type II-b Reference Profile. No major differences are notable between the two viscosity profiles.

somehow immobilized. The consequence is an almost identical apparent viscosity behavior to Type II-b experiment. The state and structure of the polymer solution is, so to say, preserved.

11.2.3.2 Storage Condition at Room Temperature

The next step shall be an experimental configuration that excludes temperature effects as far as possible and focuses mainly on time effects on the polymer solution during storage. The experiment of choice is a Type III one, involving storage that come close to previously introduced downhole conditions. The reference sample was taken right behind a Type III-a polymer flood and stored at a room temperature of 22 °C in an opaque container. The avoidance of sunlight and the storage temperature come very close to the environment encountered at the wellbore without sunlight and a temperature of 30 °C. Despite this slight change of temperature, conditions shall be assumed as roughly equal and more or less consistent throughout the whole experiment runtime. Due to this maintaining of experimental temperature, it can be assumed that the setup investigates solely time storage effects. This alteration, entirely based on time, is thought to exert viscosity healing on the polymer solution. The previously deformed polymer chains are stored under calm and unchanged conditions for two months. In this time they are free to float in the polymer solution and change their shape without external forces. It is expected that they are able to remember their original form, engraved in their mechanical structure, and strive to restore this shape somehow. This inclination will entail a slow and steady reformation to undue the previously

imparted deformational strain. As individual polymer chains unravel and change their form to partly regain their original structure, the macroscopic viscosity will grow, if a stochastically sufficient number of reshaped entities is reached. The core that was used to be flooded

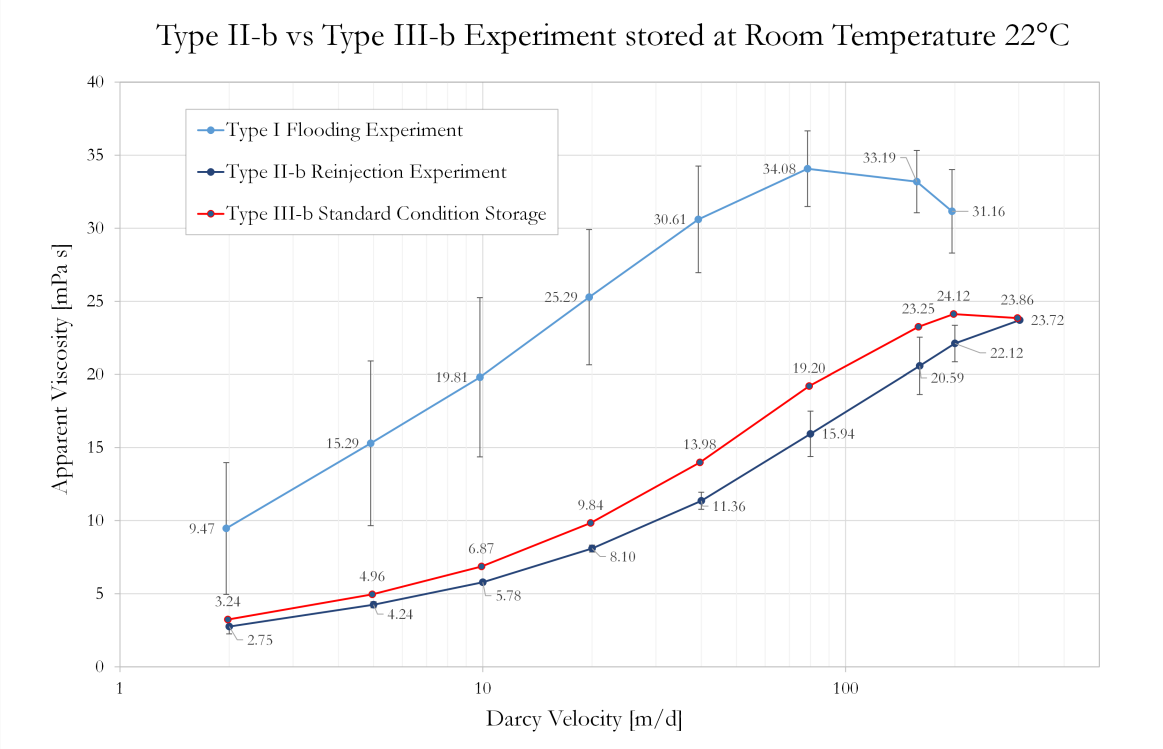

Figure 54: Comparison of Type III 22°C Storage Apparent Viscosity Profile on Berea 6-119 with Type II-b Reference Profile. Berea 6-119 clearly overperforms the II-b reference profile, especially at higher rates.

with Type III-a polymer solution stored at 22 °C was Berea 6-121. The result of this Type III-b experiment is presented in figure 54 and shows, that there was indeed some kind of polymer restoration process active. Individual apparent viscosity values are markedly higher than II-b reference points or values from the low temperature III-b experiment. The viscosity profile for the Berea 6-121 Type III-b polymer solution lies notably outside the error bars of Berea 6-111 and 6-100. The apparent viscosity curve is increased and shows a tendency, even though a slight one, to fresh III-a profiles. A small viscosity regain can be stated for this kind of experiment.

11.2.3.3 Storage Conditions with Elevated Temperatures

Having investigated pure time and lowered temperature effects, it must now be examined what elevated temperatures do to degraded polymer. For this reason a Type III-b was executed on core Berea 6-119 with degraded and stored polymer at 50 °C. Solution that has been stored at elevated temperatures, will most probably yield a different, an elevated viscosity profile. The assumption for this expectation is, that deformed polymer chains will reshape over time, gaining back parts of their initial viscosity enhancing capability. The consequence of this restoration process will be a reduction in viscosity loss. The expectation is, that the viscosity profile for this kind of experiment will show a tendency away from the perfectly degraded II-b curves from Berea 6-110 and 6-111, approaching the fresh polymer apparent viscosities of Type I experiments or Type II-a reinjection floods. The theory behind

that, in more detail, is that polymer chains will regain their shape, when allowed to rest in a solute state. Individual chains are free to unravel and bestow the solution with a higher macroscopic viscosity than a coiled and deformed polymer solution that just underwent a Type II-a experiment. The elevated temperatures are thought to assist the restoration respectively unravelling process. Higher temperatures enforce viscosity healing by endowing them with the ability to move faster or to perform more elaborate actions. By doing so, the natural restoration process gets accelerated and facilitated. The second mechanism, closely related to the speedup of natural reshaping, is thought to be connected to the activation energy, needed to start the unravelling process. Activation energy is defined as the amount of energy, that has to be raised in order to trigger a certain effect, in this case the relaxation of chain deformation. Similar or comparable to other concepts of activation energy, for example, the activation of chemical processes, there will be a bump or hurdle of minimum energy necessary, that must be spent, in order to get the process going. Further supply of

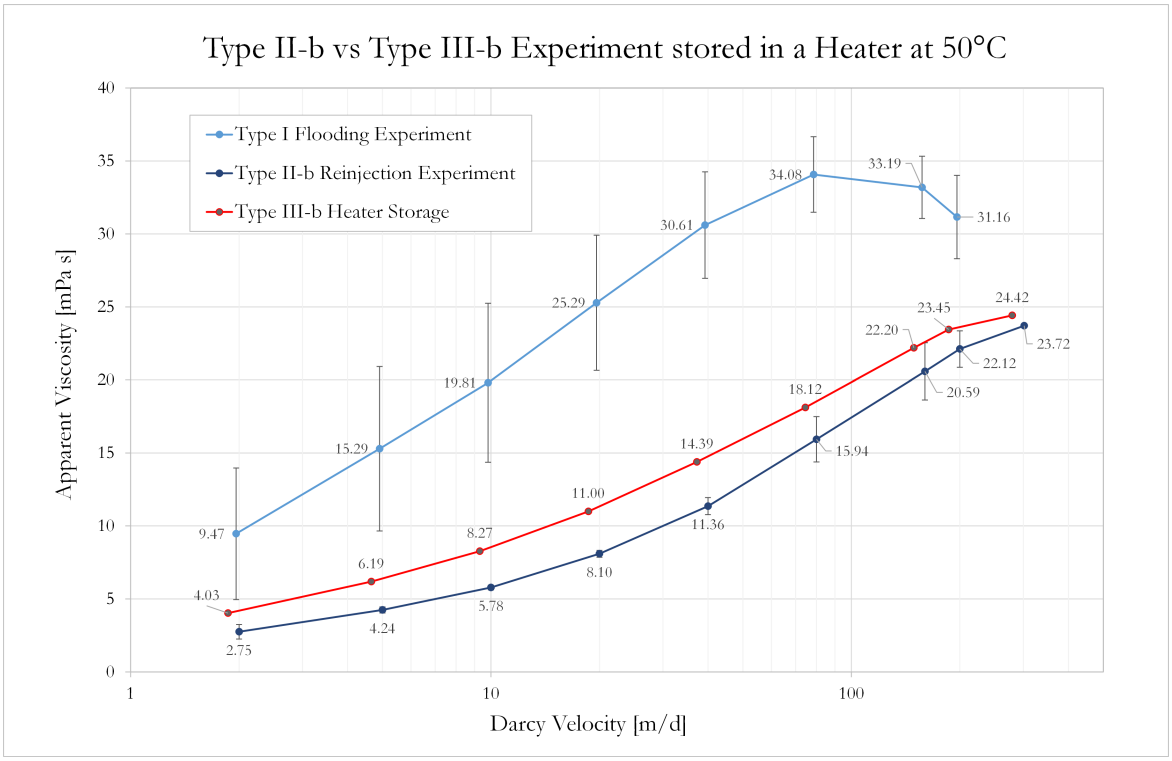

Figure 55: Comparison of Type III 50°C Storage Apparent Viscosity Profile on Berea 6-123 with Type II-b Reference Profile. Berea 6-119 clearly overperforms the II-b reference profile. Compared to Berea 6-119, the 50 °C samples prefers low rates for viscosity healing effects.

energy by elevated heat, helps the polymer chains to overcome the natural activation energy hurdle and start the reformation procedure. The outcome of this process is an apparent viscosity profile as in figure 55. Like the room temperature III-b experiment, the characteristic viscosity profile lies above the II-b curve but shows a slightly different behavior. At low rates, the 50 °C curve outperforms the 22 °C experiment and regains more viscosity than the room temperature sample. Conversely, this trend is inverted at medium and elevated rates. Especially at higher rates, the 50 °C experiment performs worse than the 22 °C with lower apparent viscosity values. At this point it cannot be decided whether this is due to some regeneration effect or due to random spread encountered in Type I experiments. One explanation could again be linked to the polymer chains ability to adapt to certain external circumstances like collision and deformation. A polymer chain that has been deformed in the

first place and subsequent to that partially restored its original shape, will most probably exhibit a strong susceptibility to fall back into the core imposed deformational state. This property wont be distinctive at lower flow rates, because the exerted forces are too small to really have influence on the chains. At higher rates, when the experienced stresses overstep a critical value, the chains are more prone to bending back and re-deform. The resulting effect will be a diminished apparent viscosity in comparison to low rates. Elevated temper-

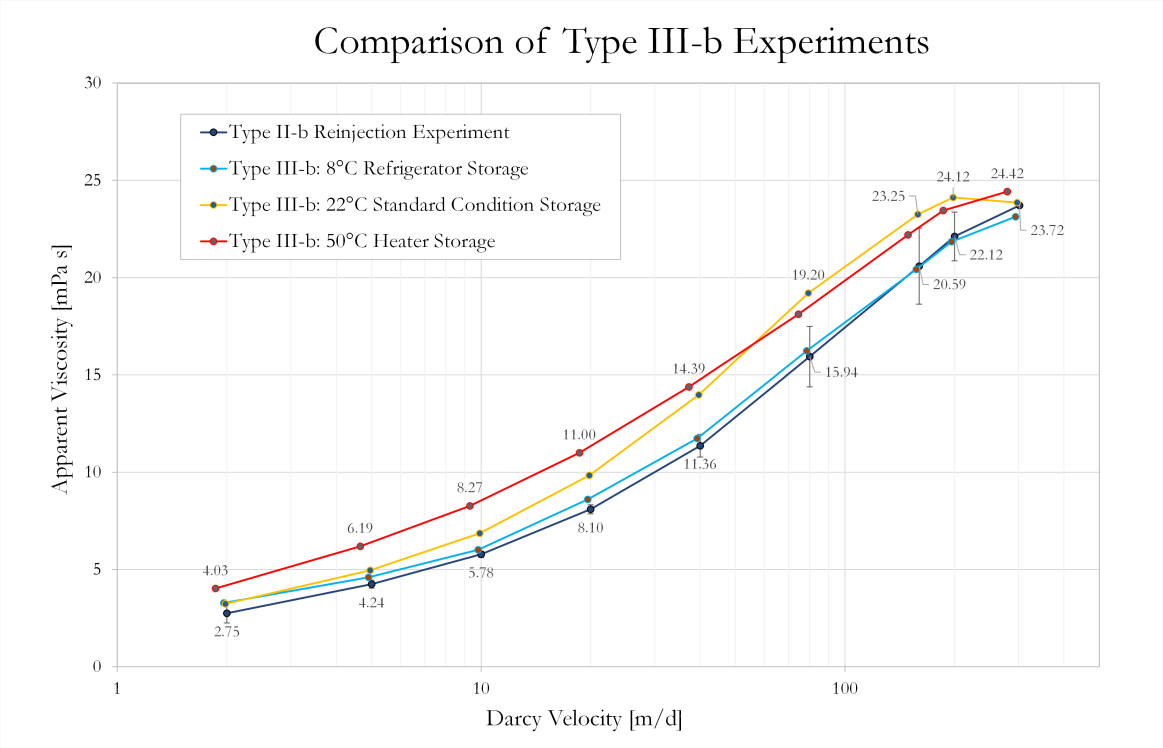

Figure 56: Comparison of all Type III-b Storage Experiments with the II-b Reference. The focus on these cores shall grant better comparability for a Method III analysis.

atures could have an influence on the molecules resistance to mechanical deformation or on its elasticity. Both effects could trigger the above stated incoherence between low and high rates when a stored polymer is re-injected. The temperature could render polymer chains more flexible and deteriorate their mechanical structure and thus stability at higher stress conditions.

11.2.3.4 Storage Conditions at the Upper Temperature Limit

The last III-b experiment shall investigate the viscosity behavior of stored polymer solutions at the highest possible temperature that the polymer can bear. The manufacturer states a thermic stability to up to 80 °C. The according experiment operates at this upper edge of polymer stability and shall confirm the findings of the 50 °C Type III experiment and maybe explain the observed effect of different viscosity restoration at low and high rates. The last experiment was added to the end of the regular experimental schedule and wasn't part of the original setup. For that reason, the chosen rock core does not belong to the original rock series with a little lower air permeability. The outcome of this Type III-b experiment is shown in figure 57. The core, Berea 25-08, shows surprisingly low apparent viscosity values in this configuration. Most probably, this can be explained with massive thermal degradation. Polymer chains in the solution were most probably disintegrated during the 2 months relaxation time, resulting in a high concentration of much smaller polymer entities.

This leads to much lower apparent viscosities in the area of about 2 mPas. The 80 °C experiment is obviously not suitable for the investigation of mechanical degradation, but proofs vividly the effect of too high temperatures on partially hydrolyzed polyacrylamide solutions.

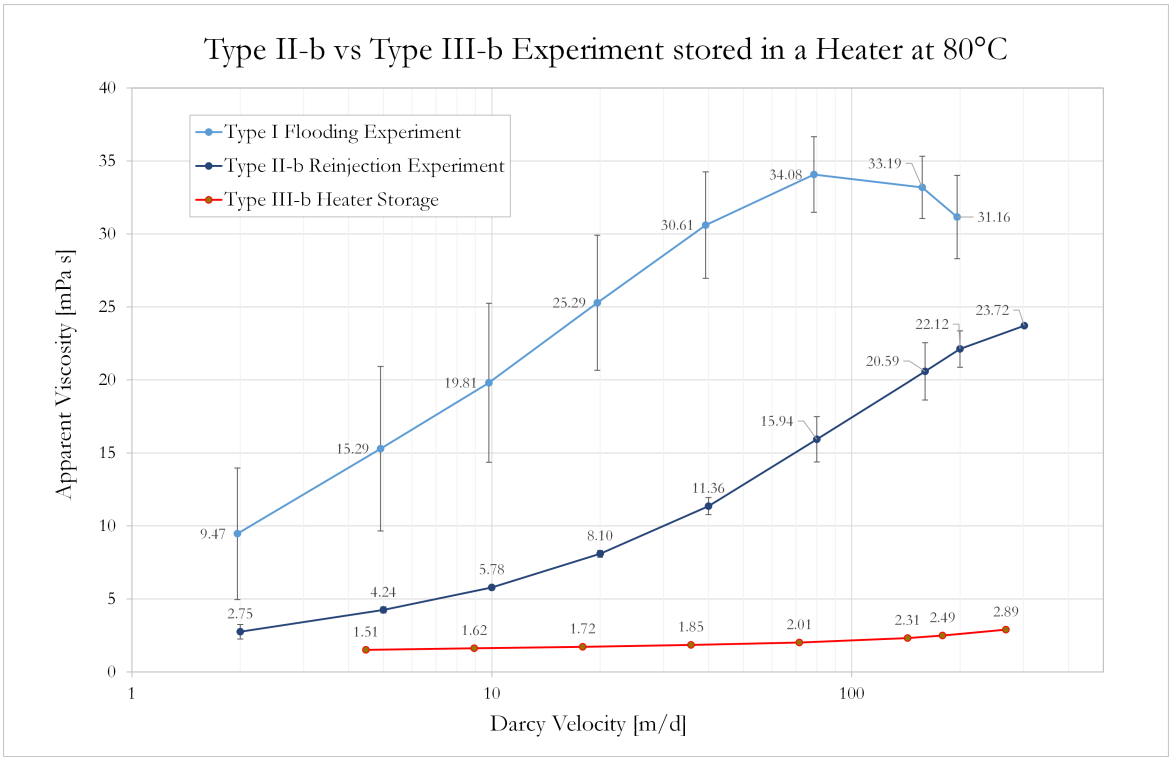

Figure 57: Comparison of Type III 80°C Storage Apparent Viscosity Profile on Berea 25-08 with Type II-b Reference Profile. Berea 25-08 exhibits a drastically deteriorated viscosity profile. Most probably temperature effects did destroy viscosity enhancing polymer chains in the solution, leaving the liquid with such a low apparent viscosity curve.

11.2.4 Critical Offset Rate of Mechanical Degradation

An additional experimental module was inserted into the original schedule to investigate the onset of mechanical degradation on polymer solutions. Although, there are many researches, who propose that mechanical degradation is a continuous process without a distinct kick-off point, the viscosity profiles for this system suggests that such an offset does exist. In order to proof this theory, a larger sample was taken at a rate of 4 ml/min for a Type II experiment. The rate of 4 ml/min was chosen because it lies right below the suspected onset of mechanical degradation indicated by Type I viscosity profiles. If no degradation has been taking place at this point of the experiment, the according Type II-b experiment will yield a viscosity profile similar to Type I or II-a curves. This means that the viscous behavior of the solution hasnt changed due to the first flood. If degradation was imposed upon the polymer chains in the sample, the result of the second II-b flood will be deteriorated viscous behavior. Most probably, the apparent viscosity will not fall as deep as 20 ml/min reinjections floods like Berea 6-111 or 6-100, but a significant loss of viscosity would be observable. Figure 58 indicates that reinjection samples at a rate of 4 ml/min will yield similar apparent viscosity profiles as virgin Type I floods. This means that there is no viscosity loss notable at this rate. Polymer chains will not be subjected to deformational or scission processes inflicting

permanent harm on them. On the contrary to that, type II experiments at 20 ml/min will yield enduring apparent viscosity losses as proven in figure and table 51. This means that there is for sure no notable kind of mechanical degradation going on below a rate of 4 ml/min. The offset of degradation must lie inbetween 4 and 20 ml/min. Most likely the

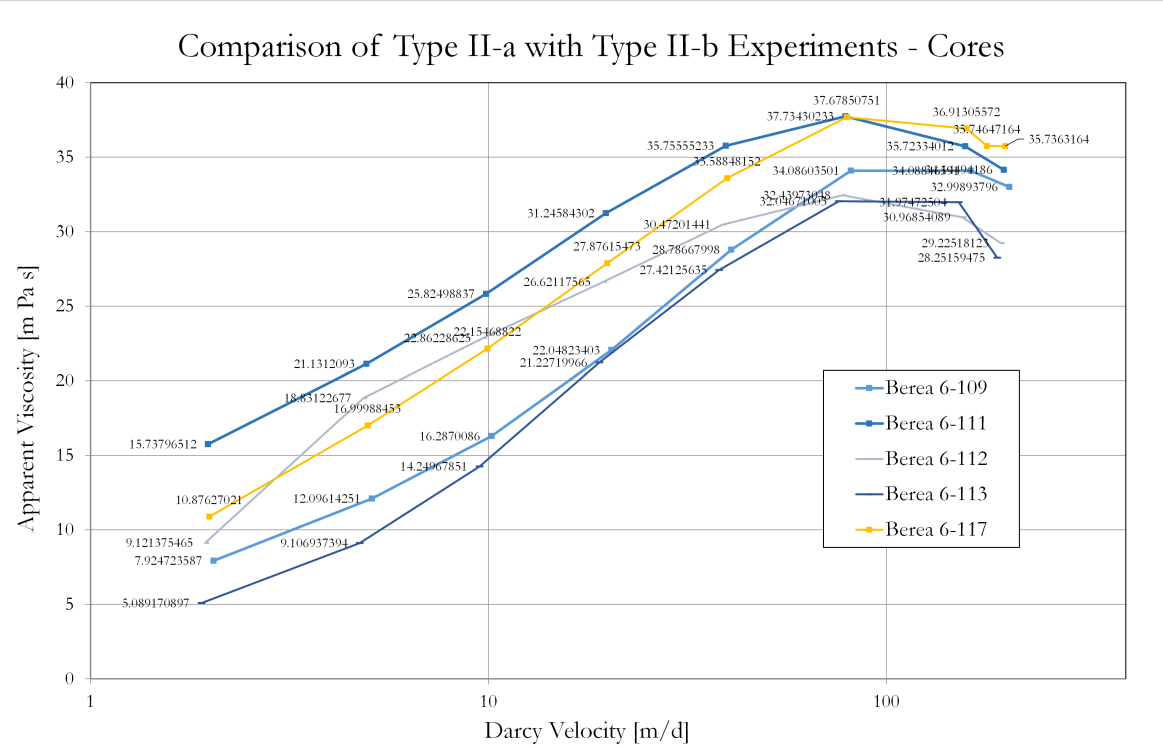

Figure 58: Apparent Viscosity Profiles for Type II Experiments at 4 ml/min. The already known blue lines are all Type I/II-a experiments. The yellow line indicates a Type II-b experiment performed on Core 6-117 with polymer which has been sampled at 4 ml/min instead of 20 ml/min. The characteristic viscosity profile is almost identical to Type I virgin experiments.

kick-of point will be in the vicinity of 10 ml/min, because roughly at this rate, the shear thickening behavior of a Type I experiment will be transduced into shear thinning behavior. That is a strong indicator for mechanical degradation. Hence, when the shear thickening trend is flattening, the apparent viscosity trend will be inverted soon. The first sign of such a behavior must be declared as the offset point of mechanical degradation.

12 Data Conditioning and Correction

Agilent Chemstation is a historically grown software and can be very bulky to handle. In order to bypass the restrictions imposed by this proprietary software, measured data has to be exported and conditioned to be used in a data processing software such as Excel or Matlab. The first macro written in Agilent proprietary code exports raw data to a comma separated file CSV that consists of simply one column with all data stored as long plain text. The task of the second macro which is simultaneously the first Excel macro in this workflow is to convert raw Chemstation data into a form that Excel or any other mathematical software will be able to handle properly. A third macro has the function of correcting and smoothing the original signals and bring them into a form that they reflect the true nature of the examined polymer samples. The last step and forth macro creates a plotting environment that allows the comparison of tremendous amounts of sample data. This is necessary in order to capture trends, tilts, proper corrections and main effects of the core flooding experiments. To put it in a nutshell, the workflow can be condensed to four distinct steps, which are

- Agilent Chemstation Export
- Data Conversion and Conditioning
- Correction and Smoothing
- Data Depiction and Analysis

Normally the procedure of data conditioning, correction and preparation wouldn't be part of a typical master thesis summing up results and discussing conclusions. In this special case, it was necessary to construct a data processing workflow because otherwise the tremendous load of data material wouldn't have been manageable. The development of macros to handle this full workload was an integral part of the whole master work and an important prerequisite for the actual experimental analysis work. The predecessor to this project Dipl. Ing. Sledz, who established the specific HPLC environment and confirmed the feasibility of chromatographic measurements at OMV lay his focus mainly on the practicability of this method. The outcome of his work comprised just a few sample sequences which were manually exported and corrected. This work turned out to be tedious, time consuming and inefficient. Because of much higher data throughput expected in this sub-project, a method of automatize data processing had to be implemented. In the end, a resulting data source of three times Mr. Sledz's samples and five times his data rows, had to be conditioned, corrected and prepared for later analysis. This made it essential to provide a systematical and mainly automatized workflow for HPLC usage. The end workflow was meticulously documented and implemented straight at the HPLC coordinating machine for further application within the hosting company OMV. Individual steps and primary ideas of the workflow shall be discussed in advance to the chromatographic analysis section and introduced to confirm data integrity and the validity of later analyses.

12.1 Data Conditioning

The first phase of the overall chromatographic workflow is the Agilent Chemstation export. The second step is the data conditioning phase and has the purpose of converting proprietary data material from Agilent Chemstation to universally usable files for further processing.

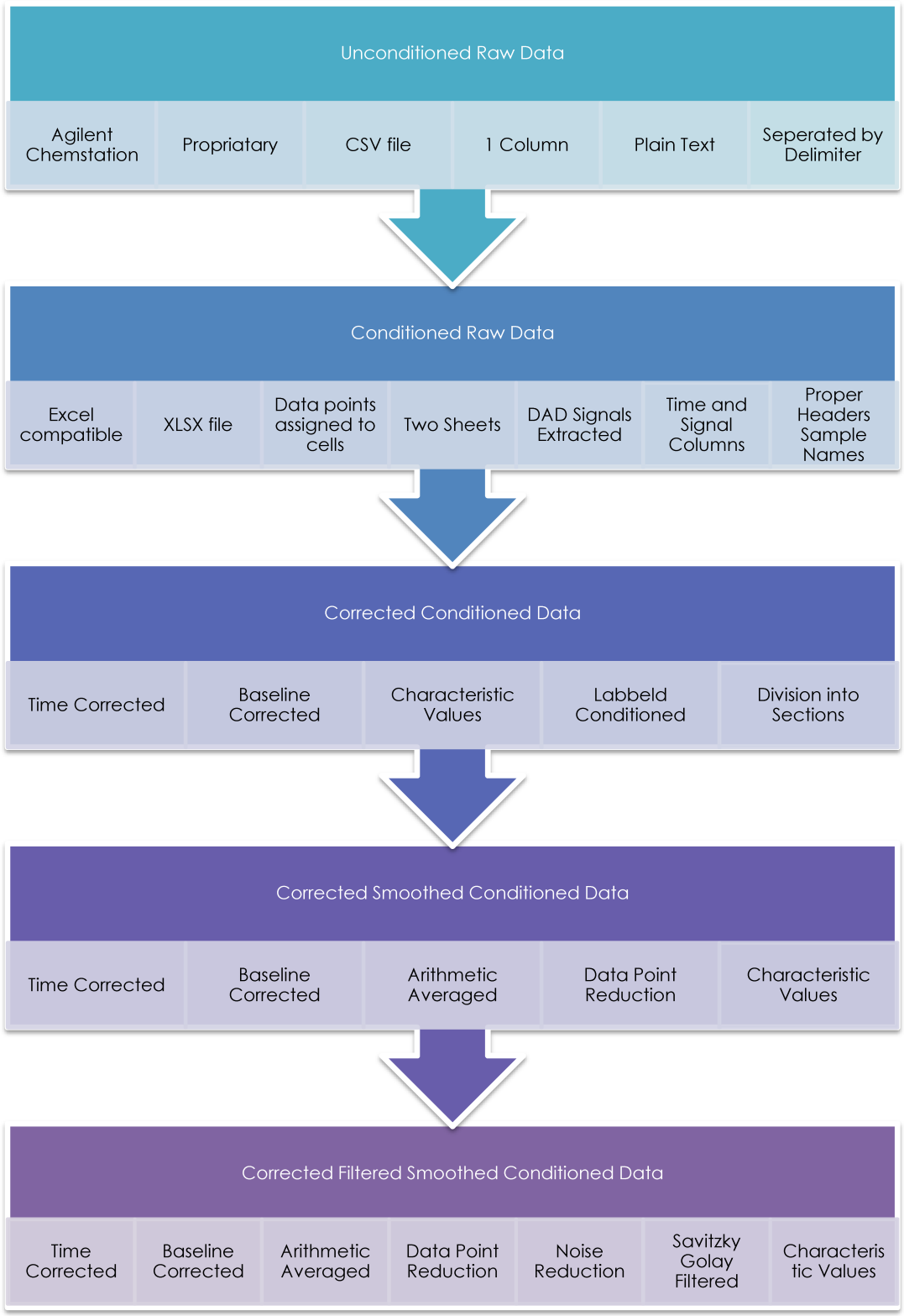

Figure 59: General Workflow of HPLC Data - The workflow describes different steps and prerequisites on data for each distinct phase

12.1.1 Intended Conditioning Targets

The intended objective of this conditioning step is an an excel file as end-product that contains two sheets of data material. The first sheet holds all diode array signals for every single sample in the sequence. The second sheet contains all data that has previously been loaded and exported starting from diode array signals, over chromatographic pump pressures, to fluid composition and refraction index signals. Every data point is assigned to an individual cell. Every Sample has two columns containing time and according signal strength values.

12.1.2 Macro Structure

12.1.2.1 Dialog Box

The first part of the macro at hand has the purpose of targeting the exported Chemstation file so that the actual conditioning work can be performed. For this reason the macro has to know the file name and the position of the raw data. Hitting the condition button will open a dialog box using the excel command *Application.FileDialog(msoFileDialogFilePicker)* which enables the user to pick the raw data csv file. Two methods *fileNameFromPath()* and *FolderFromPath()* extract the file name and the directory from the entire path, where the raw file is located. The macro now knows position and name of the file in question.

12.1.2.2 Open CSV

The raw data csv file is opened via the command *Workbooks.Open(directory & fileName)* and activated in order to be operable.

12.1.2.3 Text to Column Conversion

The first step in treating Chemstation raw data is to perform a Text to Column conversion where all plain text data from column one is converted to actual excel manageable points where every number is assigned to a single and individual cell. This is done by the *Selection.TextToColumns* command and the option *OtherChar:="|"* This means that all data points are separated by the | delimiter in text mode. The effect of this command is a data point assignment to multiple columns and rows.

12.1.2.4 Correction Algorithm

The original Chemstation macro hasnt been designed for handling multi-sample export and thus some misleading mechanisms deep inside the code cause exporting errors that distort the exported data points. The first error that occurs is an offset of data points after a certain number of values. This is due to different time steps and hence resulting different numbers of data points for different signals. The offset of data points is corrected by a mere *Sheets().Range().Cut* and .Paste command. A shift by one cell to the right suffices to restore the integrity of raw data. A second error that emerges from the Chemstation macro is that useless rows are inserted below the title which contain inconsistent names of the signals. Normally there are two kinds of headers assigned to each data sample. One displays the sample name and one marks the column as time or signal column. Chemstation doesnt have proper labels for all hardware signals. When an empty label signal is exported, a line in the code forces a new header row to be created. These misplaced headers are again shifted to the right position by this conditioning macro. All superfluous rows are deleted by a loop that stops erasing rows when the labels "Time" and "Signal" occur in the second row.

12.1.2.5 Extraction

The macros correction module results in a neat and usable dataset that could be used right away. The "Raw Data" sheet is finished and remains untouched. It contains all necessary

data about the sequence starting with diode array and refraction index signals, over fluid compositions and pressure data up to very detailed hardware related signals like lamp voltage etc. The most important signal is of course the diode array signal, which provides information about the polymer solutions molecular weight distribution. For this purpose it is convenient to have access to a separate sheet with just these signals. A new sheet labeled "DAD1" is created via the *Sheets.Add* command. This new sheet is supposed to store the significant DAD1A signals of every sample. Based upon the number of samples and signals per sample all diode array signals are transfered to the new sheet.

12.1.2.6 Save to New File Format

The end result of the conditioning process are two sheets, one with just the diode array signals and one with all additional hardware signals. All data is properly labeled and consistent now. The last step of the procedure is to delete the original csv file and save the conditioned raw data as an XSLX file.

12.2 Correction and Smoothing

The third phase which is treated by the second excel macro is the correction and smoothing phase. Conditioned raw data shall here be corrected in a way that different measurements and samples can be compared. This phase of data processing is the most complex one and the most tedious chore to do.

12.2.1 Problems with Distorted Signals

Hhigh performance liquid chromatographic measurements exhibit a broad range of behaviors that aggravate the comparability of data sets and make straight statements on data difficult. Some of them are intrinsic, corresponding to the measurement method of the diode array detection measurements, some of them are extrinsic hailing from outside influence like gas bubbles in the fluid resulting in unwanted pressure and signal fluctuations.

12.2.1.1 Intrinsic Effects

Intrinsic effects lead to a distorted signals like tilted baselines or baselines that go straight but on a level other than the expected zero line. For this effects baseline corrections have to be performed that shift the baseline down to the zero-line or tilt it back to a linear plain shape.

12.2.1.2 Extrinsic Effects

Extrinsic effects lead to pressure shocks and thus signal pulses which are unwanted in the final data plots. This pressure shocks may origin from gas bubbles in the continuous fluid or contaminations in the flow paths. They could also hail from work that was performed near the HPLC hardware or from not properly working valves or pumps. Be that as it may these pressure or signal shocks delay the diode array signal which reduces comparability again. For the purpose of correcting this retardation a time shift has to be performed. All sample signals are corrected towards a fixed time value. The distribution curves are then stacked and can be compared properly.

12.2.2 Data Enhancement by Smoothing

Conditioned raw data that was baseline corrected and time corrected is very well suited to be compared and analyzed. But it has to mayor disadvantages.

12.2.2.1 Hardware and Software Requirements

On the one hand conditioned and corrected original data is very large and bulky. The data set for one sample can be assembled from up to 80 000 data point pairs for an effluent rate of 0.1 ml/min. An average sequence comprises 20 to 40 samples which results in approximately 6.4 million data points per sequence or 200 to 1500 MB files per sequence. Apart from these huge storage needs for multiple comparable sequences and calculation durations both hardware and software equipment are facing tremendous challenges with regard to internal memory and CPU power. Even the provided data processing software Microsoft Excel reaches the boundary of its capacity in handling such amounts of data on the fly. These problems suggest the strategy of data reduction. The aim to cope with this large amounts of data is to reduce the number of data points without losing shape and characteristics of the measured molecular weight distribution.

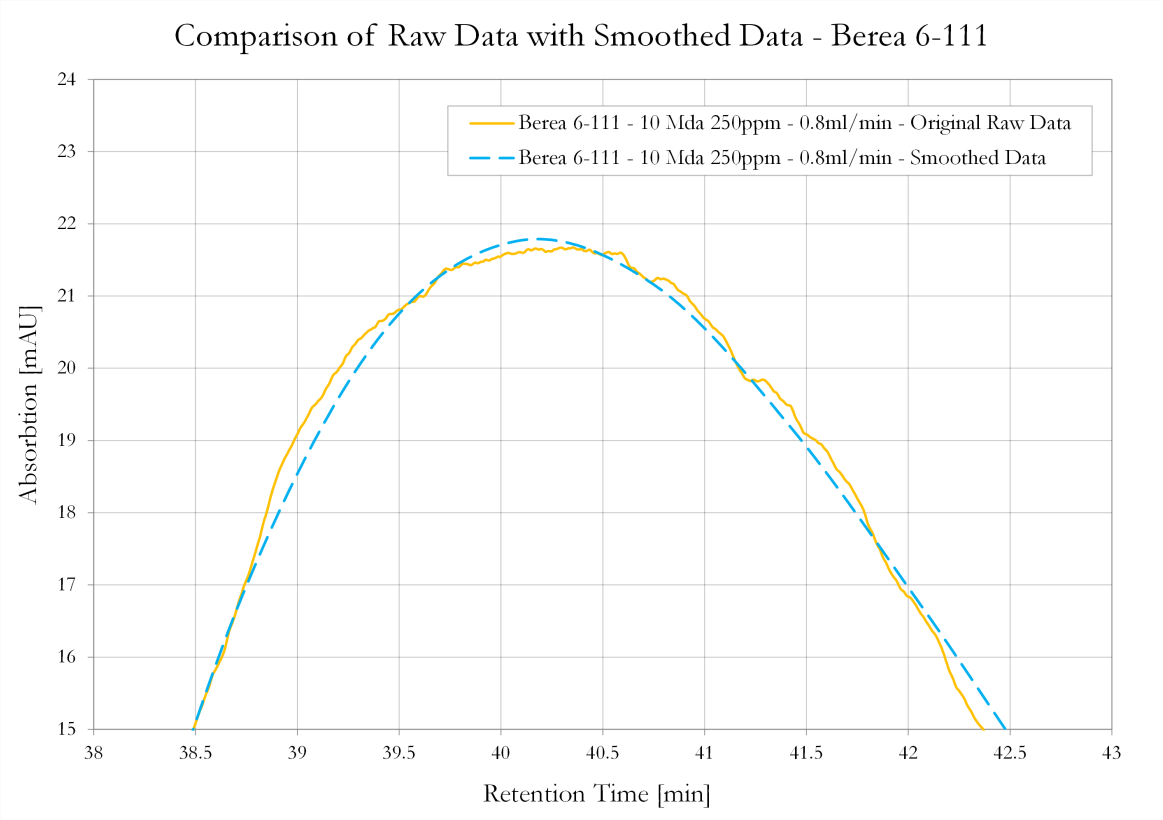

Figure 60: Comparison of Raw Data and Smoothed Data - Unsteady raw data is most likely to not fully represent the characteristic shape of the polymer curve. Smoothed data captures these peculiarities much better.

12.2.2.2 Natural Oscillations and Peaks

The second disadvantages of the original corrected data sets are natural signal fluctuations. The pump used in within the HPLC hardware is a piston pump and thus generates a certain pressure shock which is inherent to the entire system. Although it was achieved to restrict the pressure fluctuation to a limit below 0.5 bar per pulse (mostly in-between 0.1 and 0.3 bar) the pressure variation causes an unsteadily oscillating diode array signal. A reduction of data points would also smoothen these signal buckles. The second origin of non-representative signals or values hails from the fluid sample's consistency. As mentioned before, very little is known about the polymer solution and the actual composition with respect to manufacturers

specifications. Also the size exclusion process inside the separation column is not transparent and happens statistically in a microscopic scale resulting in similar but not identical depictions of the molecular weight distribution. The polymer curve can have sections of over- or under-measurement that doesnt really depict the actual distribution. For the reason of catching the true shape of the characteristic curve it is necessary to straighten these data relics or overestimated trends. In order to meet these two major disadvantages, it was decided to smoothen the full length conditioned and corrected data. The smoothed data will be assembled from much fewer data points resulting in less calculation time, smaller space and hardware requirements and more stable and more representative distributions. The crucial parameter is the number of target data points because the aim is to reduce the data set as much as possible without losing characteristic shapes and the according key parameters.

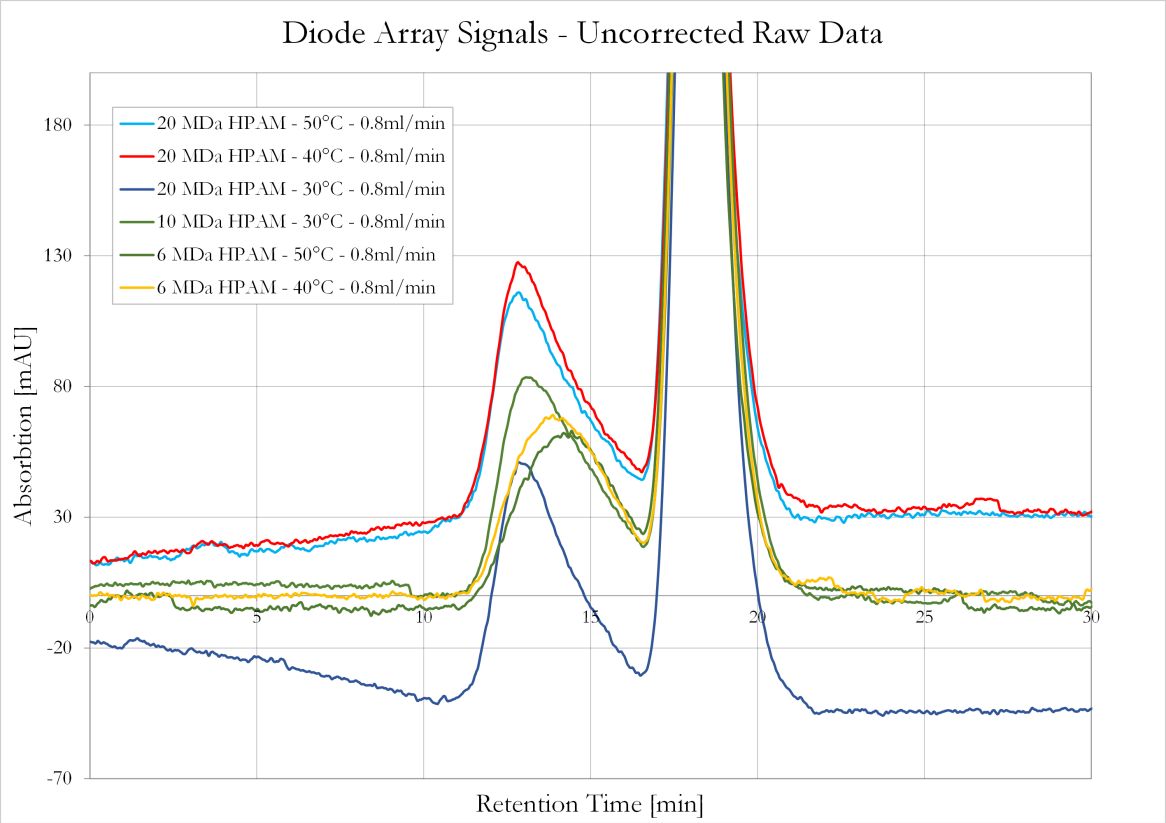

Figure 61: Uncorrected Raw Diode Array Signals - Different sets of DAD signals exhibit unsteady, tilted, shifted and distorted behavior. For better comparability correction processes and stacking is necessary.

12.2.3 Iterative Approach

Both procedures, the correction process and the smoothing process, are designed to be iterative processes. For the correction phase it is necessary to get an overview from a distant point of view in order to see the trend of the baseline, whether it is tilted, shifted or somehow otherwise distorted. There are mostly a few iterations required to find the correct baseline correction. Experience showed that once found, these parameters hold true for the entire sequence and can be applied to all individual samples at once. Time corrections are very straight forward because the time shift is a simple difference value that is characteristic for each sample. The smoothing procedure is more sophisticated but follows the same iterative approach. In order to understand if the curve has been altered during the smoothing process

the smoothed signal has to be compared to the original signal. For this purpose it is a good choice to plot corrected signals and smoothed signals at the same time and compare how their shape has been altered. The second quality sign on how well the smoothing process went are characteristic values of the curve such as maxima and inflection points. If they are preserved by the smoothing procedure and the shape remains more or less the same, the smoothed data set can be accepted and used for further calculations and comparisons. This method has the advantage to be able to decide qualitatively over certain artifacts and distortions whether they shall be smoothened or whether they shall be conserved.

12.2.4 Requested Output Format

The desired outcome of the second excel macro is now clarified by the above prerequisites. Three output data sets are requested. The input conditioned raw data has to be transformed into a baseline and time-corrected output format. In addition to that it shall be smoothed appropriately and at the same time be noise filtered.

12.2.5 Characteristic Values

For the purpose of comparing different samples, standardized characteristic key values turned out to be best suited.

12.2.5.1 Polymer Peak

The most important and most striking specific value is for sure the polymer peak. Both the time value when the peak occurs and the signal value how high the peak climaxes are important. The absorbance value gives evidence about the concentration of a certain chain length. The delay or retention time value gives evidence about the size of the molecule when it is properly calibrated with manufactured fresh polymer solutions. The easiest way to find the polymer peak is a simple search for the modal value. The value with the highest occurrence frequency is thus defined as the polymer peak. It gives a first glimpse on the characteristic of the polymer curve and enables rough comparisons and quality control on how well the smoothing process was performed. But simple modal values have their downsides too. As discussed in the smoothing section the diode array detection measurement can cause intrinsic or extrinsic distortions of real curve characteristics. The maximum value can sometimes be found at positions that do not reflect the real curve form. Sometimes a pressure peak or an oscillation climax represents the maximum which is then obviously a misleading value. The top of the polymer curve on the other hand can be very flat, very similar to a plateau. The problem here is that a pressure or signal fluctuation at any point of the plateau would indicate a maximum where there is actually none. In order to meet these difficulties in peak detection a more stable mechanism was used to get grip of the real apex of the polymer curve. To overcome the problem of a flattened top signal section, it is necessary to consider and include the actual shape of the curve. A good way to integrate the characteristic form into the maximum detection is to fit tangents to both flanks of the curve and calculate the intersecting point of both lines. This intersection indicates where on the plateau or where in the distorted upper section of the signal, the characteristic maximum value can be found. This method turned out to be much more stable than a mere modal value comparison. The difficulty of this method though is to find proper tangents, because the flanks of the curves arent that regular either. The best way to calculate appropriate tangents was to fit them to the curves characteristic inflection points. This is again a difficult task due to the unsteadiness of the signal and the non-ideal behavior of the flanks. A smoothing treatment solves this problem and yields proper inflection points for the tangent maximum detection. A second for coping with this problem is to fit the crest of the characteristic

polymer section with a polynomial fit, compute the according equation and set it zero for the purpose of extremum detection. The poly-fitted maximum is similarly stable as the intersection maximum.

12.2.5.2 Salt Peak

The position of the salt peak is crucial information from all chromatographic measurements. Due to the identical brine composition within all samples the salt peak will roughly be identical for each probe. This fact enables normalization and better comparability. When stacking signals it is an easy and robust way to bring the curves in the right position, fitting exceedingly stable identical salt peaks. When they are aligned properly, it can be presumed that comparability is given. This is in a nutshell the mechanism behind the time correction process. Delays are canceled out by matching all salt peaks to one reference value. It would have been possible to simplify the baseline correction process by simply fitting the salt peak height of each sample whilst they are overlain. The problem here is that small amounts of concentration differences would distort this kind of baseline correction. For certain polymer solutions of lower molecular weight and smaller concentration in the area of 250 or 100 ppm, smaller polymer chains could also influence the salt concentration peak. The conventional baseline correction process turned out to be more stable than that.

12.2.5.3 Polymer and Salt Areas

A second powerful key value is the area below the curve of the polymer and the salt section. On the one hand it can be validated if concentrations and molecular weights approximately fit the manufacturers specifications. It is a simple check if the right chemicals were used and all preparation and experiments were performed properly so far. On the other hand it is well suited basis material for further investigations. The total area can be split to single sections and thereof changes over time can be compared. This indicates how the distribution has changed during individual experiments.

12.2.5.4 Inflection Points

Inflection Points belonging to the curve flanks are primarily calculated for the purpose of tangent fitting for the maximum detection procedure. A second very useful statement of these curve characteristics is that they should display approximately the same time shift behavior as the maximum point while degradation. In addition to that, it enables a comparison of left and right flank and thus the relation of high and low weight molecules.

12.2.5.5 Tangent Equation Parameters

Tangents can indicate a similar behavior as inflection points. Their steepness gives evidence on how the characteristic signal is curved and thus how the relation of heavy weight molecules on the right side to low molecular weight molecules on the left side is constituted. This will be further discussed in the analysis section.

12.2.5.6 Polynomial Fit Parameters

For better maximum detection a polynomial fit can also be performed and set zero to find the equation maximum. Since it is most commonly a sixth order fit, the essential parameters are the seven corresponding coefficients and the matching derivative. The polyfit sub-macro will furthermore yield the equation maximum as retention time and signal strength.

12.2.6 The Correction Macro Structure

The actual correction macro has quite a complex structure and fulfills a lot of different tasks. The code of this macro is historically grown during the data processing procedure and thus at some passages patched up. A huge documentation had to be written to explain the whole code in detail. The rough workflow of the macro is described by organigrams and flow charts provided here. The code is written in a modular form. It is composed of eight functional core macros which are applied in a slightly altered form at several different code passages of the main macro. Counting all variations of modules and plain code, the main macro comprises 31 macro modules, that execute in combination with simple excel commands and an overall of 42 auxiliary columns of changed data per corrected sample, the entire correction and smoothing process. All work has to be done in triple versions because whenever the number of data points changes, new values for local minima and maxima and starting points have to be detected and calculated.

12.2.7 User Handling of the Correction Macro

The working principle of the macro is though pretty simple. Raw and unconditioned data is copied to the raw data sheet. Based upon one exemplary plot and frame data like the number of data points and the maximum peak, the user decides upon input data like the quality of smoothing and where the baseline shall start and end. By hitting the correction button, the macro starts performing the above mentioned correction steps sample by sample. Time and signal data pairs for one sample are copied to the conversion sheet. All corrections, smoothing and filtering is done in the conversion sheet. When the macro loop is executed the "simple corrected", "smoothed corrected" and "filtered smoothed corrected" data sets are exported to according export sheets and calculated key values of the three data sets are saved to an additional sheet. The overall correction loop continues with the next sample by copying new data pairs to the conversion sheet after previous clearing. This is done till all samples of the raw data sequences have passed the conversion sheet and all raw data has undergone the correction loop. Subsequent to the overall loop it is possible to choose from the command sheet single samples and correct them by hand or automatically with a special macro that is roughly structured similar to the big correction macro but specially tailored for the use of one single data set. The results of the whole process are four sheets with data. Three sheets of data points and one sheet with characteristic values for corresponding sets.

12.2.8 Core Modules

Each section of the macro works a similar way. Initially it is necessary to detect the boundary of each section of the signal. There is a baseline at the front of the signal. Then the curve rises, indicating the polymer section. Behind the peak the signal drops to a local minimum where the polymer section ends and the salt section begins. Behind the salt peak the signal is going back to zero to the rear baseline. When the limits have been found, local minimum and maximum searches will yield the middle point and the polymer peak.

12.2.8.1 Copy and Paste Module

The copy paste module is a very simple one. It realizes all the import and export tasks and duplicates data wherever necessary. It is a functional auxiliary macro to keep the actual correction process going.

12.2.8.2 Detect the Actual Value Module

In order to work properly the user has to decide upon a few input values. These values cannot be used straight away because it is very unlikely that there exists a data point that has exactly the desired value. Designated input values first have to be translated to actual data points. The task is to find the closest possible data point to the target value. This is realized by a simple search loop that stops when a value close to the input value has been crossed. The very data point is then saved. Major applications for this macro are searches for time values where the baseline ends and the polymer curve starts and where the salt curve ends and the baseline starts again. For example when a starting value of 15min is determined, the loop will stop at the first value past 15mich which is for example 15.0043min and saves this time data point as starting value where the signal starts to rise, further indicating the polymer section.

12.2.8.3 Detect the Salt Peak Module

The localization of the salt peak is a very important task. The salt peak position is essential for time corrections and is furthermore used for several additional detection algorithms. The realization of this search is again quite simple. An auxiliary variable is created and set to zero. A loop and an if-condition searches the whole data set and replaces the helping variable whenever the current value is larger than the saved one. At the end of the loop the largest signal value of the data set plus the according time value is saved and written to the value sheet.

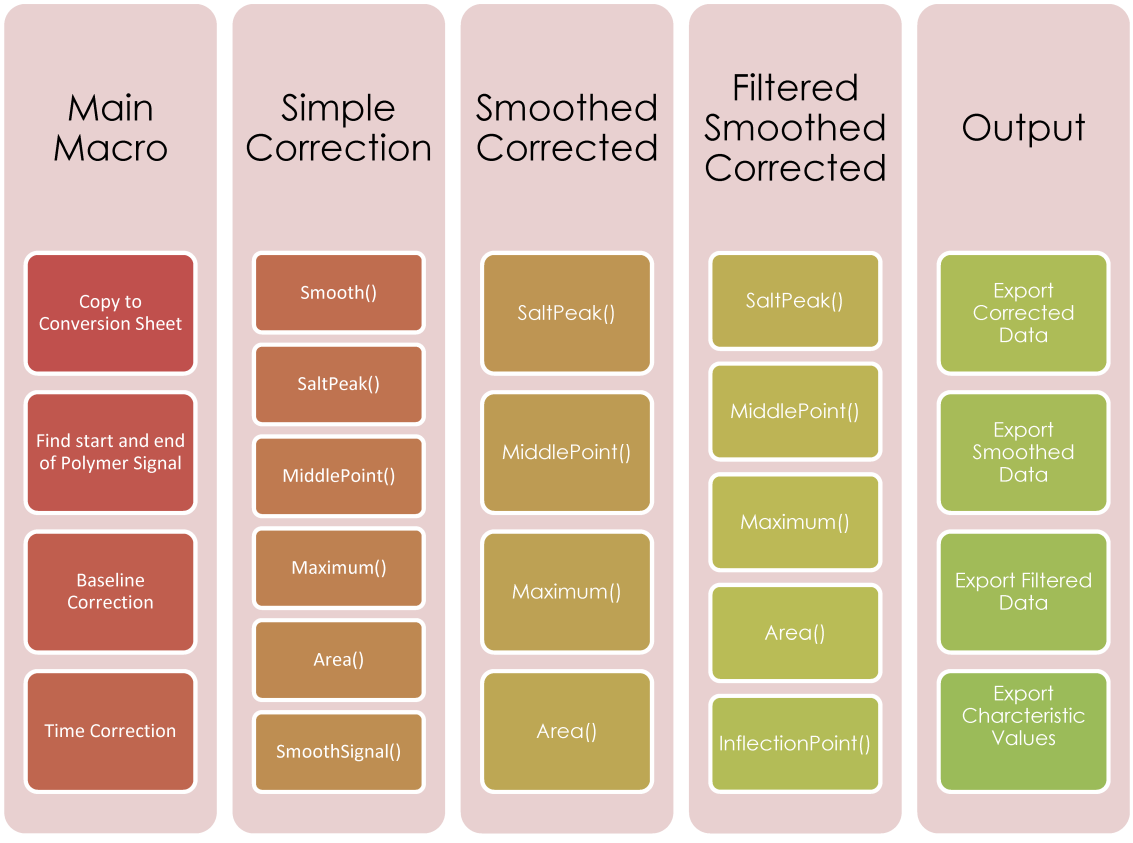

Figure 62: Overview on the Structure of the Correction Macro. All core modules of the main macro plus their integration in the overall system

12.2.8.4 Detect the Local Minimum Module

The local minimum detection is a bit more complex and sophisticated than the other macros. Due to the different shapes of curves depending on the actual molecular weight and concentrations, the local minimum will show different shapes too and may be overlain by other effects or even parts of the polymer curve. Several approaches were necessary to manufacture a procedure stable enough to work for all samples. The position of the local minimum is presumed to be in-between the polymer peak and the salt peak. The salt peak is known at this moment of the correction phase. It is also known that the salt peak exhibits relatively steep flanks. The basic idea is grounded on the fact that the first derivative of the signal shows if the curve is increasing or decreasing and if so, how steep. This fact can be used to search the signal backwards starting at the salt peak. The signal will fall very steeply so the first derivative will yield a negative value. The first positive value indicates that the signal is rising again and thus that the local minimum has been passed. Two values added to this value as a safety margin makes sure that the local minimum has by any means been passed by. This second limit in combination with the salt peak as first limit creates a perfect validity span where a simple absolute minimum search can be performed. Due to the limits it is ensured that this absolute minimum is equal to the local minimum between the two peaks. In order to avoid pressure or signal buckling and to make sure that the first rise of the signal as indicated by the derivative is really the start of the polymer section, a strongly smoothed version of the signal has to be created and browsed through. This is done by a variation of the smoothing macro module. The strongly smoothed limits that have been found by this algorithm have to be translated again to the original data set. This is done by the second macro module that finds the closest match to a target value. Once the two limits have been defined the absolute local minimum detection is easily performed. A loop within these boundaries checks each value and compares it with the value in a helper variable. Whenever the current value is smaller, it is replaced, which will lead to the smallest value within the previously defined search radius. Having identified the starting point, the local minimum and the ending point of the polymer and salt curve it is easily possible to handle these curves and find further key values.

12.2.8.5 Detect the Local Maximum Module

The fifth macro has exactly this purpose. It is able to find the local maximum of a signal section. The main application of this code is of course to detect the polymer peak modal value. Based upon the previous macros and their finding, this important key figure is very easy to trace down. An absolute maximum search as done by the salt peak macro is performed within the boundaries of the starting point of the polymer section and the local minimum. Again an if-condition checks within a for-loop if the current value is larger than the one of a helper variable. If so, the value is replaced, resulting in the local maximum. This macro is slightly altered applied to the simply corrected, the smoothed and the filtered data set yield the three corresponding maximum points.

12.2.8.6 Calculate Areas Module

Having found the boundaries of each section and corrected the signal down to the zero baseline, it is easy to roughly estimate the area below the signal curve. The method is a very simple approach to that. The area between two time values and from the signal height to the baseline is thought as plain rectangle. This incremental area rectangle is defined by its width, which is nothing more but the mere time step and hence the difference between time value 2 and time value 1. The height is defined by the average of the two signal values divided by 2. Multiplication of these two values gives the incremental area. A helper variable sums up all these increments inside a loop and saves it to the sheet for the characteristic

values. The area below the signal curve of the polymer section is restricted by the starting value and the local minimum. The area of the salt section is limited by the local minimum and the ending point.

12.2.8.7 Smooth Signal Module

Whenever a smoothed signal is required this macro module gets activated. A derivative or an algorithm that needs an extraordinarily robust signal sometimes demands a strongly smoothed auxiliary data set. Characteristic values may not be required to be preserved by this data set but only the rough shape of the signal. The actual smoothed signal that should represent the original signal and conserve all its characteristics is also produced by this macro variation but with finer and more elaborate settings. Either way the macro needs an input variable that governs the quality and intensity of the smoothing process. This value prescribes how many data points shall be melted down to one new point. It may be determined by user input in the commando sheet. Based upon this value the macro subdivides the entire signal to sets of this amount of data points furthermore called an interval. The large smoothing loop jumps from interval to interval and triggers a smaller loop that adds up all values within the data set and divides it by the number of given data points. The remaining values are separately handled and again subdued to this averaging procedure. This simple averaging process leads to much fewer data points while basically preserving the actual shape of the curve.

12.2.8.8 Detect Inflection Points and Tangents Module

The inflection point macro has several purposes. It searches the signal for the two characteristic inflection points that belong to the polymer curve. From that data it calculates the according tangent linear equations and hence the intersecting point of the two, which is equal to the tangent maximum value. The real difficulty of this macro module is the detection of the two characteristic inflection points of the polymer section. An inflection point is found by forming the second derivative of the curve and seeking the zero points of this data set. An unsteady original signal would lead to uncountable inflection points. This means that the resolution of the algorithm has to be decreased. In order to achieve it, a very strong smoothing process is executed by the smoothing module. But even this strongly smoothed curve could still have multiple inflection points depending on the quality grade of the measurement. In order to avoid this, the second derivative is smoothed again until just one sole inflection point for each flank remains. The actual macro code creates a loop and searches the produced second derivative of the signal. When the trend shifts from negative to positive or the other way round the two data points are saved and linearly interpolated to determine the accurate zero point by solving the belonging linear equation. This time value and the according signal value mark the inflection point. A near data point is used to create the tangent equation which is in the next step solved to acquire the two constants k and d of the characteristic linear equation. Crossing these two tangents for each flank leads to the intersecting point which is computed by solving the intersecting equation. The inflection point and intersection point values are again transformed from the strongly smoothed signal to the actual corrected signal by the second macro and written to the characteristic value sheet.

Figure 63: Workflow of the Correction Phase with all major steps

12.2.8.9 Detect the Fitted Crest Maximum Module

The last macro was implemented after the recognition of peak inaccuracies in the smoothed diode array signal. The observed imprecision hails from too large time steps after the smoothing procedure. The standard maximum detection macro is able to find the highest value of the smoothed data set, but the real maximum is most often situated somewhere in-between two distinct data points. This is especially true for very strong smoothing. The proper way to circumvent this problem is to describe the crest of the polymer bump in terms of an equation and perform an extremum analysis. The implementation of such an analytical method is very sophisticated in Microsoft Excel but at this point it would have been inefficient to switch data processing software. As a first step, the detection macro searches the complete data series and copies the highest value of the polymer section plus three data points before and after that maximum to a different sheet. A simple plotting command creates an Excel chart and adds all seven data points to the series collection. Another VBA command creates a trendline to the chart, fitting the previously inserted polymer crest with a sixth order polynomial and displaying the corresponding equation. The data label containing the requested equation has to be copied and split at the "x"es in order to attain the matching coefficients. These coefficients had to be converted from string to double data-type and be integrated in a scheme to form the first derivative of the characteristic equation. The last step includes a loop reaching from the first data point before to the first data point after the highest data set value and inserts x values of 0.00001 incremental steps. The loop stops, when the first negative value occurs, indicating that the zero point has been reached. Both, the zero time point which is simultaneously the maximum extremum of the crest equation and the corresponding signal value plus the fitting error are saved to the value sheet. The polyfit error is negligibly small. The detected polyfit maximum describes perfectly the smoothed and filtered characteristic polymer crest.

12.3 Plotting and Comparing

12.3.1 Massive Data Handling

The last phase of the data processing procedure is the plotting and comparison of signals. It is already part of the correction and smoothing phase whenever actions have to be checked on their validity, if baselines have properly been corrected or the smoothing algorithm hasnt cut too many data points or messed with the characteristic shape. Whenever iterative correction and smoothing circles have been paced properly, a readily processed usable data set is available. The next step then is analyzing the signals and examining how they have been altered by different experiments. A simple core flooding experiment can be comprised of up to nine samples. An extended core flooding experiment can have double that value. For the reason of repeatability and cross-checking it is sometimes necessary to compare samples from different cores but the same experimental setup. These requirements show that ten to sixty samples have to be handled at once and shall be available for comparison. Again it has to be considered that every signal is assembled from two data columns with huge amounts of data points. The comparison of these data masses calls for a powerful and automatized tool of data plotting and handling. Copying, pasting and plotting this all by hand would be a very inefficient tedious waste of time, which would furthermore entail errors, inaccuracies and data mishandling. The plot macro can handle two different kinds of data. Most probably this will be original corrected data and filtered smoothed data. The number of samples is limited only by Microsoft Excel itself, so it is no problem to compare hundreds of samples at a time. The macro has three functionalities. It can either plot the first kind of data or the second one or it can plot both kinds of data to the same plot. The two differently treated data sets are plotted alternating and are labeled " raw dated" and " corrected data". These

are historically grown labels which are preset but can be changed inside the macro code very easily.

12.3.2 Plotting Macro Mechanism

The core of this last macro is pretty straight away. A loop jumps from sample to sample and adds every data set to the appropriate chart via the command:
ActiveChart.SeriesCollection.NewSeries()
Each data set is labeled according to their header row. The chart type is preset as a X-Y-scattered plot with smoothed connections but without markers. A self-written sub-macro within each loop-step creates check boxes and data labels for each data serie with the command *ActiveSheet.CheckBoxes.Add()*. Again they are labeled accordingly with the appropriate sample name. In addition to the mere name of the sample, the associated polymer peak retention time value and signal strength is written next to it for immediate comparison when these samples are plotted. All data series and checkboxes are by default unchecked and filtered. When the overall loop is finished, the charts are ready for comparison. The actual comparison is simple. Every sample that shall be displayed can be checked by user interaction. The button "Compare Signals" triggers a macro loop that enables or disables data sets based upon the check-mark of the matching box. All requested sample signals are shown and stacked in the according plots. The key figures like polymer peak time values are shown right next to it. Additional data must be looked up in the value sheet if necessary. The macro ensures that all plots are labeled the same way, have the same position and scaling and all data sets are named correctly. It functions as an additional quality control tool. The plotting sheet provides even more functionality than that. An additional macro facilitates the scaling of chart axes and enables therefore an easier detail view on the data plot. Scale limits are simply typed to the provided cells and according buttons assign the values to the axes without going to the property area of Microsoft Excel. A reset button restores the original automated axes scale. This macro helps saving time because detail examination of signal sections is very common and frequent work and thus small time saving will accumulate to a lot of easement. A separate clearing macro was additionally implemented for the purpose of deleting all previous data, plots, data series, checkboxes and labels. The original state is reconstituted. All macros and auxiliary macros are provided in triple realizations for all three necessary plots. Provided all these data sets and key values, analysis work can begin.

13 Chromatographic Analysis and Results

13.1 Weight Calibration and Detectability

The process of chromatographic calibration has already been drafted in the methodological section of this thesis. The next two sub-chapters will deal with the overall calibration curve of a distinct 500 MDa exclusion limit separation column and individual calibrations for distinct sample sequences.

13.1.1 Global Calibration

The manufacturer of the deployed separation column provides a calibration curve based on Pullulan samples already shown in figure 42. The problem here is, that this calibration curves solely cover a range of 200 Dalton to 800 000 Dalton, which lies clearly below the requested application range of 1 000 000 to 20 000 000 Da for this kind of experiment. The highest sample weight validated by the manufacturer is a 0.8 MDa Pullulan sample. Everything beyond that is simply interpolated. Figure 64 shows the translation of rough manufacturer's data from figure 42 into a usable model for the experiment at hand with a validated low-weight calibration curve and an interpolated calibration area starting at 0.8 MDa. In order to capture the trend both curves where fitted polynomially for the purpose

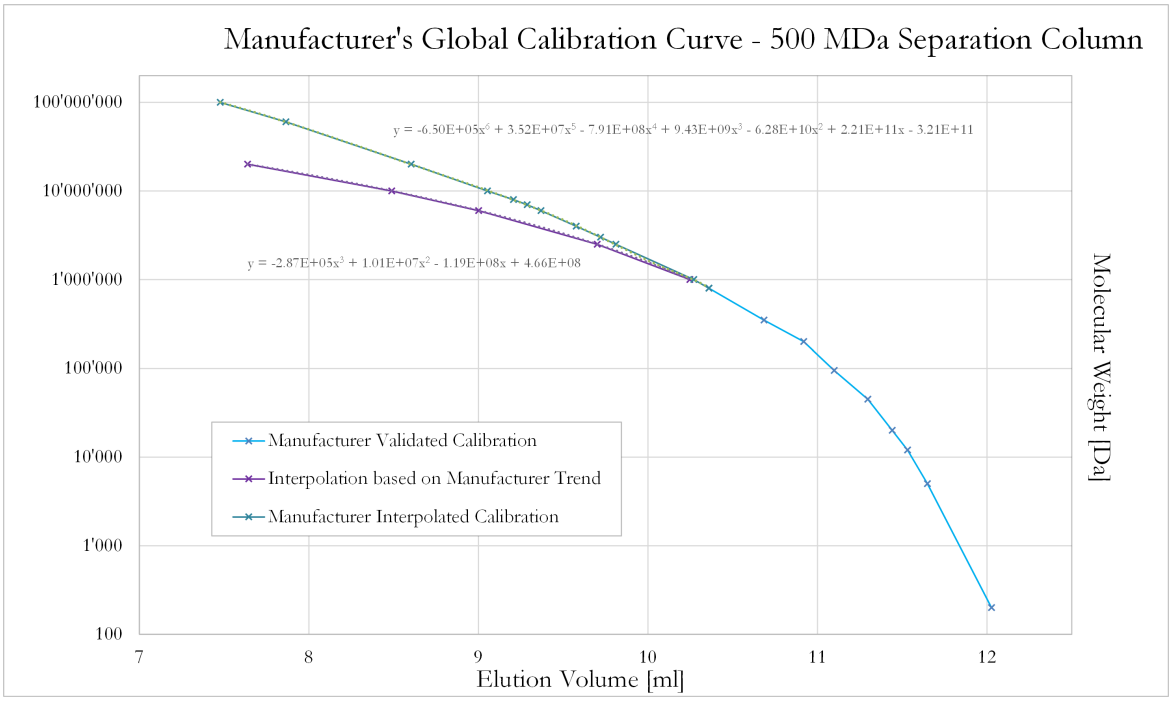

Figure 64: Global Calibration Curve - The manufacturer's proven Pullulan calibration in light blue with proposed interpolation in turquoise. Violet shows the authors interpolation based upon the trend of validated calibration values and a third order poynomial fit.

of later correlation between the individual retention times respectively elution volumes and corresponding molecular weights. The low-weight range could best described by a third order polynomial, the heavy-weight area was fitted with a sixth degree polynomial. A third calibration trend was inserted, extending the manufacturer validated low weight trend into higher mass regions in order to have a second interpolation basis.

13.1.2 Heavy Weight Calibration

Comparing sequences of measured polymer standards between 1 and 20 MDa with the manufacturer-provided calibration curve showed that the heavy weight interpolation trend didn't hold true. Inserted SNF standards suggest, that the trend of low-weight values is more or less going on beyond the 0.8 MDa data point. The prolonged interpolation curve of figure 64 resembles very strongly the measured modal values of SNF polymer standards as shown in figure 65. Seven sample sets at two different rates were examined proofing the general trend of the interpolation curve. Although the overall trend could be roughly validated, the

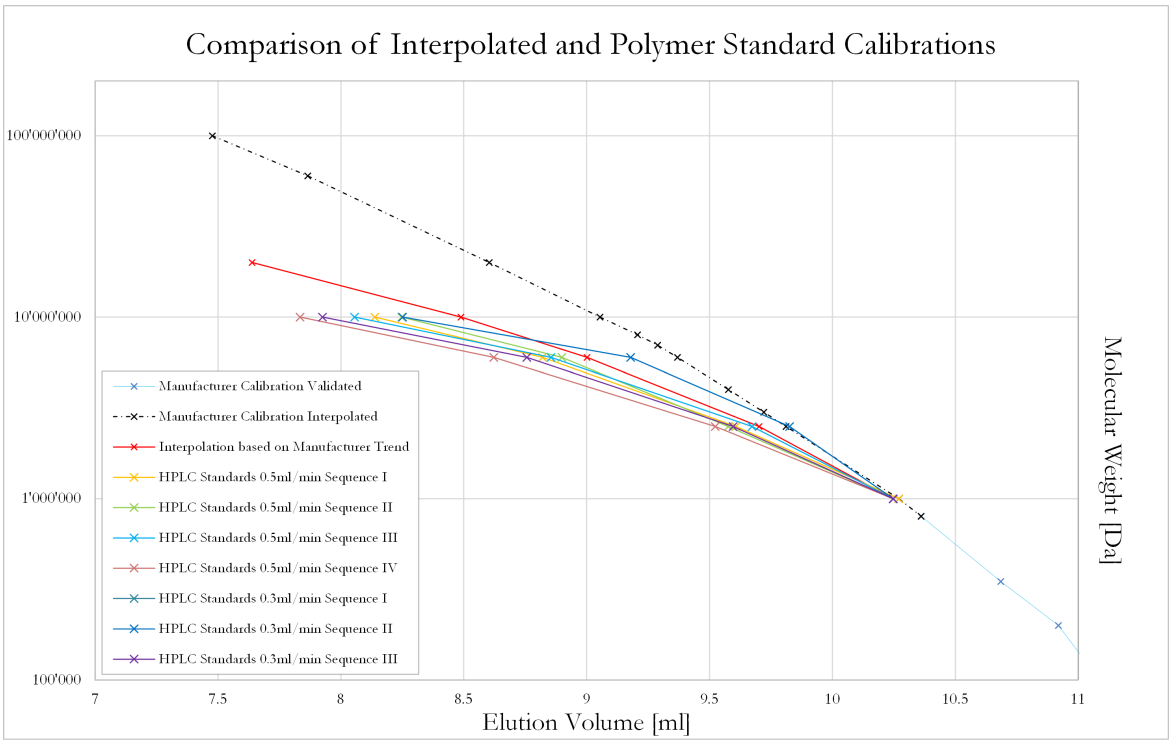

Figure 65: Heavy Weight Calibrations - A more detailed view of the global calibration curve with SNF polymer standards suggest a continuation of the low-weight trend. The trend provided by the column manufacturer is most probable too steep.

SNF sequences exhibit notably flatter lines than the low-weight interpolation, with a too wide spread of individual calibration sequences. This gaping of standard deviations can be explained with flow rate effects of the mobile phase, optical inaccuracies and random errors resulting in not perfectly reproducible sample sets. Reproducibility is given within individual sequences of chromatographic measurement, but not between distinct measurements. The farther away in time the experiments were performed, the higher the standard deviation of samples has been. In order to circumvent this problem, it was decided to built calibration environments for each set of chromatographic measurements by appending polymer standards to the actual sample sequence. Every set of 5 polymer standards (20, 10, 6, 2.5 and 1 MDa) was plotted and described by a third or fourth order polynomial, whichever yielded the most accurate fit. The 10 and 6 MDa area was put under special survey because most of the molecular size reduction happened inbetween those two. The above mentioned procedure was the most accurate way to establish a conversion environment considering the given resources.

13.1.3 Data Integrity

Having applied the conditioning workflow on chromatographic data sets, the introduced macros will export properly corrected and smoothed diode array signals. Depending on the original flow rate of the mobile phase, either 0.5 or 0.3 ml/min, a smoothing parameter of 100 to 200 data points was chosen. The original data length of 20 000 to 50 000 data points was reduced to 80 to 240 values by doing so. It was secured, that all characteristics, especially peculiarities of the polymer sections, have been preserved during the smoothing process. Figure 66 shows the complete data material of an exemplary core Berea 6-121 and the according flooding rates of 0.2 to 30 ml/min. It can be seen that data integrity is fully given.

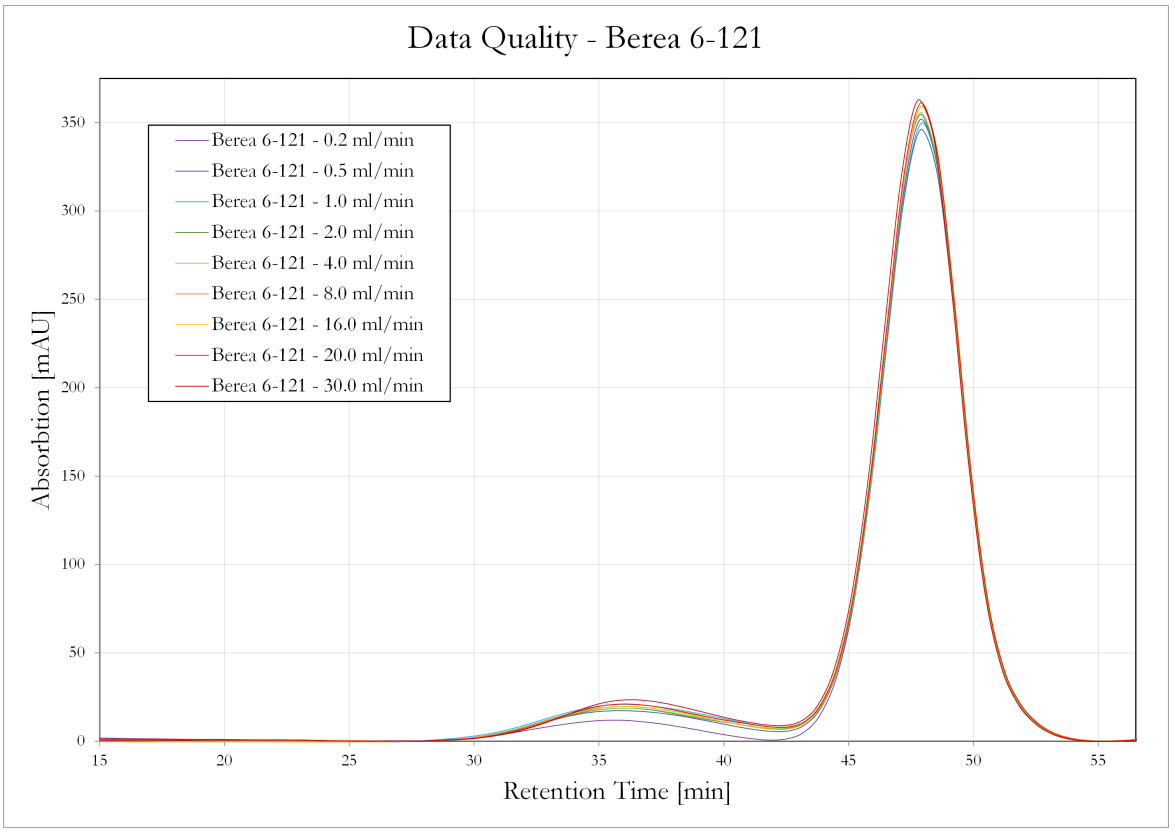

Figure 66: Proof of Data Quality exemplarily proven for Core Berea 6-121. All corrections yield proper diode array signals, snugging perfectly to the zero line and neatly stacked to a reference salt peak. A general trend of retardation can be observed at the polymer associated first signal peak.

The baseline signal is neatly corrected to the zero line and goes very flat. The salt peaks are properly stacked. No major buckles or fluctuations deteriorate the signal anymore. The lines exhibit a high degree of smoothness by simultaneously preserving all original characteristics. As can bee seen in figure 66, there is a significant change of signal maximum and height at the polymer associated section of the diode array signal. The differences in polymer peaks are in this figure overlain by the disproportionately huge salt peak, extending the plot scale and covering the changes in this section. But even on the first glimpse, it is possible to see that there is a shift in retention time between the lowest rate of 0.2 ml/min and the highest one of 30 ml/min.

13.1.4 Characteristic Values of the Polymer Peak

Rescaling the plot and focusing on the polymer associated part of the signal, leads to a characteristic pattern as shown in figure 67. The blue line signifies the smoothed and Savitzky Golay filtered corrected diode array signal. The original maximum is denoted by a red x-mark, being the polymer peak of the corrected but unsmoothed full-length signal. The dark blue mark shows the maximum value of the smoothed diode array signal. Due to larger signal steps, this value will not depict the real maximum of the polymer curve, but only the highest value of the data set. One way to cope with this problem is by fitting the crest of the polymer bump with a polynomial curve of order six, deriving this equation and setting it zero in order to get the maximum value of this polynomial fit. The polyfitted maximum is indicated by a light blue mark in this chart. The polynomial fit as such is shown in the form of a yellow trend curve with the corresponding sixth order equation in its vicinity. The

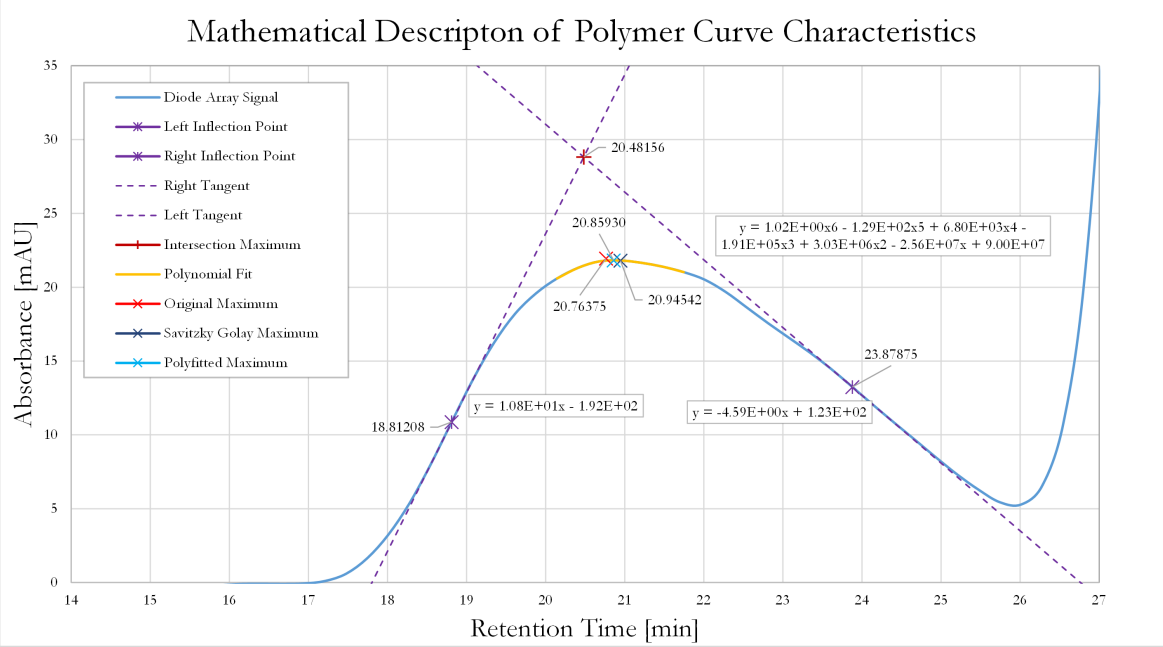

Figure 67: Mathematical Description of the Polymer Curve with characteristic values like different maxima (oringal, smoothed and filtered), inflection point tangents, intersection point and a polynomial fit to the curve crest with the matching maximum value.

second way to find a more characteristic maximum value for the polymer peak is by crossing tangents snugged to the flanks of the polymer curve. The two violet star shaped dots in the middle of both polymer flanks are their characteristic inflections points. They are detected by forming the second derivative of the curve equation and setting them zero. The tangents are found by simply taking values from the inflection point vicinity and constructing linears out of them, with matching equations given left and right of the tangents. The intersection point can be computed, by equalizing both tangent equations. The crossing point is marked in this chart by a dark red square cross. The most common applied practice of polymer peak comparison is performed either with polynomially fitted maxima or tangent intersect maxima, whichever provided more expressiveness. Although the requested trend can be seen in all of the above introduced maximum detections methods, these two illustrate shifting trends best and render it clearest observable.

13.2 Characteristic Peak Comparison - Type II-IV Analysis

Having established a sufficiently high data quality and being able to extracting all necessary curve characteristics, it is at this point possible to let the aforementioned macros apply previously described conditioning treatments on each of the overall 563 samples in all the 62 sample sequences.

13.2.1 Type I Experiments - Virgin Polymer

The sub-chapter about data integrity and figure 66 gave an overview on the changes, that can be expected when comparing individual rates of diode array signals. The first effect that shall be examined, is the alteration of molecular size of a virgin Type I core flooding experiment. Figure 68 enlists some representative flooding rates and their corresponding chromatographic signals. The scale is maximized and focused on the crest of the curve for better comparability. The salt peak and the baselines remain untouched for all samples of the sequence. Applying a Type II-IV analysis involves the comparison of individual peak values belonging to different core flooding rates. Contrasting distinct low rates with later high rates, makes it evident, that the maximum peak is significantly wandering from low retention times to higher ones as the flow rate increases. The difference in retention time between the lowest rate being 39.747 min and the highest flow rate of 40.603 min is almost 1 minute. This means that there

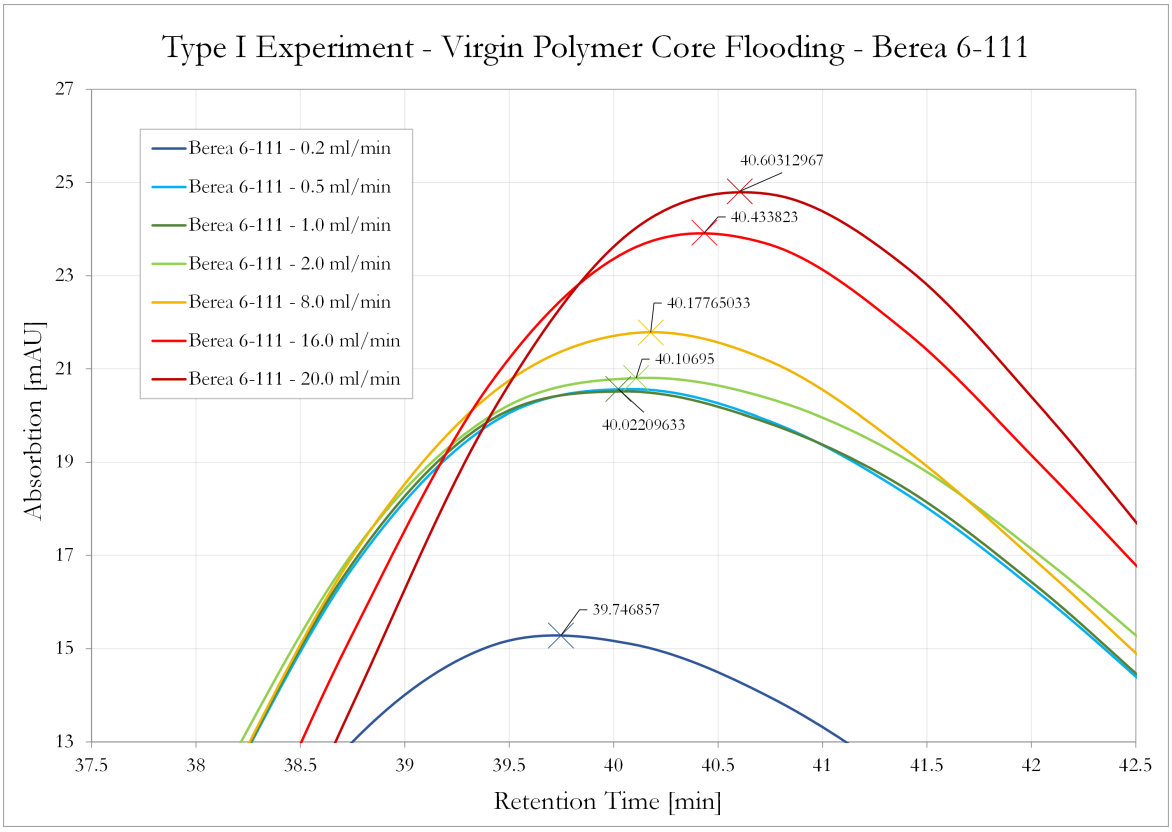

Figure 68: Comparison of Diode Array Signals for different Flow Rates of a Type I Experiment conducted on core Berea 6-111. The characteristic polymer peak exhibits a clear trend towards higher retention times at higher rates, meaning lower modal molecular size.

has been going on a striking reduction of modal molecular size during this Type I flooding experiment. The observed trend of successively decreasing molecular sizes can also be shown for other Type I experiments performed throughout the entire project. Therefore figure 68

with core Berea 6-111 stands representative for other Type I experiments conducted on cores Berea 6-109, 6-112 and 6-113. Albeit some outliers and high fluctuations at low rates, the general trend is reproducible and can be observed especially at elevated rates of 4 ml/min and beyond with high stability and due significance. Figure 68 proposes a more elaborate view on that phenomenon. In this figure each peak value is plotted against its according core flow rate. This is done for all four type I experiments and indicated by dashed lines in different shades of blue. The strong light blue curve is a summation of all four experiments, generated by simply averaging relating data points and finding representative values for each rate. In addition to that, standard deviations are derived and plotted as error bars on the average size reduction curve. The trend of molecular size reduction is again obvious and can be declared proven by now. For the purpose of quantifying the amount of coil size reduction, the retention time of individual polymer peaks are converted to molecular weight by means of previously introduced calibration curves. As explained in the last chapter, calibration curves were specifically constructed for each of these sequences and exhibit the accuracy of an order three polynomial fit. The modal value of investigated virgin polymer solutions

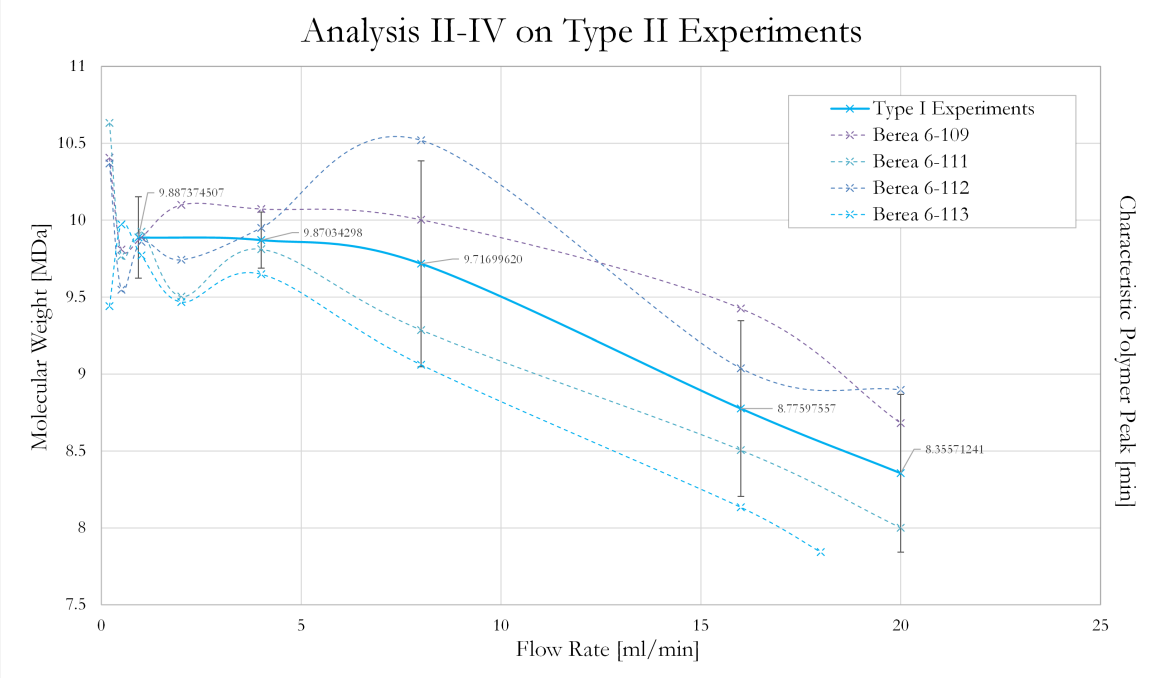

Figure 69: Comparison of Peak Maxima of Type I Experiments. Dotted blue lines mark individual Type I cores ranging from Berea 6-109 to 6-113. The bold blue curve represents the averaged characteristic curve of Type I experiments with respect to their molecular size reduction and retention time retardation. The molecular weight drops from 10 MDa to 8.356 MDa during a virgin core flooding experiment.

dropped from an originally denoted nominal 10 MDa molecular mass to calibrated 8.3 MDa on average. Some experiments showed an even more drastic reduction below 8 MDa, for example Berea 6-113 with a drop to 7.8 MDa. Numeric figures can be looked up in the provided result table.

13.2.2 Type II Experiments - Reinjected Polymer

A reinjection experiment of Type II-b uses polymer from a previously conducted Type I experiment and flushes a second core with the very same polymer solution. Figure 70 shows

the diode array signal of the lowest and the highest rate of a Type I respectively Type II-a experiment executed on core Berea 6-109 and the lowest and highest rate of a Type II-b experiment performed on Berea 6-110. The pattern observed on these two cores could be reproduced with a combination of a I-a core Berea 6-112 and a II-b core Berea 6-100. The result featured an overall lower expressiveness, but the general trend was the same. The reduction of molecular size of a virgin polymer, as described in the previous sub-chapter can, once more, be observed here with core Berea 6-109. The lowest rate of the reinjected Type II-b probe has roughly the same retention time as the peak of the highest rate of Type II-a samples. This means that the second experiment starts more or less with the same molecular size as the first kind of experiment. The phenomenon indicates, that alterations

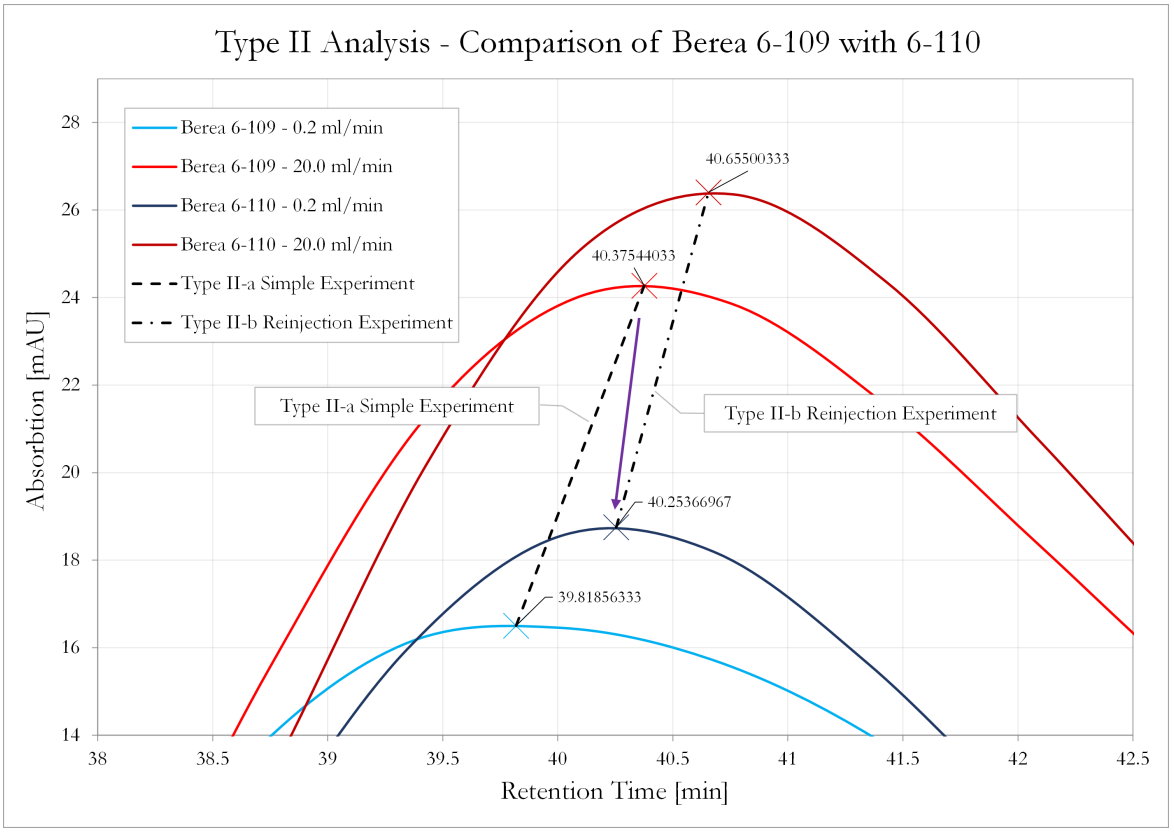

Figure 70: Comparison of Diode Array Signals of a Type II Experiment. The lighter lines signify diode array signals for a Type II-a experiment through Berea 6-109 at the lowest rate of 0.2 and the highest rate of 20 ml/min. The darker curves represent a Type II-b reinjection experiment performed afterwards on core Berea 6-110. The second experiment is notably shifted to smaller molecular sizes and starts at roughly the same molecular size, at which the first experiment ended.

are imprinted on the polymer chains in the long term and are not just temporary effects. This can be declared true for the small amounts of time between II-a and II-b experiments. Longer term experiments will be discussed in the analysis section of Type III experiments. For the time being, it can be stated that the molecular alteration seems to be stable over few hours to an entire day, when subjected to the highest rate of 20 ml/min.The retention time and thus modal molecular size doesn't however fit the previous highest rate perfectly. The second experiment starts with a slightly earlier peak time, meaning larger molecular weight. This could be explained by either mere statistical fluctuations or a slight amount of relaxation happening in the few hours between the two experiments. The consequence could be a small

amount of uncoiling and thus a slightly enlarged molecular size. Which of these theories are correct cannot be decided at this point of the work and with so few experimental runs. Nevertheless, the greater part of the molecular size reduction does not recover, which is surely the main effect. Molecular size between experiment A and B does not change significantly. Examining the second series of flow rates, belonging to the Type II-b experiment conducted

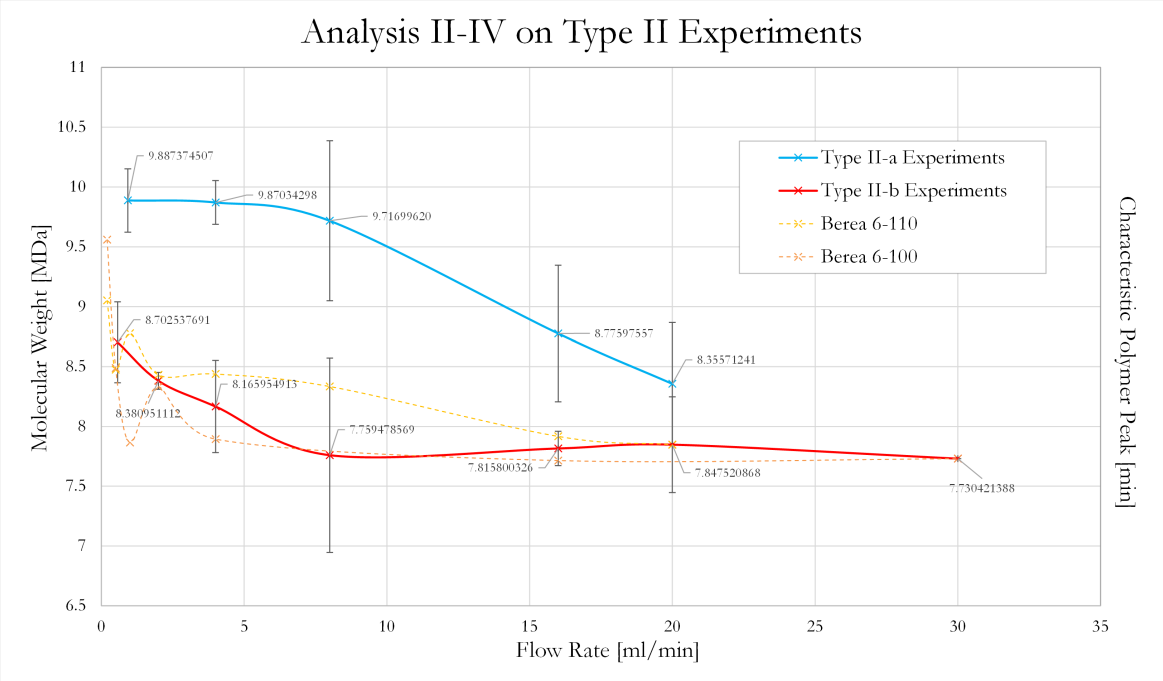

Figure 71: Comparison of Peak Maxima of Type II Experiments. Dashed redish lines mark individual Type II cores being Berea 6-100 and 6-101. The bold blue curve represents the averaged characteristic curve of Type I experiments with respect to their molecular size reduction and retention time retardation. The bold red line represents the averaged characteristic curve of Type II experiments with error bars. The second experiment starts approximately with the end value of the previous experiment 8.7 and drops to 7.7 MDa.

on Berea 6-110, shows a similar evolution of molecular size. The higher rates are delayed in comparison to lower ones, implying again a reduction in molecular size respectively weight. The decrease is smaller for Type II-b experiments, resulting in a time shift of 0.2 to 0.4 minutes, roughly. In the second set of Type II experiments the degradation of molecular weight isn't clearly visible but only mathematically detectable. Figure 71 is again a plot of peak maxima converted to molecular weights versus corresponding flow rates. Both cores, Berea 6-110 and Berea 6-100, indicated by dashed lines, start roughly at the highest rate of Type II-a experiments. Further deterioration during reinjection seems to be much smaller, resulting in a flatter drop of molecular weight as indicated by the summarized red Type II-b line with error bars. The conclusion of Type II experiments is, that the molecular size after a Type I experiment is mainly maintained when starting a II-b flood and that a further decrease of molecular weight and size is going on. This secondary degradation is much smaller than the original deterioration.

13.2.3 Type II Experiments - Offset of Mechanical Degradation

When comparing different plots in the style of figure 68, it is striking that low rates most probably show a large amount of fluctuation. The time shift of these low rates, mostly between 0.2 and 4 ml/min is somehow chaotic, and when systemically occurring, then much slower and less bold than the time shift and molecular size reduction of higher rates. This property indicates that mechanical degradation is an effect of elevated rates, as previously suggested in the literature review section. Both inflection points, especially the left one, and polymer maxima are somehow densely crowded in a point cloud at low rates. Elevated rates however, are standing out prominently with 8, 16, 20 and 30 ml/min. This can be nicely seen, when stacking polymer curves as in figure 68 but at a larger scale. All low rate signals are melting into one bold line with very little differences, whereas signals of higher rates are clearly shifted to later times or smaller sizes. Referring to figure 69, the same trend is detectable. The first low rates can be described as nearly flat with a very small slope. The

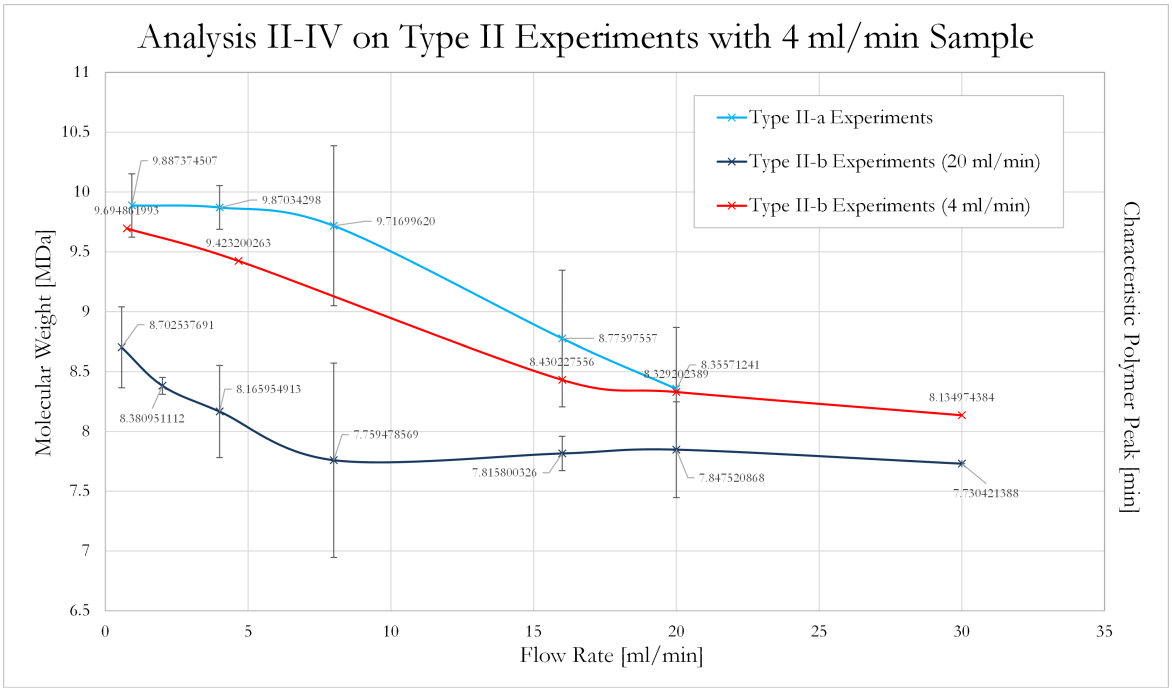

Figure 72: Comparison of Peak Maxima of a Type II Experiment at 4 ml/min. The bold light blue curve represents the averaged characteristic curve of Type I experiments with respect to their molecular size reduction and retention time retardation. The bold dark blue line represents the averaged characteristic curve of Type II experiments with error bars. The red line indicates the diode array peaks for a Type II-b experiment conducted with polymer sampled at 4 ml/min. Comparable to the corresponding viscosity profile, the characteristic drop is similar to the Type I experiment.

macroscopic explanation for that is, that polymer chains have enough time to adjust and react to contact and collision with other molecules or the rock's inner surface. At a rate of roughly 5 to 6 ml/min the curve starts to fall off dramatically with much lower modal molecular weights emerging. The explanation for that behavior is that the flow rate is now too high for polymer chains to cushion motion and collisions. They are affected by contact with each other and the rock, leading to deformation or even breakage. This is congruent to former described trends of curve flanks and maxima crowds. The rate of 8 ml/min is clearly affected by strong mechanical degradation, whereas samples of 4 ml/min seem mostly untouched or

just slightly subjected to these forces. In order to prove the theory, a Type II experiment was conducted with a polymer sample just below the critical offset point of 5 to 6 ml/min instead of normally the highest rate of 20 ml/min. The result of this experiment is shown in figure 72. For the purpose of comparability the averaged Type I and Type II curves with error bars were inserted too. The experimental outcome, signified by the red line, shows that 4 ml/min samples behave more or less like Type I probes. The curve performs in the lower part of the error bars of plain core floods. One of the two offset experiments through Berea 6-101 and Berea 6-117 resulted in a characteristic maximum curve that mostly lay inside the error limits, but sometimes dropped slightly below them, especially at lower rates. This behavior means that Type II-b offset experiments are very similar to Type I experiments in their traits. Either mechanical degradation was not strong enough, or three hours between the two experiments were sufficient to restore the slight degradation effects. Anyways, the modal

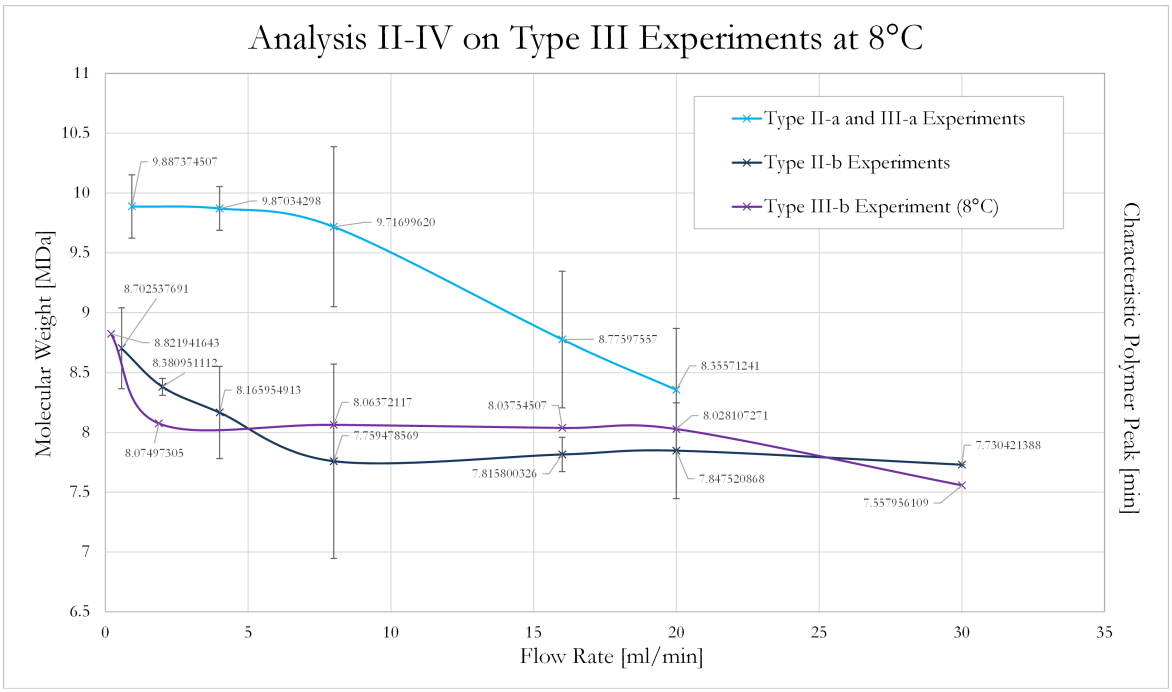

Figure 73: Comparison of Peak Maxima of a Type III Experiment at 8°C Storage Temperature. The bold light blue line and the bold dark blue line indicate characteristic size reductions for Type I and Type II experiments. The violet curve signifies a Type III-b experiment at 8°C and moves inside the boundaries of the reference Type II size curve.

molecular size featured more or less the same composition as the virgin polymer solution. The fact that characteristic molecular mass reduction curves performed on the lower edge of the error band, can be interpreted as slight degradational effects having reduced the modal molecular size by just a bit. At this point it is not possible to say, if this is really true or if the encountered effect is simply due to the wide spread of Type I experiments mentioned in earlier discussions. Howsoever, it can be stated that there is a critical flow rate present after which graver degradational processes get activated. This offset value lies surely inbetween 4 and 8 ml/min with the highest probability 6 ml/min.

13.3 Temperature Effects - Type II-IV Analysis

It has been shown so far, that the time between any A and B experiment for Type II setups is not sufficient to have an effect on the modal molecular weight of examined solutions. As described in the methodology section of this thesis, the impact of time and temperature shall be further investigated within this piece of research. For that reason 4 different temperature scenarios where created and larger polymer samples been stored at different conditions for 2 months or 62 days. The effects on molecular level can best be displayed in plots with peak maxima respectively molecular weights versus core flooding rates. In order to ensure comparability both Type I and Type II-b outcomes are depicted too with their corresponding error bands.

13.3.1 Type III Experiments - Low Temperature Conditions

The first and easiest plot is figure 73. The violet line is a Type III-b 20 ml/min degraded polymer solution, which was stored at 8 °C and reinjected into core Berea 6-121. The initial molecular weight is pretty much the same as in a plain Type II-b experiment and thus equivalent to the highest rate of a Type I core flood. The curve of this III-b experiment

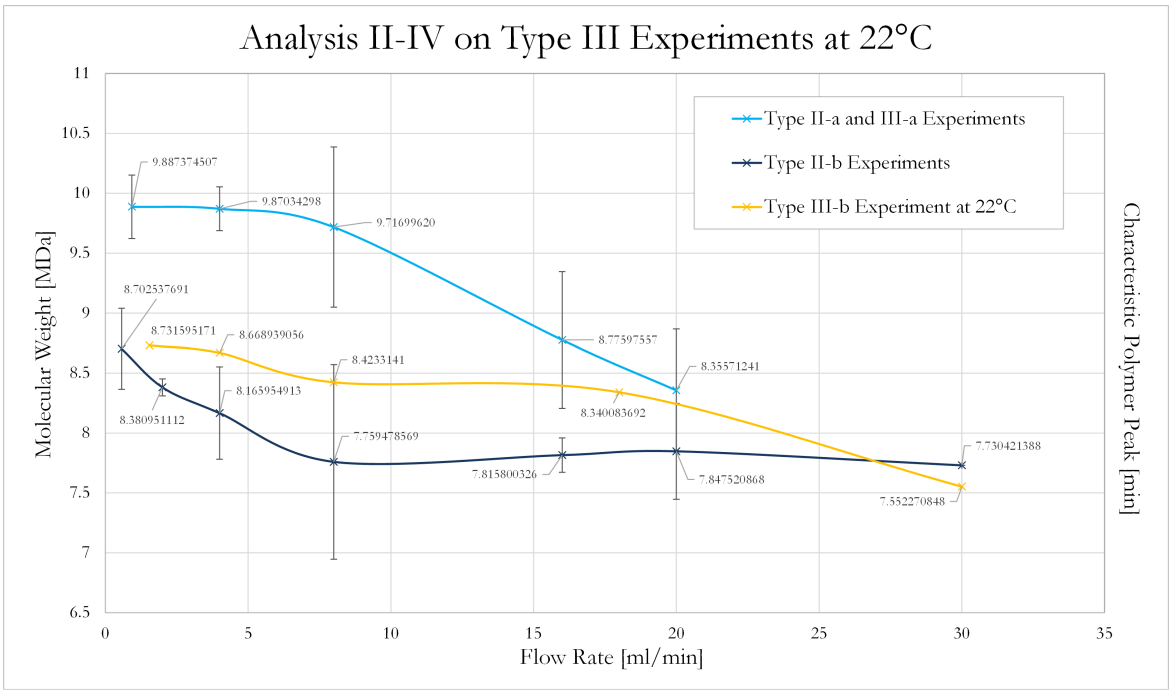

Figure 74: Comparison of Peak Maxima of a Type III Experiment at 22°C Storage Temperature. The bold light blue line and the bold dark blue line indicate characteristic size reductions for Type I and Type II experiments. The yellow curve signifies a Type III-b experiment at 22°C, which outperforms the dark blue Type II reference by a little. It is similar but not identical to the second core flood.

follows more or less the lead of the averaged Type II-b line and its corresponding limits. This means that neither time nor temperature had a measurable impact on the polymer solution. Molecular size is similarly reduced as a simple Type II-b experiment would have been, without storage or chilling. A macroscopic explanation for the like behavior could be, that low temperatures hindered the polymer chains to uncoil and restore their shapes. The refrigerator kind of extracted energy from the system, disabling molecular movement in the entire solution. Metaphorically spoken the polymer chains have been "frozen" or their

molecular structures have been cast to stone. The specific trend of weight reduction cannot be interpreted because it exhibits no clear trend.

13.3.2 Type III Experiments - Room Temperature Conditions

The second set of Type III experiments marginalizes the effect of temperature and focuses solely on the effect of time on degraded polymer. The outcome is presented in figure 74. The yellow line in this chart illustrates the according Type III-b experiment through core Berea 6-119. It reveals that the characteristic weight reduction curve performs at the upper edge of the reference Type II band, mostly over-performing the limits of this type of experiment. Although it sometimes touches the boundaries of Type II curves, the 22 °C curve lies above the plainly sheared polymer solution of Berea 6-100 and 6-110. This means that the stored solution has regained parts of its molecular size over time. This restoration effect is comparatively small with regard to Type I performance and its limits, but a rise is still noticeable. The macroscopic explanation for this effect has already been given in the literature and ex-

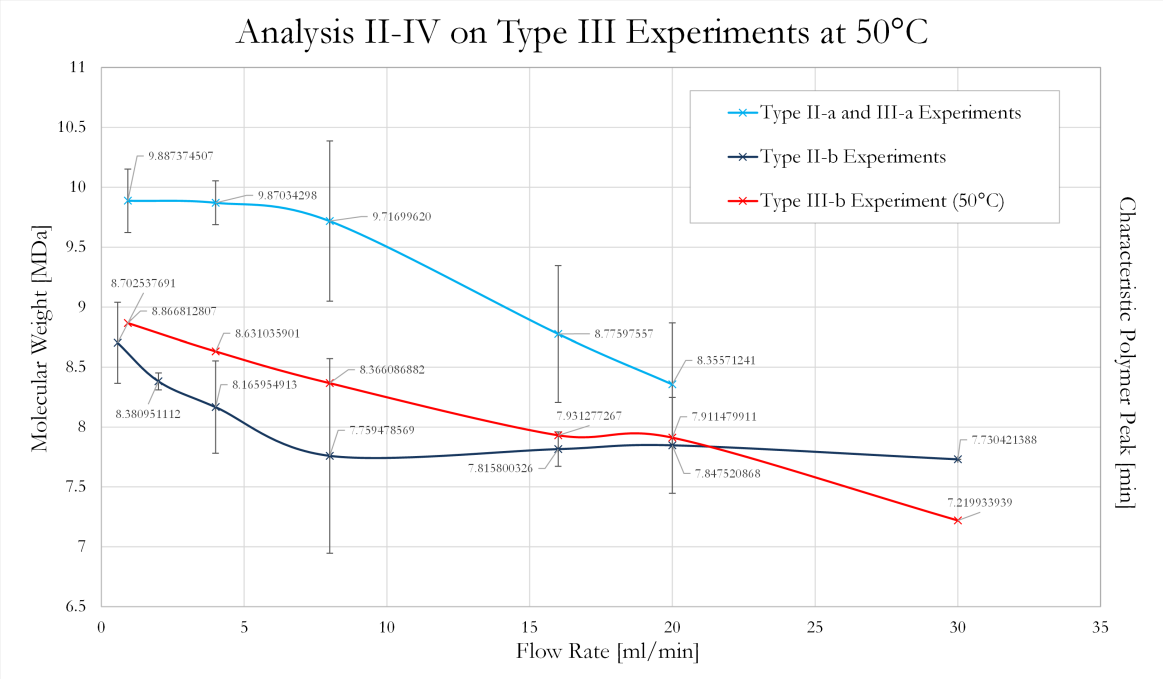

Figure 75: Comparison of Peak Maxima of a Type III Experiment at 50°C Storage Temperature. The bold light blue line and the bold dark blue line indicate characteristic size reductions for Type I and Type II experiments. The red curve signifies a Type III-b experiment at 50°C, which performs similar to the 22°C experiment, leaving the limits of Type II-b reference area.

pectation section, but, in a nutshell, the polymer chains are able to unravel and regain parts of their original shape. The unraveling process enlarges their volume, a property that can be detected by size exclusion methods. The experimental setup was able to show that most probably some of the previously inflicted deformation could be undone by simply letting the sheared polymer solution rest at standard conditions. The remnants of molecular size loss must be attributed to whether permanent deformation or, more likely, chain scission.

13.3.3 Type III Experiments - Elevated Temperature Conditions

Figure 75 shows the last examined III-b experiment with storage condition of 50 °C. The red curve in this very figure denotes the specific experiment conducted on core Berea 6-123. The outcome resembles very strongly the behavior of Berea 6-119 and the Type III-b experiment at 22 °C storage conditions but lies a little lower. This slightly deterioration renders the according characteristic curve operating mostly in the probability band of the reference Type II-b curve. It is hard to say, if the elevated temperature really had an impact on the solution's development of molecular size over time, but the trend performs at the upper edge of the II-b band at lower rates. This suggests that there is some sort of size restoration active at these rates. Conversely, elevated rates clearly contradict this early trend, dropping to the lower limit of the Type II-b curve. It is a curious effect that 22 °C behavior outperforms the

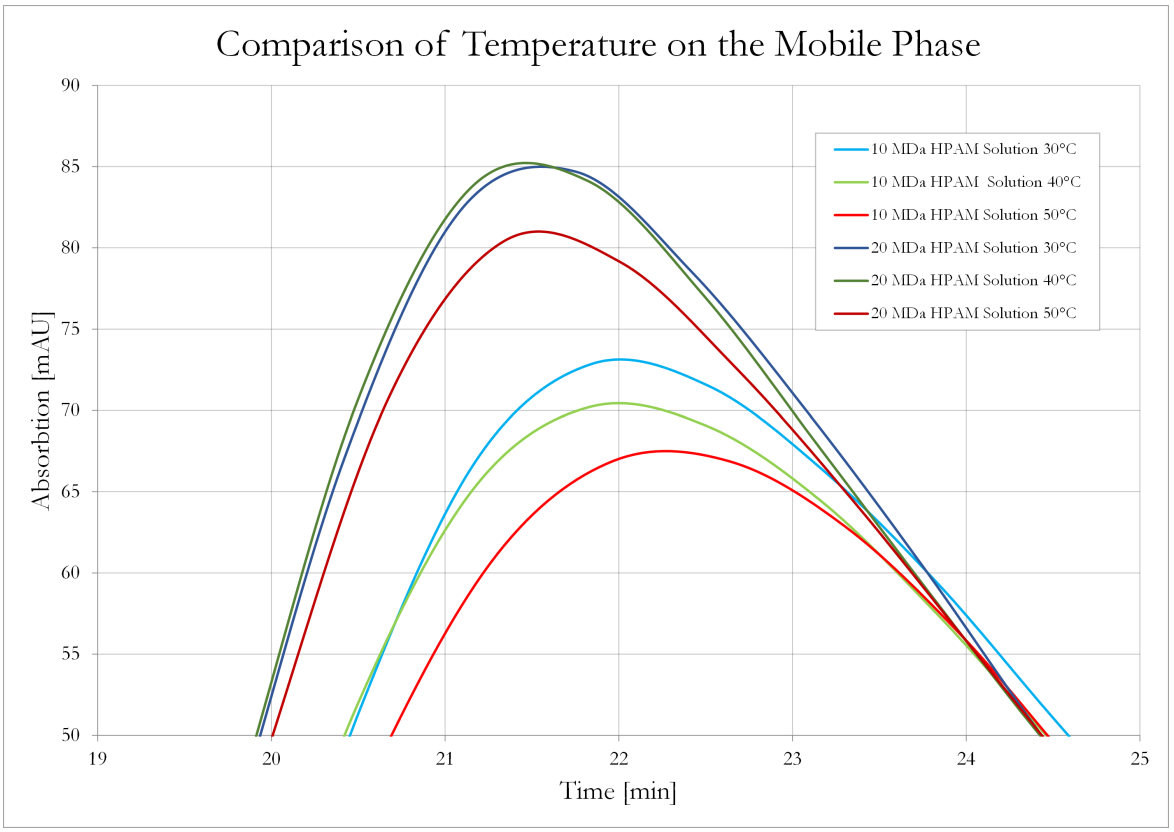

Figure 76: Temperature Effects on the Mobile Phase. Two data series of 20 and 10 MDa in comparison with 30, 40 and 50°C surrounding temperature for the thermostatted column compartment and thus the mobile phase.

higher energetic 50 °C degree line. What is striking though, is the high slope of that specific experiment. Figure 74 already showed a much steeper reduction of molecular sizes than the reference II-b experiment, but figure 75 distinctly exceeds this tendency. The phenomenon provides no hints for interpretations nor a direct or straight explanation. It could again be thinkable that elevated temperatures soften the chains' molecular structure and render them more vulnerable for further degradation. However, no proof for that theory can be provided given the available data.

13.3.4 Temperature Effects on the Mobile Phase

This subchapter belonging to the secondary objectives section turned out to be relatively irrelevant to the measurement process. Figure 76 shows the diode array signals of different flooding rates for Core Berea 6-108 at different temperatures of the thermostatted column compartment. Three distinct temperature scenarios were tested, being 30, 40 and 50 °C. Higher temperatures resulted in a time shift to later retention times of the signal and a reduction in signal strength. The characteristic curve and all key figures remained consistent. The observation of these small differences leads to the conclusion that temperature effects on the mobile phase are negligible.

13.4 Degradation due to Pumping Equipment

As described in the last module of the secondary objectives section, an aspect of the overall research aim was defined to be the examination of pumping equipment's impact used in polymer flooding treatments on the above kind of polymer solutions. For that reason a progressive cavity pump Type Nemo 4NE20, typically used for polymer dosage, was scrutinized with regard to changes in the pumped-through liquid. The polymer solution was taken from

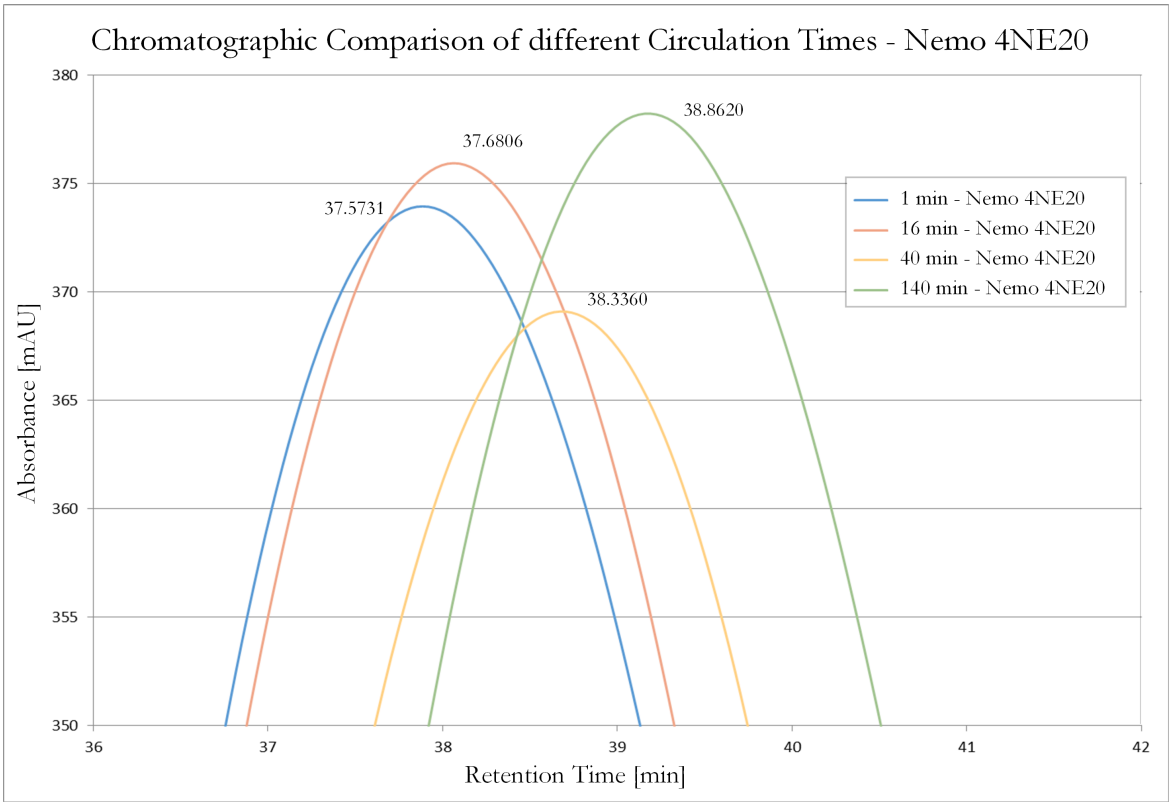

Figure 77: Comparison of Diode Array Signals for different Circulation Durations between 1 and 140 Minutes. A clear shift in retention time is observable.

the field, being a 20 MDa FLOPAAM 3630 polymer with a concentration of 4100ppm. The used polymer has already been degraded by field deployment which is why no calibration environment could be created for that specific experiment. A simple relative comparison of retention times was applied to detect changes in the polymer solution's composition. The first part of the pump experiment involved filling the storage container of the pump with field polymer and pumping the liquid through the system at different rates ranging from

stage 1 to stage 8 with a throughput of inbetween 3.2 and 20 l/min as enlisted in the below table.

Stage	Rate	Unit	Rate	Unit
1	3.2	[l/min]	0.192	[m^3/h]
2	3.8	[l/min]	0.225	[m^3/h]
3	5.5	[l/min]	0.328	[m^3/h]
4	6.6	[l/min]	0.394	[m^3/h]
5	8.5	[l/min]	0.512	[m^3/h]
6	11.7	[l/min]	0.703	[m^3/h]
7	16.0	[l/min]	0.957	[m^3/h]
8	20.0	[l/min]	1.199	[m^3/h]

Table 13: Different Stages and the According Pump Rates for Nemo 4NE20

The result of this first experiment yielded a blank result, meaning that no alteration was noticeable after one single run, regardless of the used stage and applied flow rate. This experiment clearly showed that none or negligible small amounts of mechanical degradation are inflicted by the like pumping equipment. More interesting was the second part of the experiment. The exit hose of the pumping system was-short circuited with the inlet hose,

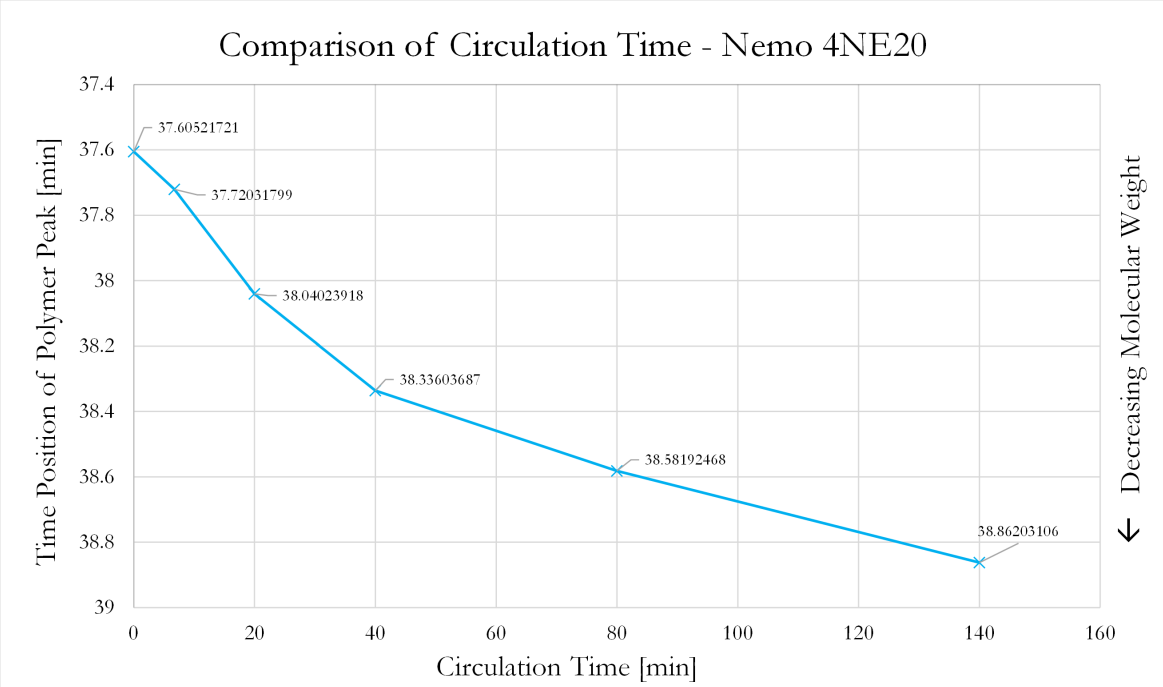

Figure 78: Comparison of Diode Array Signal Peaks for all Circulation Times between 1 and 140 minutes. A steady drop of polymer peak time is the general trend.

creating a circulating flowpath through the pump. Samples were taken at different times and compared to the virgin solution and each other. The outcome of comparing diode array signals is shown in figure 78. It is clearly observable that there is a huge time shift occuring between different circulating durations. The retardation of the polymer peak between one minute circulating time and 140 min of circulation is 1.3 minutes. Figure 77 shows the well established technique of maximum reduction versus circulating time for this case. The successive drop of retention time and thus molecular weight is unmistakably evident. In comparison to previously discussed core flooding experiments, there is no critical offset

point detectable. Mechanical degradation is therefore continuously proceeding. The steady progress of polymer deterioration suggests that every through-put adds a slight amount of degradation to the polymer chains, accumulating damage over time. A second explanation for this kind of behavior would be that the mechanical structure of polymer chains is softened by every run, leading to lower degradation resistance and ongoing breakage or deformation after this softening process. Anyways, the general trend of degradation is obviously non-linear. This could be linked to many different causes, but none of them are provable at this stage of the research considering the given resources. Most probably, diverging susceptibility of different chain lengths causes the non-linearity in the reduction-curve. Due to the lack of calibration environments, size losses are not exactly quantifiable.

14 Conclusion and Discussion

Having presented all results by now, this last chapter will summarize the findings of this thesis and discuss their significance and interpretation.

14.1 Minor Objectives and their Outcome

First of all the fulfillment of minor objectives shall be described, because they were prerequisites without which no further investigation of the main subject would have been possible. The outcome shall be summarized in a nutshell:

1. A fast and accurate correction and conditioning workflow could be established
2. Intersection maxima and maxima based on crest fits turned out to be most expressive
3. Findings of previous experiments could be reproduced
4. Identical results suggested system and sample stability
5. Time shifts of polymer peaks were clearly distinguishable
6. Calibration curves were established to convert peaks to molecular mass
7. Temperature had no major effect on the mobile phase with regard to measurments
8. Higher Temperatures shifted the DAD signal slightly downwards and to later times
9. PCP pumps do not inflict significant damage on polymer solution at one pass-through
10. Mechanical Degradation can be detected at higher circulating performance through the pump

14.2 Working Hypotheses Decision and Core Objective Discussion

Having now provided all necessary data, it is possible to decide on the previously constructed logical table of working hypotheses. On the first level, hypothesis I and II have to be declared falsified for time and elevated temperature effects, because the resulting viscosity and molecular sizes curves did neither match Type I experiments, which would have been a proof for full restoration Hypothesis I, nor did it fully overlay with Type II experiments, which would have been the final proof for entirely long lasting if not permanent damage. The one theory that can be verified is Hypothesis III with parts of both models being true. Analysis method I-III suggests, that a small amount of viscosity can be regained, when polymer solution is allowed to rest at 22 to 50 °C. Although the effects are comparably small, apparent viscosity values do suggest, that some of the lost viscosity during core flooding was regained, because the according III-b curves are situated in between the two reference curves of Type I and II experiments. The fact that stored polymer curves are rather sticking to the degraded II-b viscosity and molecular size, proposes that the restoration effect has been rather small in comparison to permanent damages. These chain scissions represent the greater part of the losses. In this conclusion section temporary viscosity losses are attributed to chain unfolding due to former deformation, although it is also possible that chain entanglement triggered the restoration process. The same is true for permanent damage, which is described here as a chain scission process, although it would also be possible to refer to it as permanent deformation. The main explanations, chain unfolding for temporary and chain breakage for permanent losses, are most likely. On the one side, these were the major assumptions and explanations by previous researches and they themselves based their claims on their own meticulousus experiments. On the other side, the amount of each effect, proposes the above-mentioned explanations. The tremendous amount of viscosity and chain size loss, is very unlikely to be explained by permanent deformation, because a densification and further

compaction of polymer coils is only legitimate to a certain degree. Very soon there will a point be reached, at which all of the void space is occupied by chain branches and no further packing is possible. The polymer solution looses a third to a half of its original viscosity, which is a clear indicator that it cannot be mere permanent deformation. The conclusion from this disparity must be, that only chain scission can cause such a grave and continuous loss effect, although permanent deformation can still play a minor role in that process. The same, but less significant is true for temporary losses, which must be attributed to chain unfolding due to the small amounts of restoration observed. Chain entanglement would most probably lead to stronger and more systematic viscosity healing. On the other hand, the low concentration of 250 ppm contradicts the theory of chain entanglement because in comparison to experiments of previous sub-projects using 1000 ppm and even higher concentrations, the polymer chains have four times more space to unfold and float without affected each other or entangling. The slight amount of viscosity and size recovering and low concentrations on the other hand, are a strong indicator to favor Hypothesis I-I polymer unfolding over I-II chain entanglement. But, as a matter of fact, these are just assumptions and can't be quantitatively verified at this point.

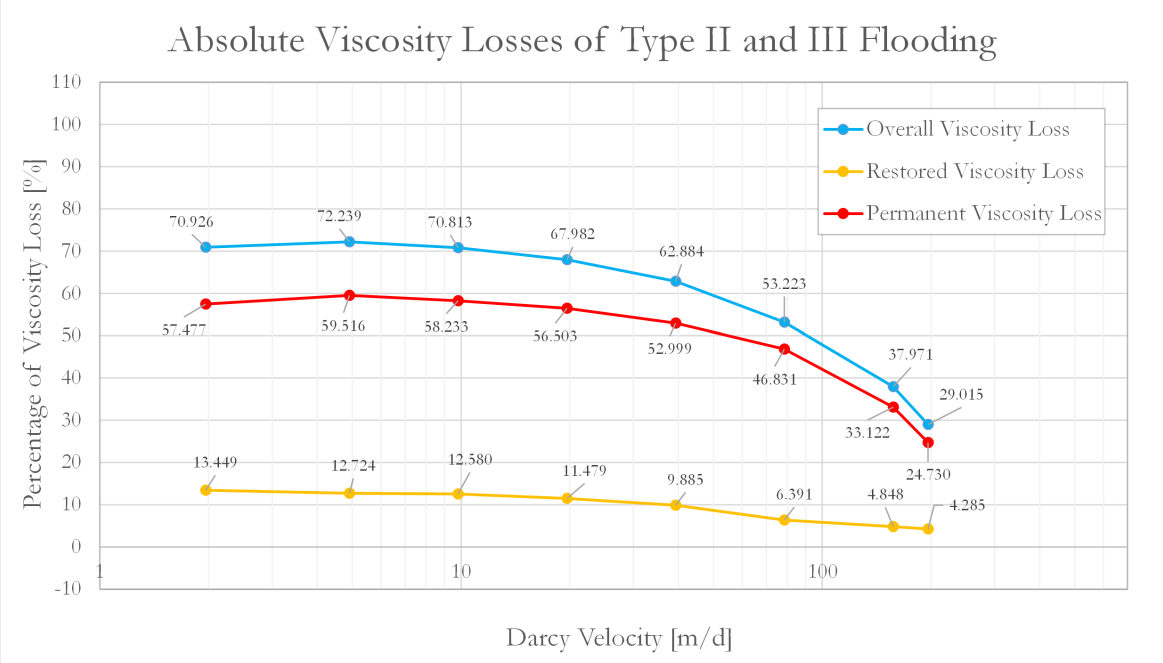

Figure 79: Total Viscosity Loss of Type III Experiments with Absolute Percentages of Permanent and Temporary Losses

What can be measured and quantified is the ratio of restorable to permanent viscosity loss. For that reason two calculations have been executed. The first one issues the overall loss of apparent viscosity as the ratio of virgin Type I values and degraded Type II viscosities. The second ratio describes the percentage of viscosity restoration in comparison to the absolute total loss. This is done by bringing the average Type II apparent viscosity curve to the zero line and measuring the percentage of the 50 °C Type III-b experiment as the highest expressive data series in comparison to the virgin Type I curve. The results are shown in the below table. The overall viscosity loss equals an average 70.926% for lower rates with a successively ongoing shrinkage to 29.015% for elevated ones. A non-linear trend is observable between both limits, as shown in figure 79. The average total viscosity loss equals 58.132%

of the original viscosity. Shares of permanent and restorable viscosity loss are provided in figure 79 on an absolute scale and in figure 80 in a relative framework.

Flow Rate as Darcy Velocity	Total Viscosity Loss Type II Experiment	Relative Temporary Viscosity Loss	Relative Permanent Viscosity Loss	Absolute Permanent Viscosity Loss
[ml/min]	[%]	[%]	[%]	[%]
1.96	70.926	18.963	81.037	57.477
4.91	72.239	17.613	82.387	59.516
9.82	70.813	17.765	82.235	58.233
19.63	67.982	16.886	83.114	56.503
39.26	62.884	15.719	84.281	52.999
78.53	53.223	12.008	87.992	46.831
157.06	37.971	12.769	87.231	33.122
196.32	29.015	14.767	85.233	24.730
Average	58.132	16.265	83.734	48.676

Table 14: Viscosity Losses of a Type III Analysis

The relative percentage of viscosity loss is best suited to picture the amount of each type of loss for these kind of time experiments. It is evident, that despite the non-linear overall viscosity loss, the ratio of temporary to permanent reduction is comparably stable, ranging from permanent deterioration of 81.037% for low to 85.223% for high rates. Vice versa,

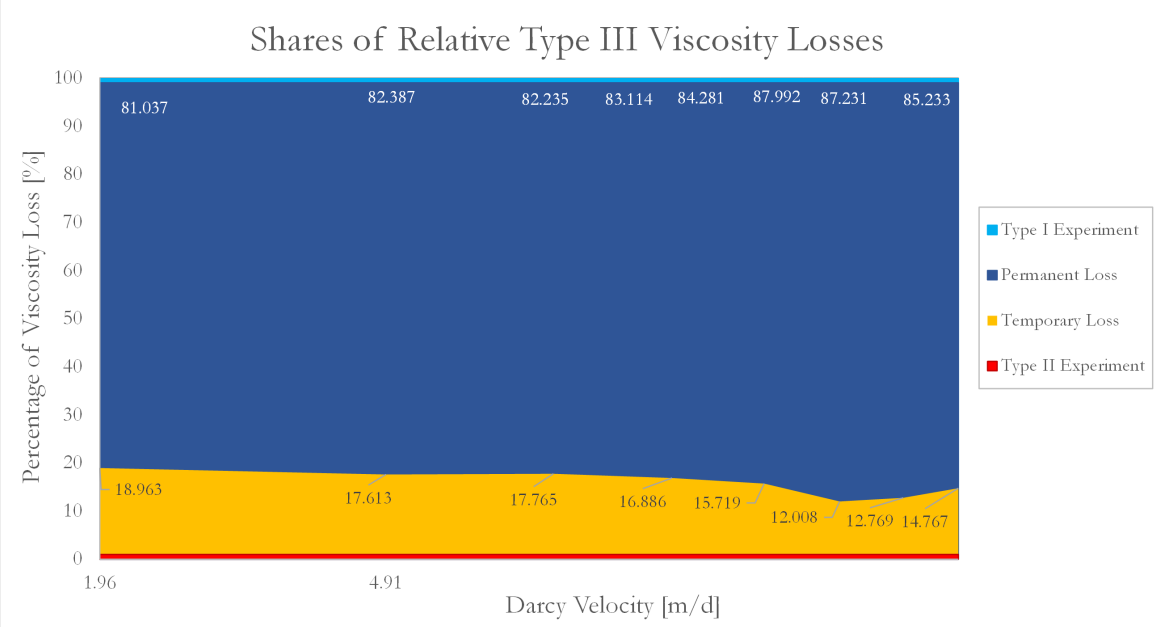

Figure 80: Total Viscosity Loss of Type III Experiments with Relative Shares of Permanent and Temporary Losses

restorable viscosity losses range inbetween 18.963% for low and 12.760% for high rates. The average ratio is 15.811% temporary to 84.189% permanent viscosity loss or expressed in one number 0.812. According absolute values are given in figure 79. The amount of absolute permanent polymer damage is given by absolute loss minus restorable diminution. Comparison of reduction results leads to a range of 57.477 to 24.730% for absolute permanent loss

instead of 70.926% to 29.015% total damage including temporary effects. The average apparent viscosity loss for these experiments can be quoted 48.676% and must be declared not as grave as the originally observed 58.132%. This means that roughly an absolute 10% and a relative 16% gain of viscosity wasn't totally lost during the polymer flooding treatments.

Molecular size losses feature a similar trend but are much more difficult to display and tainted with graver errors and higher uncertainties. The overall molecular size loss ranges from 1.12% for the lowest rate to 16.44% for the highest one during a Type I experiment. A reinjection experiment decreases the molecular size of examined molecules further from 14.58%, which doesn't match exactly the previous value of 16.44%, to another 22.69%. This is the total loss in molecular size experienced throughout the whole flooding experiment.

Flow Rate	Molecular Weight	Absolute Loss	Relative Loss
[ml/min]	[MDa]	[%]	[%]
0.925	9.887	1.126	1.126
4	9.870	1.296	1.296
8	9.716	2.830	2.830
16	8.775	12.240	12.240
20	8.355	16.442	16.442
Average	Losses	16.442	16.442
0.2	8.541	14.582	0
1.875	8.165	18.340	1.897
8	7.759	22.405	5.962
16	7.815	21.841	5.399
20	7.847	21.524	5.081
30	7.730	22.695	6.252
Average	Losses	22.695	6.252

Table 15: Molecular Weight Losses - Type II-IV Analysis

What is striking is the fact, that the total viscosity loss of 58.132% is much more grave than the loss of modal molecular size, 22.69%, would propose. The conclusion that can be drawn from this discrepancy is that there exists a disproportional relation between molecular size and solution viscosity. It seems that larger molecules contribute much more to the overall viscosity than smaller entities. This finding is congruent to assumptions and theories of former researches from the literature review section. An accurate comparison or linkage between viscosity loss and loss of hydrodynamic volumes isn't exactly feasible due to the strong rate dependency of solution viscosity. The size shrinkage of experiment I is with about 16.4% nearly three times larger than the value 6.3% of the subsequent experiment. What this means in terms of interpretation is unclear. Most probably the encountered non-linear trend will flatten out with higher molecular size losses leading to much smaller viscosity losses with higher size reductions. Restoration effects are nearly undetectable and range inbetween 1 and 3% compared to II-b experiments. The meaning of that statement is that these few percent of chain unfolding are responsible for a share of 16% viscosity restoration. This shows again the disproportion between particle size and viscosity and the impact of larger molecular chains on the overall solution flow resistance.

14.3 Problems and Obscurities encountered during the Research Work

The above statements must be read carefully and with all due doubt. The core flooding experiments are a well established examination technique and are based on few, very reasonable assumptions. All findings connected to apparent viscosities and core flooding results can be taken as reliable, reproducible and significant. The chromatographic examination method on the other hand is a newly configured technique and is founded on many assumptions which hold a high degree of uncertainty. For example the description of polymer coils during the measurement process, the assumed straight correlation between molecular size and molecular mass and the lack of knowledge of accurate shapes, positions and extents of involved molecules. Even the calibration method is error afflicted, considering the industrially produced partially hydrolyzed polyacrylamide and the wide range of constituent sizes and weights. The problem with size exclusion is, that the whole chromatographic system is designed to detect molecular sizes and not weight, which is presumably correlated later on in the process. Another problem was the impossibility to say if just the packing of the molecular chains changed during an experiment or also their molecular weight. A denser packed or rougher deformed chain coil will have larger retention times as a less packed chain coil with the same molecular weight. It was neither possible to distinguish between the permanent deformation and the chain scission theory, nor was it for the unfolding and the entanglement hypothesis. It was furthermore not possible to catch the trend of large to small chain ratio during the degradation process. Therefor all data and interpretations concerning chromatographic measurements must be understood as trends with high uncertainties implied. Although the size exclusion data matches quite well the core flooding findings, caution is still advisable and statements must be made with all due restrictions in mind. Especially slight trends in the range of few percents have to be taken critically. More significant trends and differences with proven reproducibility are of course valid for usage and further interpretation as it was done in the analysis section above.

Further restrictions are for example storage time, reproduction of single runs and the chosen temperature scenarios. The storage time span was limited to two months due to the extent of a master thesis. In addition to that it wasn't possible to conduct a second run of III-b experiments due to the tremendous effort and limited storage room plus available time. Therefore, it couldn't be verified whether the observed storage effects are fully reproducible or just statistical outliers. The similar over-performance of 22 and 50 °C curves, on the other hand, strongly suggest that the viscosity and molecular size healing is indeed happening and provable. Despite some remaining doubts, in the context of this thesis and the available data and methods, all the above statements must be passed for ascertained. Of course, the above given interpretations and explanations cannot be fully verified. They are just a qualitative means for better understanding of quantitative experiment trends. Theories beyond the above interpretations must be called pure speculation and cannot be proven with provided data sets. What remains, in any case, are hard, reproducible data series and results presented in the last two chapters.

14.4 Summary of Findings and Final Statements

1. Core flooding experiments are well established, reliable data sources.
2. Chromatographic measurements illustrate trends and rely strongly on assumptions.
3. Despite HPLC method restrictions general trends and relative relations could be quantified.
4. A global calibration curve based on newly generated and manufacturer data could be generated.
5. Individual third order calibrations for each sequences proved most feasibly.
6. 62 sequence sets were examined with a total of 563 samples.
7. The examined system possesses a critical offset point below which no substantial mechanical degradation will occur.
8. The critical offset rate is roughly 6 ml/min or 61 m/d.
9. Highest apparent viscosity is typically reached at 8 ml/min or 76 m/d.
10. Critical temperatures of 80 °C provably destabilize polymer solutions.
11. Subjected to that high temperatures, the solution's apparent viscosity is dramatically diminished.
12. Storage (III-b) at 8 °C yielded identical values as Type II experiments.
13. Storage at 22 °C and 50 °C exhibited some degree of viscosity and molecular size alteration in comparison to II-b.
14. Hypotheses I and II have to be declared falsified.
15. Hypothesis III is stated verified.
16. A combination of permanent and temporary viscosity loss was discovered.
17. It was not distinguishable whether chain unfolding (I-I) or chain entanglement (I-II) was responsible for the temporary viscosity loss.
18. The small amount of temporary loss and low concentrations point to molecular unfolding (I-I).
19. It was not possible to distinguish between chain scission (II-I) and permanent deformation (II-II).
20. Due to the amount of permanent damage and literature hints, chain scission (II-I) is though to be the major cause for permanent damage.
21. The average ratio between temporary and permanent damage is 15.811 to 84.189%.
22. The average total observed viscosity loss is 58.132%
23. Without regained viscosity, the permanent and thus total viscosity loss is 48.676%
24. The loss of molecular size during a Type I experiment is 16.44 %.
25. The absolute loss of a further Type II experiment is 22.69 %
26. The relative loss of a second coreflooding experiment is roughly 6.5 %.
27. The molecular size at the beginning of a Type II experiment equals roughly the size of the last rate of a Type I experiment.
28. Type III-b experiments show a restoration of 1 to 3% of molecular size.
29. The 1 to 3% of size growth seems to be responsible for 16% of viscosity healing
30. There is a non-linear relation between molecular size and apparent viscosity reduction present.

References

Agilent. Agilent 1200 infinity series - user manual. *http://www.agilent.com/*, 2013.

J.-F. Argillier, T. Aubry, A. Dupas, P. Poulain, D. Rousseau, and R. Tabary. Impact of polymer mechanical degradation on shear and extensional viscosities: Towards better injectivity forecasts in polymer flooding operations. *SPE-164083-MS*, 2013.

Andrew R. Barron and Yen-Hao Lin. Physical methods in chemistry and nano science. *Rice University Research Course*, 2009.

A. M. Basedow, K. H. Ebert, and H. Hunger. Effects of mechanical stress on the reactivity of polymers: Shear degradation of polyacrylamidea and dextran. *Macromolecular Chemistry*, 1979.

B. A. Buchholz, J. M. Zhan, M. Kenward, G. W. Slater, and A. E. Barron. Flow-induced scission as a physical route to narrowly distributed, high molar mass polymers. *Polymer*, 2004.

James L. Buchwalter, Abdus Satter, and Ghulam Iqbal. *Practical Enhanced Reservoir Engineering: Assisted with Simulation Software*. Gulf Professional Publishing, 2008. ISBN 978-1593700560.

F. Bueche. Mechanical degradation of high polymers. *Journal of Applied Polymer Science No 10*, 1960.

Torsten Clemens, Marie Deckers, Martin Kornberger, and Thomas Gumpenberger. Polymer solution injection near wellbore dynamicsand displacement efficiency, pilot test results, matzen field, austria. 2003.

Torsten Clemens, Thomas Gumpenberger, M. Kornberger, and M. Deckers. Polymer viscosity in porous media and near wellbore behaviour of a polymer pilot in the matzen field. *OMC-2013-166*, 2013.

L. P. Dake. *The Practice of Reservoir Engineering (Revised Edition) (Developments in Petroleum Science)*. Elsevier Science, 2001. ISBN 978-0444506719.

L. P. Dake. *Practical Reservoir Engineering and Characterization*. Gulf Professional Publishing, 2015. ISBN 978-0128018118.

M. Delshad, D. H. Kim, Oluwaseun Adedej Magbagbeola, Chun Huh, Gary Arnold Pope, and Farhad Tarahhom.

US DOE. Polymer flooding, August 2015. URL `"http://www.energy.gov"`.

Healthcare GE-Liefscience. Size exclusion chromatography - principles and methods. *www.gelifesciences.com/sizeexclusion*, 2000.

Glynn, Van der Hoff, and Reilly. A general model for prediction of molecular weight distributions of degraded polymers development and comparison with ultrasonic degradation experiments. *Journal of Macromolecular Science A6*, 1972.

Bhavsar Kaumil. High performance liquid chromatographic principles. *http://de.slideshare.net/kaumilbhavsar/kaumil-hplc-presentation*, 2008.

Bruce L. Knight. Reservoir stability of polymer solutions. *SPE-4167-PA*, 1973.

L. W. Lake. *Enhanced Oil Recovery*. Englewood Cliffs, 1989. ISBN 314-353.

J.M. Maerker. Shear degradation of partially hydrolyzed polyacryl solutions. *SPE-5101-PA*, 1975.

B.K. Maitin, W.O. Sohn, and H. Volz. Preconditioning concepts in polymer flooding in high-salinity reservoirs: Laboratory investigations and case histories. *SPE Res Eng 5: 503507. SPE-17675-PA*, 1990.

C. W. Morris and K. M. Jackson. Mechanical degradation of polyacrylamide solutions in porous media. *SPE 7064*, 1978.

A. J. Muller, J. A. Odell, and S. Carrington. Degradation of semidilute polymer-solutions in elongational flows. *Polymers*, 1992.

R. C. Putz, A. G. ; Rivenq. Commercial polymer injection in the courtenay field. *J. Petroleum Sci. and Eng.*, 1992.

T. Sato and D. E. Nalepa. Shear degradation of cellulose derivatives. *Journal of Applied Polymer Science 22*, 1978.

Abdus Satter and Ghulam M. Iqbal. *Reservoir Engineering: The Fundamentals, Simulation, and Management of Conventional and Unconventional Recoveries*. Gulf Professional Publishing, 11 edition, 2015. ISBN 3257227892.

R. S. Seright, Fan Tianguang, and Kathryn Wavrik. New insights into polymer rheology in porous media. *SPE-129200-MS*, 2010.

R.S. Seright. The effects of mechanical degradation and viscoelastic behaviour on injectivity of polyacrylamide solutions. *SPE-9297-PA*, 1983.

Shodex. Shodex - size exclusion chromatography - operation manual. *https://www.shodex.de*, 2015.

Waseem Ahmad Siddiqui. New protein purification approaches. *Omics Groups*, 2015.

Christian Sledz. Consequences of degradation forces on molecular weight distribution of high-weight hydrolyzed polyacrylamide solutionsl. *Montan University Leoben, Master Thesis*, 2015.

K.S. Sorbie and L.J. Roberts. A model for calculating polymer injectivity including the effects of shear degradation. *SPE/DOE-12652-MS*, 1984.

C. G. Southwick and C. W. Manke. Molecular degradation, injectivity, and elastic properties of polymer solutions. *SPE-15652-PA*, 1988.

J.J. Taber, F.D. Martin, and R.S. Seright. Eor screening criteria revisited-part 1 : Introduction to screening criteria and enhanced recovery field projects. *SPE35385*, 1997.

Ahmed Tarek. *Reservoir Engineering Handbook*. Butterworth Heinemann, 2010. ISBN 978-1856178037.

Paul A. Tipler, Jenny Wagner, Gene Mosca, and Christoph Kommer. *Physik: fr Wissenschaftler und Ingenieure*. Springer Spektrum, 2015. ISBN 978-3642541650.

J.L. White, J.E. Goddard, and H.M. Phillips. Use of polymers to control water production in oil wells. *3672-PA*, 1973.

Markus Zechner, Markus Buchgraber, and Torsten Clemens. Flow of polyacrylamide polymers in the near-wellbore-region, rheological behavior within induced fractures and near-wellbore area. *SPE-166085-MS*, 2013.

List of Figures

List of Tables

List of Equations